

Sheffield Hallam University

Buckling behaviour of slender structural elements under interactive axial static and cyclic loading.

HIRST, Paul B.

Available from the Sheffield Hallam University Research Archive (SHURA) at:

<http://shura.shu.ac.uk/19797/>

A Sheffield Hallam University thesis

This thesis is protected by copyright which belongs to the author.

The content must not be changed in any way or sold commercially in any format or medium without the formal permission of the author.

When referring to this work, full bibliographic details including the author, title, awarding institution and date of the thesis must be given.

Please visit <http://shura.shu.ac.uk/19797/> and <http://shura.shu.ac.uk/information.html> for further details about copyright and re-use permissions.

POLYTECHNIC LIBRARY
POND STREET
SHEFFIELD S1 1WB

6811

100217444 9

TELEPEN



Sheffield City Polytechnic Library

REFERENCE ONLY

ProQuest Number: 10697099

All rights reserved

INFORMATION TO ALL USERS

The quality of this reproduction is dependent upon the quality of the copy submitted.

In the unlikely event that the author did not send a complete manuscript and there are missing pages, these will be noted. Also, if material had to be removed, a note will indicate the deletion.



ProQuest 10697099

Published by ProQuest LLC (2017). Copyright of the Dissertation is held by the Author.

All rights reserved.

This work is protected against unauthorized copying under Title 17, United States Code
Microform Edition © ProQuest LLC.

ProQuest LLC.
789 East Eisenhower Parkway
P.O. Box 1346
Ann Arbor, MI 48106 – 1346

BUCKLING BEHAVIOUR OF SLENDER STRUCTURAL ELEMENTS
UNDER INTERACTIVE AXIAL STATIC AND CYCLIC LOADING

PAUL BRENDAN HIRST BSc

A thesis submitted to the Council for National Academic Awards
in partial fulfilment of the requirements for the degree of

Doctor of Philosophy

Sponsoring Establishment

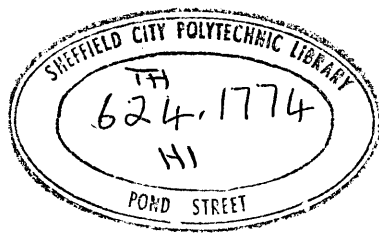
SHEFFIELD CITY POLYTECHNIC

Department of Civil Engineering

Collaborating Establishment

University of Surrey

July 1987



CONTENTS

Advanced Studies Undertaken	(v)	
List of Tables	(vi)	
List of Figures	(viii)	
List of Plates	(xiii)	
Acknowledgements	(xiv)	
Abstract	(xv)	
CHAPTER 1	INITIAL CONSIDERATIONS	1
1.1	Introduction	1
1.2	Basic Structural Instability	3
1.3	Strut Buckling - Historical Résumé	13
1.4	Basic Theoretical Modelling	16
1.5	Experimental Considerations	20
1.6	Digital Computer Incorporation	24
1.7	Summary	25
CHAPTER 2	THE ESTABLISHMENT OF A LARGE SCALE STRUT TESTING SYSTEM	27
2.1	Introduction	27
2.2	Initial Schenck Configuration	28
2.3	Schenck Enhancement - Peripheral Hardware	31
2.3.1	Strut Facility	31
2.3.2	Stub Facility	34
2.3.3	Cyclic Testing Aspects	36
2.3.4	Out-of-Straightness Monitoring	38
2.4	Schenck Enhancement -	

	Digital Computer Incorporation	40
2.5	Preliminary Tests	47
2.5.1	Static Strut Tests	47
2.5.2	Stub Tests	49
2.5.3	Cyclic Strut Tests	51
2.5.4	Résumé	53
2.6	Tensile Testing Facility	54
2.7	Ancillary Features	56
2.8	Summary	57
CHAPTER 3	EXPERIMENTAL PROGRAMME	60
3.1	Introduction	60
3.2	Specimen Definition	62
3.2.1	Configuration	62
3.2.2	Reference System	64
3.2.3	Metrology Aspects	64
3.3	Testing Procedures	73
3.3.1	Stub Tests	73
3.3.2	Stub Tests - Cyclic	77
3.3.3	Tensile Tests	77
3.3.4	Strut Tests - Imperfection Monitoring	78
3.3.5	Strut Tests - Static	82
3.3.6	Strut Tests - Cyclic	85
3.4	Constitutive Behaviour - Results	87
3.4.1	Stub Tests	87
3.4.2	Tensile Tests	90
3.5	Imperfection Assessment Results	93
3.5.1	Initial Curvature	93

3.5.2	Load Eccentricity	100
3.6	Static Strut Testing - Results	101
3.6.1	Parametric Response	101
3.6.2	Semi-Empirical Analyses - Southwell and Lundquist Plots	113
3.7	Cyclic Strut Testing - Results	119
3.7.1	Pseudo-Static Parametric Response	119
3.7.2	Time-Dependent Parametric Response	140
3.7.3	Semi-Empirical Analyses - Southwell and Lundquist Plots	147
3.8	Additional Strut Tests	156
3.8.1	Comments	156
3.8.2	Cyclic Stub Tests	156
3.8.3	Synthetically Curved Struts	158
3.8.4	Re-Tested Struts	160
3.9	Summary	163
CHAPTER 4	THEORETICAL STUDY	165
4.1	Introduction	165
4.2	Formal Static Moment-Thrust-Curvature Constitutive Relationships	167
4.3	Novel Constitutive Modelling	172
4.4	Spring-Link Strut Model	175
4.5	Analytical Virtual Work Formulation	179
4.6	Application and Solution Procedures	181
4.6.1	Static Studies	181
4.6.2	Cyclic Studies	181
4.6.3	Non-Linear Solution Routine	184

4.6.4	Static Strut Analysis, $\lambda_m=1$	185
4.7	Case Studies; Static Analyses	187
4.8	Case Studies; Cyclic Analyses (Pseudo-Static Modelling)	190
4.9	End-Shortening Conditions	206
4.10	Summary	210
CHAPTER 5	DISCUSSION	213
5.1	Introduction	213
5.2	Static-Cyclic Correlation	216
5.2.1	Experimental Considerations; Data Control	216
5.2.2	Pseudo-Static Modelling	229
5.3	Design Implications	237
5.4	Summary	241
CHAPTER 6	CONCLUSIONS	244
6.1	Primary Assessments	244
6.2	Associated Factors	245
6.3	Suggestions for Further Work	247
CHAPTER 7	APPENDICES	
I	Publications	A1
II	Typical Numerical Output	A36
III	Typical x,y/t Output	A39
IV	List of Computer Programmes	A42
V	Sample Computer Programme	A44
VI	Nomenclature	A76
VII	Bibliography	A81

ADVANCED STUDIES UNDERTAKEN

1981	Dynamic Analysis of Offshore Structures
27-29 January	Course
	Computational Mechanics Centre, Southampton
1981	Fortran Programming Course
Autumn Term	Computer Services
	Sheffield City Polytechnic
1982	Computing short courses (including computer
Spring Term	graphics and microcomputing)
	Computer Services
	Sheffield City Polytechnic

LIST OF TABLES

Table	Title	Page
2.1	Preliminary Static Strut Test Results	50
2.2	Preliminary Stub Test Results	52
2.3	Preliminary Cyclic Strut Test Results	52
2.4	Error Analysis	58
3.1	Sample Outer Diameter and Wall Thickness Measurements	67
3.2	Sample Data for Ovality and Eccentricity of Loading Assessment	71
3.3	Sample Cross-Sectional Area Measurements	72
3.4	Sample Stub Test Data	88
3.5	Tensile Test Data	92
3.6	Sample (Pin-Ended) Out-of-Straightness Values	94
3.7	Sample (Pin-Ended) Out-of-Straightness Angular Displacement Values	95
3.8	Pinned-Encastré Mode Correlation	95
3.9	Sample Experimental Static Strut Data	109
3.10	Sample Southwell and Lundquist Plot Data	116
3.11	Cyclic Experimental Data	121
3.12	Primary Experimental Data	124
3.13	Supporting Experimental Data	127
3.14	Quasi-Cyclic Struts - Southwell and Lundquist Plot Data	152
3.15	Southwell and Lundquist Plot Data	153
3.16	Cyclic Stub Test Data	157

Table	Title	Page
3.17	Synthetically Deformed Strut Test Data	157
3.18	Retested Strut Test Data	157
4.1	Sample Static Strut Data - Theoretical Buckling Load Assessment	189
4.2	Sample Quasi-Cyclic Strut Data - Theoretical Buckling Load Assessment	189
4.3	Theoretical Buckling Loads for Cyclic and Corresponding Static Struts	195
4.4	Post-Cyclic Phase Buckling Loads, P_C , Expressed as a Percentage of their Fully Equivalent Static Values, P_{CS}	204
4.5	Theoretical Fully Equivalent Static and Cyclic Buckling Displacements	
4.6	Average Theoretical Buckling Loads Given as Percentages of their Corresponding Experimental Buckling Loads	211

LIST OF FIGURES

Figure	Title	Page
1.1	Idealised Linear Systems Theory	4
1.2	Quasi-Idealised Buckling Considerations	6
1.3	Initially Curved Strut	9
1.4	Buckling Loci	12
1.5	Quasi-Idealised Spring Link Model	17
1.6	Imperfect Spring Link Model	17
1.7	Model: Action-Response Loci	21
2.1	Computer Control and Monitoring Features	42
2.2	Line Diagram of Enhanced Testing System	48
3.1	Reference System	65
3.2	Outer Diameter and Wall Thickness Measurements	65
3.3	Outer Diameter Histogram	68
3.4	Wall Thickness Histogram	69
3.5	Non-Dimensionalised Cross-Sectional Area Histogram	74
3.6	Out-of-Straightness Monitoring Configuration	81
3.7	Central Monitoring Facility	84
3.8	Stub Loci - Yield and Roundhouse Type	89
3.9	Stub and Tensile Test Loci	89
3.10	Direct Modulus and Yield/Proof Stress Histograms	91
3.11	Out-of-Straightness Components - Strut Ref. 6S	91
3.12	Non-Dimensionalised Maximum Initial Lateral Displacement Histogram	97
3.13	Imperfection Parameters	98
3.14	P vs u - Strut Ref. 12S	102

Figure	Title	Page
3.15	P vs $w_{cL}-w_{ocL}$ - Strut Ref. 12S	102
3.16	P vs ϵ_n - Strut Ref. 12S	103
3.17	Vector Trace ($P \leq P_c$) - Strut Ref. 12S	103
3.18	Vector Trace - Strut Ref. 12S	104
3.19	P vs u - Strut Ref. 20S	104
3.20	P vs $w_{cL}-w_{ocL}$ - Strut Ref. 20S	105
3.21	P vs ϵ_n - Strut Ref. 20S	105
3.22	Vector Trace ($P \leq P_c$) - Strut Ref. 20S	106
3.23	Vector Trace - Strut Ref. 20S	106
3.24	P vs u - Strut Ref. 21S	108
3.25	P vs $w_{cL}-w_{ocL}$ - Strut Ref. 21S	108
3.26	Vector Trace ($P \leq P_c$) - Strut Ref. 6S	111
3.27	Vector Trace - Strut Ref. 6S	111
3.28	Pin Ended/Encastré End Condition Correlation	115
3.29	Southwell and Lundquist Plots - Strut Ref. 21S	118
3.30	Southwell Plot - Strut Ref. 5S	118
3.31	Cyclic Strut Studies - Pseudo-Static Considerations	120
3.32	Cyclic Step/Peak Cyclic Load Ratio vs Modified Slenderness	128
3.33	Peak Cyclic Load vs Cyclic Step Response	128
3.34	P vs u - Strut Ref. 13C	130
3.35	P vs $w_{cL}-w_{ocL}$ - Strut Ref. 13C	130
3.36	Vector Trace ($P \leq P_c$) - Strut Ref. 13C	131
3.37	Vector Trace - Strut Ref. 13C	131
3.38	P vs u - Strut Ref. 26C	133
3.39	P vs $w_{cL}-w_{ocL}$ - Strut Ref. 26C	133

Figure	Title	Page
3.40	Vector Trace ($P < P_C$) - Strut Ref. 26C	134
3.41	Vector Trace - Strut Ref. 26C	134
3.42	P vs u - Strut Ref. 27C	135
3.43	P vs $w_{cL} - w_{ocL}$ - Strut Ref. 27C	135
3.44	Vector Trace ($P < P_C$) - Strut Ref. 27C	136
3.45	Vector Trace - Strut Ref. 27C	136
3.46	Vector Trace ($P < P_C$) - Strut Ref. 19C	137
3.47	P vs u - Strut Ref. 20C	139
3.48	P vs $w_{cL} - w_{ocL}$ - Strut Ref. 20C	139
3.49	Quasi-Elastic Hysteresis: P vs u Trace - Strut Ref. 13C	141
3.50	Quasi-Elastic Hysteresis: P vs $w_{cL} - w_{ocL}$ Trace - Strut Ref. 13C	141
3.51	Single Band Hysteresis: P vs $w_{cL} - w_{ocL}$ Trace - Strut Ref. 19C	143
3.52	Multiple Band Hysteresis: P vs $w_{cL} - w_{ocL}$ Trace - Strut Ref. 21C	143
3.53	Cyclic Creep: P vs $w_{cL} - w_{ocL}$ Trace - Strut Ref. 26C	144
3.54	Cyclic Creep: P vs $w_{cL} - w_{ocL}$ Trace - Strut Ref. 27C	145
3.55	P vs u Hysteretic Trace - Strut Ref. 26C	146
3.56	P vs u Hysteretic Trace - Strut Ref. 27C	146
3.57	Cyclic Buckling: P vs u Hysteretic Trace - Strut Ref. 20C	148

Figure	Title	Page
3.58	Cyclic Buckling: P vs $w_{cL}-w_{ocL}$ Hysteretic Trace - Strut Ref. 20C	149
3.59	Southwell Plot - Strut Ref. 7C	150
3.60	Lundquist Plot - Strut Ref. 7C	150
3.61	Southwell and Lundquist Plots - Strut Ref. 24C	154
3.62	Southwell Plot - Strut Ref. 18C	155
3.63	Lundquist Plot - Strut Ref. 18C	155
3.64	Cyclic Stub Test (Autographic) Output - Stub Ref. 2D(a)	159
3.65	Cyclic Stub Test: Computer Graphic Output - Stub Ref. 2D(a)	159
3.66	P vs $w_{cL}-w_{ocL}$ - Strut Ref. 32(a)	161
3.67	Vector Trace ($P < P_c$) - Strut Ref. 32(a)	161
3.68	P vs $w_{cL}-w_{ocL}$ - Strut Ref. 1R	162
3.69	Schedule of Tests	164
4.1	Three Phase Constitutive Topology	168
4.2	Formal M-P-V Contours	171
4.3	Formal M-P-V and Curve Fit Contours	174
4.4	Typical Spring-Link Configuration	176
4.5	Theoretical Model	177
4.6	Quasi-Idealised and Imperfection Buckling Loci: $\lambda_m = 1$	186
4.7	Case Study - Strut Ref. 18S	188
4.8	Case Study - Strut Ref. 21S	188
4.9	Case Study - Strut Ref. 3C	192
4.10	Case Study - Strut Ref. 7C	192

Figure	Title	Page
4.11	Case Study - Strut Ref. 3C	193
4.12	Case Study - Strut Ref. 18C	197
4.13	Case Study - Strut Ref. 19C	198
4.14	Case Study - Strut Ref. 21C	199
4.15	Case Study - Strut Ref. 22C	199
4.16	Case Study - Strut Ref. 26C	200
4.17	Case Study - Strut Ref. 27C	201
4.18	Pseudo-Static Model Characteristics	201
4.19	P vs $u-u_0$ Case Study - Strut Ref. 19S	209
4.20	P vs $u-u_0$ Case Study - Strut Ref. 20S	209
5.1	Normalised Experimental Buckling Loads vs λ_m	222
5.2	Non-Dimensionalised [P_e] Experimental Buckling Loads vs λ_m	223
5.3	Non-Dimensionalised [P_p] Experimental Buckling Loads vs λ_m	224
5.4	Normalised Theoretical Buckling Loads Based on Direct w_{oc} Values vs λ_m	232
5.5	Normalised Theoretical Buckling Loads Based on Interpolated w_{oc} Values vs λ_m	233
5.6	Normalised Theoretical Buckling Loads Based on Southwell a_{os} Values vs λ_m	234
5.7	Normalised Theoretical Buckling Loads Based on Lundquist a_{o1} Values vs λ_m	235
5.8	Experimental Imperfection Data vs λ_m	239
5.9	Non-Dimensionalised Cyclic Step Parameter vs λ_m	242

LIST OF PLATES

Plate	Title	Page
1	Initial Schenck Configuration	30
2	Load Cell and Collett Assembly	30
3	Strut Test Rig - Transducer Monitoring Network	35
4	Stub Test Rig	37
5	Cyclic Stub Test Rig	37
6	Out-Of-Straightness Monitoring Rig-Base Assembly	39
7	Digital Computer Annexe	39
8	Enhanced Schenck Configuration	46
9	Avery - Tensile Testing Rig	55
10	Stub Specimens	76
11	Tensile Test Specimen	76
12	Ruptured Tensile Test Specimen	79
13	Buckled Strut Specimen (partial recovery)	79

ACKNOWLEDGEMENTS

The author would like to express his appreciation to Dr Neil Taylor, Director of Studies, and Professor A C Walker, External Supervisor, for their help and guidance.

This opportunity is also taken to thank Mr P F Lonsborough, Department of Civil Engineering, and Mr M Andersons, Department of Computer Services, for their assistance with respect to the testing system enhancement programme.

Material support for the programme was received from the British Steel Corporation, Tubes Division, Corby. This support is most gratefully acknowledged.

ABSTRACT (P B HIRST)

Buckling behaviour of slender structural elements under interactive axial static and cyclic loading

The objective of the research programme has been to investigate the effects of pre-buckling low frequency inelastic cyclic hysteresis upon a range of imperfection sensitive circular hollow section struts. The programme has involved experimental and theoretical studies and computer graphics are widely employed throughout. The subject matter is introduced from a variety of perspectives, phenomenological, historical, theoretical and experimental in Chapter 1, together with an appreciation of the role of the digital computer within the research programme. Experimental factors are initially presented in Chapter 2 whilst the formal testing programme is described in Chapter 3. Original findings are definitively set out in Sections 3.3 and 3.7 wherein the concept of the 'cyclic step' is first introduced, the remaining sections in the chapter providing the necessary supporting data.

Theoretical studies are reported in Chapter 4 with the novel moment-thrust-curvature modelling described in Sections 4.2 and 4.3 being of central importance. This modelling enables the formulation of a predictive cyclic strut system effectively requiring of the end user the solution of only a pair of simultaneous equations and yet capable of providing data trends consistent with the experimental findings.

Design interpretation together with an overview of the experimental and theoretical studies and their interrelationship are set out in Chapter 5. A practical design procedure oriented about the effect of a pre-buckling cyclic action phase upon otherwise static strut performance is delineated and an appropriate design chart is provided.

Conclusions are drawn with respect to the primary research findings in Chapter 6 wherein suggestions are also made regarding possible further studies. An Appendix is included providing the bibliography, nomenclature and respective published work; selected supporting documentation is also presented.

CHAPTER 1

INITIAL CONSIDERATIONS

1.1 INTRODUCTION

Basic static structural analysis employs linear systems theory which prescribes the deformations to be indefinitely small and the constitutive properties to be of linear form. However, current structural design practice is increasingly concerned with the limit state concept⁽¹⁾ whereby these conditions, particularly the latter, are subject to revision. Consequently, inelastic behaviour is of notable interest in bridging between linear (elastic) and limit (plastic) states. Further, current trends are towards the employment of slender structural elements, with emphasis on economic strength-to-weight ratios. This, in turn, leads to increased importance being attached to stability considerations which necessarily involve some measure of regard being given to finite deformations and, crucially, incorporation of initial imperfection effects⁽²⁾.

Accepting that no service load is truly static⁽³⁾, and given that there exists a wide range of dynamic configurations, then the incorporation of dynamic action in nominally static analyses also requires careful consideration. Severe dynamic action generates inertial forces⁽⁴⁾ whilst resonance⁽⁵⁾, a singular phenomenon involving the structure's natural frequency, is of major importance in the design of structures subject to vibration.

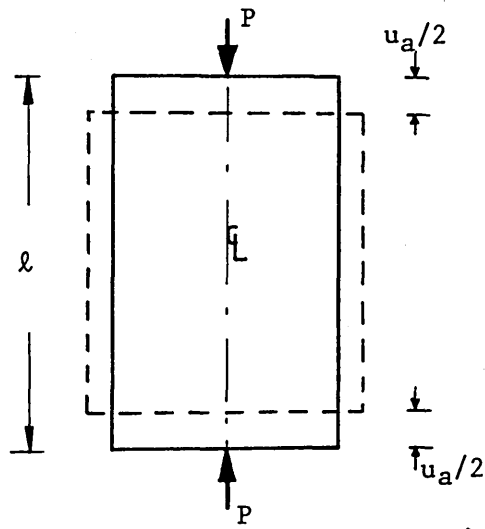
Given the prevention of rigid body motion in static systems, then essentially static studies which involve some dynamic modelling are primarily concerned with vibration or cyclic considerations. Vibrations can be of free or forced excitation forms(6). Regarding free vibration modes, which relate to impulse or transient disturbing forces, the presence of damping effects generally assures a diminishing dynamic response. Conversely, forced vibration involves continually applied action, generally cyclic in nature, in which the vibration profiles may be of known, that is deterministic, configuration or otherwise(7). For low frequency action, inertial effects are minimal(8), permitting some correlation between vibrational effects and static studies involving incremental plasticity shakedown and alternating plasticity(9,10). Fatigue failure must be considered, of course, although its importance diminishes in cases involving relatively few cycles ($\leq 10^4$) and the absence of net tension.

Given the foregoing and the recommendations of recent studies delineating research needs(11,12), the present work relates to the effects of pre-buckling low frequency inelastic cyclic hysteresis upon a range of imperfection-sensitive circular hollow section (CHS) struts. Whilst there exists substantial data relating to the effects of fully reversed cyclic loading upon axially loaded structural elements(13-21), little investigation appears to have been undertaken with respect to the effect of a pre-buckling cyclic loading phase upon the otherwise static strut buckling performance(22). This would seem somewhat arbitrary given the importance of imperfections upon strut behaviour and the

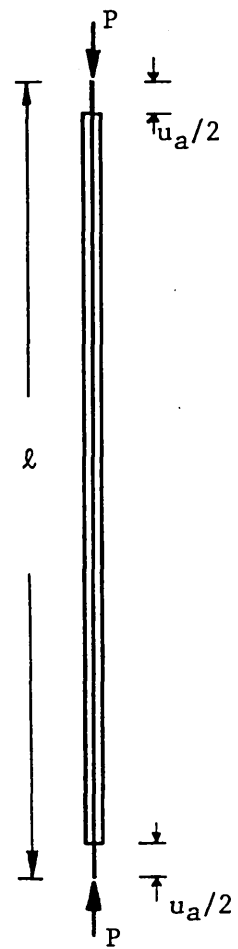
possibility of interaction between inelastic hysteresis and imperfection sensitivity. Accordingly, amplification of the effects of any initial imperfection due to pre-buckling cyclic action is considered together with its concomitant effects upon load carrying capacity and serviceability.

1.2 BASIC STRUCTURAL INSTABILITY

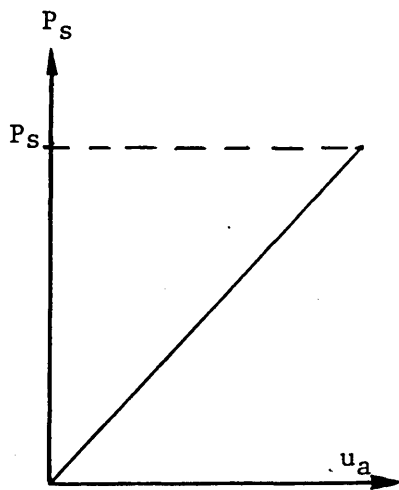
Within the field of elastostatics⁽²³⁾, idealised structural behaviour can be typified by recourse to the stub and slender axial compression systems illustrated in Fig 1.1(a) and (b) respectively. As action parameter P , equivalent to the axial force in the respective member, is uniformly increased, the primary response parameter, axial deformation u , represented herein by the overall axial shortening u_a , correspondingly increases. For systems involving linear constitutive properties and indefinitely small deformations, $u_a = P\ell/AE$, where ℓ is the length, A is the cross-sectional area and E is the direct modulus of the member. The governing action-response locus is of linear form as depicted in Fig 1.1(c). All structural response parameters, including axial stress for example, afford a corresponding behavioural pattern. The axial or direct stress generated in the member is given by $\sigma_a = P/A$. System linearity ceases with the onset of either constitutive non-linearity, that is the onset of yield in ductile steel structures for example, or finite deformations which, with regard to the purely axial system herein, refers to the state at which the induced change in cross-sectional area becomes significant. In terms of flexural



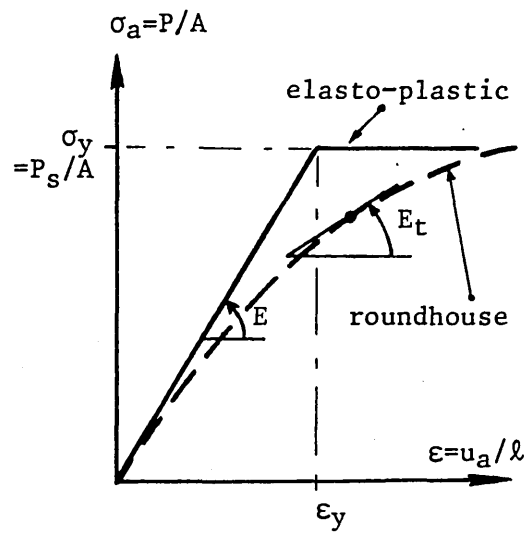
(a) Stub Topology



(b) Fully Idealised Slender Topology



(c) Action-Response Locus



(d) Constitutive Loci

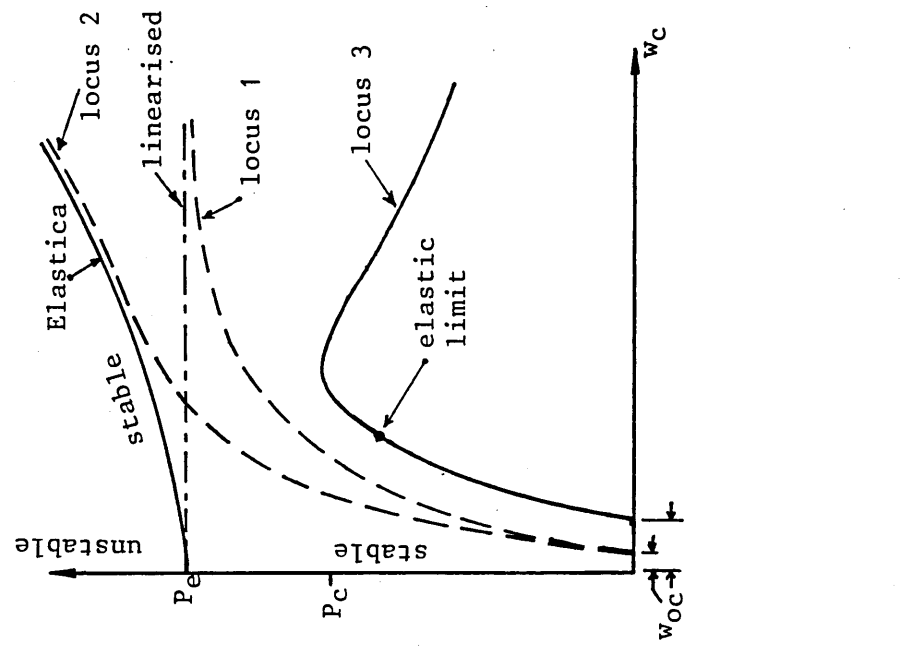
Figure 1.1 ; Idealised Linear Systems Theory

system behaviour, of particular relevance to the later work, finite deformations are typified by slopes exceeding 0.1 radians(24).

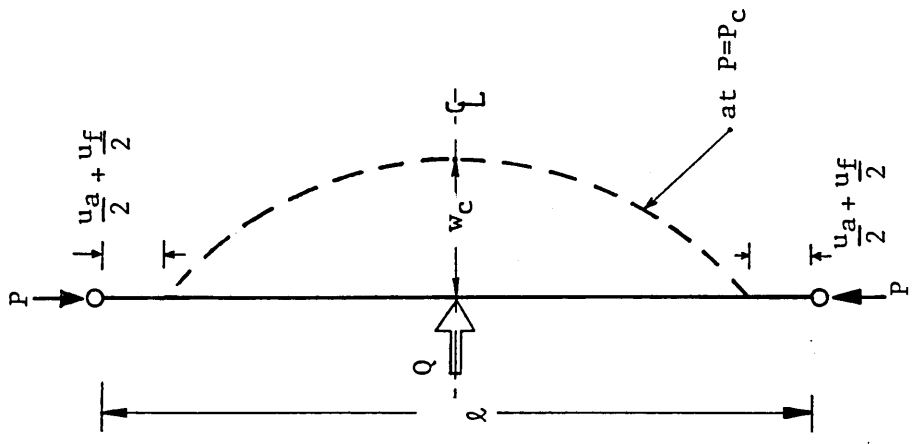
In conjunction with the above, idealised elasto-plastic constitutive behaviour, as associated with mild steels (eg grade 43), is typified in Fig 1.1(d). Stress-strain behaviour is therefore linear for $\sigma \leq \sigma_y$. Actual constitutive loci are derived from tensile(25) or stub tests(26).

Consider now the introduction of some relatively small, transient, lateral interference force Q into each of the foregoing idealised axial compression systems in the manner denoted in Fig 1.2(a) and (b), by means of which the systems concerned become only quasi-idealised compression systems. The respective responses of the stub and slender systems become quite distinct. The behaviour of the former is effectively unchanged, whilst the latter will undergo (elastic) instability. The study of instability(27,28) relates to systems which experience a singular and sudden change in structural response despite the action parameter being only gradually and uniformly increased. The fundamental nature of instability studies can be classified in terms of Thom's Catastrophe Theory(29).

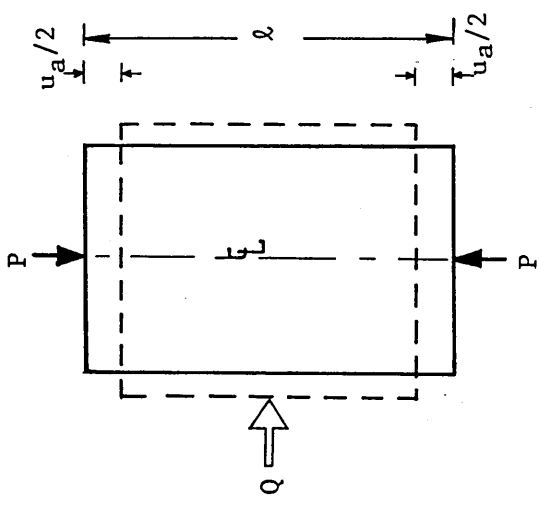
Elastic instability can thereby be typified by reference to the slender compression system depicted in Fig 1.2(b). Noting the presence of the relatively small, transient force Q , then, as the action parameter P is gradually increased, axial response in terms



(c) Action - Response Loci



(b) Quasi-Idealised Slender Topology - Buckling



(a) Stub Topology

Figure 1.2 ; Quasi-Idealised Buckling Considerations

of u_a is again exhibited. However, at some singular or critical loading state P_e , a sudden change in structural response is observed; flexural deformation, represented by the central (mid-span) and maximum transverse deflection parameter w_c , is statically incurred. Further, a flexurally induced axial end-shortening u_f is set up. That is, an apparently axial system is replaced by a predominantly flexural system at, and beyond, a singular state associated with compression P_e . The system typified in Fig 1.2(b) thereby suffers strut buckling action which onsets at $P_e = \pi^2 EA / (\ell/r)^2$ (30) with r denoting the minimum radius of gyration - note Fig 1.2(c). The degree of slenderness, assessed in terms of the so-called slenderness ratio, ℓ/r , is clearly of importance with regard to the possible onset of flexural behaviour. In linearised terms, that is assuming relatively small deformations, the critical load P_e represents the limiting load carrying capacity of the member. Experimentation has shown that such members can sustain loads higher than the critical or conceptual buckling load P_e , the necessary modelling requiring a finite deformation study - the 'Elastica' (31). The appropriate behavioural locus is included in Fig 1.2(c). Within the linear elastic constitutive range, the overall end-shortening now takes the form

$$u_a + u_f = \frac{P\ell}{AE} + \frac{1}{2} \int_0^{\ell} \left(\frac{dw}{dx} \right)^2 dx \quad \text{for } P > P_e \quad (1.1)$$

whilst the appropriate maximum stress induced in the member σ_m , $\sigma_m \leq \sigma_y$, can be represented by

$$\sigma_m = P/A + Pw_c/Z \quad \text{for } P > P_e \quad (1.2)$$

where Pw_c is the maximum bending moment and Z is the elastic modulus of the member. For completeness, it is useful to note that for roundhouse constitutive loci, as associated with aluminium alloys or mild steel suffering substantial residual stress effects(32,33), the critical load can be expressed in terms of a tangent modulus E_t or as a reduced derivative(34) - note Fig 1.1(d).

The foregoing slender strut analysis requires the incorporation of the ill-defined transient parameter Q ; such analyses are thereby deemed to be quasi-idealised. In practice, physical imperfections in the structural system are unavoidable and prompt flexural response, note Eqns (1.1) and (1.2), for $P > 0$; Q conceptually serves to represent this fact. Physical imperfections can be classified into three major groups; initial curvature, eccentric loading and residual stresses(1).

Accordingly, Fig 1.3 illustrates a strut suffering an initial central deflection, w_{oc} . Assuming a sympathetic initial profile, $w_0 = w_{oc} \sin(\pi x/\ell)$, then the response, in linearised terms, is given by(35)

$$w_c = w_{oc} (1 - (P/P_e))^{-1} \quad (1.3)$$

This behaviour can be typified by imperfection locus 1 depicted in Fig 1.2(c), where the maximum load converges to the asymptote, P_e .

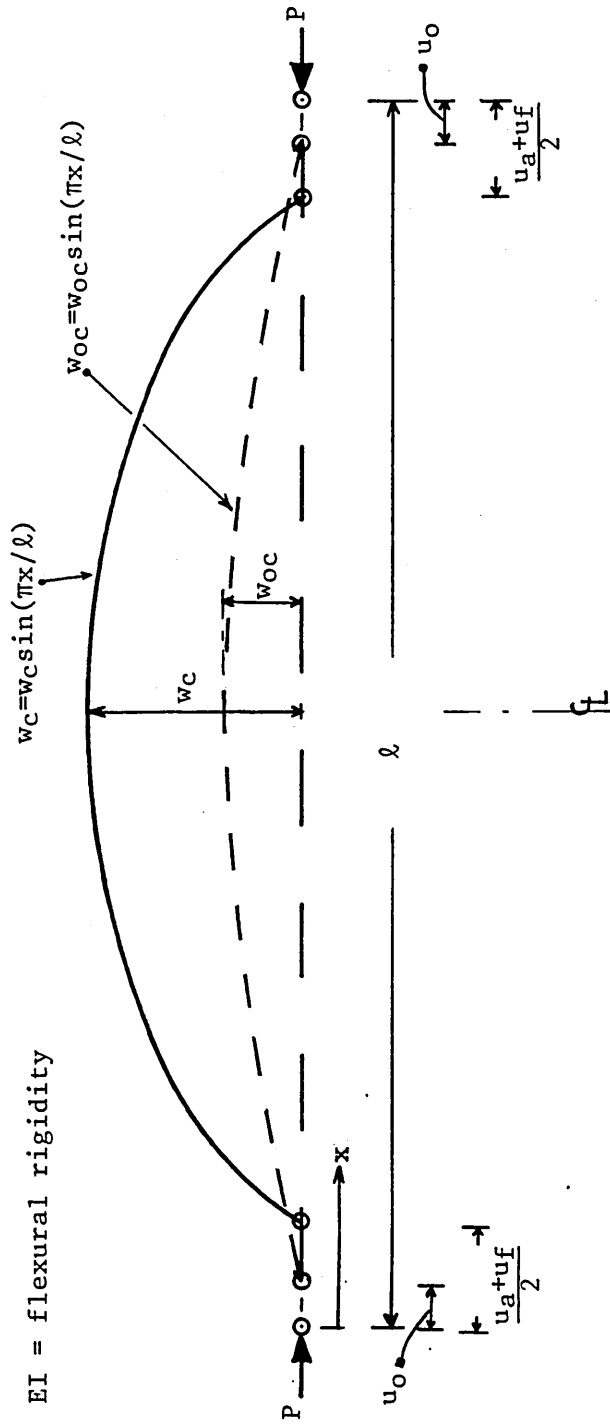


Figure 1.3 ; Initially Curved Strut

Similar treatment can be instituted for the other types of imperfection either by direct analysis or by employing some effectively equivalent w_{oc} in Eqn (1.3)(1). More formally, and subject to the availability of a suitable yield strength, employment of a finite deformation study can lead to imperfection loci of type 2 form as shown in Fig 1.2(c). Loci 1 and 2 both involve linear elastic constitutive properties being extant throughout the loading process. The theoretical load carrying capacity is effectively unaffected by the incorporation of w_{oc} . Such behaviour is classified as being imperfection insensitive. However, in practical terms, loci of type 3 as depicted in Fig 1.2 (c) are generally incurred in which the linear elastic limit or yield stress is breached below P_e , with flexurally inelastic response governing system behaviour where the maximum induced strain $\epsilon_m > \epsilon_y$. This results in the institution of a maximum load P_c , which is termed the crippling or buckling load, where $P_c < P_e$. The magnitude of P_c is dependent upon the initial imperfections (eg w_{oc}) and the yield stress σ_y . This form of strut behaviour is therefore deemed to be inelastically imperfection sensitive(3).

The inclusion of an initially curved strut profile, as illustrated in Fig 1.3, together with the elastic limit state or first yield criterion, forms the basis of the Perry formula(35). Its subsequent derivative, employed in the current strut or column design code of practice BS 5950(36), is given by

$$\frac{P_p}{A} = \frac{P_e P_s}{A^2} \left[\frac{P_s + (\eta+1)P_e}{2A} + \left[\left(\frac{P_s + (\eta+1)P_e}{2A} \right)^2 - \frac{P_e P_s}{A} \right]^{\frac{1}{2}} \right]^{-1} \quad (1.4)$$

with P_p and P_s denoting the unfactored design and squash (yield) loads respectively, where $P_s = \sigma_y A$. The empirically based Perry factor η is determined by

$$\eta = 0.001 a_r (\lambda - \lambda_0) \quad : \quad \lambda_0 = 0.2 \left(\frac{\pi^2 E}{\sigma_y} \right)^{\frac{1}{2}} \quad (1.5)$$

where λ and λ_0 denote the slenderness and limiting slenderness ratios respectively. The Robertson constant a_r is assigned prescribed values according to the cross-sectional configuration and testifies to the employment of multiple column curves. For hot rolled and finished CHS struts, which are of primary concern herein, $a_r = 2$. The necessarily empirical basis for η is due to the essentially statistical nature of practical strut performance, given both the highly variable and ill-defined form of strut imperfections.

Fig 1.4 graphically illustrates the appropriate design curve relating to hot and finished rolled CHS struts, together with the elastic critical (Euler) and yield loci. The ordinate is normalised to the squash load P_s , and the abscissa is evaluated in terms of the modified slenderness ratio $\lambda_m = \lambda / \lambda_1$ (35) such that

$$\lambda_m = \lambda / \lambda_1 = \frac{\ell / r}{\pi (E / \sigma_y)^{\frac{1}{2}}} = (\sigma_y / \sigma_e)^{\frac{1}{2}} = \ell / r (\sigma_y / \pi^2 E)^{\frac{1}{2}} \quad (1.6)$$

with λ_1 denoting the value of λ at the state $P_s = P_e$. This takes explicit account of the respective constitutive properties and provides for normalised abscissa values. Also indicated in the figure is the classification of imperfection sensitivity by

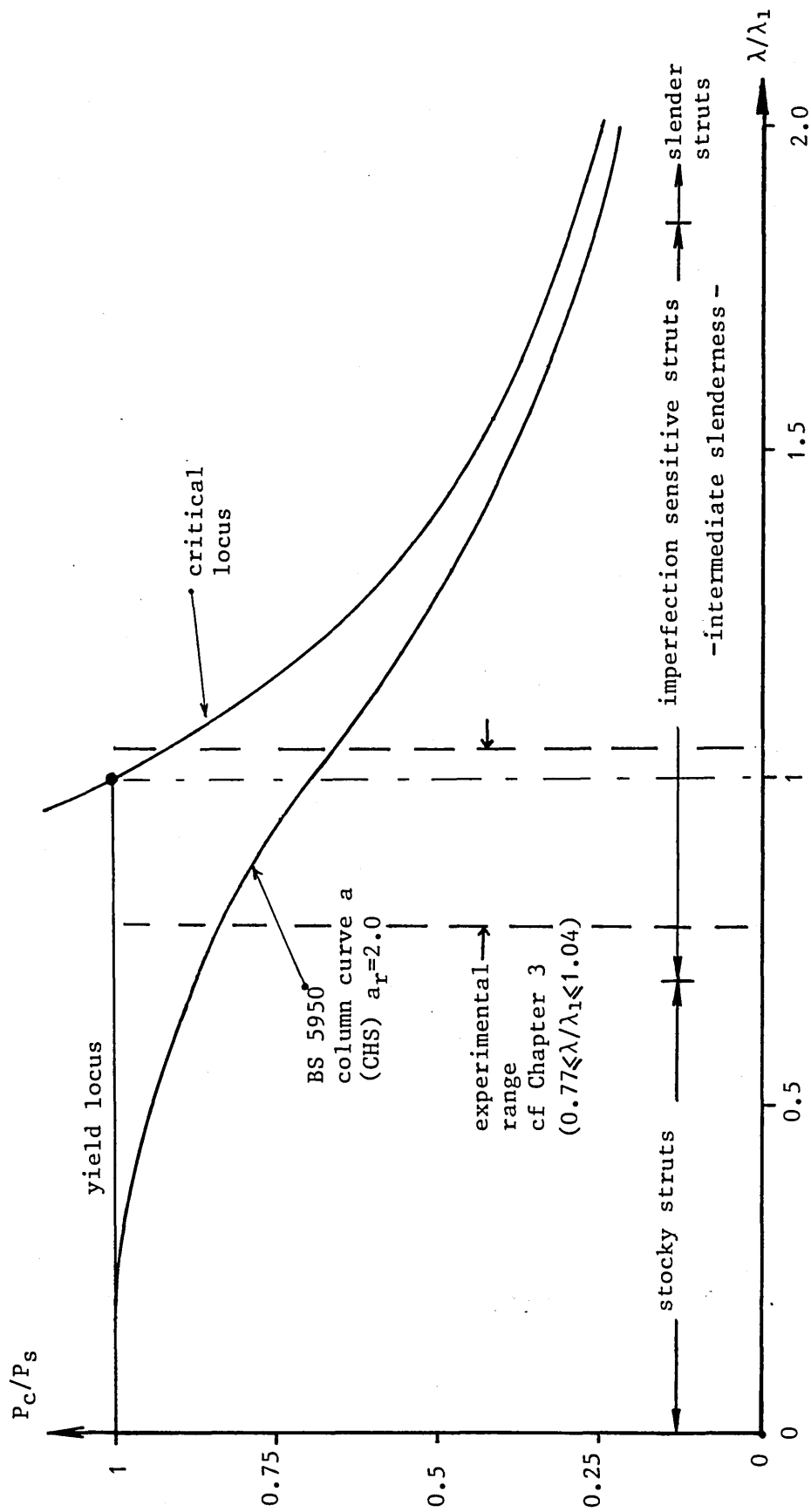


Figure 1.4 ; Buckling Loci

slenderness⁽³⁷⁾, with extreme imperfection sensitivity occurring at $\lambda/\lambda_1=1$.

General inelastic strut behaviour is of complex form, and its treatment is considered at length in the ensuing study. Effort has been centred about the modified slenderness ratio of unity, important because of its service practicality and imperfection sensitivity.

1.3 STRUT BUCKLING - HISTORICAL RÉSUMÉ

The study of structural systems can be said to begin in earnest with the Egyptians, surely the first culture to institute structural forms on a large scale. Developments through Grecian and Roman studies ebbed with the onset of the Dark Ages and scientific thought only re-emerged with the Renaissance. Da Vinci (1452-1519) considered the basic philosophy of the equilibrium of forces, this being typified in his quote 'Mechanics is the paradise of mathematical science, because here we come to the fruits of mathematics'. Amongst his many achievements was his experimental work on columns⁽³⁸⁾.

Key developments in the seventeenth century may be concisely represented by the definition of elasticity by Hooke, the introduction of the principles of 'infinitesimal' calculus by Leibnitz and Newton, and, of course, Newton's Laws of Motion.

The study of structural instability proper was initiated in the

eighteenth century by Euler (1707-1783). Employing the 'infinitesimal' calculus he provided an analysis and solution to the problem of the *Elastica*, determining the critical load of the strut under quasi-ideal conditions and subject to linear elastic constitutive properties. Euler also extended the associated theory of moment-curvature and propounded the condition of small or indefinitely small deformations. The original formal concepts of first order linear structural theory were introduced by Young (1773-1829).

The nineteenth century saw a dramatic expansion in the study of mechanics. Particular interest centred on the work of Rankine, who, in 1858, presented a semi-empirical formula that predicted the crippling state of struts for a wide range of slenderness ratios. In 1886, the semi-empirical Perry Formula was introduced. An important step, this formula has formed a basis for column design through this century.

Robertson published results from an extensive series of steel column tests in 1925 and, on the basis of these tests, developed the applicability of Perry's work by proposing an improved value for the empirical imperfection constant η in Perry's formula⁽³⁵⁾. It is to be noted that Perry originally attempted to define, albeit on an empirical basis, the limiting elastic or first yield state despite involving the statistically necessary employment of a load factor approach to design. This useful revision led to the Perry-Robertson formula being adopted in British practice. In 1929, the Steel Structures Research Committee was set up under one

of the earliest cooperative ventures between British industry and the Government Department of Science and Industrial Research⁽³⁹⁾. This committee was responsible for introducing the first edition of BS 449 in 1931. This standard, suitably revised, served until the publication in 1985 of the current code of practice, which employs limit state philosophy, BS 5950. Herein, the Perry formula has been modified in line with a study commissioned by the European Convention of Constructional Steelwork (ECCS). As a result, a set of design loci or multiple column-strength curves are provided which account for the influence of both cross-sectional geometry and fabrication methods on strut performance.

The field of inelastic strut buckling, with which the present study is intimately concerned, has received considerable attention, the first notable contribution being from Considère in 1889. He indicated the limited applicability of the Euler analysis, notwithstanding Euler's own intuitive understanding of the process of inelastic buckling⁽⁴⁰⁾. Supported by experimental evidence, Considère proposed a modified inelastic Euler formulation employing a reduced tangent modulus, whose value he qualified as being intermediate between the direct (Young's) and tangent moduli. A contemporary study by Engesser⁽⁴⁰⁾, whilst being independent of Considère's contribution, led to the now well established tangent modulus formula. In 1895, Jasinski brought Considère's work to the attention of Engesser, who produced a general reduced tangent modulus approach. In 1910, Kármán developed this generalised approach in deriving explicit

expressions for the reduced tangent moduli of certain standard structural cross-sections. For the 35 years following Kármán's work, controversy surrounded the relative merits of the tangent and reduced moduli. In 1946, Shanley reconciled this discord with a rational explanation of the phenomenon in favour of the tangent modulus approach. A year later he validated this theory by the analysis of a buckling model that has become eponymous with him⁽⁴¹⁾

More generally, with the twentieth came the development of a variety of refined analytical principles, together with an attendant improvement in the quality of experimental techniques. Further, the relatively recent advent of the electronic digital computer has had a dramatic impact upon both analytical and experimental studies. Modern computers are capable of undertaking algorithmic computations at phenomenal speed and facilitate the storage of vast amounts of data in a readily accessible manner. Since the advent of the first computer, ENIAC, constructed in 1948 in the USA, engineering analysis and experimental techniques have in turn developed to take advantage of the digital computer's attributes. Given the highly variable, statistical nature of strut behaviour, these factors are of particular relevance to the research programme herein discussed.

1.4 BASIC THEORETICAL MODELLING

The representative spring-link model illustrated in Fig 1.5 consists of two rigid and incompressible links, connected by a centrally located torsional spring of stiffness c - this is a

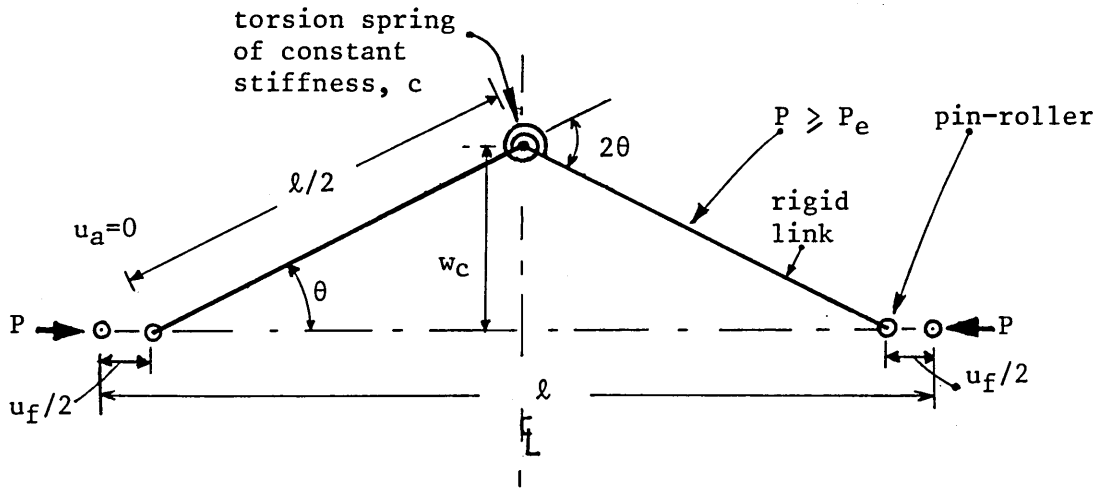


Figure 1.5 ; Quasi- Idealised Spring Link Model

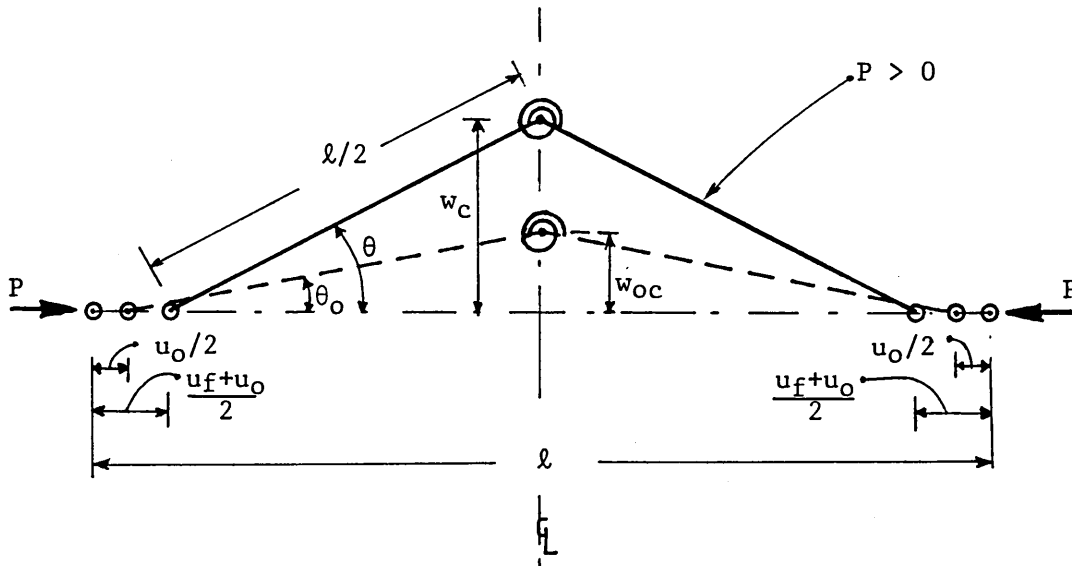


Figure 1.6 ; Imperfect Spring Link Model

constant for linearly constitutive systems. Such models afford considerable computational amenability. The spring represents the flexural stiffness of the model in discretised terms. The response moment M , due to the rotation of the spring, is given by $M=2c\theta$ (3), where θ , the angular link displacement, is the single kinematic generalised coordinate in this 1 degree-of-freedom system. Presently, $c=2EI/\ell$ in accordance with linear elastic constitutive properties. The spring-link topology is taken to be initially straight and the attendant analysis is thereby of quasi-idealised form.

Employing a potential energy approach(35), then, with V denoting the total potential energy of the system,

$$V = U - W \quad (1.7)$$

where U and W are the strain energy and external work functions respectively. These functions may be derived explicitly in terms of θ , such that Eqn (1.7) becomes

$$V = 2c\theta^2 - P\ell(1-\cos\theta) \quad (1.8)$$

The condition that V is stationary with respect to θ for static equilibrium affords

$$\partial V/\partial\theta = 4c\theta - P\ell\sin\theta = 0 \quad (1.9)$$

Eqn (1.9) can be satisfied either with $\theta=0$ throughout all P , which forms a flexurally trivial solution, or with

$$P = 4c\theta/\ell\sin\theta \quad (1.10)$$

Linearising (1.10), such that $\theta/\sin\theta=1$ for small displacements of θ , affords the critical load

$$P_e = 4c/\ell = 8EI/\ell^2 \quad (1.11)$$

with $(\theta|_{P_e}=0)$. Accordingly, the quasi-idealised post-buckling equilibrium path $(\theta>0)$ is given by

$$P = P_e \theta / \sin\theta \quad (1.12)$$

To establish the nature of the stability of the pre- and post-buckling loci, the second differential of V with respect to θ is sought⁽³⁾, whereby

$$\partial^2 V / \partial \theta^2 = 4c - P\ell \cos\theta \quad (1.13)$$

noting that maximum V ($\partial^2 V / \partial \theta^2 < 0$) and minimum V ($\partial^2 V / \partial \theta^2 > 0$) are associated with unstable, $\theta|_{P < P_e} = 0$, and stable $\theta|_{P > P_e} \neq 0$, equilibrium respectively.

If an imperfect initial profile is introduced into the former idealised model as illustrated in Fig 1.6, which is analogous to the initial curvature profile depicted in Fig 1.3, then V becomes

$$V = 2c(\theta - \theta_0)^2 + P\ell(\cos\theta - \cos\theta_0) \quad (1.14)$$

with the equilibrium condition

$$\partial V / \partial \theta = 4c(\theta - \theta_0) - P\ell \sin\theta = 0 \quad (1.15)$$

affording

$$P = 4c(\theta - \theta_0) / l \sin \theta \quad (1.16)$$

Normalising the loading to its critical value

$$P/P_e = (\theta - \theta_0) / \sin \theta \quad (1.17)$$

The locus given by this expression is typically represented by the imperfection locus illustrated in Fig 1.7; also shown are the equilibrium loci of the former quasi-idealised analysis.

Spring-link models can provide quantitatively representative data at low computational cost. This is particularly attractive when considering more complex inelastic studies and further use of the spring-link procedure is made in the ensuing theoretical work.

1.5 EXPERIMENTAL CONSIDERATIONS

Given the previously denoted statistical nature of inelastic strut performance, then experimentation and empiricism suitably form a major part of the research programme. Associated with this, the actual establishment of an accurate large scale testing system formed an integral part of this programme during the early stages of the study. Wherever applicable, the necessary compliance with

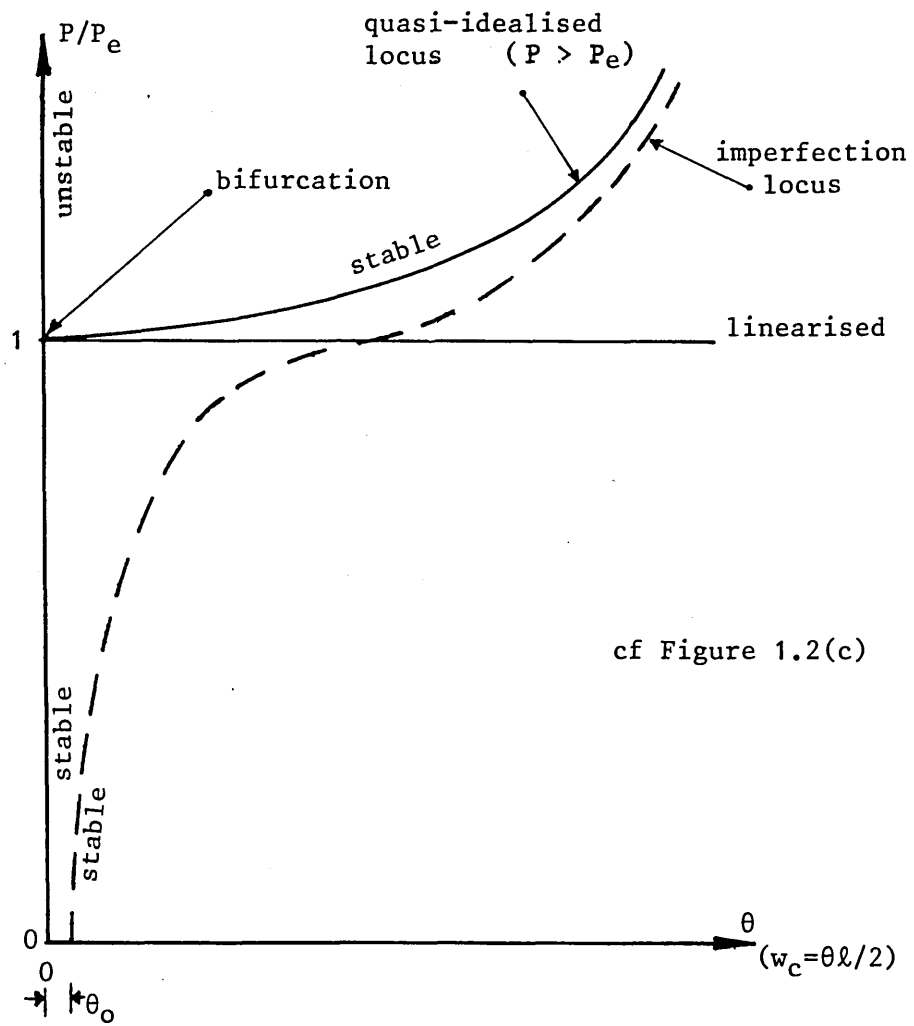


Figure 1.7 ; Model : Action - Response Loci

British Standards Codes of Practice was ensured; in aspects of the work not covered by these codes, recommendations from established literature sources in the field were sought(26).

The experimental system was based on a Schenck 250 tonne servo-hydraulic stiff column testing machine, possessing over 3m of available 'daylight'. Stroke or axial displacement control was employed, providing for static post-buckling path definition. Cyclic loading capability was made available through an in-board function generator. CHS steel strut specimens were chosen for testing purposes. A doubly encastré configuration was considered to afford the most readily definable form of boundary conditions. Such configurations afford a common effective length ($l_e=L/2$) in both the elastic and inelastic material ranges(42). Further, using circular sections should, given a sufficiently large number of tests, enable a check to be made upon specimen behaviour being machine independent. That is, the testing machine must not prejudice the buckling path direction response of the strut, there being no preferred failure direction (weak axis) resulting from the geometry of the specimen cross-section. Specimen geometry was to be based on λ_m values of about unity, the nominal strut lengths thereby being between 2.2m and 3.0m.

Material support from the tubes division (Corby) of the British Steel Corporation led to the provision of 7.5m runs of CHS electric-weld stretch reduced (EWSR) grade 43C steel; these sections are stress relieved. Two strut specimens were cut from each run, one being tested statically, the other being additionally

subjected to cyclic loading phase, thereby affording some degree of specific static/cyclic strut performance correlation to be made. Such correspondence is limited by imperfection variability, however; if the static strut is substantially more imperfect, correlation of performance is greatly reduced. Consequently, the large number of tests is again important to statistically provide for a sufficient degree of correlation. Further, employing offcuts, a stub test⁽²⁶⁾ was performed for each strut experiment undertaken to determine individual specimen constitutive data. Geometric properties of individual cross-sections were obtained by recording the relevant measurements. Datum out-of-straightness measurements were undertaken for each strut prior to actual testing whilst wall thickness and outer diameter measurements were employed for ovality and eccentricity of loading assessment⁽⁴³⁾. Residual stresses were not explicitly considered in view of their relative unimportance in the (stress relieved) sections employed herein⁽³⁵⁾. It is considered that such individual specimen assessment assists in accurate experimentation.

The Schenck column testing rig was adapted and developed through the earlier part of the research programme to accommodate the various types of testing denoted above - static strut, cyclic strut, stub and initial curvature tests. These developments were undertaken as part of the general enhancement of the basic testing system which also involved substantial digital computer provision. This provision resulted in considerable improvements in system accuracy, repeatability, control, 'turnround' time and safety; convenient manipulation of the large data sets generated was also

provided. Various types of computing facility were employed, depending on the particular requirements involved. This feature is further discussed in the following section.

Additionally, a supplementary set of tensile tests were carried out to provide for control on the stub data. These tests were conducted on an Avery 7110 universal testing machine which provided for tensile testing to BS 18, Part 4(25).

1.6 DIGITAL COMPUTER INCORPORATION

The experimental phase of the research programme was heavily influenced by the capabilities of modern computing equipment. The enhancement of the basic testing facility, whereby diverse computing systems were interfaced with the Schenck testing machine, led to improvements in both the quality and production of experimental data, as denoted in the foregoing section. The enhanced computer governed testing facility involved micro, mini and mainframe computers, which were employed in the control, data monitoring/acquisition and graphical parametric output phases respectively. The RML380Z microcomputer afforded a '10-bit' DAC (digital-to-analogue converter) and ADC control unit whilst the PDP1104(DEC) 16-bit minicomputer provided for high speed accurate data recording. The IBM4341 mainframe computer supplied both high resolution graphics software support, together with substantial and readily accessible data storage facilities.

In addition to interfacing the testing machine with both the micro

and minicomputers, the micro was further interfaced with the mini and mainframe systems for data transfer purposes.

All drive, monitor and data reduction software was developed in-house. The BASIC language was used for the smaller computers, whilst 32/64-bit (per byte) FORTRAN/GINO programming was employed on the mainframe. The inelastic theoretical studies undertaken in support of the experimental programme were also implemented on the mainframe computer. This was considered necessary given the highly non-linear nature of the expressions involved.

1.7 SUMMARY

The history and nature of strut stability studies have been identified. The important role of imperfections has been set out, particularly with regard to struts possessing industrially relevant slenderness ratios ($\lambda_m=1$). Attempts to model the complex inelastic behaviour of these common structural elements should pay due regard to the requirements of design engineers in practice. Accordingly, a spring-link modelling procedure which provides for computationally amenable expressions has been introduced.

Given that the objective of the programme is to determine the otherwise static behaviour of an inelastically imperfection sensitive strut subject to a pre-buckling cyclic loading phase, the need for substantial experimental study has been identified and discussed. Testing at large scale is demanded if direct definition of the effects of imperfections are to be made

available. Incorporation of the digital computer is to be made throughout the experimental and theoretical phases of the research programme. The following chapter sets out the preliminary factors associated with the experimentation.

CHAPTER 2

THE ESTABLISHMENT OF A LARGE SCALE STRUT TESTING SYSTEM

2.1 INTRODUCTION

Experimentation and empiricism, employing a suitably large number of tests, are of particular importance with regard to the study of inelastic strut behaviour⁽¹⁾. This is due to the sensitivity displayed with respect to the presence of imperfections; the substantial scatter of the data accompanying strut testing is well-established⁽⁴⁴⁾. Indeed, most recent studies on design criteria are concerned with the probabilistic basis of the parameters involved⁽³⁴⁾. Accordingly, considerable effort has been taken in the present programme to ensure high quality experimentation, with the substantial number of large scale tests involved being a particular feature.

The fulcrum of the compression testing system employed in the experimental studies was a +5 volt Schenck 250 tonne column testing machine. This was employed for the stub and strut compression tests and initial out-of-straightness monitoring of the strut specimens. A number of supporting tensile tests were to be undertaken on an Avery testing machine, with geometric data obtained from metrology studies completing the experimental programme.

An integral part of this programme was concerned with enhancement

of the Schenck machine for reasons of accuracy, test repeatability, fine control, turnaround time and safety. Of particular interest was the incorporation of digital computer control and monitoring which enabled fully automatic experimentation and generation of graphical/numerical output data of high (digital) resolution. Concurrent with this enhancement was a preliminary series of strut and stub tests undertaken for purposes of testing system validation; these two activities formed the first phase of the experimental programme and are discussed in the following.

2.2 INITIAL SCHENCK CONFIGURATION

The basic Schenck facility essentially consisted of a stiff mechanical rig, RV-10 servo controller and hydraulic power pack. The machine cross-head was adjustable on twin threaded columns; the actuator was located at the base, where the compressive loading, under axial stroke (displacement) control was applied. This form of 'loading' control enables identification of the post-buckling path. Machine 'daylight' provision allowed for over 3m vertical clearance and 0.6m lateral clearance in the plane of the columns; there was no effective restriction in the third dimension. The testing machine was of servo-hydraulic form with the electronic (analogue) commands of the RV-10 servo controller governing the power pack's delivery of high pressure hydraulic oil to the actuator. Equivalence of the controller's signal with that fed back from the Schenck inboard transducer was indicative of the required incremental axial displacement being achieved. Cyclic

action was provided for by means of a function generator in the RV-10 controller. Axial load was determined from an inboard 2500kN load cell.

Plate 1 shows the Schenck mechanical rig being employed in its pre-enhancement or basic form. The specimen involved is a 50mm by 3.2mm SHS - both SHS and CHS specimens were used in the preliminary tests - with encastré conditions being established using end caps bolted to the upper and lower plattens, bond between these caps and the ends of the strut being achieved by the use of proprietary resin. This arrangement was effective in restricting rotation of the ends of the strut but inconvenient to implement. Plate 1 also shows the dial gauges which were initially employed to measure specimen end-shortening whilst the centrally mounted strain gauges set a pattern for future tests. It is to be noted that the deflected shape conforms to that expected in the post-buckling range. Further discussion on the preliminary compression tests follows delineation of the actual testing system enhancement undertaken. It is to be understood that Sections 2.3 and 2.4 relate to the testing system and procedures as finally established in the enhanced configuration, ie the system and procedures employed in the formal testing programme described in Chapter 3. Section 2.5 deals with tests undertaken concurrently with this enhancement, these preliminary tests being integral with the enhancement process itself.

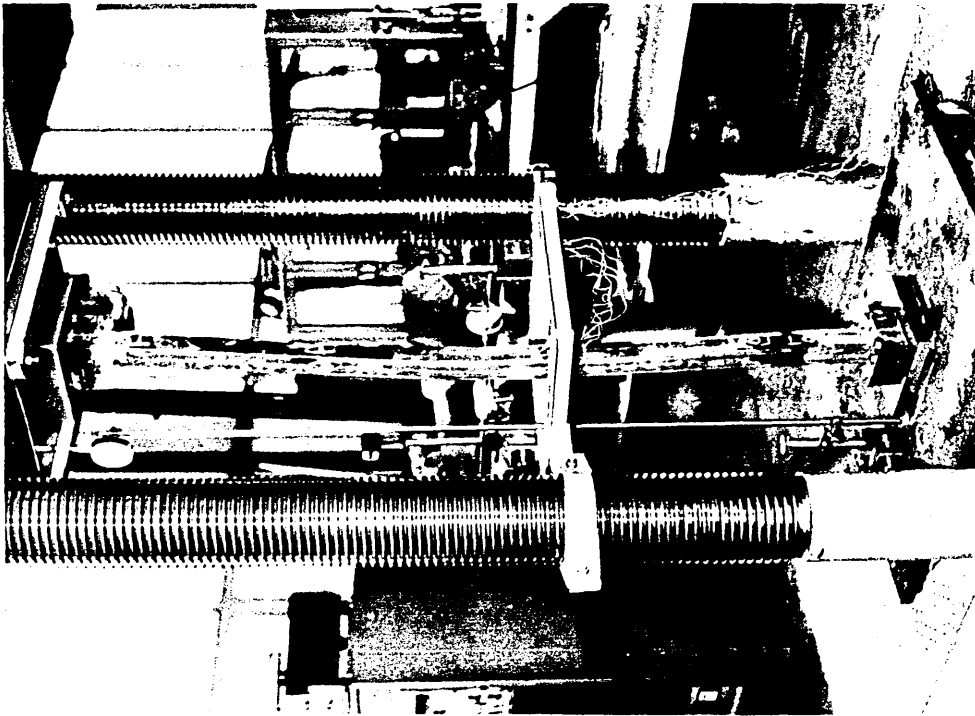


Plate 1 ; Initial Schenck Configuration



Plate 2 ; Load Cell and Collett Assembly

2.3 SCHENCK ENHANCEMENT - PERIPHERAL HARDWARE

2.3.1 Strut Facility

Provision of an outboard 225kN Strainert (low profile) load cell and the associated load cell amplifier, constructed in-house, ensured that the testing system complied with the highest grade, 0.5, of BS 1610⁽⁴⁵⁾; ie load measurement was accurate to $\pm 0.5\%$ of full scale. Plate 2 depicts the load cell located between purpose-built hardened steel housing units. The lower housing unit was located on the machine actuator by a central locating spigot, all relevant surfaces being milled flat to obviate alignment errors. As illustrated in Plate 2, the upper housing unit was recessed in the centre to accept a mechanical split taper lock collett which is displayed alongside. Colletts were employed to provide for end fixity.

Considerable thought was given to the means by which effective clamping action, to be maintained throughout the loading procedure, could be provided. Several mechanical devices were considered and, after trials, the use of taper lock colletts, a familiar item in mechanical engineering systems, was accepted as providing the best means by which the desired effect could be achieved. As shown in Plate 2, each collett accepted a 50mm length of section which was then gripped circumferentially upon mounting the collett in the appropriately recessed housing and fitting the two grub screws provided. Further, and importantly, the grip increases upon application of axial compression. End

bearing on the extreme cross-sections completed the requisite end fixity definition. In addition to the lower mounting unit displayed in Plate 2, a similar but simplified - no load cell being required - unit was employed at the upper end of the strut where connection to the cross-head platten was effected. Initially, struts were turned down to fit the collets. This was unsatisfactory as it introduced unnecessary effort and additional cross-sectional geometric imperfections. Accordingly, a set of collets was obtained, these being turned to a variety of internal diameters to provide for a range of tolerances appropriate to the nominal section diameter - formal testing was to be made using 48.3mm by 3.2mm CHS as noted in Section 1.5.

The necessary slack on the Schenck threaded column permitted movement of the cross-head under strut loading. It was considered that this could be problematical, particularly in the cyclic tests. A tie-rod arrangement was therefore implemented to pull the cross-head up against the threads of the columns using the top plate of the Schenck as an anchor point. The cross-head was forced back onto the column threads, under a load in excess of the maximum anticipated compressive test load; the tie-rod was then pre-tensioned to secure the cross-head in position.

A further development saw the provision of transducer monitoring of the primary kinematic response parameters - that is end-shortening and central transverse displacement. In addition, a more precise level of actuator control would be made available. This development consisted of a transducer network made up of a

ten ± 50 mm stroke transducer monitoring array located on a purpose built framework independent of specimen and machine strain. The stroke range employed was dictated by the prescribed limiting magnitude of the net central transverse displacement $w_{cL} - w_{ocL}$. This prescribed magnitude was determined from the concurrent preliminary strut tests - cf Section 2.5. Six transducers were mounted to monitor the upper and lower end displacements and thereby provide definitive net axial strut movement. At each end, the respective transducers were located, radially, at 120° intervals, minimising any rotational effect of the platten mounted housings. (This arrangement indicated that no measurable rotation occurred throughout the testing programme.) Denoting the lower three transducer readings by A, B and C and the upper readings by D, E, and F, then the net axial shortening, denoted u (for convenience), is given by

$$\left[\frac{A + B + C}{3} \right] - \left[\frac{D + E + F}{3} \right] = u \quad (2.1)$$

The algorithm was implemented using an in-house constructed, hard-wired analogue device. The lower three readings were themselves averaged, this similarly hard-wired reading supplanting the cruder inboard transducer in providing for a more accurate feedback signal regarding actuator movement. The remaining four transducers, denoted by G, H, I and J were mounted to record net central transverse displacement $w_{cL} - w_{ocL}$. These were orthogonally located so as to bear onto the facets of a square target, itself centralised using knife-edges on the strut. Average values, taking account of the vectors provided by the respective transducers, of opposing pairs afforded a non-prejudicial net

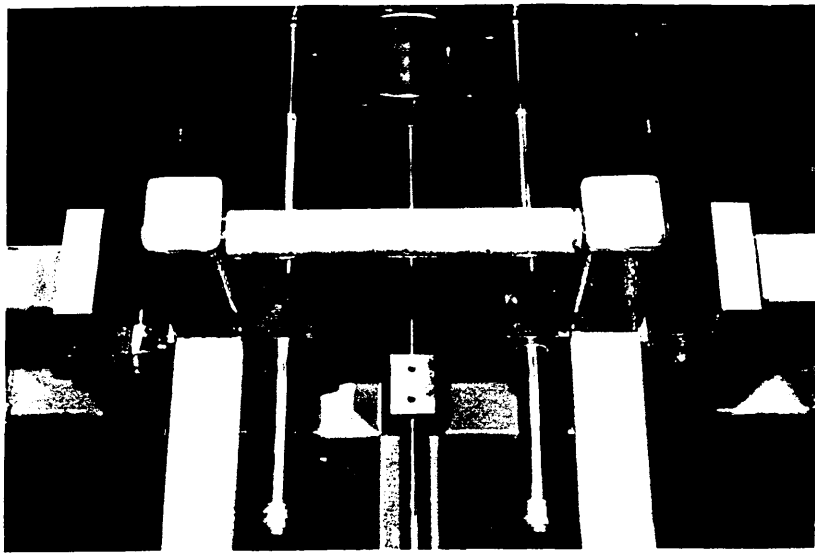
resultant vector value of $w_{cL}-w_{ocL}$ by the following Pythagorean transformation;

$$\left[\left(\frac{G-I}{2} \right)^2 + \left(\frac{J-H}{2} \right)^2 \right]^{\frac{1}{2}} = w_{cL}-w_{ocL} \quad (2.2)$$

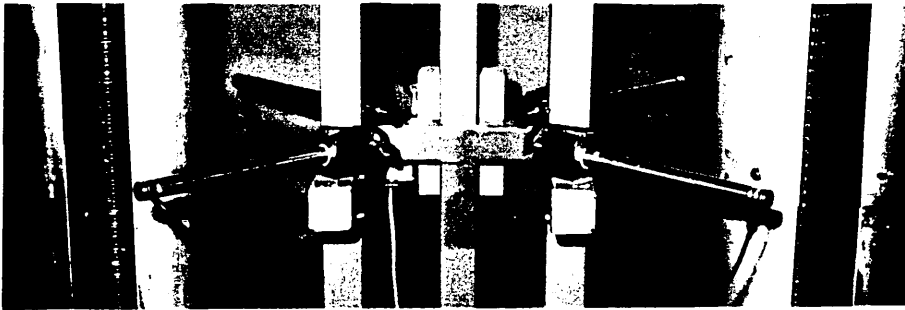
which was also employed in hard-wired form using an in-house constructed analogue device. The transducers were served by the necessary amplifying units, and the three sets of transducer assemblies are shown in Plate 3. Additional monitoring was provided by four centrally mounted axially oriented strain gauges, located in a radially symmetric pattern. These enabled a close inspection to be made of the constitutive states appertaining to this highly stressed region of the strut.

2.3.2 Stub Facility

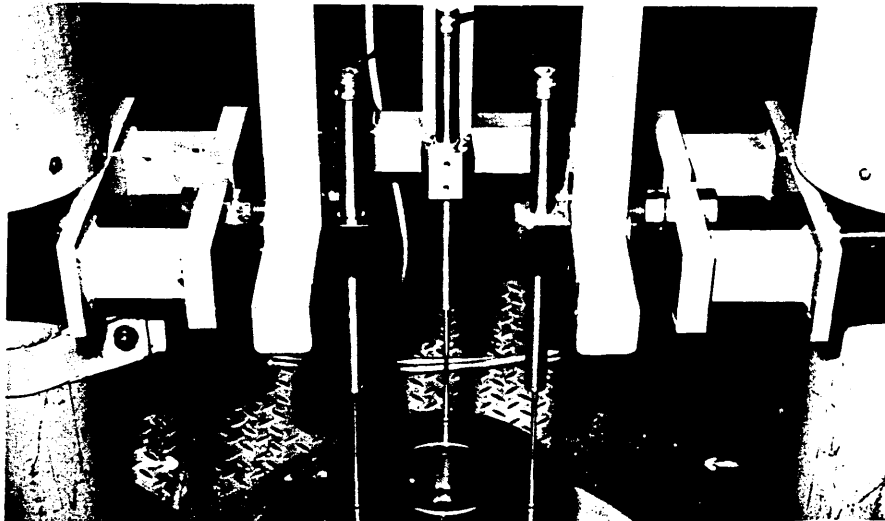
An important aspect of the experimental programme was the provision of appropriate yield/proof stress σ_y and direct modulus E data. This data was obtained from stub tests, the respective specimens being approximately 200mm in length, this length being dependent upon the specimen sections involved - note later. The tests were conducted with the Schenck cross-head lowered accordingly, the previously mentioned tie-rod being extended to accommodate this feature. In particular, and as required by the stub test procedure(26), these tests necessitated the provision of case-hardened upper and lower bearing plate assemblies which were mounted on spigots, these being located in the previously discussed collets. The upper housing unit was adjustable to ensure parallelism of the bearing surfaces between which were



(a) Upper Transducer Assembly



(b) Central Transducer Assembly



(c) Base Transducer Assembly

Plate 3 ; Strut Test Rig - Transducer Monitoring Network

mounted four short stroke precision gauges - NER5 ± 5 mm stroke. The complete but unmounted stub testing unit is depicted in Plate 4 together with a typical CHS specimen. The directly obtained (ie hard-wired) analogue average of the four transducers, mounted in a radially symmetrical manner, served both as the necessary end-shortening data output and actuator feedback signal. Axial load monitoring was again provided by the 225kN load cell.

2.3.3 Cyclic Testing Aspects

As noted in Section 1.1, the primary objective of the research programme was to determine the effect of a pre-buckling cyclic phase of loading upon otherwise static strut performance. The duration and frequency of this cyclic phase were to be based on offshore values in the absence of more definitive data. Accordingly, target values of $n_c=1000$ cycles at $f=1/16\text{Hz}$ ⁽⁴⁶⁾ were established. A familiar sinusoidal forcing function was to be employed using the RV-10 function generator under manual control, the appropriate amplitudes and mean cyclic axial displacements to be determined once typical static strut performance had been identified.

For those compression tests involving a phase of cyclic action, additional and continuous monitoring was provided by the use of x,y and x,y/t plotters. For strut testing purposes, these were interfaced with the axial load, axial displacement and central transverse displacement output channels. This arrangement provided axial load/axial displacement, axial load/central

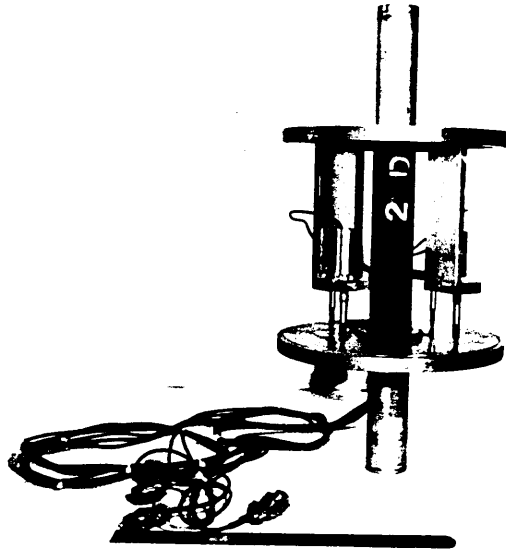


Plate 4 ; Stub Test Rig

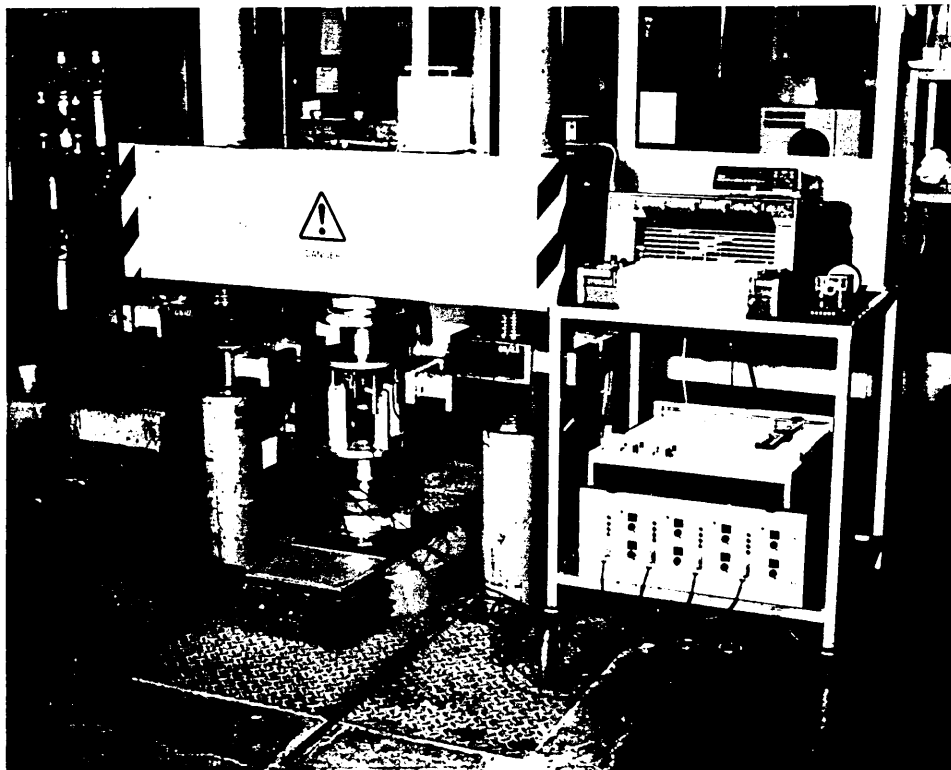


Plate 5 ; Cyclic Stub Test Rig

transverse displacement and each of axial load, axial displacement and central transverse displacement versus time graphical output. It was incumbent upon the system that the mean axial cyclic displacement or stroke was maintained constant throughout the cyclic phase. Pre- and post- cyclic action phase values of axial stroke were checked accordingly. For data control regarding slenderness ratio effects, a number of later stub tests, see Chapter 3, were also subject to a cyclic loading phase and facilities for the continuous monitoring of axial load and axial displacement against time and one another were incorporated in a similar manner to that described above. Plate 5 illustrates a stub specimen undergoing a test involving a cyclic action phase.

2.3.4 Out-of-Straightness Monitoring

Attempts to automatically monitor the initial out-of-straightness of the strut specimens were focussed on the fitting of a motorised lathe rotating centre to the lower collett seating together with a similar slave unit fitted into the upper collett seating. The lower mounting is illustrated in Plate 6. Out-of-straightness measurements were obtained using seven transversely mounted +12.5mm transducers fitted with T heads to allow for the circular nature of the specimens chosen for the main strut testing programme. The transducers were mounted on the previously mentioned main transducer framework and were evenly distributed along the length of each strut, with one at mid-span. Having fitted a specimen onto the lathe rotating centres, the specimen was automatically rotated and monitored, readings being taken at

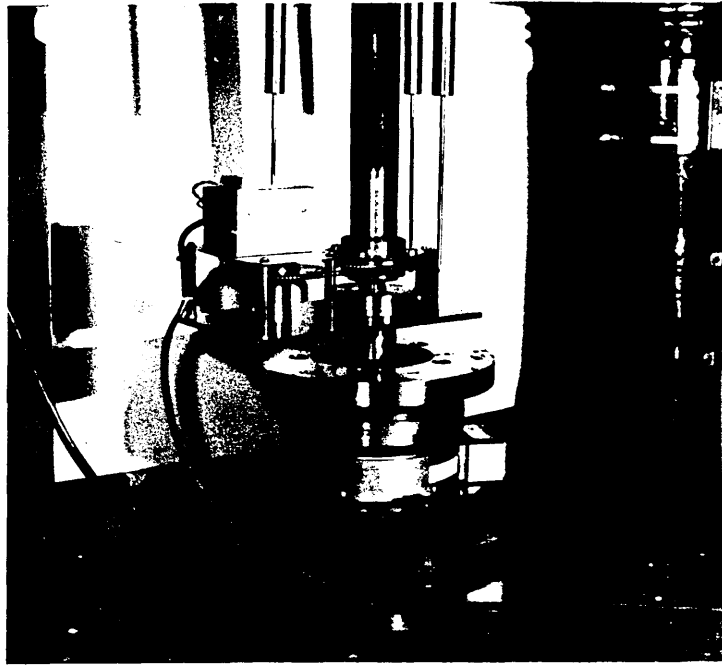


Plate 6 ; Out - of - Straightness Monitoring
Rig - Base Assembly

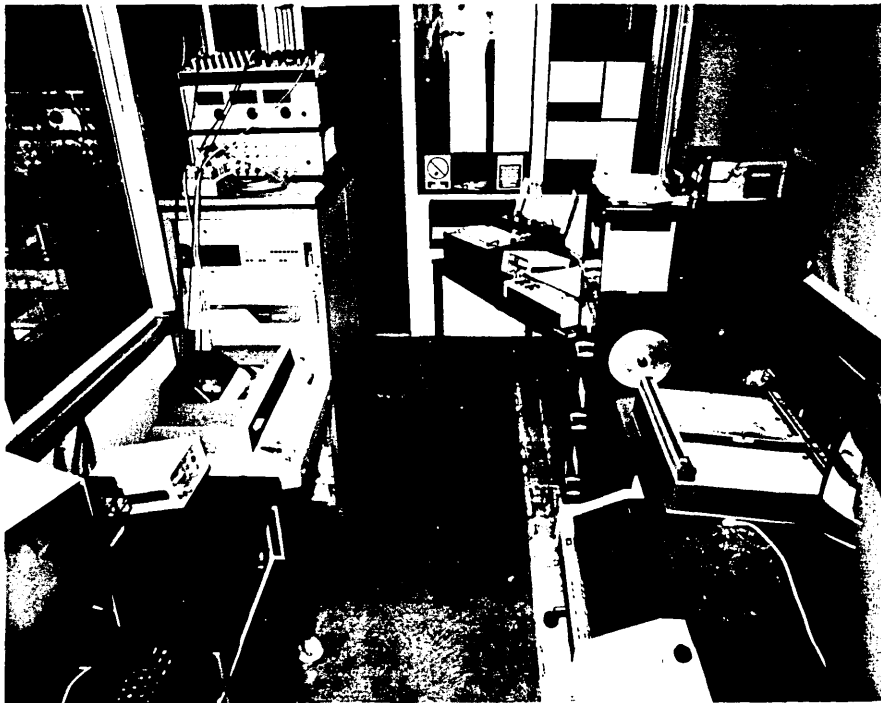


Plate 7 ; Digital Computer Annex

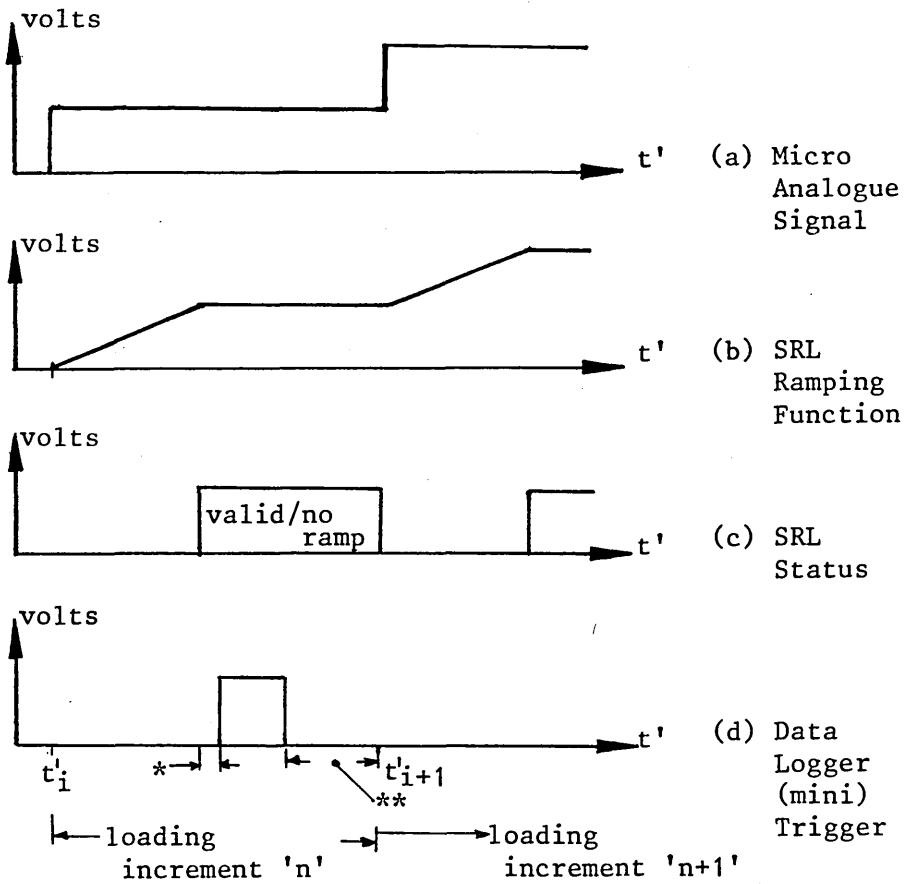
intervals of $\pi/2$. The lathe rotating centres enabled assessment of the initial out-of-straightness against BS4848, Part 2(47). Aware of the possibility that these readings might not be directly relevant to the encastré compression testing mode, readings were also taken with specimens fully mounted in the collets. In this approach, the specimens were manually rotated - an awkward procedure - clamping being effected as required prior to the readings being taken. A representative sample of the struts formally tested and delineated in Chapter 3 were assessed in this manner and correlation established between the two sets of data. Attempts to motorise encastré mode out-of-straightness assessment were investigated but no convenient system was determined.

2.4 SCHENCK ENHANCEMENT - DIGITAL COMPUTER INCORPORATION

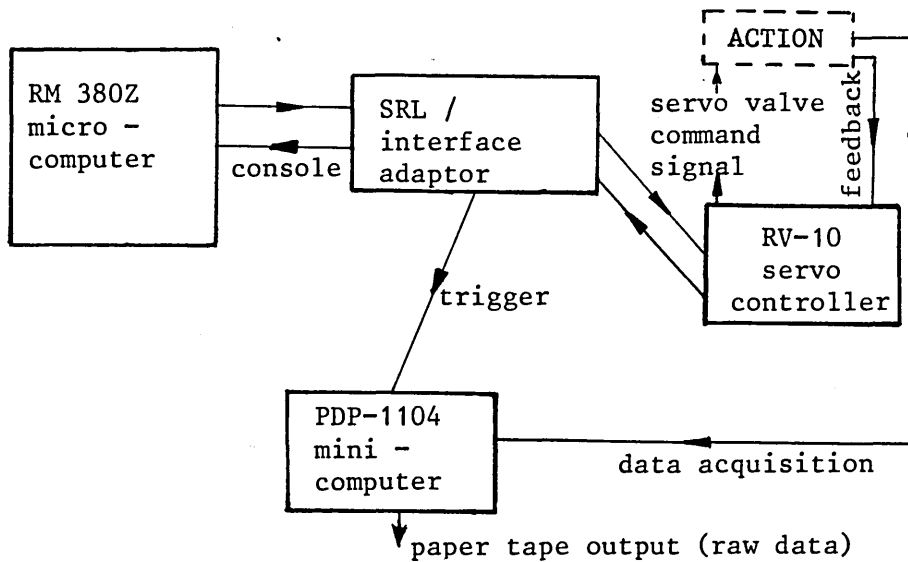
In conjunction with the foregoing mechanical enhancement, thought was given to the incorporation of digital computing facilities in order to establish a modern automated system. Initially a DEC PDP 1104 mini-computer/data logger was interfaced with the appropriate transducer, strain gauge and load cell channels. This was essential if a substantial number of static increments were to be employed in the (static) compression tests - some 2000 data items per test was the desired target figure. This implementation was a relatively straightforward task, with all software produced in-house; 16-bit digital accuracy was thereby readily made available. In parametric terms, an accuracy of 0.01% was obtained at a reading speed of ten channels per second; this performance was markedly superior to that previously available.

With newer but similar testing equipment also providing inboard computer control, it was then determined to employ a standard micro-computer for control purposes with the Schenck. An RML380Z computer was chosen in view of its 10-bit DAC (digital-to-analogue converter), made available by paired combination of the machine's basic 8-bit architecture. Its 56K bytes memory and twin disc drive facility were ample for the tasks involved. With the necessary software again produced in-house, the interfacing took considerable effort to implement, most of this effort being expended on effectively setting up an accurate incremental loading or 'ramping' signal, in real-time, that would override the RV-10 controller. Safety considerations were a further major factor, as was the need to coordinate the micro-drive with the mini-monitoring, again in real-time.

The essential features of the resultant control and monitoring system, as applicable to static testing, are illustrated in Fig 2.1. With regard to the drive signal, the micro-computer set up a digital pulse as shown in Fig 2.1(a). Interfacing through the DAC enabled conversion of this pulse into the voltage regulated analogue linear ramp and plateau configuration depicted in Fig 2.1(b). This regulation corresponded - note the +5 volt Schenck machine stroke range - to limiting both the stroke and stroke rate per 'loading' increment of the Schenck machine. The interface adaptor/stroke rate limiter (SRL) was controlled in real-time and the ramped signal was then passed, via the RV-10 controller now acting as a 'slave', to the actuator - note Section 2.2. Following actuator displacement, the channels corresponding to the



* : delay before data logger trigger
 ** : delay after data acquisition



(e) Hardware Flow Diagram

Figure 2.1 ; Computer Control and Monitoring Features

lower platten outboard transducers, recall readings A, B and C delineated in Section 2.3.1 for strut testing and the four precision gauge readings with respect to the stub testing configuration denoted in Section 2.3.2, were then 'interrogated' for completion of the now computerised servo-loop. This servo check on the status of the actuator movement was again completed in real-time during the 'plateau' stage referred to above - note Fig 2.1(c). The servo-loop data was checked using the interface adaptor/SRL and the resulting status displayed on the micro-computer's VDU employing the computer's ADC (analogue-to-digital converter) as denoted in Fig 2.1(c). The micro- and mini-computers were themselves interfaced so that a trigger signal could be despatched, satisfactory SRL status having been achieved, from the micro to the mini to initiate channel (ie data) monitoring of all parametric output by the latter computer. To have employed the controlling micro-computer for full data monitoring would have resulted in slower and less accurate testing. The micro/mini trigger signal and the mini channel scanning data acquisition process were again established in real-time t', as denoted in Fig 2.1(d). Failure to achieve or maintain satisfactory SRL status resulted in automatic test shut-down; this never occurred throughout the experimental studies.

The complete incremental procedure was duly programmed with each increment occupying a prescribed time period, the procedure being repeated through to test completion, computer control and monitoring having begun once the specimen had been initially

mounted in the Schenck. A total of 1K bits was attributed to driving the overall actuator stroke. For those compression tests involving a cyclic action phase, an interrupt was provided to enable use of the RV-10 cyclic function generator under manual control. A sketch of the appropriate hardware features is given in Fig 2.1(e). Finally, a safety cut-out was made available by passing control to the micro-computer's 'space-bar' key whenever signals, either to/from the Schenck or to the mini-computer (ie trigger signal), were not active in the micro's CPU (central processor unit). This resulted in real-time cut-out being made available for 'virtually' the whole duration of a test. The computer coding required was simple but effective. On one occasion, for example, problems due to electronic interference were incurred resulting in vibration of the Schenck during a test. This was quickly overcome using the controlling computer's 'space-bar' key. In conjunction with the displacement control approach employed, the testing system was actually safer than it had been under manual control; improved response time in all related aspects was the essential product of computer implementation.

Given the foregoing implementation, then, upon completion of a test, all data, relating to both raw individual sensor readings and their refined parametric equivalents, was resident in the mini-computer's CPU. This was then transferred, using paper-tape interfacing, to the micro-computer now free from its test control role. This computer had been interfaced with the (SCP) Computer Unit's IBM4341 8Mb mainframe - the first such interfacing between a micro-computer and the Polytechnic's mainframe to be achieved.

The raw test data was transferred to the mainframe whereupon it was processed into engineering parametric graphical form. The stub and strut data processing programmes were written in Fortran/GINO and included linear regression routines for interpolated parametric values (eg determination of 0.2% proof stress from constitutive data plots).

With respect to out-of-straightness monitoring as conducted in the formal tests described in Chapter 3, a small control programme was written for the RML380Z (micro). Monitoring was undertaken using the mini-computer in a manner similar to that described above. Increments herein took the form of angular rotations, mechanical power being supplied by a small proprietary motor interfaced with the micro and connected to the lower lathe rotating centre - note Plate 6. Each test involved five full rotations of the strut making for twenty-one sets of initial displacements at each of the respective seven transducers. Data output was again transferred to the mainframe whereby mean initial displacements and their orientations were evaluated.

Clearly, considerable effort went into providing digital computing support to the experimental programme. Indeed, it was considered desirable to construct a 'digital computer annexe' to provide a clean air atmosphere for the micro- and mini-computers and attendant peripherals. An interior view of the annexe is given in Plate 7 whilst the testing system in its enhanced strut testing guise is illustrated in Plate 8, the annexe forming the backdrop; it is instructive to compare Plates 1 and 8. It must be recalled



Plate 8 ; Enhanced Schenck Configuration

that, together with the previously discussed mechanical enhancement, the foregoing digital computing support only came on-line towards the end of the preliminary series of compression tests and that the procedures discussed essentially relate to the formal testing programme described in Chapter 3. Fig 2.2 gives a schematic representation of the finalised Schenck testing system.

Attention is now drawn to the preliminary series of stub and strut tests undertaken during the period of testing system enhancement. These tests provided for testing system validation and important data such as suitable limiting stroke values for both formal stub and strut test purposes. Experience in large scale testing was gained and a review of methodology enabled.

2.5 PRELIMINARY TESTS

2.5.1 Static Strut Tests

In these tests both 50mm by 3.2mm SHS and 48.3mm by 3.2mm CHS specimens were employed. All sections were tested at a slenderness ratio of 80 and were of Grade 43C material. The effective length was deemed to be half the nominal length, ie $\lambda=L/2$. Axial stroke was gradually applied, through buckling, up to some maximum axial stroke beyond which it was considered that data would not be of practical engineering interest. At each increment, the corresponding axial load was recorded together with further response data as available, this being dependent upon the degree of system enhancement extant. The number of increments

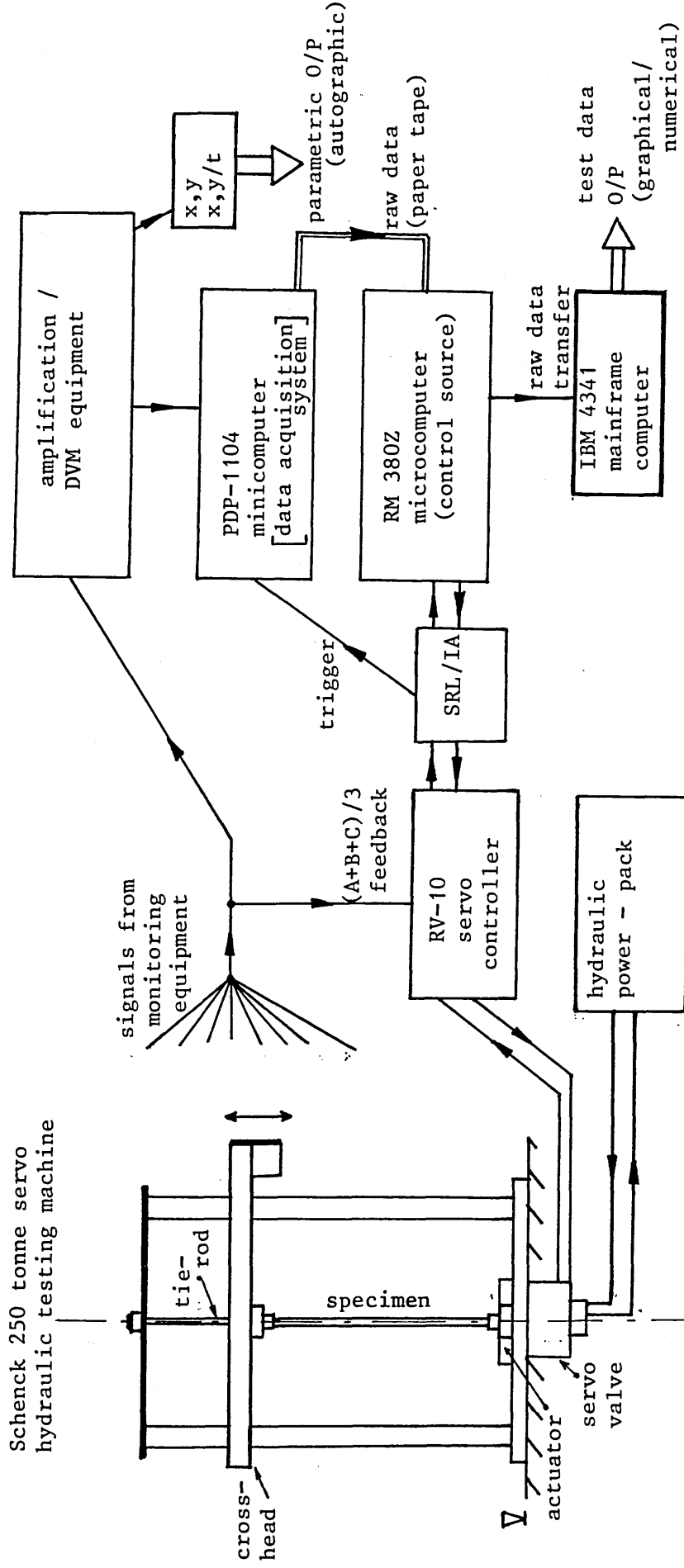


Figure 2.2 ; Line Diagram of Enhanced Testing System

involved in a given test was similarly variable. The early tests were conducted using as few as twenty increments involving only axial displacement and load parametric monitoring.

Key experimental data is given in Table 2.1 together with the respective Euler/Critical and ECCS/Perry⁽³⁶⁾ (unfactored) load values. In these latter evaluations, the effective length has been taken as above, $l \neq 0.7L$ ⁽³⁶⁾, whilst values for direct modulus E and yield/proof stress σ_y have been taken from code values⁽³⁶⁾, ie $E=205\text{kN/mm}^2$ and $\sigma_y=275\text{N/mm}^2$. (nb; At the time of testing BS 449 was in force.) Tests P9-P21 involved initially restricted but developing use of the mini-computer/data logger, whilst tests P17-P21 involved some form of digital control. By the end of this preliminary series of static strut tests the testing system was fully on-line and the formal testing described in Chapter 3 was imminent. With particular respect to CHS specimens, the maximum value of net central displacement recorded was of the order of 50mm, this evaluation being of importance to the design of the transducer network under development. The corresponding limiting axial displacement was of the order of 5mm. Of note is the fact that the average CHS buckling load was 1.12 times the respective ECCS limit state load.

2.5.2 Stub Tests

Six preliminary stub tests were carried out towards the end of the enhancement programme under full computer control and monitoring as delineated in Sections 2.3 and 2.4. Only the number and

Test Ref.	Buckling Load P_c (kN)	Axial or End Shortening $u P_c$ (mm)	Net Central Transverse Displacement $w_{cL} - w_{ocL} P_c$ (mm)
P1	131.3	-	-
P2	137.5	-	-
P3 SHS	136.2	-	-
P4 CHS	105.5	2.92	9.49
P5	102.5	2.85	5.95
P6	109.0	2.67	4.23
P7	101.5	2.91	4.35
P8	101.6	2.96	5.07
P9	101.9	2.89	8.15
P10	100.3	2.88	5.76
P11	103.5	2.89	4.21
P12	103.0	2.83	5.66
P13	100.5	2.91	5.78
P14	106.8	3.06	4.12
P15	102.5	2.98	6.23
P16	95.2	2.86	6.65
P17	105.4	3.00	4.74
P18	99.6	2.96	5.65
P19	108.6	3.01	7.31
P20	98.8	2.92	7.12
P21	108.2	3.05	4.82
Average (SHS)	135.0	-	-
Average (CHS)	103.0	2.92	5.85

SHS Euler Load = 187.8kN
CHS Euler Load = 121kN

SHS ECCS Load = 143kN
CHS ECCS Load = 92kN

Table 2.1; Preliminary Static Strut Test Results

magnitude of the 'loading' increments remained to be established whilst the only non-automated aspect concerned the transfer of data to the mainframe and the manner of data reduction/graphical interpretation employed. Indeed, this experimentation 'back-end' was finally established employing the six data sets provided by these tests. The number of increments employed in an individual stub test increased from approximately twenty to in excess of one hundred in the course of this small series of tests. Essentially, the overall stub test procedure was formally established by this means and key preliminary test data is given in Table 2.2. All tests were carried out on 48.3mm by 3.2 mm CHS specimens; the spread of data for yield/proof stress and direct modulus is noteworthy.

2.5.3 Cyclic Strut Tests

Three cyclic strut tests formed the final set of preliminary tests and were conducted under appropriate computer control and monitoring. Employing experience obtained from the former static strut tests, the primary purposes of these tests were cyclic testing system validation and determination of suitable amplitude ($2u_{am}$) and mean cyclic axial stroke values (u_m'), this latter parameter being that value of axial static displacement at which the cyclic action was implemented. In all three cases, 48.3mm by 3.2mm CHS specimens were employed and the cyclic action incurred varying degrees of inelastic behaviour as indicated by the values for $u|_{P_c}$, u_{am} and u_m' in Table 2.3. Consideration was given to the relationship between u_m' and the axial displacement corresponding

Test Ref.	Yield/Proof Stress σ_y (N/mm ²)	Direct Modulus E (kN/mm ²)
P25	312	197
P26	292	197
P27	293	206
P28	276	211
P29	280	207
P30	314	204

Average values: $\sigma_y = 295\text{N/mm}^2$, $E = 204\text{kN/mm}^2$, $u|_{P_s} = 0.29\text{mm}$

Table 2.2; Preliminary Stub Test Results

Test Ref.	Buckling Load P_c (kN)	Axial Displacement $u _{P_c}$ (mm)	Net Central Transverse Displacement $w_{cL} - w_{ocL} _{P_c}$ (mm)
P22	100.0	2.97	4.76
P23	100.5	3.03	7.67
P24	110.0	2.84	5.21

$f = 1/16\text{Hz}$, $u_{am} = 1\text{mm}$, $n_c = 100$ cycles, $u'_m = 1.4\text{mm}$

Table 2.3; Preliminary Cyclic Strut Test Results

to the unfactored/factored 'Perry' loads - this matter is discussed further in Chapter 3. For machine proving purposes, cyclic durations were limited to 100 cycles and no variation in u_m^i was detected; this is as required under displacement or stroke controlled action. Strain gauges were dispensed with, there being a surfeit of data otherwise made available, the data monitoring procedure being suitably amended. A slenderness ratio of 80 was once more employed. As with the preliminary static tests, imperfections were not monitored a priori. No indication of loss in end fixity due to cyclic action was recorded.

It was determined that efficient testing was readily available employing the established computerised static strut procedure subject to machine interrupt upon attainment of axial stroke u_m . Control was then passed to the RV-10 and a sinusoidal forcing function implemented under manual control. The tests enabled the dynamic monitoring to be 'tuned' during the cyclic action phases. Control was passed back to the micro-computer upon completion of the respective cyclic action phase.

2.5.4 Résumé

The preliminary tests set out above resulted in the proving of the testing system through the various stages of the mechanical and digital computer enhancement programme. Chronologically concurrent activities, the preliminary tests and enhancement programmes resulted in the procedures discussed in Sections 2.3 and 2.4 being fully operative by their completion. Further

consideration of these procedures follows after delineation of two additional developments whose necessity was identified as a result of the work undertaken in this initial experimental phase of the research programme.

2.6 TENSILE TESTING FACILITY

Given the variation in yield/proof stress data noted in Table 2.2 for the limited number of tests undertaken and in view of established arguments relating to stub test based constitutive data⁽⁴³⁾, it was considered necessary to supplement the compression tests with a series of tensile tests on a representative sample of specimens. An Avery 7110 testing machine was therefore configured to BS18, Part 4⁽²⁵⁾ standards, this requiring the addition of key peripherals to the basic machine. An x,y plotter was employed to record axial load/average axial strain whilst an x,y/t plotter recorded the strain rate⁽⁴⁸⁾. Load was monitored using an outboard 300kN load cell and manual control was employed throughout. CHS specimens were centrally 'waisted' and four axially oriented strain gauges applied in a radially symmetric manner, their hard-wired average being provided by a supplementary analogue amplifier. Plate 9 illustrates the Avery system, as established, in operation. Further details of the tensile testing programme are given in Section 3.3.2.

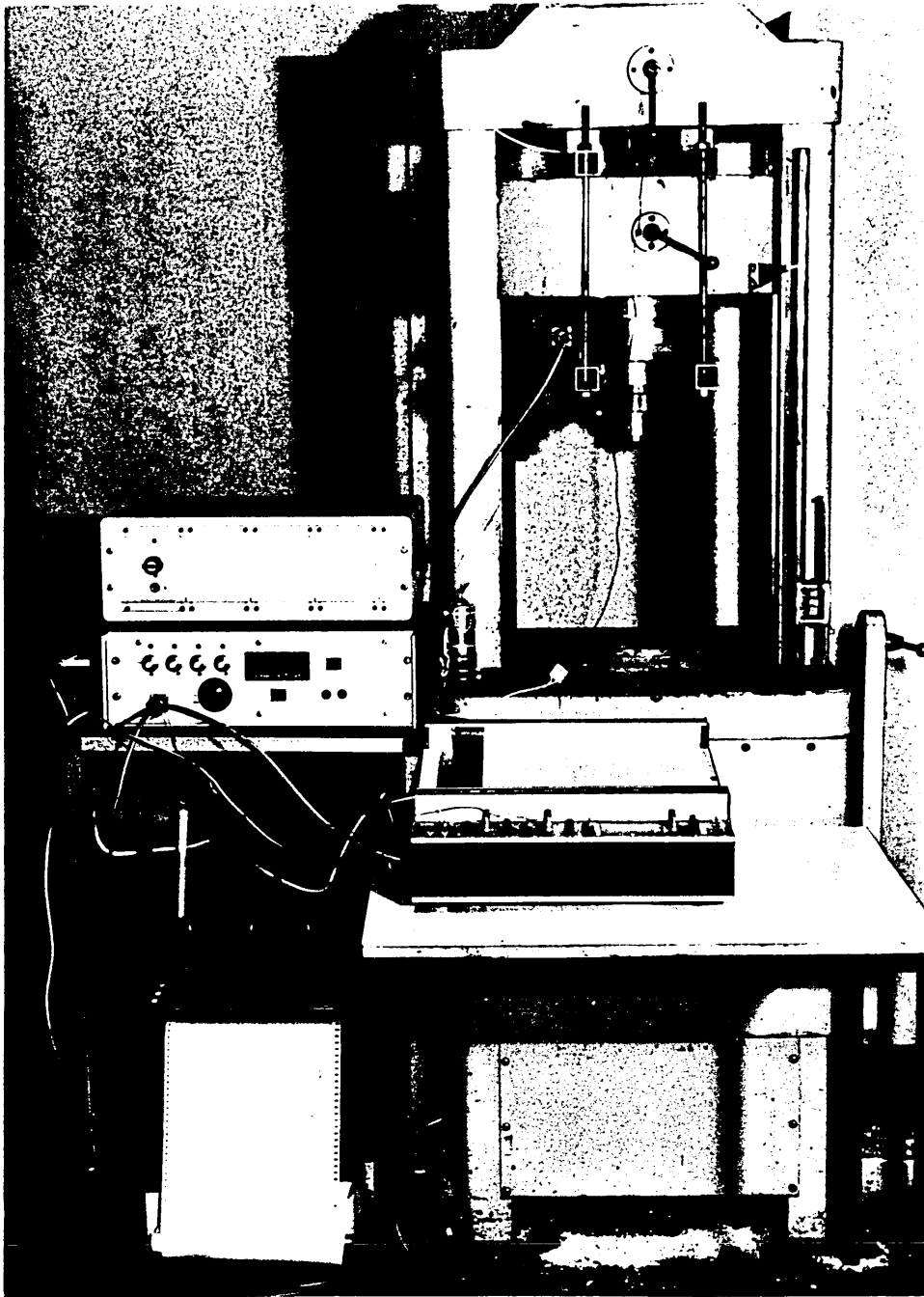


Plate 9 ; Avery - Tensile Testing Rig

2.7 ANCILLARY FEATURES

During the first experimental phase it also became apparent that, for purposes of accuracy, the means of geometric measurement should be carefully assessed. To this end, recourse was to be made in the formal experimental programme to use of the Polytechnic's Metrology Laboratory. Geometric dimensions recorded during the formal testing programme and noted in Chapter 3 included CHS stub specimen length, diameter and wall thickness measurements together with checks upon the planarity of the respective stub end sections and their orthogonality with respect to the specimen length. Further, weight assessments were to be undertaken for purposes of sectional area assessment. Throughout, such experimental measurements were supported by checks being made employing the Metrology Laboratory facilities. In particular, all stub specimen length and end section parallelism assessments were checked in this way.

Inevitably, errors or inaccuracies will occur. Tolerances attending peripheral hardware - eg transducers - are available; tolerances attending the actual electronic acquisition of the data, however, can only be estimated. The former tolerances consist of non-linearity (the deviation from the 'true' value of the measured value) and repeatability (variation of a measured value due to repeated observations of that value) types. Tolerance values, given as a percentage of full scale, take the form $\pm 0.09\%$ and $\pm 0.1\%$ non-linearity for the load cell and the transducers respectively, and $\pm 0.03\%$ repeatability for both items.

The x,y and x,y/t plotters each involve total tolerances of $\pm 0.6\%$. Electronic acquisition tolerances are taken to be individually $\pm 0.1\%$ for the amplifier, supply voltage fluctuations and logging errors, with $\pm 0.01\%$ mini-computer resolution. Table 2.4 presents the resultant tolerances or errors incurred in the various monitoring systems employed. Each resultant consists of the square root of the sum of the respective component errors squared.

2.8 SUMMARY

The work discussed in this chapter has been primarily concerned with the establishment of an enhanced compression system and the preliminary strut and stub tests concurrently undertaken for purposes of testing system system validation. This work accounted for the first eighteen months of research study. During this time, the decision was taken to employ 48.3mm by 3.2mm CHS of Grade 43C for testing purposes, and BSC were approached for assistance. This resulted in the prompt provision of fifty such 7.5m runs by BSC Tubes Division (Corby). The EWSR tubes conformed to BS4360(49) and BS4, Part 2(50), the manufacturing process involving hot rolling and forming, induction welding, stretch reducing to size and hot finishing (stress relieving). This material support is gratefully acknowledged.

The material was received some nine months into the programme and some of this stock was employed in the preliminary tests. It is a pity that more use could not have been made of the data obtained

Device	Digital		x,y and x,y/t plotters	
	Non-linearity + repeatability + data acquisition system		% of full scale	actual
	% of full scale	actual		
Load cell (full scale = 225kN)	+0.198	+0.45kN	+0.624	+1.40kN
+50mm transducers (full scale = 100mm)	+0.203	+0.203mm	+0.625	+0.625mm
+5mm transducers (full scale = 10mm)	+0.203	+0.020mm	+0.625	+0.063mm
+12.5mm transducers (full scale = 25mm)	+0.203	+0.051mm	n/a	n/a

Table 2.4; Error Analysis

during these tests. (It is to be appreciated that the refined facilities and procedures detailed in Sections 2.3 and 2.4 only became available as a complete system towards the end of the preliminary testing programme.) However, with every test, ideas for refinement led to a continuous improvement in experimentation and programme specification. Accordingly, the following chapter sets out the formal experimental programme consisting of in excess of two hundred computer controlled and monitored tests. Given the importance of the digital computing aspects discussed in the foregoing with respect to the ensuing experimental programme, some further details of the software involved are given in the Appendix.

CHAPTER 3

EXPERIMENTAL PROGRAMME

3.1 INTRODUCTION

The central feature of the mainstream or formal testing programme was the set of strut tests undertaken involving a pre-buckling cyclic action phase. In support of this set, static strut, stub and tensile tests were conducted for purposes of data control. As noted in Section 1.1, despite an intensive literature search - witness the Bibliography - little previous work directly relevant to this area of study has been uncovered(22).

The primary objective of the programme was to determine the effect of a pre-buckling cyclic action phase upon otherwise static performance, emphasis being placed upon imperfection sensitive struts and consideration of the effective amplification of initial strut imperfections due to the hysteresis incurred. In-depth time-dependent study per se was not undertaken. As noted in Section 2.3.3, offshore values for cyclic duration and frequency were employed in the absence of more definitive data, notwithstanding the more general consideration that no structural loading is truly static. Accordingly, cyclic action as implemented in the programme involved durations centred on approximately 1000 cycles (n_c) at a frequency(f) of 1/16 Hz(46), thereby obviating inertial and resonance effects. The sinusoidal forcing function employed is detailed in Section 3.3.6.

The mean states at which the cyclic action phases were to be introduced were based upon the factored Perry and 'unfactored' ECCS/Perry loads. The former effectively relates to service conditions, the latter guaranteeing inelastic cyclic excursions. Given axial displacement or stroke control, therefore, the respective mean strokes u_m' were prescribed to correspond to axial compressions of approximately 45 kN and 70 kN respectively for the CHS sections employed at a slenderness ratio of 80; some two-thirds of the strut tests were conducted at $\lambda=80$. As noted in the previous chapters, a doubly-encastred testing mode was to be employed relating to an effective length factor of 0.5. The basic 70 kN load given above lies between the ECCS loads corresponding to the use of the 0.5 factor (92 kN) and the maximum code value of $0.7^{(36)}$ (60 kN).

Amplitudes were to be such as to constrain behaviour to the sub-buckling compression regime throughout. Relatively low amplitudes centred on a mean axial compression of approximately 45 kN would primarily involve quasi-elastic hysteresis⁽⁵¹⁾ whilst larger amplitudes centred on the higher mean value of 70 kN would produce significant inelastic excursions. The remaining cyclic tests would cover the intervening range.

It should be noted that fatigue⁽⁵²⁾ generally involves net tension and a large number of cycles ($\leq 10^8$); low cycle fatigue⁽⁵¹⁾ involves $\leq 10^4$ cycles but even this remains far in excess of the prescribed n_c . At no stage during the experimental study were signs of fatigue failure observed; indeed, some cyclic-tested

struts were later re-tested statically - see Section 3.8.

The ensuing experimentation is initially discussed in terms of specimen configuration and testing procedures. The respective data and findings are then presented. Clearly, a vast amount of data was generated from the large number of tests involved - in excess of 200 - and data presentation takes the form of sample tabulations and statistical techniques, in the form of histograms, in an attempt to display data concisely, whilst affording definitive data trends. All key data is presented in a summary table towards the end of the chapter.

3.2 SPECIMEN DEFINITION

3.2.1 Configuration

The 48.3mm by 3.2mm CHS employed in the experimental programme was delineated in Section 2.8. This section was chosen to enable suitable slenderness ratios to be achieved given the available Schenck 'daylight' and to meet the large scale testing requirement. Slenderness ratios (λ) of 70-90 were deemed appropriate, most tests being based on a ratio of 80. Modified slenderness ratios ($\lambda_m = \lambda/\lambda_1$) were thereby centred on unity as required for maximum imperfection sensitivity. Nominal strut length $L=2\ell$ therefore ranged between 2.2m and 3.0m; $L=2.56m$ for $\lambda=80$. An additional 50mm was provided at each end of a specimen for gripping in the collets described in Chapter 2.

Accordingly, two strut specimens were cut from each 7.5m run provided by BSC. From each run, therefore, one specimen could be tested in a formal static manner whilst the other would be subject to testing involving a cyclic action phase or, as in a number of cyclic tests, phases. This specimen procedure enabled some degree of data control to be provided between corresponding static and cyclic 'partners'.

For purposes of control over constitutive data, E and σ_y , two stub specimens were cut from each 7.5m run at locations adjacent to the strut specimen metal, thereby providing individual strut constitutive data. In accordance with established guidelines⁽²⁶⁾, the stub specimens were about 200mm in length, with minimum length $> 2D + 25\text{cm}$ or $3D$ and maximum length $< 20r$ or $5D$ where D and r denote diameter and minimum radius of gyration respectively. Additionally, provision was made to provide for a number of tensile specimens as control on the stub test data, further offcuts being used for geometric assessment.

Specimens were initially sawn from the 7.5m runs. Strut specimens had their ends machined square using a lathe. Stub specimen ends were additionally ground flat and parallel as required for direct bearing in the stub rig - recall Plate 4. Tensile specimens were cut to 600mm in length due to testing machine requirements. A central portion was 'turned down' or 'waisted' by lathe to approximately half wall thickness over a gauge length of 45mm, in accordance with BS18, Part 4⁽²⁵⁾, to receive strain gauges. Static strut specimens were also 'cleaned' to receive strain

gauges as noted in Section 2.3.1. Further, a small batch of strut specimens were subject to additional, synthetically produced, initial curvature; this particular feature is discussed later.

3.2.2 Reference System

A typical 7.5m run topology is illustrated in Fig 3.1; each run was assigned a consecutive serial number with sub-classifications S and C denoting the respective 'static' and 'cyclic' strut specimens, SS and SC their stub counterparts, with T denoting, where applicable, the appropriate tensile specimens. Accordingly, the main body of tests involved serial or reference numbers 1 to 27. Numbers 28 to 31 were consigned to the above noted synthetically curved specimens. For data control purposes, reference number 16 involved one additional synthetically curved specimen; this particular specimen, nominally 16S, was given the reference 32S to avoid confusion with mainstream data. As a result, 53 struts were tested effectively as supplied, a further 9 struts being subject to synthetic curvature. In addition, 6 of the former cases were subjected to re-testing for purposes of monitoring the typical 'failed' specimen; these re-tests were assigned reference numbers 33 to 38. Finally, 6 stub tests were conducted on additional CHS material for cyclic action phase data control purposes.

3.2.3 Metrology Aspects

In keeping with the overall demand for accuracy, geometric

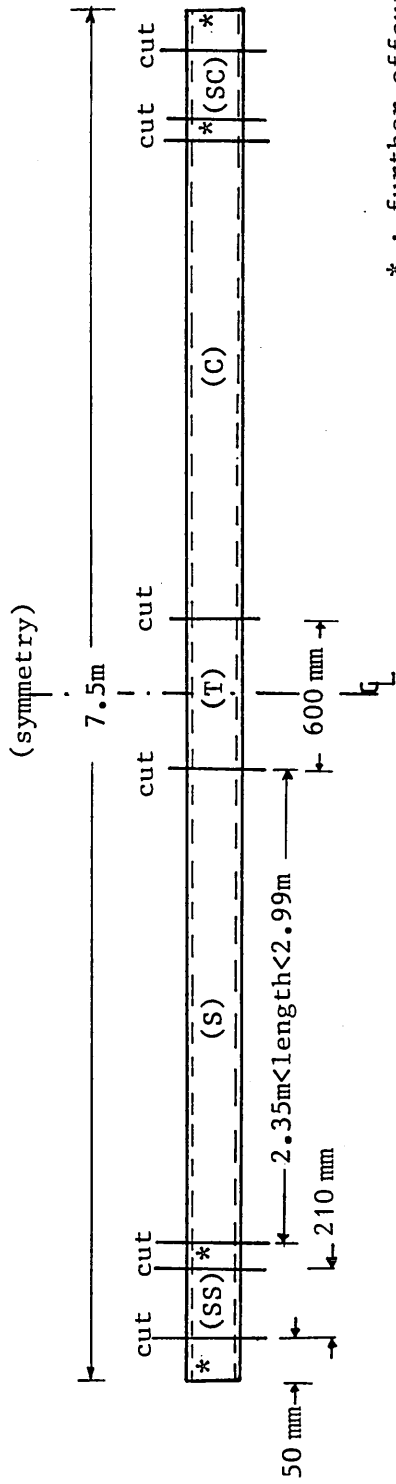


Figure 3.1 ; Reference System

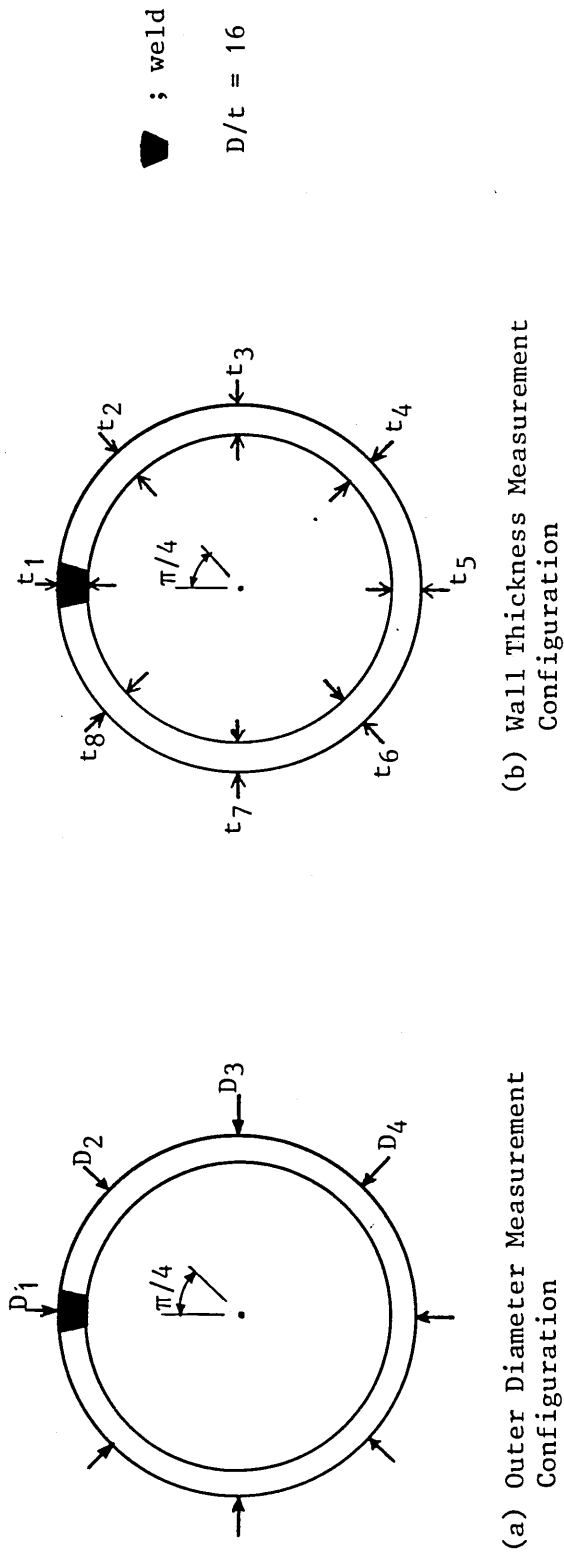


Figure 3.2 ; Outer Diameter and Wall Thickness Measurements

measurement included specific metrology study. Wall thickness t and outer-diameter D were measured for each reference or serial number specimen set using offcuts. At each cross-section concerned, 4 values of D and 8 values of t were determined as denoted in Fig 3.2 employing precision vernier micrometers; 2 cross-sections per run were assessed making for 248 final readings for D and 496 for t , these cross-sections being appropriate to the 4 stub and strut specimens cut from each run. Sample D and t measurements are given in Table 3.1 whilst the histograms of Figs 3.3 and 3.4 present the final readings in concise form.

Fig 3.3 indicates all material complies with BS4848, Part 2⁽⁴⁷⁾, and virtually all readings exceeded the nominal diameter of 48.3mm. With \bar{x} denoting the mean and s the standard deviation, then the lower 95% confidence limit, $\bar{x}-2s$ assuming a normal distribution⁽⁵³⁾, affords a lower bound on D of 48.344mm. Two histograms are presented for t owing to the variability of the thickness of the weld on the inner CHS surface. One histogram assumes a single reading for t_1 whilst the other employs the average of two such readings, these attempting to mitigate the effect of the inner surface irregularities. The two means are close but both are less than the nominal value of wall thickness. A lower 95% confidence limit of 3.041mm was recorded. For both D and t values, samples were checked in the Metrology Laboratory employing alternative gauges - readings for t involved use of conical measuring points - with close correlation obtained throughout. D and t measurements were also made on the tensile specimens, t being recorded before 'waisting', D both before and

Specimen Reference	D ₁ (mm)	D ₂ (mm)	D ₃ (mm)	D ₄ (mm)	t ₁ (average) (mm)	t ₂ (mm)	t ₃ (mm)	t ₄ (mm)	t ₅ (mm)	t ₆ (mm)	t ₇ (mm)	t ₈ (mm)
1	S	48.515	48.535	48.590	3.340	3.152	3.140	3.168	3.160	3.160	3.121	3.153
	C	48.455	48.540	48.440	3.338	3.168	3.149	3.127	3.165	3.150	3.155	3.078
5	S	48.505	48.575	48.425	3.276	3.118	3.162	3.070	3.165	3.160	3.160	3.140
	C	48.530	48.510	48.485	3.211	3.182	3.160	3.135	3.209	3.180	3.160	3.158
10	S	48.450	48.425	48.535	3.334	3.141	3.162	3.185	3.209	3.195	3.190	3.170
	C	48.465	48.455	48.525	3.415	3.241	3.170	3.222	3.240	3.201	3.200	3.131
15	S	48.465	48.550	48.475	3.351	3.238	3.262	3.200	3.182	3.242	3.231	3.211
	C	48.390	48.525	48.450	3.425	3.224	3.260	3.187	3.182	3.225	3.220	3.268
20	S	48.565	48.520	48.485	3.301	3.250	3.192	3.182	3.222	3.210	3.235	3.182
	C	48.425	48.535	48.495	3.324	3.212	3.162	3.208	3.221	3.180	3.176	3.195
25	S	48.360	48.550	48.440	3.270	3.160	3.160	3.192	3.090	3.092	3.201	3.110
	C	48.475	48.555	48.440	3.340	3.130	3.210	3.181	3.213	3.130	3.204	3.065
30	S	48.350	48.440	48.425	3.492	3.220	3.205	3.200	3.232	3.172	3.292	3.202
	C	48.540	48.420	48.450	3.372	3.239	3.165	3.205	3.212	3.190	3.222	3.200

Table 3.1; Sample Outer Diameter and Wall Thickness Measurements

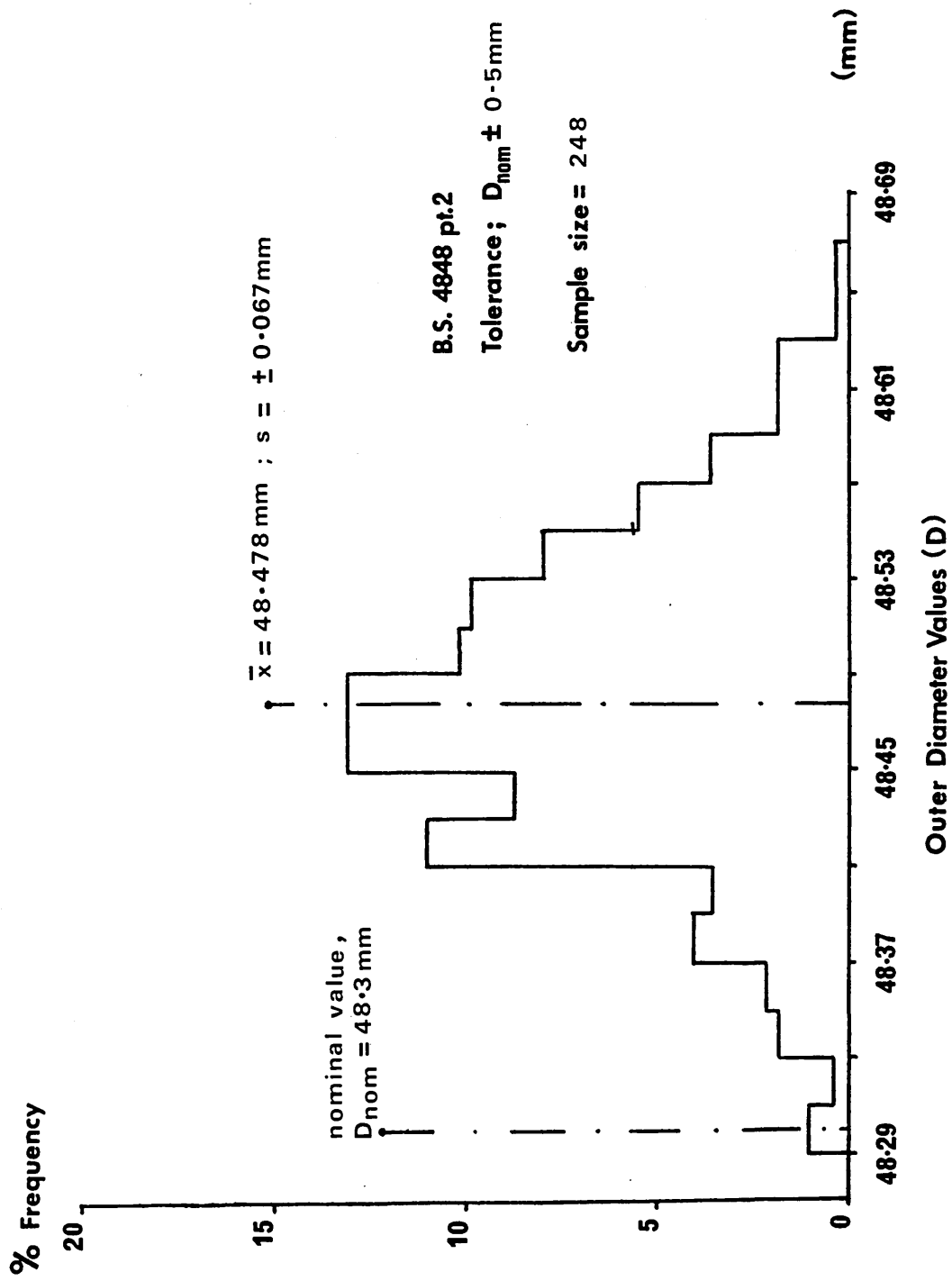


Figure 3.3 ; Outer Diameter Histogram

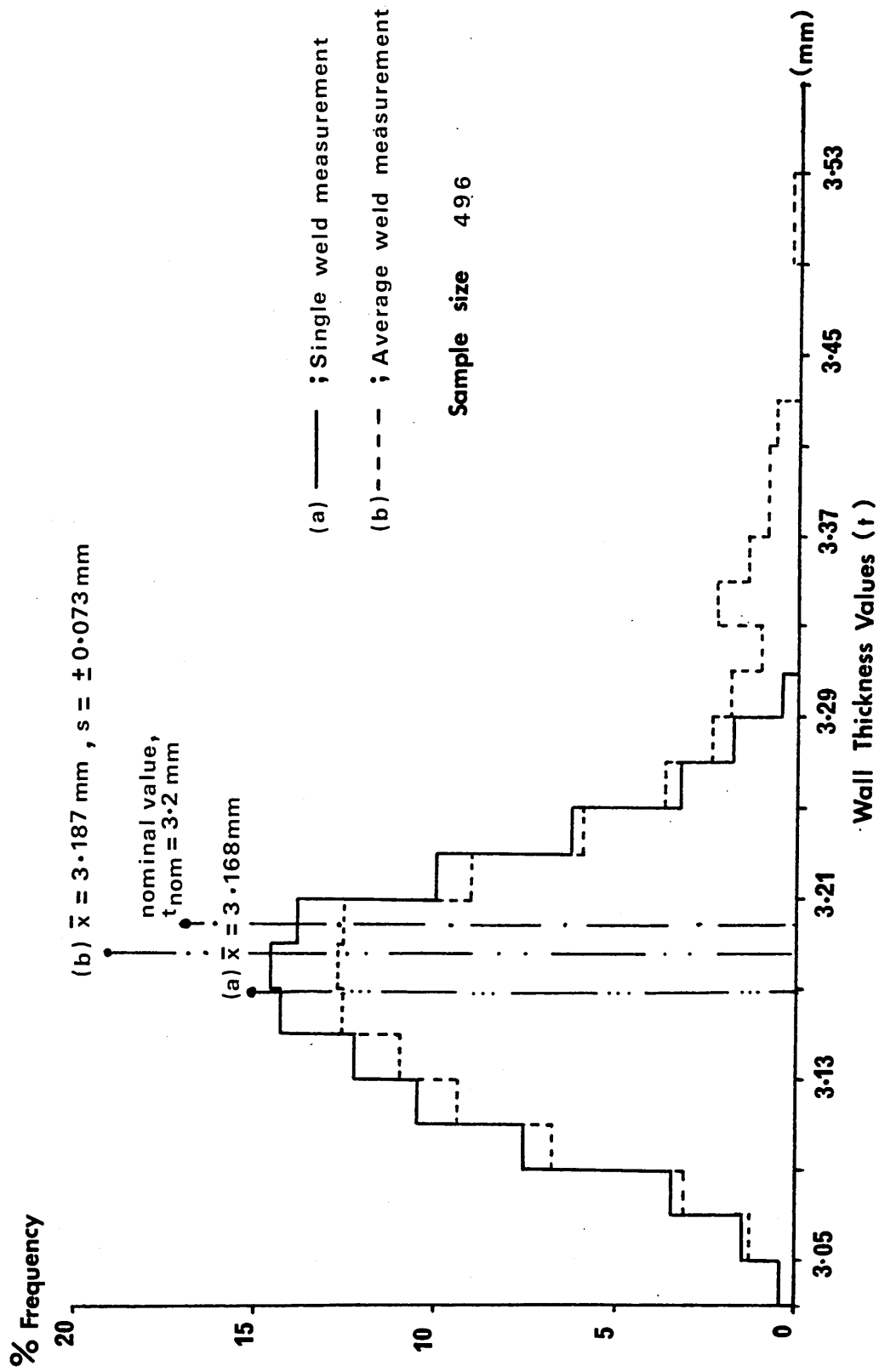


Figure 3.4 ; Wall Thickness Histogram

after.

Table 3.2 affords sample processed D and t data used in the evaluation of effective sectional eccentricity e and ovality⁽⁴³⁾, the latter being included for quality control purposes. Ovality is a localised imperfection and is given by $(D_{\max}-D_{\min})/D_{\text{av}}$. With respect to the 62 strut specimen sample, the average (\bar{x}) ovality was 0.00218 (ie 0.22%) with $s=0.00124$ (ie 0.12%). This is considered fairly low⁽⁴³⁾. Eccentricity of loading was considered to be equivalent to $e=(t_1-t_5)(D_{\text{av}}/t_{\text{av}}-2)/4$ noting the additional wall thickness invariably present in the weld vicinity⁽⁴³⁾.

All stub specimens were checked in the Metrology Laboratory for parallelism. Maximum and minimum length readings, taken around the individual section, afforded the parallel errors and average values of length for axial strain evaluation in the stub tests. Table 3.3 affords sample stub length and parallelism data. Whilst the readings appear excellent, no specification is given for parallelism⁽²⁶⁾. Also given in Table 3.3 is data on cross-sectional areas; values employing the processed geometric D and t data appertaining to the sample of stub specimens are given in accordance with

$$A = A_g = \frac{\pi}{4} (D_{\text{av}}^2 - [D_{\text{av}} - 2t_{\text{av}}]^2) \quad (3.1)$$

Values for stub cross-sectional areas were also obtained employing weight assessment undertaken in the Metrology Laboratory. Area determination by 'mass' is achieved employing

$$A_m = A_{\text{nom}} [\text{nominal mass/metre}]^{-1} (\text{stub mass/stub length}) \quad (3.2)$$

Specimen Reference		D_{max} (mm)	D_{min} (mm)	D_{av} (mm)	t_1-t_5 (mm)	t_{av} (mm)	Ovality ($\times 10^{-3}$)
1	S	48.620	48.515	48.565	0.180	3.174	2.16
	C	48.540	48.440	48.486	0.173	3.166	2.06
5	S	48.575	48.425	48.503	0.111	3.156	3.09
	C	48.550	48.485	48.519	0.002	3.174	1.34
10	S	48.535	48.375	48.446	0.125	3.198	3.30
	C	48.525	48.340	48.446	0.175	3.228	3.82
15	S	48.550	48.440	48.483	0.169	3.240	2.27
	C	48.525	48.390	48.459	0.243	3.249	2.79
20	S	48.565	48.480	48.513	0.079	3.222	1.75
	C	48.535	48.425	48.484	0.103	3.210	2.27
25	S	48.550	48.360	48.469	0.180	3.160	3.92
	C	48.580	48.440	48.500	0.127	3.184	2.89
30	S	48.500	48.350	48.427	0.260	3.252	3.10
	C	48.540	48.420	48.458	0.160	3.226	2.48

Table 3.2; Sample Data for Ovality
and Eccentricity of Loading Assessment

Specimen Reference		Average stub specimen length (mm)	Error in parallel (mmx10 ⁻³)	Stub specimen mass (g)	A _m (by mass) (mm ²)	A _g (by geometry) (mm ²)	A _{av} (mm ²)
1	S	203.457	2	724.82	453.32	452.61	452.97
	C	203.835	5	725.52	452.92	450.77	451.85
5	S	203.880	5	722.58	450.98	449.59	450.34
	C	203.890	7	723.65	451.63	452.15	451.89
10	S	202.884	5	721.32	452.41	454.60	453.51
	C	203.212	6	727.68	455.66	458.56	457.11
15	S	202.182	5	725.02	456.31	460.52	458.42
	C	203.396	2	730.33	456.90	461.46	459.18
20	S	202.710	2	727.19	456.48	458.45	457.47
	C	202.484	8	720.80	452.97	456.57	454.47
25	S	202.896	4	721.80	452.68	449.80	451.24
	C	203.120	7	724.51	453.88	453.28	453.58
30	S	201.937	5	722.42	455.21	461.55	458.38
	C	202.965	5	727.07	455.83	458.42	457.13

Table 3.3; Sample Cross-Sectional Area Measurements

where $A_{nom}=453mm^2(50)$ is the nominal cross-sectional area and the stub length is as measured above. Data control and resultant average cross-sectional area values are thereby made available. On the basis of 62 partnered strut and stub specimens, a pertinent histogram is given in Fig 3.5. Excellent correlation was obtained between A_{nom} , A_g and A_m , data spread being $A_{nom} \pm 3\%$; lower 95% confidence values were $441.766mm^2$ and $443.288mm^2$ for A_g and A_m respectively. Given the close correlation, values of the resultant A_{av} were used for partnered strut and stub specimens - note Fig 3.1.

3.3 TESTING PROCEDURES

3.3.1 Stub Tests

All 62 static stub specimens were tested consecutively to provide the first phase of the formal testing programme. General testing system factors were given in Section 2.3.2. Specimens were manually located in the Schenck-mounted stub rig, note Plates 4 and 5, and the 'zero-zero' datum state achieved as accurately as possible using manual control of the RV10 controller. Monitoring was provided by the mini-computer resulting in highly accurate 'zeroing'. Alignment was thoroughly checked before invoking computer control, transfer to which resulted in the application of 145 axial stroke increments. There were 75 'fine' increments (12 μm /increment), at least 30 of which were assigned to the linear

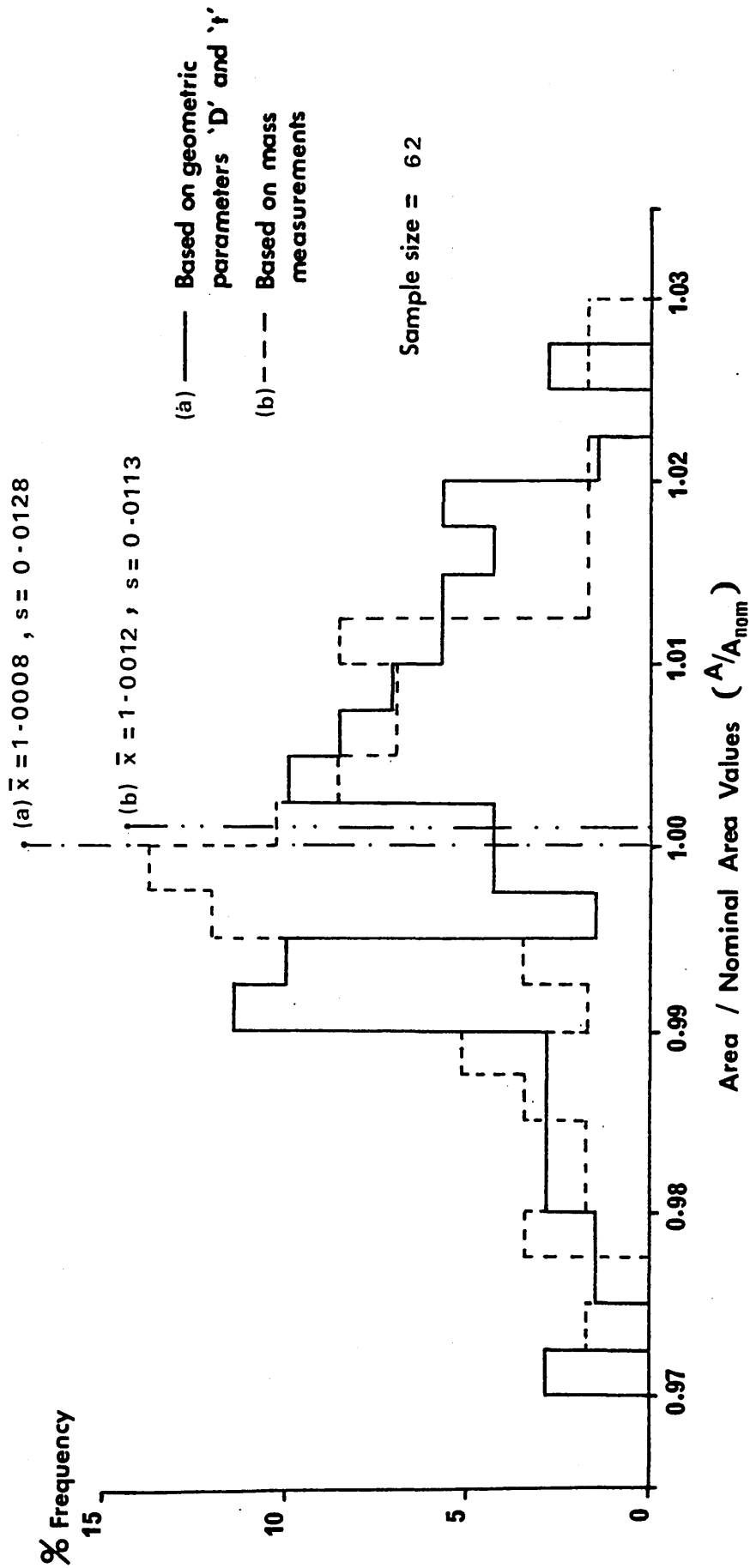


Figure 3.5 ; Non - Dimensionalised Cross - Sectional Area Histogram

elastic range⁽²⁶⁾; 35 increments were assigned to the unloading path, these forming part of the later 70 'coarser' increments (90 $\mu\text{m}/\text{increment}$).

Whilst formal output was obtained employing the IBM mainframe as discussed in Section 2.4, data on incremental values of stroke and load were also monitored on-line for purposes of experimental control and safety. Given the speed of monitoring, see Section 2.4, output was considered to be of 'dynamic' form⁽⁵⁴⁾. The applied strain rate was 20 $\mu\epsilon/\text{s}$ (ie specimen strain rate in the linear elastic range), with tests being curtailed at a strain of approximately 0.02. Experimental turn-round time was of the order of 30 minutes. Checks for non-axiality were made by investigating individual transducer readings⁽²⁶⁾; no problems were encountered. Final mainframe graphical output, discussed shortly, included provision of linear regression facilities for evaluation of E and $\sigma_y/\text{proof stress}$.

Plate 10 illustrates 3 stub specimens; to the right is an untested stub, in the centre is a typically tested stub, whilst to the left is a stub compressed well beyond a strain of 0.02. This was done to exaggerate and thereby more visually illustrate the well-established 'bulge' problem associated with stub testing. End friction coupled with the Poisson effect induces this flexural-type action which can adversely affect the constitutive values obtained⁽⁴³⁾. Given this problem, a restricted series of tensile tests were later conducted for purposes of comparative assessment.



Plate 10 ; Stub Specimens

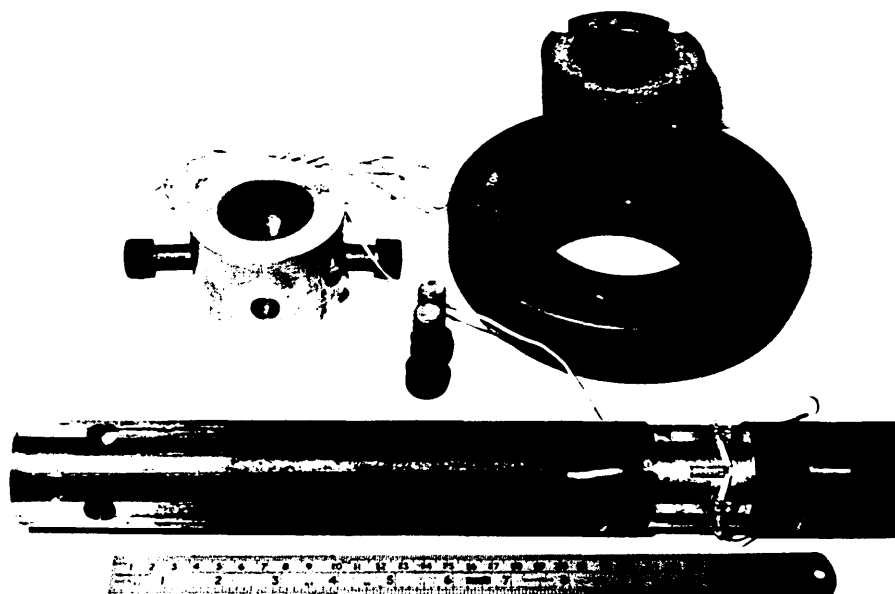


Plate 11 ; Tensile Test Specimen

3.3.2 Stub Tests - Cyclic

As noted in Sections 2.3.3 and 3.2.2, six additional stub tests were undertaken for control purposes. Three specimens were cut from each of two further (ie additional to specimen refs 1-38) 7.5m CHS runs; one specimen from each run was tested statically. Using the data obtained, the remaining four stubs were tested statically up to a state mid-way through the linear elastic range whereupon computer control and monitoring were suppressed. A sinusoidal forcing function was manually instituted through the RV10 controller with amplitudes such that cyclic action ($n_c=1000$ cycles) remained within the elastic range. Dynamic monitoring of axial stroke and load against one another and time was undertaken using x,y and x,y/t plotters as illustrated in Plate 5. Upon completion of the cyclic phase, static computer control and monitoring was re-implemented through to the limiting strain state. Primarily, the output provided control on cyclic action/slenderness ratio effects, particularly in the context of quasi-elastic hysteresis⁽⁵¹⁾. Further details on cyclic testing procedures are given in Section 3.3.6. These six tests were, in fact, the last tests undertaken, in chronological terms, with respect to the experimental programme.

3.3.3 Tensile Tests

Whilst compressive constitutive data is clearly desirable for strut testing support, the previously discussed 'end bulge' effect gives reason for concern with respect to the values obtained⁽⁴³⁾.

Some measure of control is available by undertaking tensile tests on comparable specimens. Twelve full scale tensile tests were thereby undertaken employing offcut material - see Fig 3.1.

Tests were conducted to BS18, Part 4 using an Avery testing machine, see Plate 9. Specimen details are illustrated in Plate 11. Taper-lock collets were employed in reversed mode, bearing onto which were end plates bolted to the specimen through previously drilled holes. The complete arrangement involved one collett being connected to the cross-head of the Avery machine, the specimen passing through the outboard load cell, its housing and beneath the travelling cross-beam of the machine to which the other collett was attached through a ball joint. Stroke loading was continuously applied, the rate being monitored using an x,y/t plotter⁽²⁵⁾, the respective 'K-factor' being determined as appropriate⁽⁴⁸⁾. Applied strain rate was $8 \mu\epsilon/s$.

The average axial strain in the 'waisted' section, see Section 2.6, was recorded together with the applied loading, the 'dynamic' criterion for yield stress being applicable⁽⁵⁴⁾. Cross-sectional area was determined in accordance with Section 3.2.3. Specimens were tested to failure; Plate 12 shows a typical ruptured specimen, failure being of accepted ductile form.

3.3.4 Strut Tests - Imperfection Monitoring

Following completion of the tensile tests, all strut specimens - other than the re-test cases discussed later - were subjected to



Plate 13 ; Buckled Strut Specimen
(partial recovery)

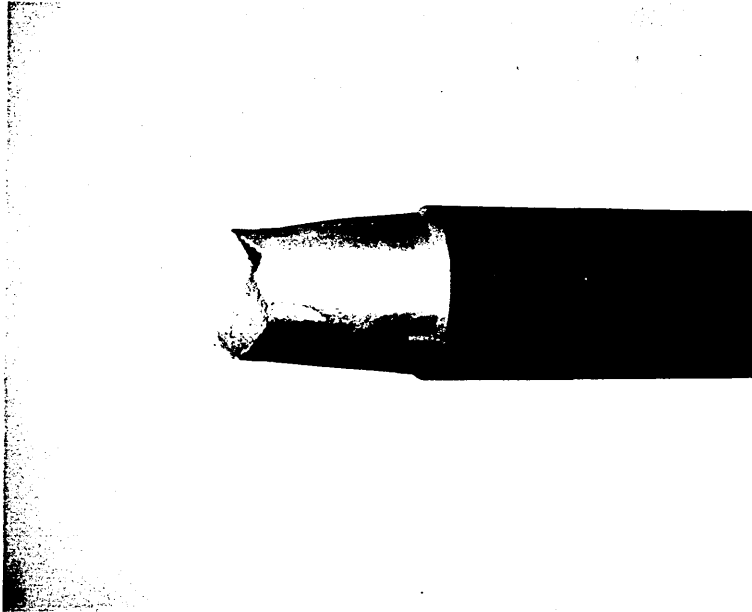


Plate 12 ; Ruptured Tensile Test
Specimen

out-of-straightness monitoring. The essentials of the equipment employed were described in Sections 2.3.4 and 2.4; see also Plate 6. With a variety of slenderness ratios being employed, the cross-head and transducers required re-location as necessary. Each strut was given 'strut-top' and 'strut-bottom' marks and then mounted in the Schenck with the weld seam in line with the central or mid-height transducer for control purposes. The 0° rotation reading was then taken and recorded using the mini-computer; subsequently, readings were taken at intervals of 90° with five full rotations employed as denoted previously. Fig 3.6 illustrates the principles involved, with the difference between diametrically opposing pairs of transducer readings being twice the respective imperfection. From the output data, resultant mean initial displacements and their orientation, conveniently expressed by β_{on} with respect to the weld, were computed, with

$$w_{on} = (e_{n1}^2 + e_{n2}^2)^{\frac{1}{2}} \quad (3.3)$$

and

$$\beta_{on} = \tan^{-1} (e_{n2}/e_{n1}) \quad (3.4)$$

for $n=1,7$, this denoting the seven transducers employed. Ovality data, as discussed in Section 3.2.3, was available for combination with this data for definitive values of initial out-of-straightness; the magnitudes of the ovality errors were considered negligible herein - see Table 3.2.

Whilst the data provided was directly relevant to the

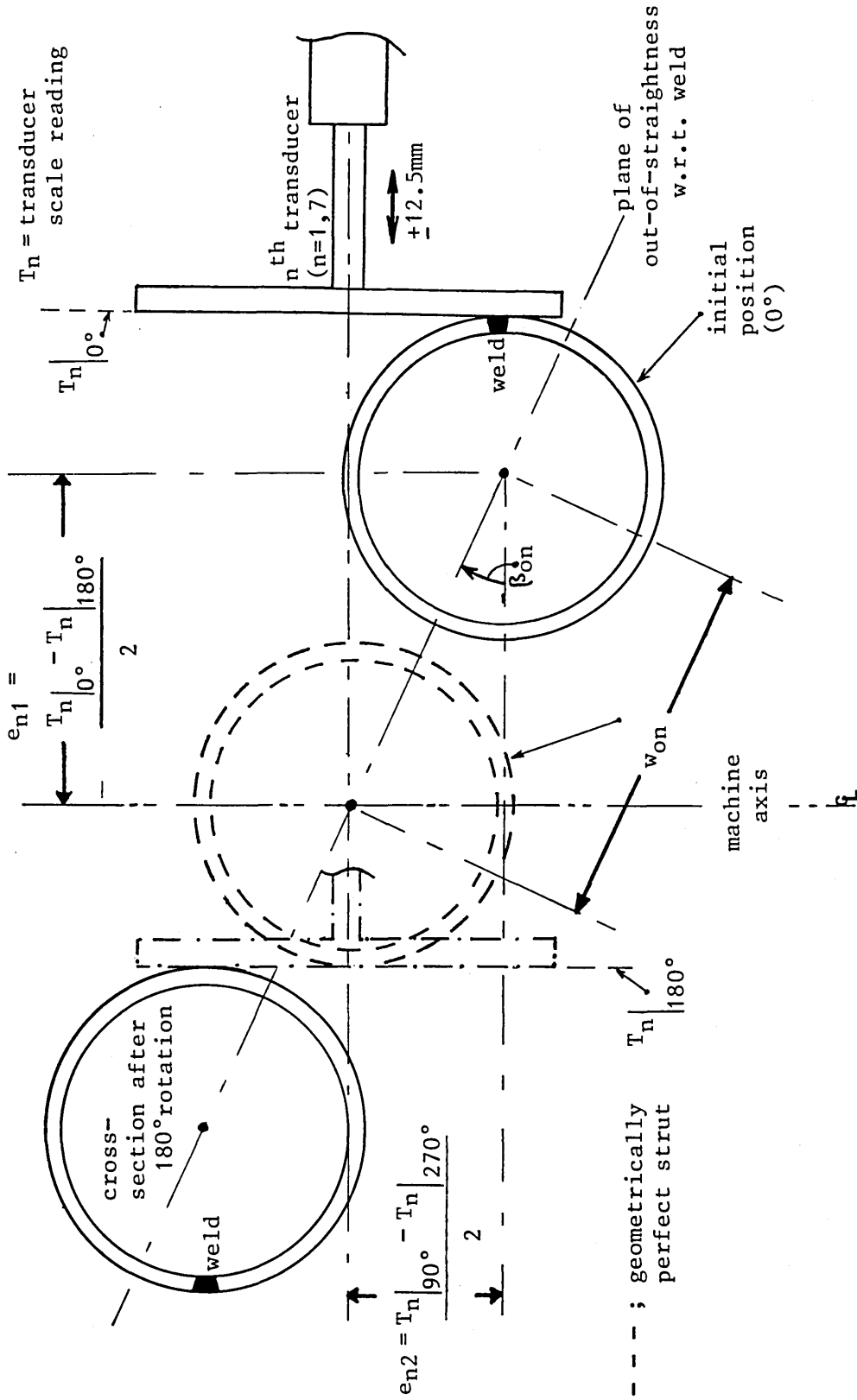


Figure 3.6 ; Out - of - Straightness Monitoring Configuration

considerations of BS4848, Part 2(47) owing to the lathe-centres employed in the procedure, relevance to the doubly-encasté support mode employed in the strut testing proper was clearly questionable. As noted in Section 2.3.4, a manual procedure was therefore adopted for the monitoring of the out-of-straightness of a representative sample of specimens fitted into the respective collets. The correlation between the lathe (pinned) and collett (encasté) data for these specimens is considered later.

As noted in Section 3.2.3, cross-sectional geometry data provided an eccentricity of loading parameter 'e', values for which are given in Table 3.2. This parameter relates to local conditions only, however, and is essentially for reference purposes only. The influence of the weld upon 'e' is marked.

3.3.5 Strut Tests - Static

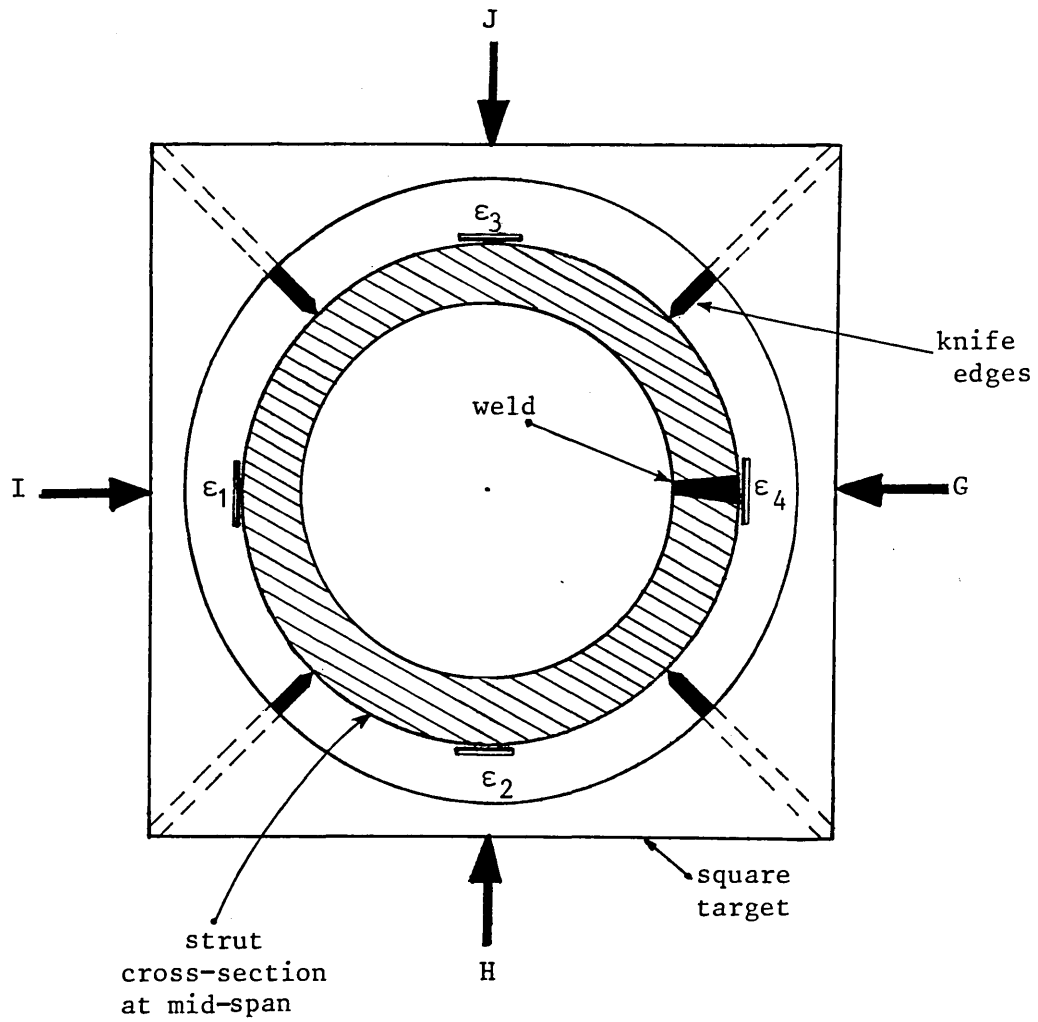
Those struts with a slenderness ratio of 80 - approximately two-thirds of the specimens - were tested as a batch following completion of the out-of-straightness monitoring. The remaining static tests were conducted following the cyclic testing, discussed below, of the $\lambda=80$ 'cyclic batch'. Re-tests and tests on synthetically deformed samples are considered separately in Section 3.8.

Having received the previously delineated strain gauges, each specimen was fitted, before being mounted in the Schenck, with the specially-designed square target discussed in Section 2.3.1 and

illustrated in Fig 3.7. Mid-height transducer G was chosen as datum location for the weld. The four transducers enabled a resultant central transverse buckling path to be plotted from readings $(G-I)/2$ and $(J-H)/2$, the negative signs being transducer-dependent. This novel feature proved to be very important in assessing strut behaviour - ie 'is planar strut modelling valid?' - and the corresponding computer graphical outputs were termed 'vector traces'. Correlation between measured central transverse displacement $w_{CL}-w_{ocL}$, see Eqn (2.2), and the strain gauge output was important and achieved employing the central monitoring topology depicted in Fig 3.7.

The collets were tightened once the specimen/actuator was zeroed-in, and computer control was then effected. Each test involved the acquisition of some 2000 discrete data items employing 145 stroke controlled increments which took the specimen well into the post-buckling range as discussed in Section 2.5.1 and illustrated in Plate 8. The initial 34 increments, each of $90\mu\text{m}$ stroke, were followed by fine increments of $25\mu\text{m}$ stroke for tight definition of the buckling state. The applied stroke rate approximated to $16\mu\text{E/s}$ (ie $16\mu\text{E/s}$ for $\lambda=80$). An experimental 'turn-round' time of 35-40 minutes was not uncommon.

Plate 13 illustrates a buckled specimen with the reversed curvature displayed. The strut is subject to elastic recovery, some 60% recovery of the central transverse displacement being achieved upon unloading. It should perhaps be noted that the specimen actually depicted comes from the preliminary series of



$\epsilon_1, \epsilon_2, \epsilon_3, \epsilon_4$:- strain gauges

G, H, I, J :- mid-span lateral transducers
(cf Plate 3)

Figure 3.7 ; Central Monitoring Facility

tests described in Section 2.5.1 as indicated by the presence of the 'turned' ends.

3.3.6 Strut Tests - Cyclic

Upon completion of the $\lambda=80$ static strut tests - ie cases 1S-16S - the testing of their cyclic counterparts was undertaken. Static data relating to buckling load P_c and corresponding end shortening $u|_{P_c}$ assisted in prescribing cyclic amplitudes ($2u_{am}$) and, given the appropriate mean state P_m^i , u_m^i , the resulting peak cyclic axial displacements u_m . Behaviour was to be of sub-buckling compressive form throughout (ie $u|_{P_c} > u_m^i + u_{am}$, $0 < u_m^i - u_{am}$). Specimens were prepared and mounted in the testing rig in the manner earlier described with respect to the static strut tests save for the omission of strain gauges. These were not considered to be necessary given the additional cyclic monitoring aspects involved - see Sections 2.3.3 and 2.5.3.

Tests therefore proceeded in accordance with the aforementioned static manner until the prescribed mean axial displacement u_m^i was achieved, this state corresponding to axial compressions of approximately 45 kN and/or 70 kN as discussed in Section 3.1. At this state, manual override control was implemented employing the RV10 controller's inboard function generator to apply a sinusoidal waveform

$$u = u_m^i + u_{am} \sin(2\pi ft') \quad (3.5)$$

where u denotes total axial displacement at time t' , monitoring

being undertaken in accordance with Section 2.3.3 for P vs $w_{CL}-w_{ocL}$ (measured central transverse displacement) and P vs u , with each of these parameters also plotted against a time (t') base. Peak cyclic parameters P_m and u_m were of obvious importance. Cyclic durations were varied but generally consisted of a total of $n_c=1000$ cycles applied at either of the lower (45kN) or upper (70kN) P_m^i , u_m^i states. Exceptions to this primarily concerned the first test, 1C, in which short durations were applied, 25 cycles, as a lower limit check upon the preliminary tests delineated in Table 2.3, and tests 13C and 14C in which 1500 cycles were employed as an upper limit check upon duration effects. Upon completion of a cyclic action phase, digital control was re-implemented, this being initiated by mini-computer logging of the post-cyclic phase values of load and displacement. This enabled accurate digital assessment of cyclic action phase effects in pre- and post-cyclic phase static terms. No effective change in mean axial displacement u_m^i was recorded throughout the cyclic experimentation, as was required of the testing system.

For tests involving only one cyclic action phase, completion of this phase was followed by re-implementation of the established static loading procedure through to the limiting post-buckling displacement state as discussed in Sections 2.5.1 and 3.3.5. For those tests involving two such cyclic phases, the static loading procedure was re-implemented between the two respective u_m^i states and again following completion of the second cyclic action phase through to the prescribed limiting post-buckling displacement state.

A variety of cyclic profiles was therefore investigated for $\lambda=80$. It became apparent that the primary action parameter, given the $n_c-u_{am}-f-\lambda$ configurations considered, was peak cyclic displacement u_m (or P_m). This was to be of major importance with respect to the final mainstream set of cyclic strut tests, 17C to 27C, these involving a variety of slenderness ratios λ . These tests all involved only one cyclic action phase, primarily based on the upper value of u_m^1 , corresponding to $P=70kN$. Values of u_m were such that concern with peak inelastic excursion took precedence over the quasi-elastic hysteresis associated with lower values of u_m . This second series of formal cyclic strut tests followed the testing of the corresponding static strut specimens 17S to 27S. The Schenck and transducer monitoring facilities were adjusted to accommodate the changes in λ as required. Detailed consideration of the results obtained follows as part of the ensuing discussion of the overall formal experimental data.

3.4 CONSTITUTIVE BEHAVIOUR - RESULTS

3.4.1 Stub Tests

Table 3.4 presents sample specimen data from the main set of 62 static stub tests. Constitutive response ranged between the typical yield and roundhouse loci depicted in Fig 3.8; most loci were of either the former or slightly rounded, quasi-yielding type shown in Fig 3.9. This figure also illustrates the typical computer graphics output resulting from a stub test, with regression providing for E and the 0.2% proof stress. Few full

Specimen Reference		$\sigma_y/\sigma_{0.2\%}$ (N/mm)	E (kN/mm ²)	Classification R-roundhouse S-slightly rounded Y-yield
1	SS	285	214	S
	SC	283	214	
5	SS	287	213	S
	SC	302	207	
10	SS	306	215	S
	SC	309	211	
15	SS	275	215	Y
	SC	277	217	
20	SS	297	218	S
	SC	300	219	
25	SS	204	213	Y
	SC	210	218	
30	SS	325	216	R
	SC	320	220	

Table 3.4; Sample Stub Test Data

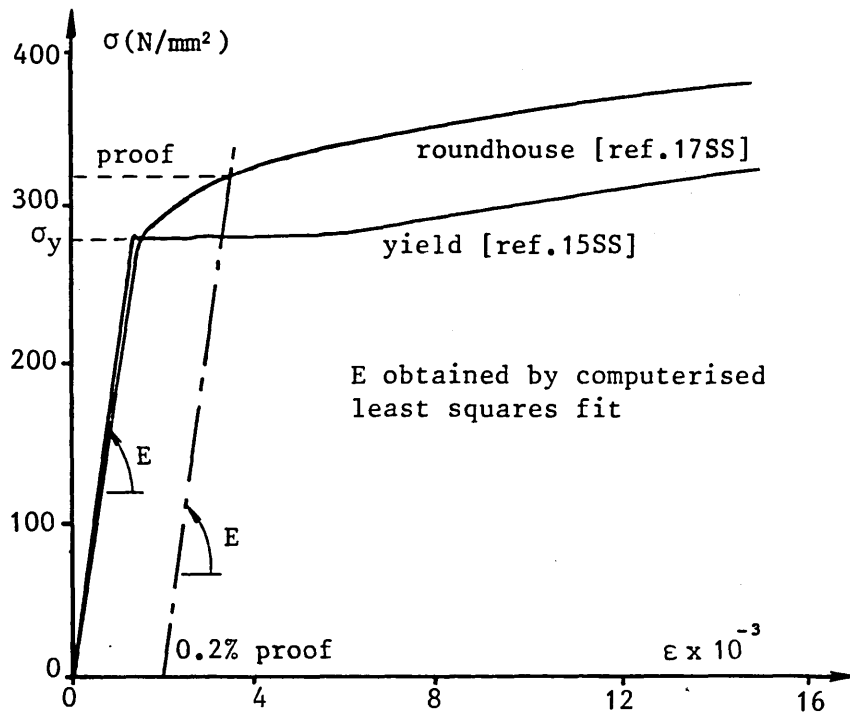


Figure 3.8 ; Stub Loci - Yield and Roundhouse Type

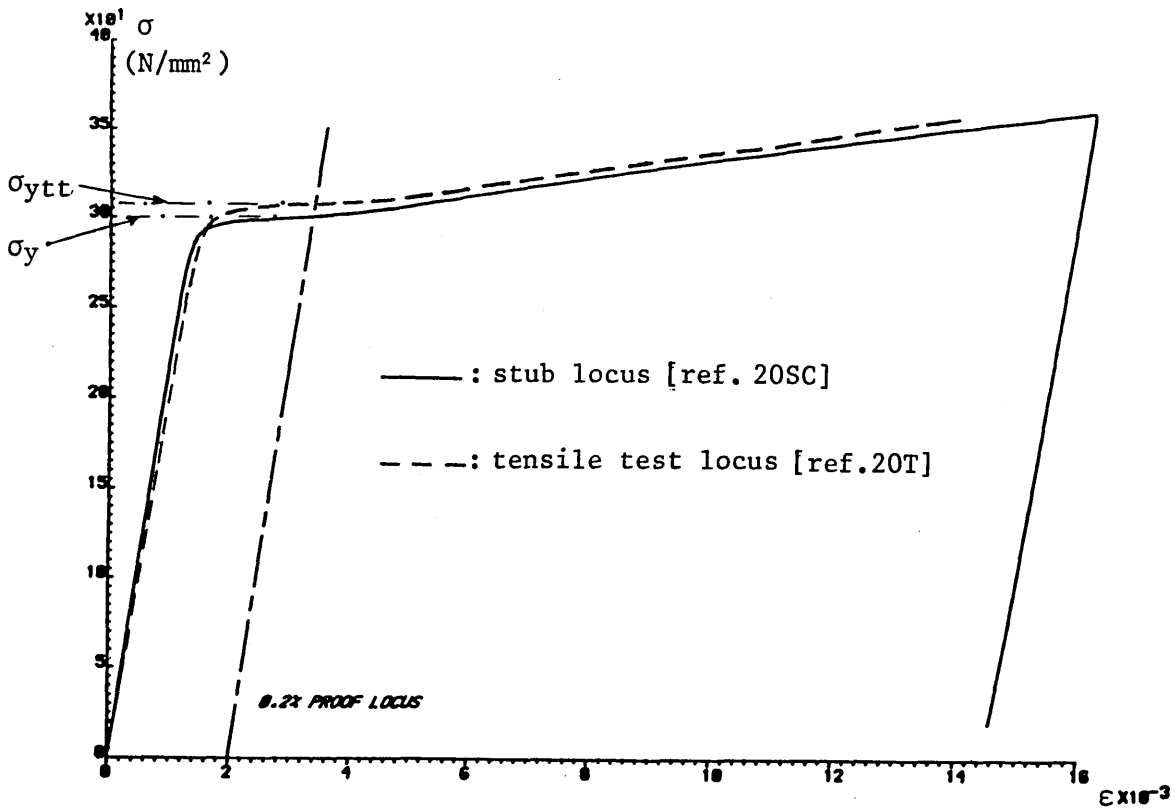


Figure 3.9 ; Stub and Tensile Test Loci

roundhouse curves were obtained, supporting the thesis that residual stresses are relatively unimportant in the hot-finished sections employed(32).

Fig 3.10 affords histograms of the $\sigma_y/0.2\%$ proof stress and E obtained from the stub experimentation. Variations from the mean of up to -33% and -13% respectively are noted. These variations from the respective means of 284.4N/mm^2 and 213.6kN/mm^2 are substantial, particularly in the case of $\sigma_y/0.2\%$ proof stress, and justify the constitutive experimentation. However, variations with respect to any given specimen reference set were generally small as typified in Table 3.4. The findings of the cyclic stub experimentation are discussed later.

3.4.2 Tensile Tests

Table 3.5 presents pertinent data from the 12 tensile tests undertaken on specimens taken at random from offcut material. Tensile test values for yield/0.2% proof stress and direct modulus are denoted by σ_{ytt} and E_{tt} . Their relationship to the corresponding stub test values of σ_y and E is given alongside showing the stub test average to be 3% down on yield/0.2% proof stress and up by 7% on the direct modulus. When comparing the average tensile test values with those from all 62 stub tests, however, the stub values show a drop of 6% in yield/0.2% proof stress and an increase of 6% in direct modulus; note Fig 3.10.

Fig 3.9 shows a typical tensile constitutive locus superposed on the corresponding stub test output, specimen ref. 20T; the struts

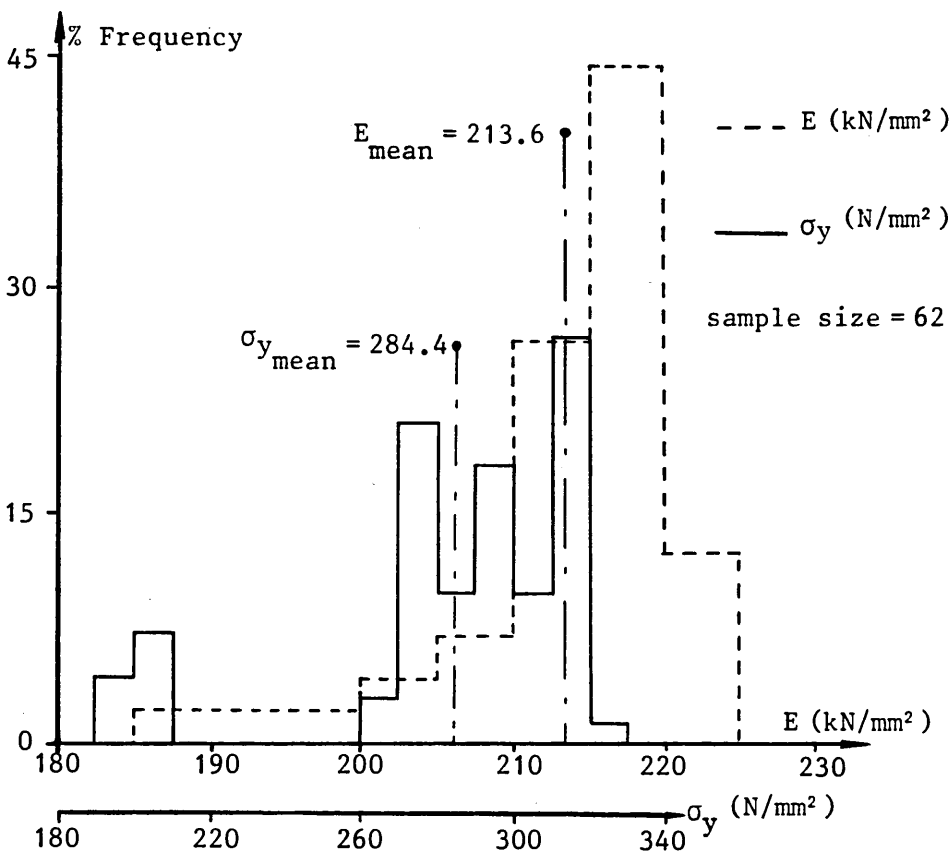


Figure 3.10 ; Direct Modulus and Yield/Proof Stress Histograms

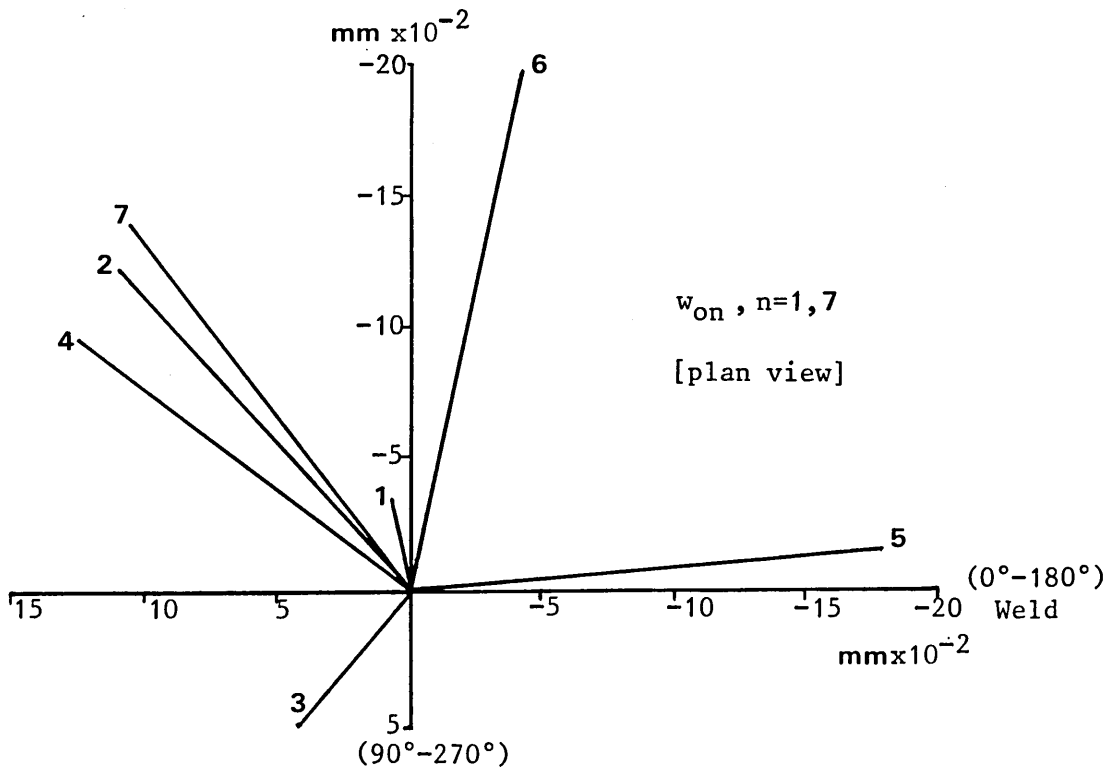


Figure 3.11 ; Out-of-Straightness Components - Strut Ref. 6S

Specimen Ref.	σ_{ytt} (N/mm ²)	$\frac{\sigma_y}{\sigma_{ytt}}$	E_{tt} (kN/mm ²)	$\frac{E}{E_{tt}}$	Classification R-roundhouse S-slightly rounded Y-yield
1T	290	0.98	200	1.07	S
3T	290	1.00	195	1.07	Y
5T	307	0.96	205	1.02	S
7T	300	0.98	200	1.07	S
8T	294	0.94	203	1.07	Y
13T	320	0.98	200	1.08	S
20T	311	0.96	205	1.07	S
a 21T	307	0.97	197	1.11	S
b 21T	306	0.97	200	1.08	S
22T	283	0.97	198	1.10	S
26T	331	0.94	206	1.06	R
27T	309	1.01	200	1.08	S
Average	304	0.97	201	1.07	n/a

Table 3.5; Tensile Test Data

21S and 21C were of slenderness ratio 75, permitting two tensile specimens, a and b, to be obtained and compared. Most tensile loci were of slightly rounded yielding form as denoted in Table 3.5.

3.5 IMPERFECTION ASSESSMENT - RESULTS

3.5.1 Initial Curvature

Data from the 53 mainstream strut tests, 1S to 27S, less 16S, and 1C to 27C, as discussed in Section 3.2.2, was reduced from a basic set of 7420 individual readings to produce average resultant values of magnitude w_{on} and orientation β_{on} , $n=1,7$, for each strut; β_{on} was measured in an anticlockwise sense from the weld in plan view. Tables 3.6 and 3.7 present sample data. The values for w_{on} indicate the struts to be well-formed or very straight; this was true for all strut samples. Indeed, it was this trend which led to the decision to subject a set of strut samples to synthetically produced additional initial curvature as discussed separately in Section 3.8. All struts were well within the requisite 0.2%L tolerance⁽⁴⁷⁾ as assessed by the maximum value of the respective w_{on} , w_{om} . This value did not always coincide with the central value $w_{o4}(=w_{ocL})$ as indicated in Table 3.6 and corkscrewed initial topologies were extant throughout; see β_{on} in Table 3.7. Fig 3.11 depicts the graphical output relating to case 6S and illustrates typical initial profile data in plan view. The complexities associated with attempting to theoretically model practical strut behaviour are well-typified by

Strut Reference	INITIAL CURVATURE VALUES										Interpolated w_{oc} (mm)
	w_{on}	w_{o1} (mm)	w_{o2} (mm)	w_{o3} (mm)	(w_{ocL}) w_{o4} (mm)	w_{o5} (mm)	w_{o6} (mm)	w_{o7} (mm)	direct w_{oc} (mm)		
1	S	0.30	0.56*	0.48	0.49	0.05	0.33	0.03	n/a	0.28	
	C	0.06	0.08	0.12	0.14*	0.13	0.11	0.12	0.04	0.10	
5	S	0.25	0.24	0.32	0.34*	0.13	0.16	0.11	0.14	0.19	
	C	0.35	0.09	0.62	0.89*	0.82	0.34	0.42	0.67	0.44	
10	S	0.81	1.41	1.37	1.45*	1.28	1.09	0.68	0.20	1.01	
	C	0.82	1.59	1.74*	1.53	1.46	0.91	0.57	n/a	1.08	
15	S	0.21	0.21	0.13	0.28	0.40*	0.33	0.26	n/a	0.23	
	C	0.16	0.32	0.47*	0.32	0.40	0.27	0.29	n/a	0.28	
20	S	0.09	0.16	0.20*	0.32	0.18	0.24*	0.11	0.12	0.16	
	C	0.08	0.12	0.27*	0.17	0.09	0.20	0.30	n/a	0.15	

* Maximum of w_{on} per strut

Table 3.6; Sample (Pin-Ended) Out-of-Straightness Values

Strut Reference	β_{0n} INITIAL CURVATURE ANGULAR DISPLACEMENT VALUES (degrees)						
	β_{01}	β_{02}	β_{03}	(β_{0cL}) β_{04}	β_{05}	β_{06}	β_{07}
1	S	242	146	272	94	6	192
	C	64	88	104	174	192	22
5	S	337	140	347	346	8	333
	C	302	216	313	94	168	103
10	S	22	99	109	66	24	352
	C	106	140	122	77	9	45
15	S	6	225	24	347	46	344
	C	350	310	66	342	32	108
20	S	84	130	273	285	278	355
	C	263	302	95	72	145	178

Table 3.7 ; Sample (Pin-Ended) Out - of - Straightness Angular Displacement Values

Strut Reference	5C	14C	16C	17C	18C	23C	24C	25C	26C	27C	Average
w_{ocL}/w_{ocE}	0.89	1.05	0.93	1.03	1.00	0.94	0.88	0.99	0.85	0.86	0.94

Table 3.8 ; Pinned-Encastré Mode Correlation $\text{nb } \beta_{ocL} / \beta_{ocE}$ affords similar correlation

this example of a three-dimensional, corkscrewed initial topology. The histogram of Fig 3.12 gives an overall mean value of 0.258×10^{-3} for w_{om}/L , an order of magnitude within the 2×10^{-3} tolerance(47).

Accepting that theoretical studies were to be undertaken in conjunction with the experimental programme and that modelling was to be undertaken on the generalised basis of effective length ℓ , then the relationship between the measured w_{on} , $n=1,7$, noting w_{ocL} in particular and that these were assessed over a length L , and an initial central transverse displacement w_{oc} defined with respect to ℓ was required. As noted in Sections 2.3.4 and 3.3.4, a manual procedure was adopted for the monitoring of out-of-straightness for a sample of ten strut specimens in the encastré mode. The two alternative modes of out-of-straightness monitoring are illustrated in Figs 3.13(a) and (b). The ten encastré tests generated 280 individual component data items. The appropriate processed data is given in relation to the corresponding pin-ended data in Table 3.8 in terms of the initial central transverse displacement values, w_{ocE} denoting the respective encastré data. The correlation was considered to indicate that, noting the relative straightness of the specimens, the pin-ended data could be used in conjunction with encastré strut testing per se.

Compromise between the importance and variability of strut imperfections with the requirements of design practice demanded the reduction of the necessary w_{on}/w_{ocL} and w_{ocE} data base into a form suited to planar strut analysis. Accordingly, Fig 3.13(c)

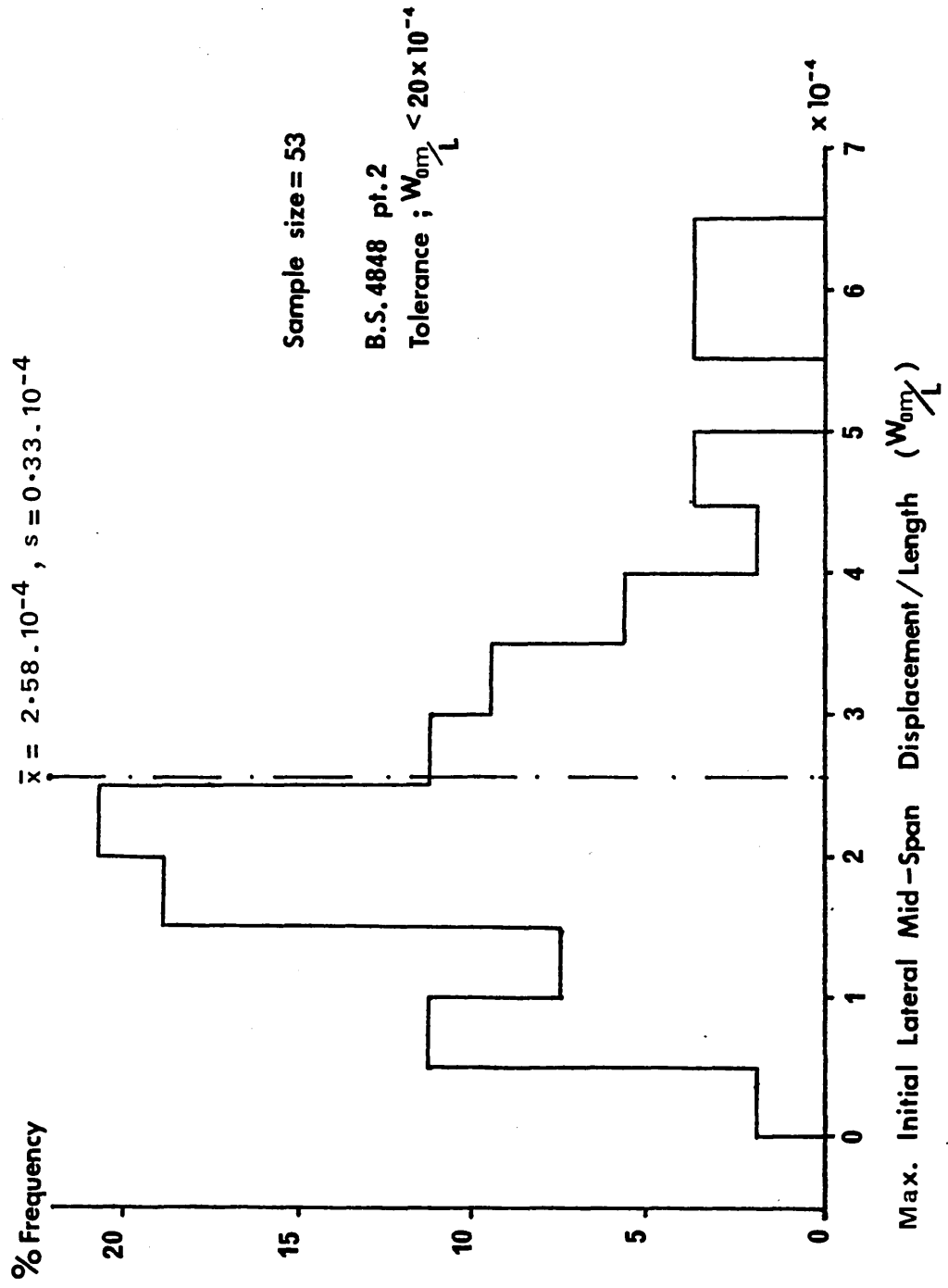
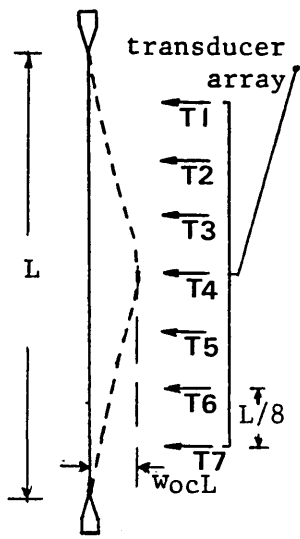
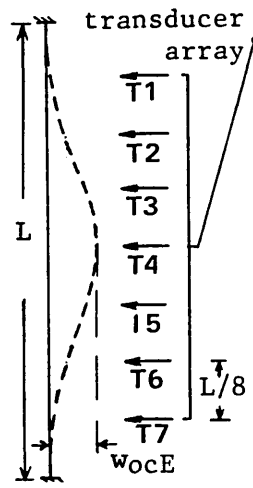


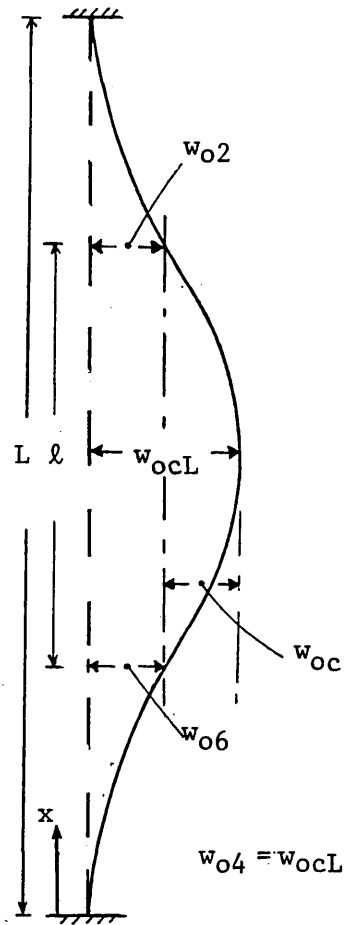
Figure 3.12 ; Non - Dimensionalised Maximum Initial Lateral Displacement Histogram



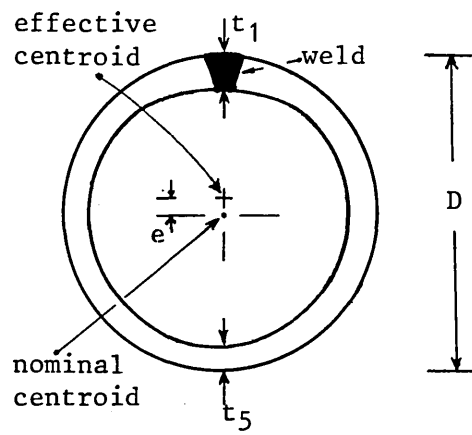
(a) Pinned End Conditions



(b) Encastré End Conditions



(c) w_{oc}



(d) Eccentricity

Figure 3.13 ; Imperfection Parameters

illustrates the basic procedure adopted, with w_{oc} denoting the processed value of initial central transverse displacement with respect to effective length $\ell=L/2$. This procedure employs

$$w_{oc} = w_{ocL} - (w_{o2} + w_{o6})/2 \quad (3.6)$$

and effectively requires that $w_{ocL}=w_{o4}$ be the respective maximum initial displacement w_{om} and that non-negative values be obtained. To provide for cases where this was not viable, an alternative, interpolating function procedure was adopted. Considering coordinate x to lie along the undeformed centreline as shown in Fig 3.13(c), then, for $\ell=L/2$, let the initial deformed profile take the form

$$w_o = w_{ocL} (1 - \cos[2\pi x/L])/2 \quad (3.7)$$

such that the area enclosed between the undeformed centreline and the initial strut profile is given by

$$A = \int_0^L w_o \, dx = w_{ocL} \cdot L/2 \quad (3.8)$$

Equating this with the non-planar area piecewise enclosed by the actual w_{on} readings affords

$$w_{ocL} \cdot L/2 = (L/8) \sum_{n=1}^7 w_{on} \quad (3.9)$$

Employing $\ell=L/2$ thereby implies

$$w_{oc} = w_{ocL} / 2 = \left(\sum_{n=1}^7 w_{on} \right) / 8 \quad (3.10)$$

which is always available for any strut.

Values of w_{oc} obtained either directly from Eqn (3.6) or by interpolation from Eqn (3.10) enable assessment of w_{oc} against the 0.1% ℓ requirement⁽⁴²⁾ or imperfection parameter η in design practice^(35,36) which gives 0.104% ℓ for $\lambda=80$ using design values for σ_y and E. Individual strut values for w_{oc} are given in the comprehensive tabulations of Section 3.7; the maximum direct and interpolated values are well within these tolerances, being 0.05% ℓ and 0.08% ℓ respectively, corresponding means being 0.02% ℓ and 0.035% ℓ . The minor discrepancies between w_{ocL} and w_{ocE} as denoted in Table 3.8 are thereby considered negligible.

3.5.2 Load Eccentricity

Equivalence of cross-section and load eccentricity was delineated in Section 3.2.3 and the appropriate processed data given in Table 3.2 with $t_{max} - t_{min} = t_1 - t_5$ due to weld effects; note Fig 3.13(d). Evaluation of eccentricity e is thereby readily available, the respective data being given in the main tabulations of Section 3.7.

Given that strut imperfections can be broadly grouped under the classifications of initial curvature (say w_{oc}), eccentricity of loading (say e) and residual stress, then it is considered that imperfection assessment has been comprehensively treated.

Consideration of the implications is left to the overview of experimental strut behaviour delineated in Section 3.7.

3.6 STATIC STRUT TESTING - RESULTS

3.6.1 Parametric Response

The software employed for the interpretation of the static strut test data provided for computer numerical and graphical output of the primary parameters, whilst additional software features generated vector traces, note Section 3.3.5, and interactively produced Southwell and Lundquist Plots; this latter item is considered in section 3.6.2.

Two sets of complete graphical output, that is P vs u , P vs $w_{CL}-w_{oCL}$, P vs ϵ_n and the associated vector trace plots, are depicted in Figs 3.14 to 3.23 inclusive. Cases 12S - Figs 3.14 to 3.18 inclusive - and 20S - Figs 3.19 to 3.23 inclusive - are considered representative in terms of their output and also display particular features of interest.

From the P vs u graphs in Figs 3.14 and 3.19, it can be seen that the dispersion of increments through the pre- and post-buckling paths - each discrete increment being delineated by a symbol - were aimed at defining the sensitive buckling region accurately. Despite the fine increment size, Fig 3.14 displays sudden load shedding, with the increment following attainment of P_c not being able to define a 'curve' around P_c , and hence a definitive P_c .

AXIAL LOAD vs. AXIAL DISPLACEMENT

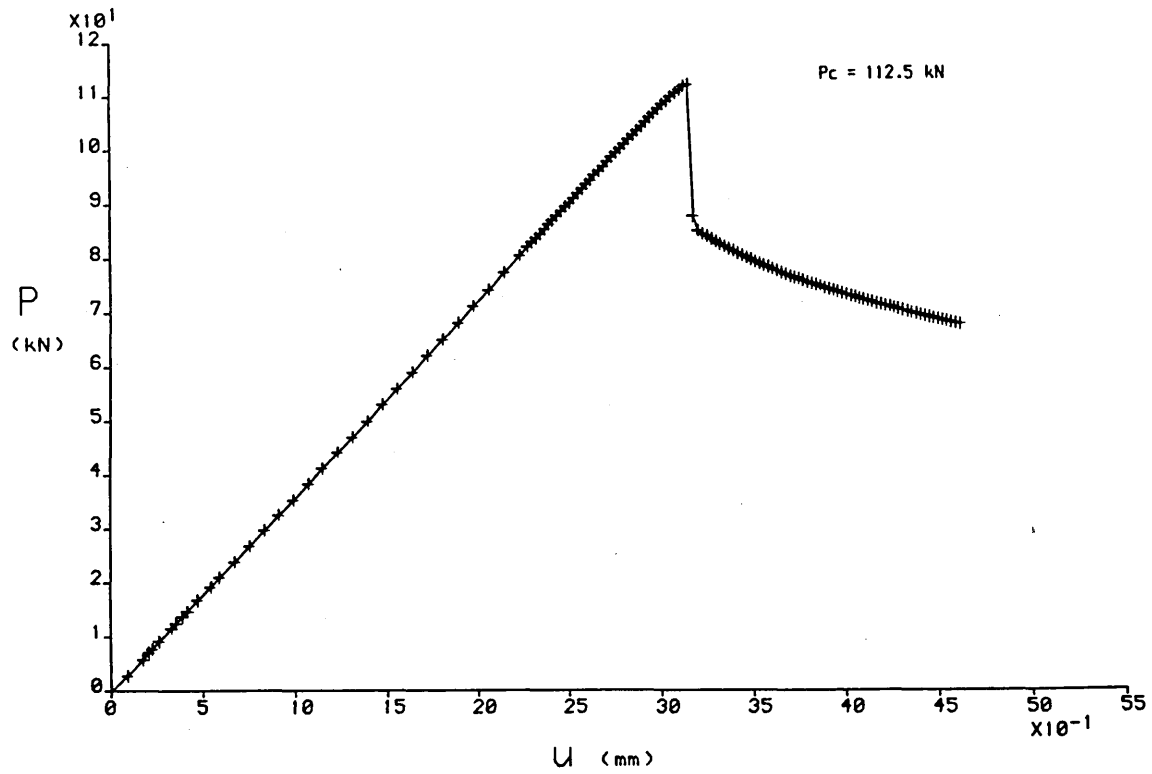


Figure 3.14 ; P vs u - Strut Ref. 12S

AXIAL LOAD vs. MID-SPAN RESULTANT LATERAL DISPLACEMENT

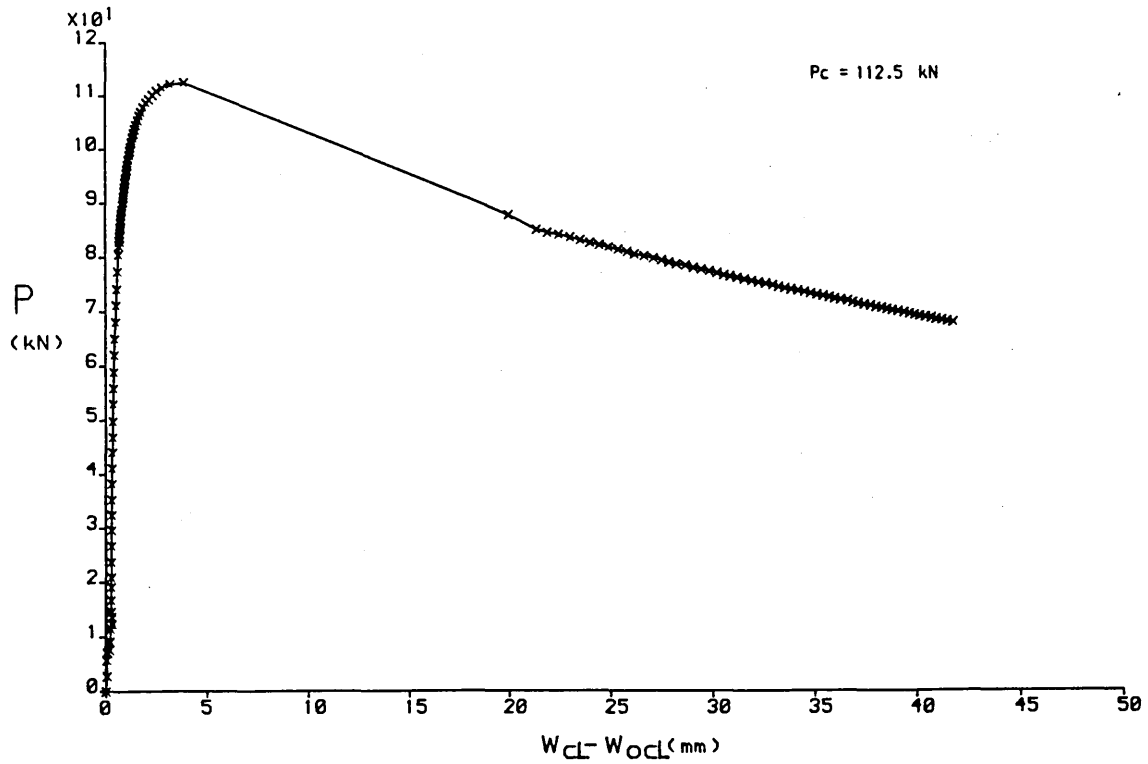


Figure 3.15 ; P vs $w_{cL} - w_{ocL}$ - Strut Ref. 12S

AXIAL LOAD vs. MID-SPAN AXIAL STRAIN

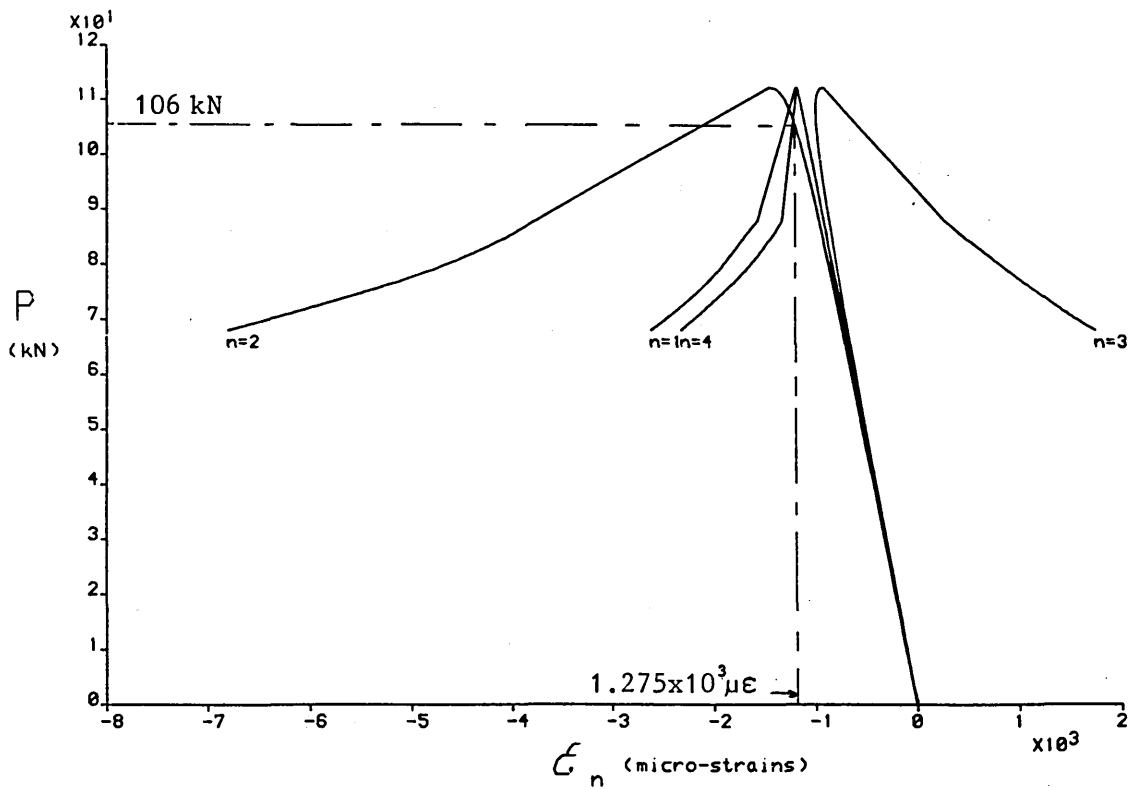


Figure 3.16 ; P vs ϵ_n - Strut Ref. 12S

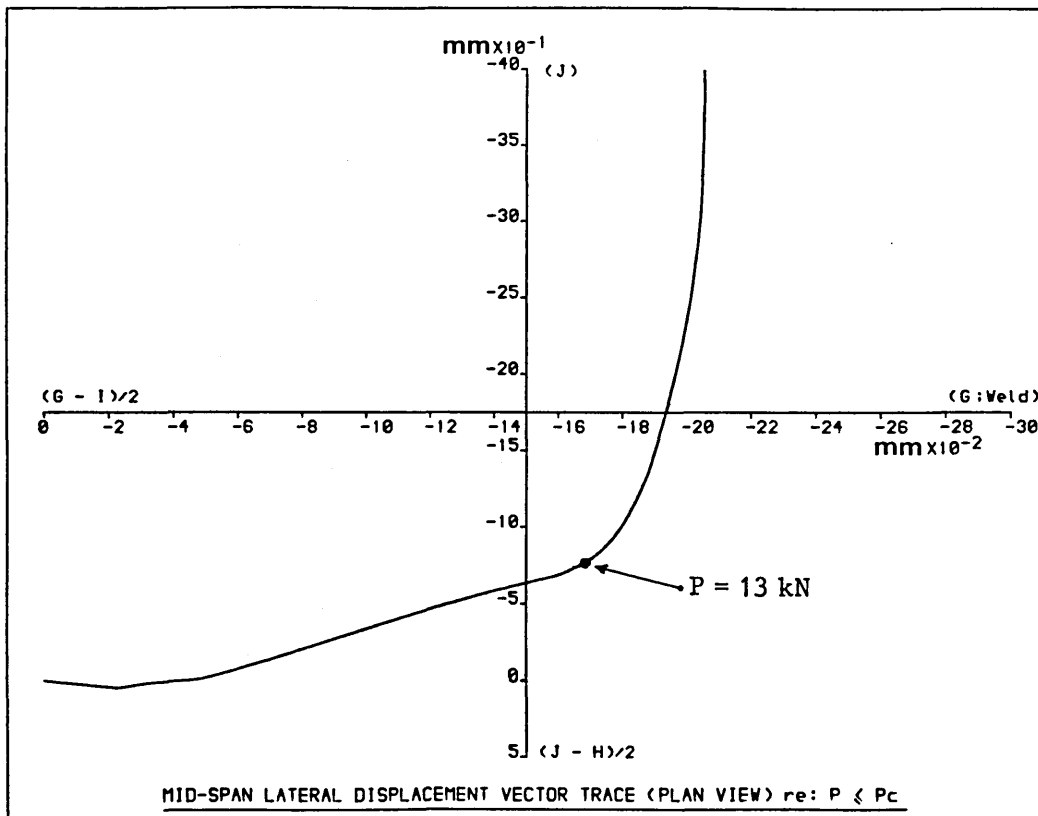


Figure 3.17 ; Vector Trace ($P \leq P_c$) - Strut Ref. 12S

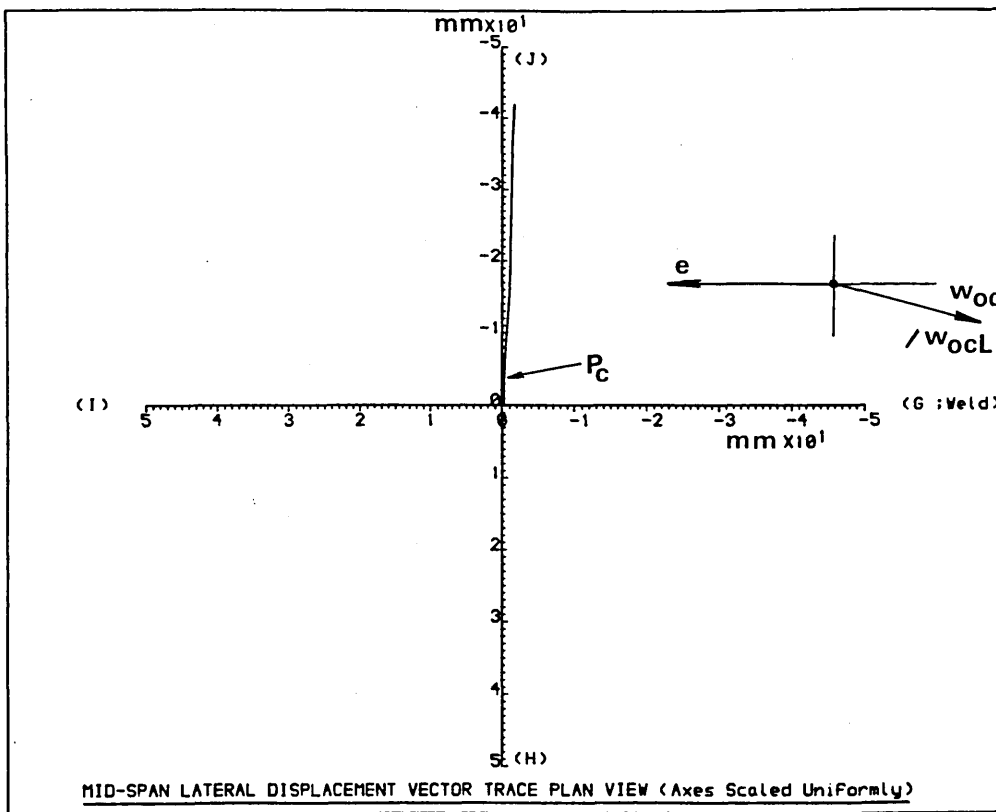


Figure 3.18 ; Vector Trace - Strut Ref. 12S

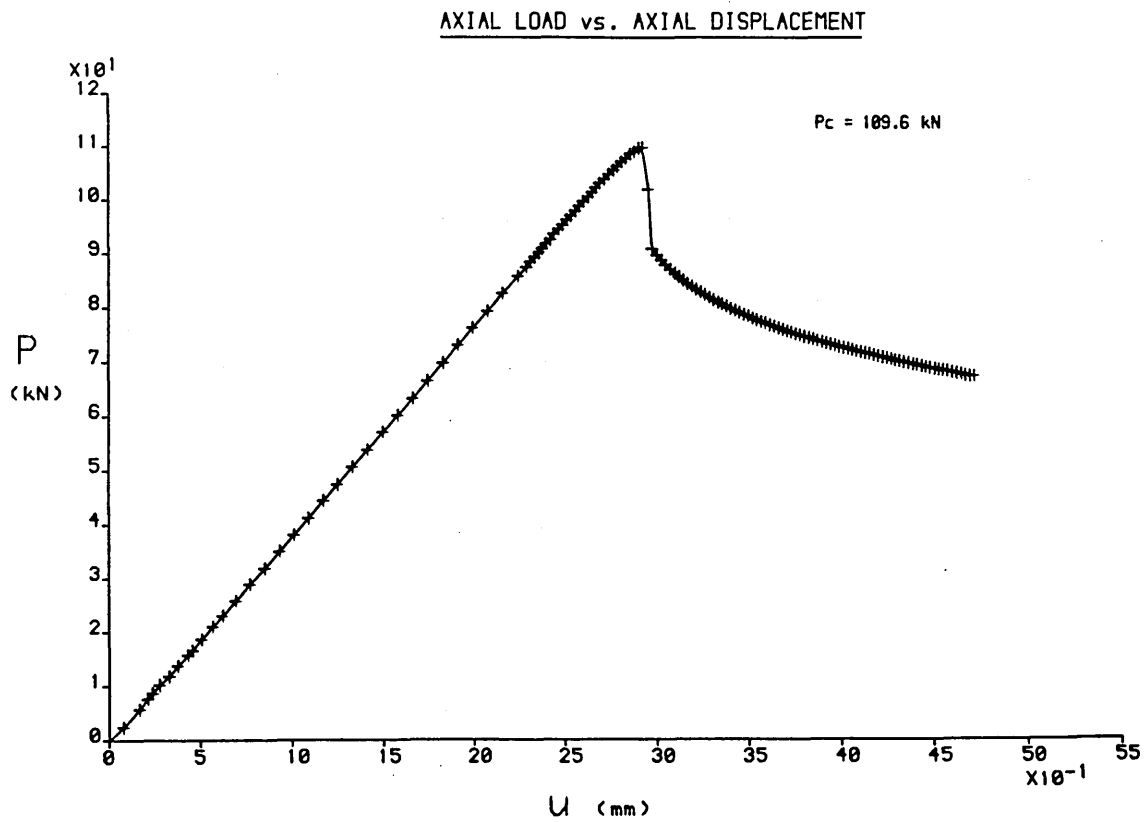


Figure 3.19 ; P vs u - Strut Ref. 20S

AXIAL LOAD vs. MID-SPAN RESULTANT LATERAL DISPLACEMENT

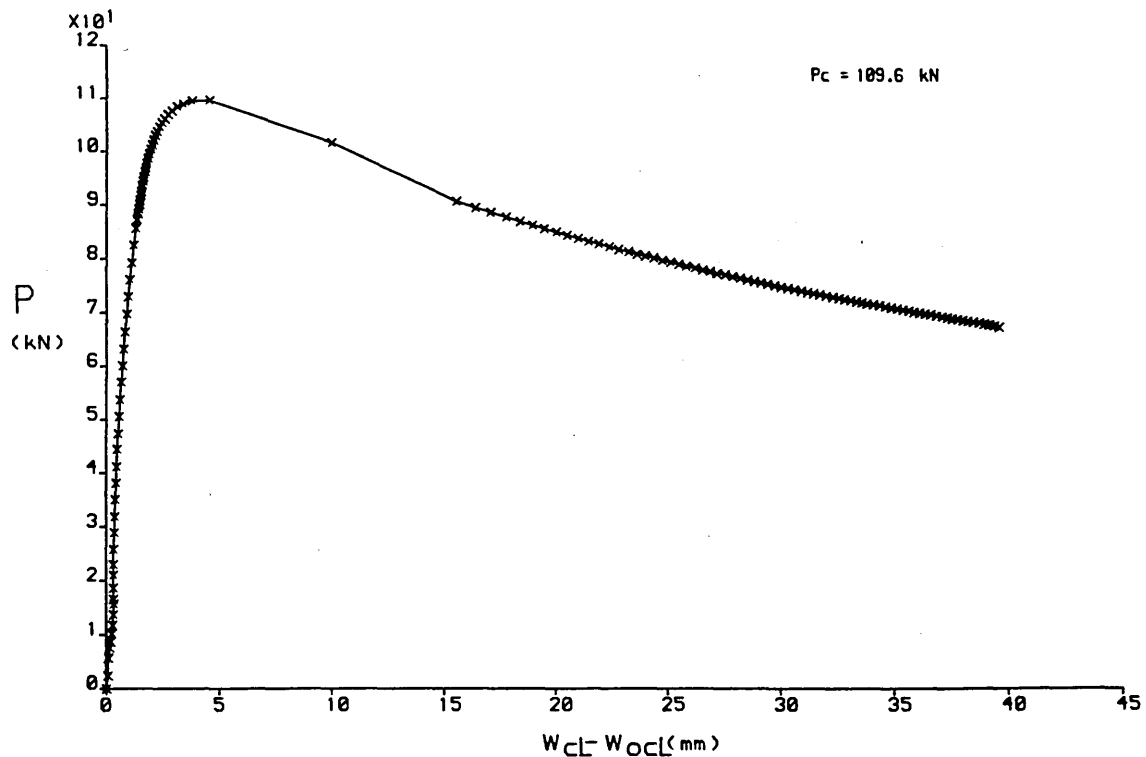


Figure 3.20 ; P vs $w_{cL} - w_{ocL}$ - Strut Ref. 20S

AXIAL LOAD vs. MID-SPAN AXIAL STRAIN

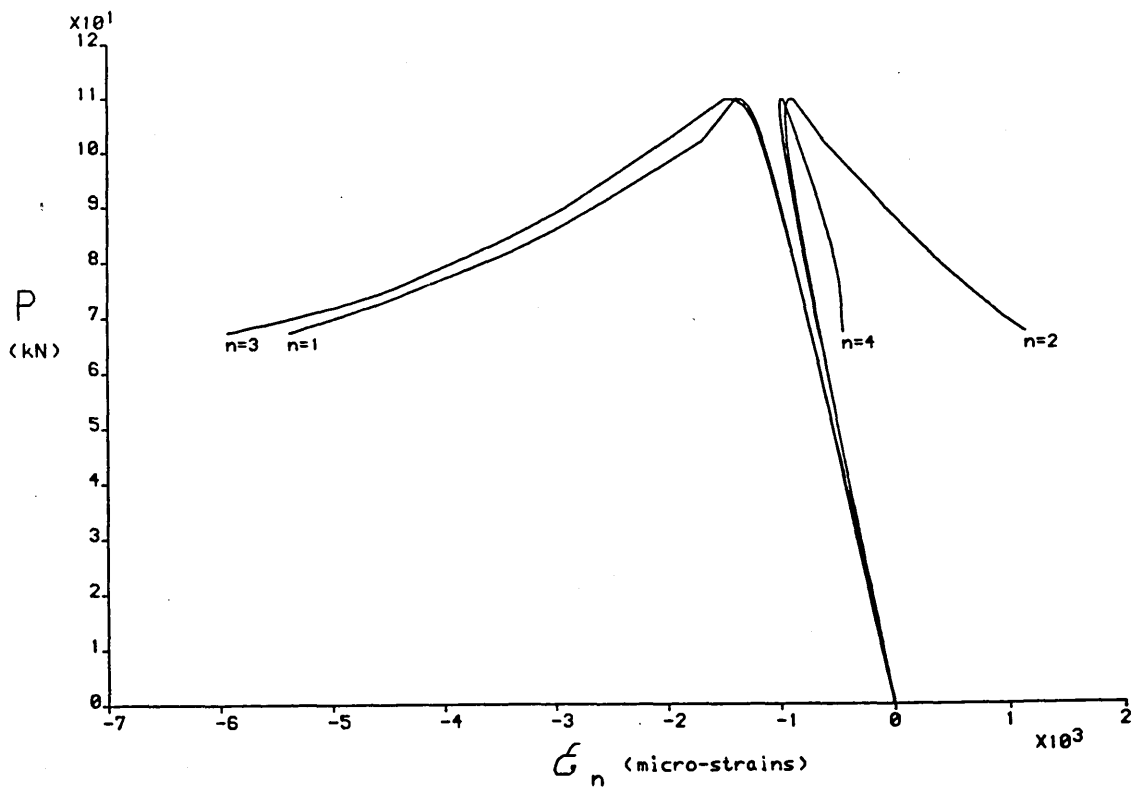


Figure 3.21 ; P vs ϵ_n - Strut Ref. 20S

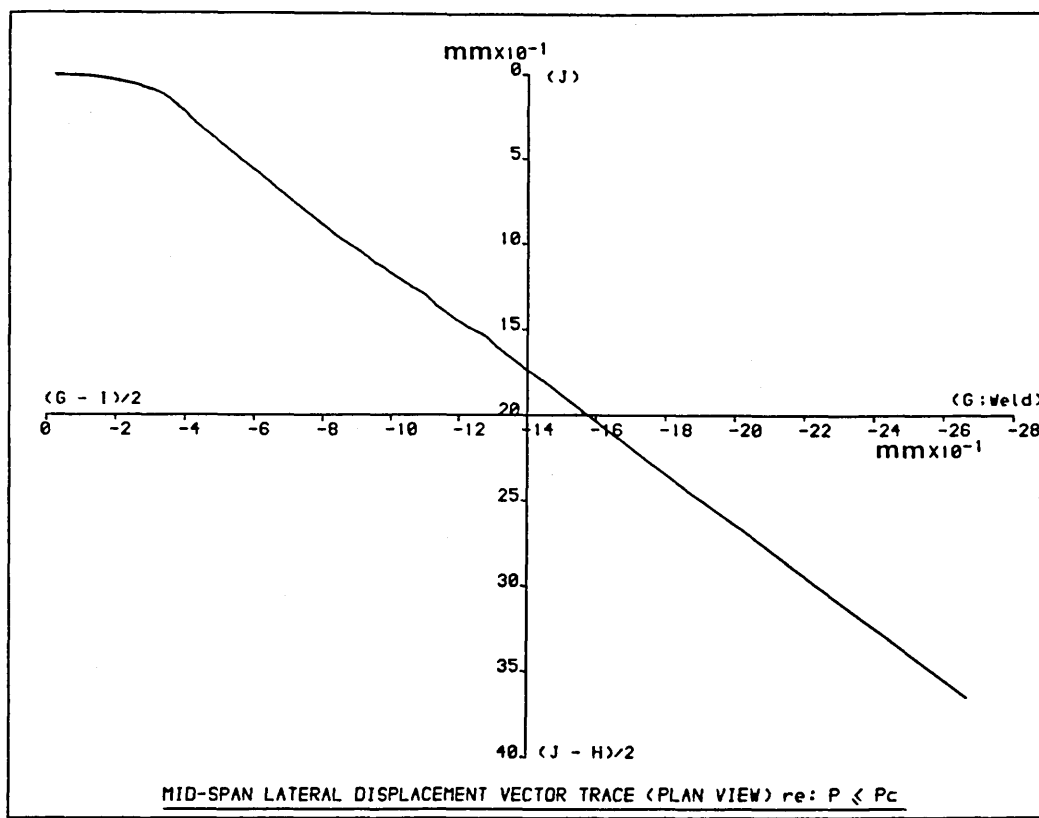


Figure 3.22 ; Vector Trace ($P < P_c$) - Strut Ref. 20S

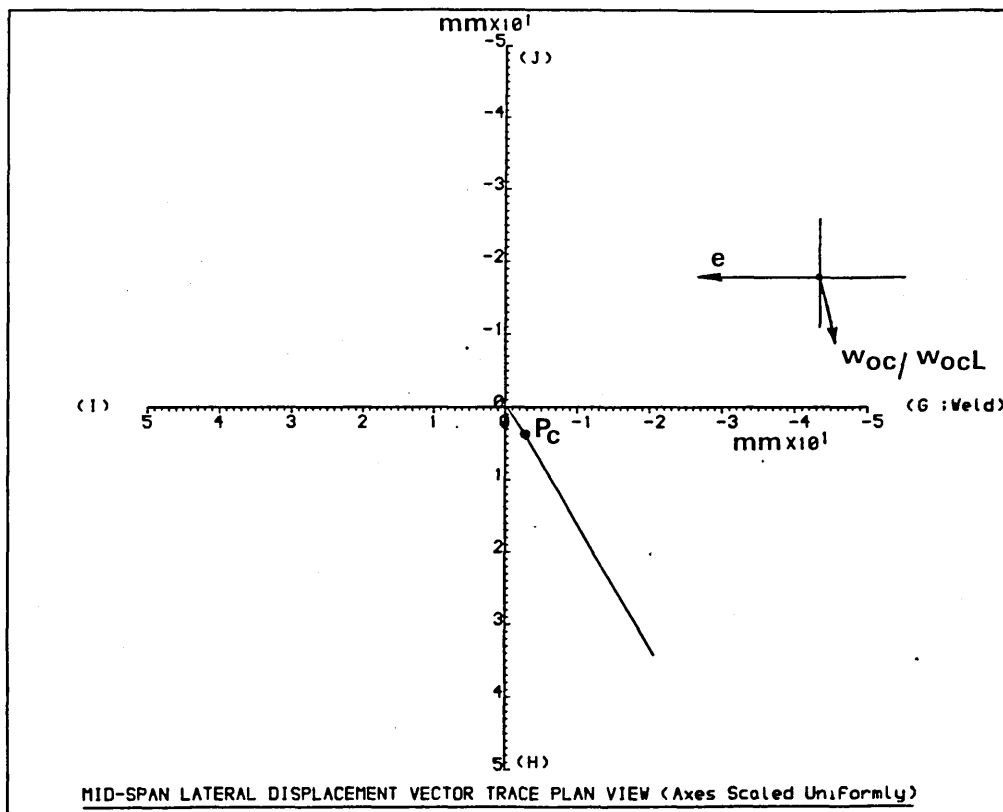


Figure 3.23 ; Vector Trace - Strut Ref. 20

This behaviour is indicative of dynamic unloading associated with rigid/stiff testing machine characteristics⁽⁵⁵⁾, where a 'sharp knee' displayed at buckling is to be expected. Fig 3.19 displays an increment being 'caught' in the process of buckling. An additional P vs u plot for case 21S is included - Fig 3.24 - to depict the foregoing 'curve' around P_c being more effectively defined; such highly specific P vs u curves were obtained from about one-third of the strut cases involved.

The most sensitive or difficult parameter to evaluate at the essentially 'dynamic' buckling state is $w_{cL-w_{ocL}}|_{P_c}$. The object is surely to obtain this value as the load begins to drop but before the full dynamic buckling process is underway. Figs 3.15 (12S), 3.20 (20S) and 3.25 (21S) are representative of the range of P vs $w_{cL-w_{ocL}}$ loci obtained. As is to be expected from the above, the locus for case 21S provides for a slightly more accurate determination of $w_{cL-w_{ocL}}|_{P_c}$, with $w_{cL-w_{ocL}}|_{P_c}$ possibly being slightly underestimated in the remaining cases.

Figs 3.16 and 3.21 depict typical P vs ϵ_n loci (central strain gauge readings, $n=1,4$) for cases 12S and 20S respectively. The pre-buckling loci for each ϵ_n trace is linear up to loads approaching P_c although the readings indicated that inelastic buckling was indeed prevalent.

Sample key static strut test data is given in Table 3.9 with experimental buckling load P_c presented in terms of the Euler critical load P_e and squash load (stub test) P_s . Further, the design load P_p (with $\ell=L/2$) is given in terms of the Euler

AXIAL LOAD vs. AXIAL DISPLACEMENT

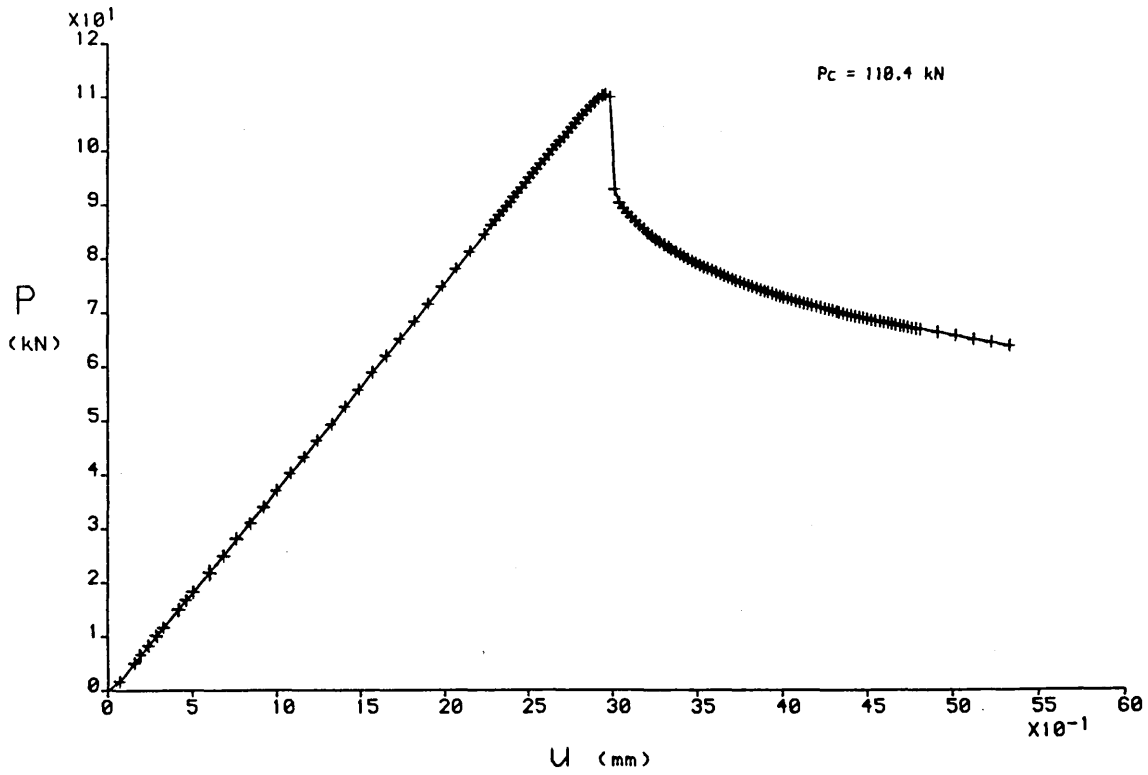


Figure 3.24 ; P vs u - Strut Ref. 21S

AXIAL LOAD vs. MID-SPAN RESULTANT LATERAL DISPLACEMENT

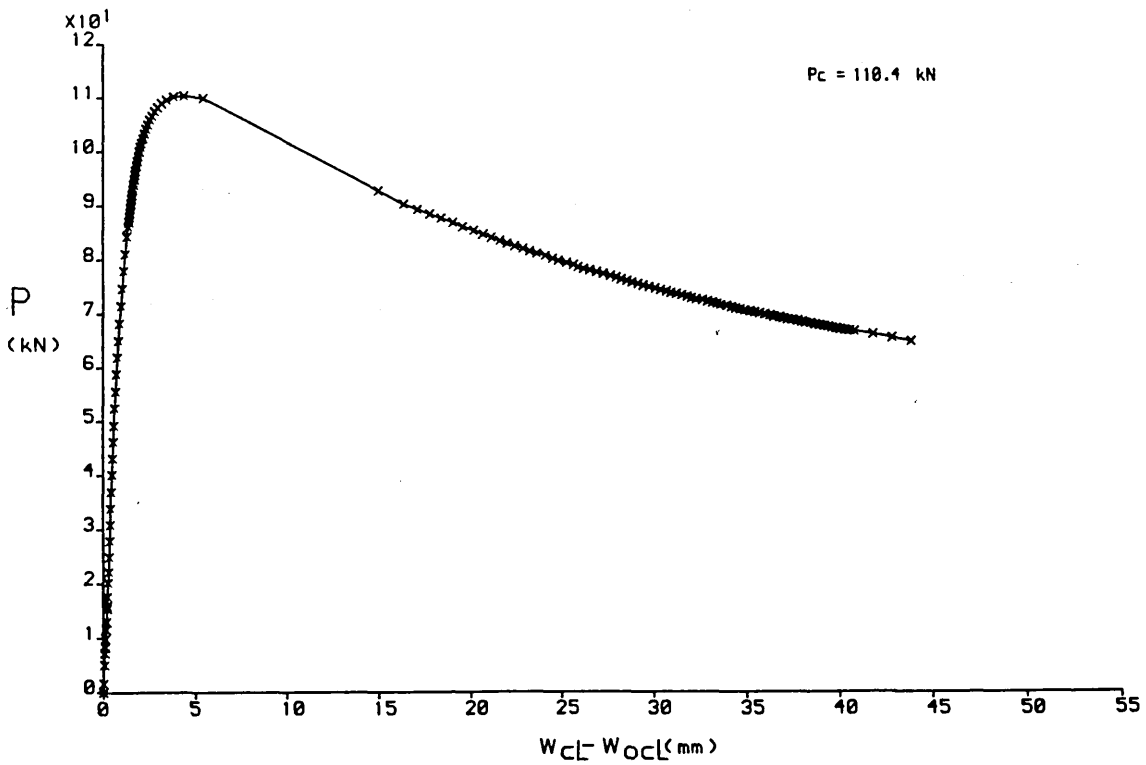


Figure 3.25 ; P vs $w_{cL} - w_{ocL}$ - Strut Ref. 21S

Strut Ref.	λ/λ_1	Direct w_{oc} (mm)	Interpolated w_{oc} (mm)	e (mm)	P_c/P_e	P_p/P_e	P_c/P_s
3S	0.94	n/a	0.67	0.74	0.70	0.65	0.80
5S	0.94	0.14	0.19	0.37	0.72	0.64	0.83
9S	1.01	n/a	0.22	0.79	0.74	0.71	0.72
15S	0.91	n/a	0.23	0.55	0.73	0.62	0.89
17S	1.02	0.52	0.84	0.23	0.75	0.71	0.72
18S	0.99	0.66	0.89	1.18	0.69	0.68	0.71
20S	0.88	0.12	0.16	0.26	0.62	0.60	0.81
21S	0.88	0.61	0.95	0.45	0.62	0.59	0.82
22S	0.85	n/a	0.43	0.72	0.62	0.56	0.87
24S	1.02	0.20	0.56	0.71	0.80	0.69	0.77

Table 3.9; Sample Experimental Static Strut Data

critical load. In all cases, individual geometric and constitutive (compressive) data are employed in these evaluations. The table testifies to the range of modified slenderness ratios λ_m employed, exhibits the direct and interpolated values for w_{oc} (note correlation where applicable) and shows that eccentricity e is of the same order of magnitude as w_{oc} .

Figs 3.17, 3.18, 3.22 and 3.23 illustrate the respective pre-buckling and full buckling loci vector traces, employment of which is considered to be of novel form. The variable and very fine scales employed in the pre-buckling traces are to be noted, with minor zero-zero datum irregularities being shown in Fig 3.17 - note abscissa scale vs ordinate scale in particular. Importantly, Figs 3.18 and 3.23 exhibit 'planar' behaviour, although the orientations should be noted in the context of the w_{oc} and e orientations provided. The resultant vector trace planarity is the product of a complex interaction of imperfections, particularly $w_{ocL}(w_{oc})$ and e herein. Indeed, the vector traces given in Figs 3.26 and 3.27 relate to case 6S for which w_{on} imperfection data was given in Fig 3.11. The apparent agreement between the orientations of w_{ocL} (and w_{oc}) and the planar buckling path belies the fact that 6S was heavily corkscrewed, note Fig 3.11, with $w_{ocL} \neq w_{om}$ and no direct w_{oc} value being available. Further, the eccentricity e was six times the magnitude of w_{oc} (interpolated). Recall that values of e and w_{oc} are fully tabulated in Section 3.7 together with all other important experimental data. The diverse orientations of the vector traces given in Figs 3.18, 3.23 and 3.27 indicate

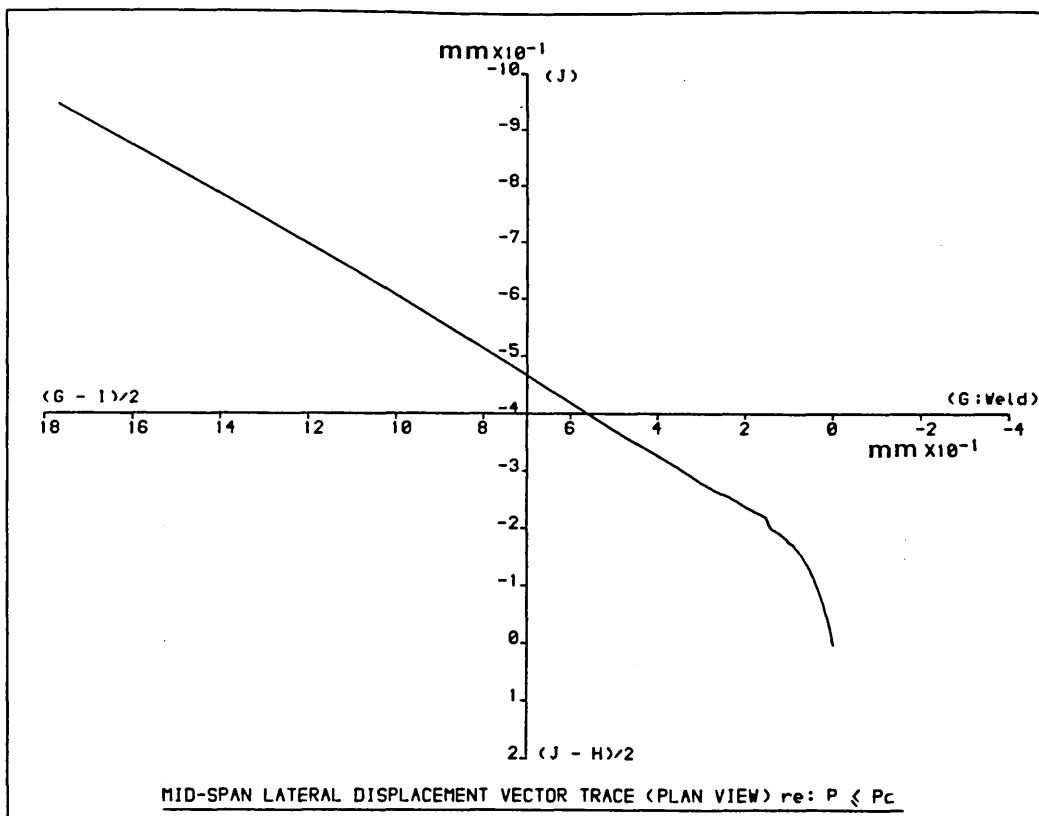


Figure 3.26 ; Vector Trace ($P < P_c$) - Strut Ref. 6S

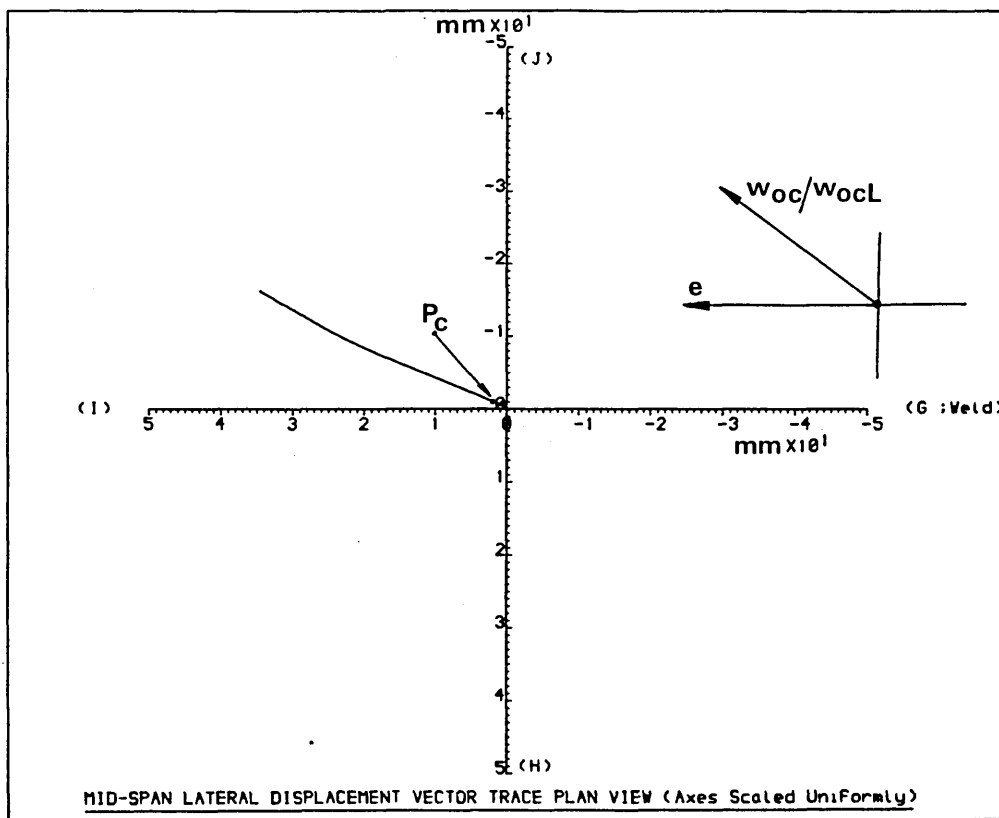


Figure 3.27 ; Vector Trace - Strut Ref. 6S

independence of buckling path from machine interference; this is clearly as required.

The interrelationship of data obtained from central strain gauge readings and the corresponding vector traces provide for control of output in accordance with the topology illustrated in Fig 3.7. All strut studies involved suitable correlation, the zone of highest compression as provided by strain gauge output correlating well with that prescribed by the direction of the buckling path given by the corresponding vector trace.

It is instructive to consider the strain gauge/vector trace correlation further. Considering case 12S, Fig 3.18 indicates strain gauge reading ϵ_2 , recall Fig 3.7, will afford the maximum compressive strain. The corresponding value of limiting linear elastic strain is available from the appropriate stub test, 12SS, which gives a value of 1.275×10^{-3} and the associated stress to be 275 N/mm^2 . From Fig 3.16, the maximum linear elastic load thereby corresponds to 106 kN , this being 6% lower than the buckling load P_c . The ECCS load⁽³⁶⁾ subject to $\ell=L/2$ and the use of stub test data gives $P_p=103.5 \text{ kN}$. This form of correlation is as anticipated and supports claims of accurate experimentation. Further, employing Eqn (1.2), a check can be made upon load-displacement characteristics. Substituting the above noted maximum linear elastic values for stress and load, together with values for A and Z, then $w_c=1.86 \text{ mm}$ at the limiting elastic state, w_c being relative to effective length ℓ . Accepting that $w_c=w_{cL}/2$ for $\ell=L/2$, note Eqn (3.7), and similarly transforming the respective imperfections

w_{oc} and w_{ocL} affords an estimate that $w_{cL}-w_{ocL}=2.48\text{mm}$ at the limiting elastic state. From numerical output (nb Fig 3.15), the experimental value for $w_{cL}-w_{ocL}$ is 2.36mm. Validity of the output data is thereby supported.

3.6.2 Semi-Empirical Analyses - Southwell and Lundquist Plots

The basis for the Southwell and Lundquist plot techniques is well established(56,35,57,58). The governing equations of the Southwell and Lundquist plots take the form

$$(w_c - w_{oc})/P = (w_c - w_{oc})/P_{es} + a_{os}/P_{es} \quad (3.11)$$

and

$$(w_c - w_{oc} - w')/(P - P') = (w_c - w_{oc} - w')/(P_{el} - P') + a_{o1}/(P_{el} - P') \quad (3.12)$$

where P' and w' denote the elastic 'pivot' state and P_{es} , a_{os} and P_{el} , a_{o1} delineate the Southwell and Lundquist estimates of the critical load and initial central displacement respectively with respect to the effective length ℓ . The Lundquist 'pivot' attempts to mitigate low load non-linearities (56). Importantly, the a_{os} and a_{o1} parameters can be considered as lumped or effective imperfections taking account, when applied to practical struts, of not only w_{oc} , but also e and residual stress effects (however small). These a_{os} and a_{o1} parameters were particularly useful herein given the initially corkscrewed/irregular strut topologies extant, this effect also rendering central w_{oc} (direct) values not

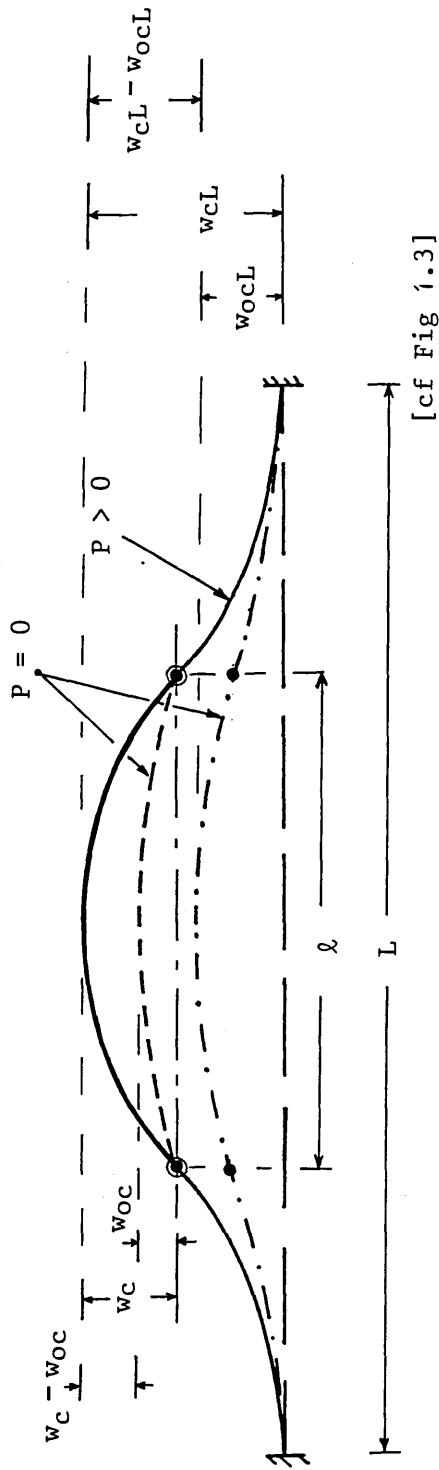
always being deemed applicable. Given the availability of experimental data, a_{0s} and a_{0l} provide convenient planar imperfection parameters highly suited to practical engineering interpretation.

Eqns (3.11) and (3.12) also provide estimates for the Euler critical load and thereby, given appropriate constitutive and geometric data, estimates for effective length from

$$\ell_s/\ell = (P_e/P_{eS})^{\frac{1}{2}} \quad \text{and} \quad \ell_l/\ell = (P_e/P_{eL})^{\frac{1}{2}} \quad (3.13)$$

where ℓ_s and ℓ_l are the Southwell and Lundquist estimates for effective length respectively.

Employing interactive linear regression, suitable Southwell and Lundquist plots were made readily available as an experimentation back-end facility. Various linear fits and Lundquist pivots were implemented for all cases, the necessary transformation $w_c - w_{oc} = (w_{cL} - w_{ocL})/2$ being applied pre-plotting. Indeed, these effective length check procedures were appreciated to be of the utmost importance to the research programme. The various applications of the $\ell=L/2$ transformation, see Sections 3.5.1 and 3.6.1 for example, demand that some control on effective length be made available. Fig 3.28 clarifies the effective length transformation details whilst Table 3.10 affords sample key data, the final values of fit range, and pivot state in the case of Lundquist plots, being those which gave the best degree of linearity. It is considered that the linear ranges quoted are



$$w_c = w_{cL}/2$$

$$w_{oc} = w_{ocL}/2$$

$$w_c - w_{oc} = (w_{cL} - w_{ocL})/2$$

⊙ : contraflexure / pin ends

Figure 3.28 ; Pin Ended / Encastré End Condition Correlation

Strut Ref.	Fit Range (% of P_e)		Euler Data		w_{oc} Data (mm)	
	Southwell	Lundquist	$l_g/\%$	$l_1/\%$	a_{os}	a_{o1}
3S	55 - 62	52 - 60	0.98	1.06	0.79	0.18
5S	58 - 69	50 - 67	1.01	1.07	0.58	0.14
9S	59 - 67	50 - 67	0.99	1.03	0.66	0.22
15S	53 - 61	53 - 61	1.01	1.03	0.30	0.10
17S	57 - 66	57 - 70	1.01	1.08	0.48	0.07
18S	38 - 55	44 - 57	1.05	1.10	0.77	0.45
20S	36 - 50	39 - 52	1.01	1.06	0.67	0.48
21S	38 - 54	38 - 54	1.02	1.10	0.66	0.32
22S	37 - 51	46 - 55	1.01	1.09	0.68	0.36
24S	66 - 78	68 - 77	1.07	1.07	0.19	0.35

Table 3.10; Sample Southwell and Lundquist Plot Data

sufficiently large and that the effective length l_s and l_1 estimates lend confidence to the deemed $l=L/2$. Imperfection parameters a_{0s} and a_{0l} appear attractive and are of the same order of magnitude as their direct and interpolated w_{0c} equivalents, note Table 3.9. As noted above, a_{0s} and a_{0l} include all imperfections considered in a planar regime.

Fig 3.29 presents the Southwell and Lundquist plots for case 21S whilst Fig 3.30 shows a typical computer graphics Southwell plot for case 5S. The latter shows more pronounced low load irregularity⁽⁵⁶⁾ than the former Southwell plot; overall, however, case 21S is the more typical. The Lundquist plots did not generally provide for larger linear 'fit' ranges, the Southwell plots themselves being, as indicated above, well-behaved. As employed herein, these two semi-graphical techniques proved very useful, providing for experimental verification as well as for alternative imperfection assessment. Given the lack of explicit residual stress analysis, this latter feature serves as a control upon this factor. The Southwell and Lundquist techniques provide an excellent example of experimental-numerical interaction⁽⁵⁹⁾, their output serving further in the theoretical modelling procedures discussed in the next chapter. Finally, it should be noted that out of the 26 static strut test cases, only 7 and 8 cases respectively failed to provide suitable Southwell and Lundquist plots⁽⁵⁶⁾. These failures were generally associated with low λ_m configurations.

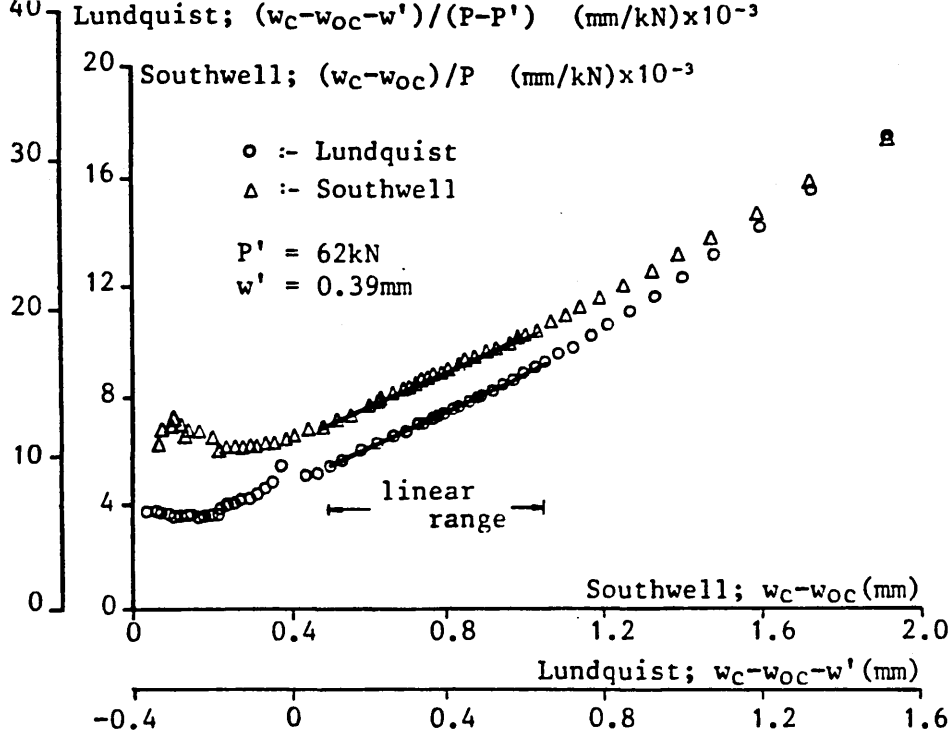


Figure 3.29 ; Southwell and Lundquist Plots - Strut Ref. 21S

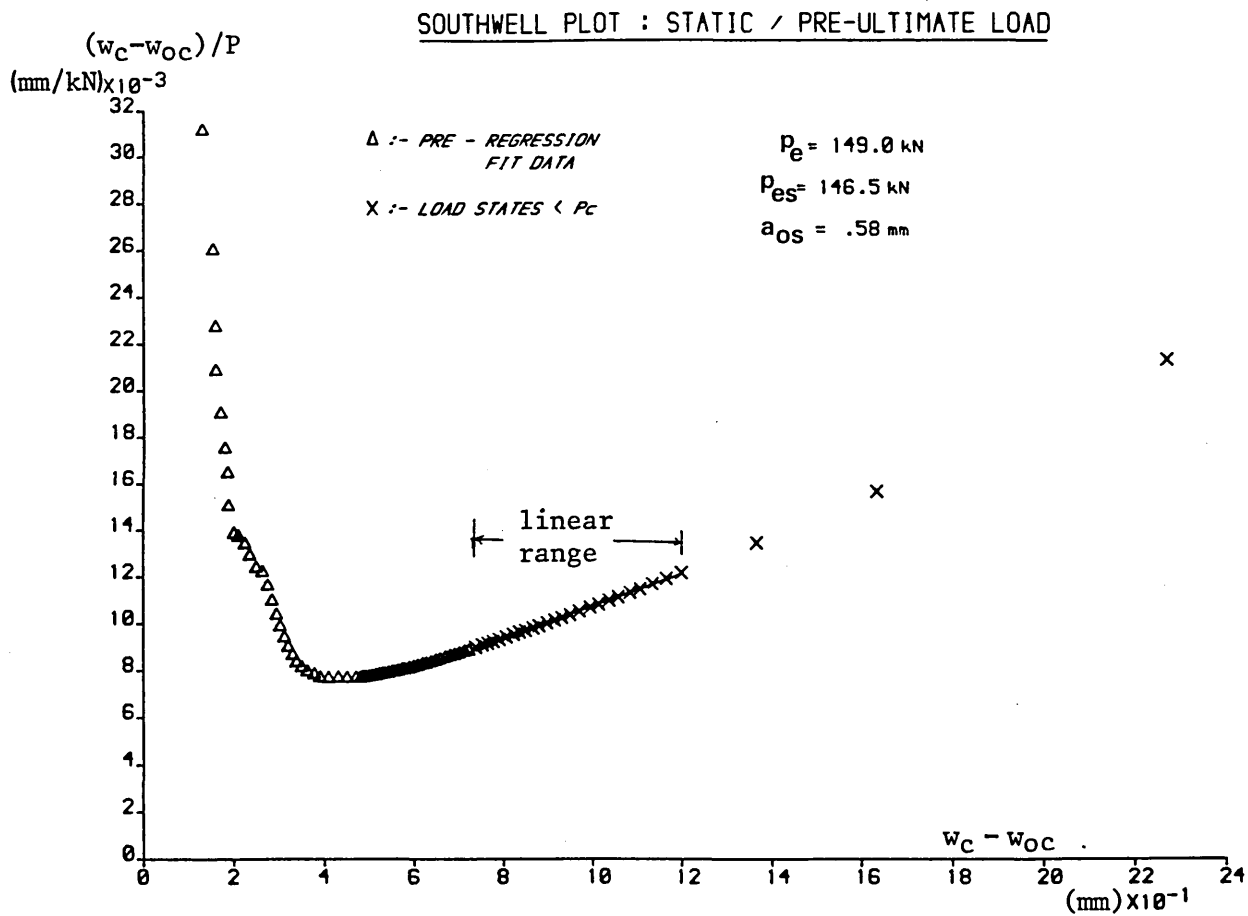


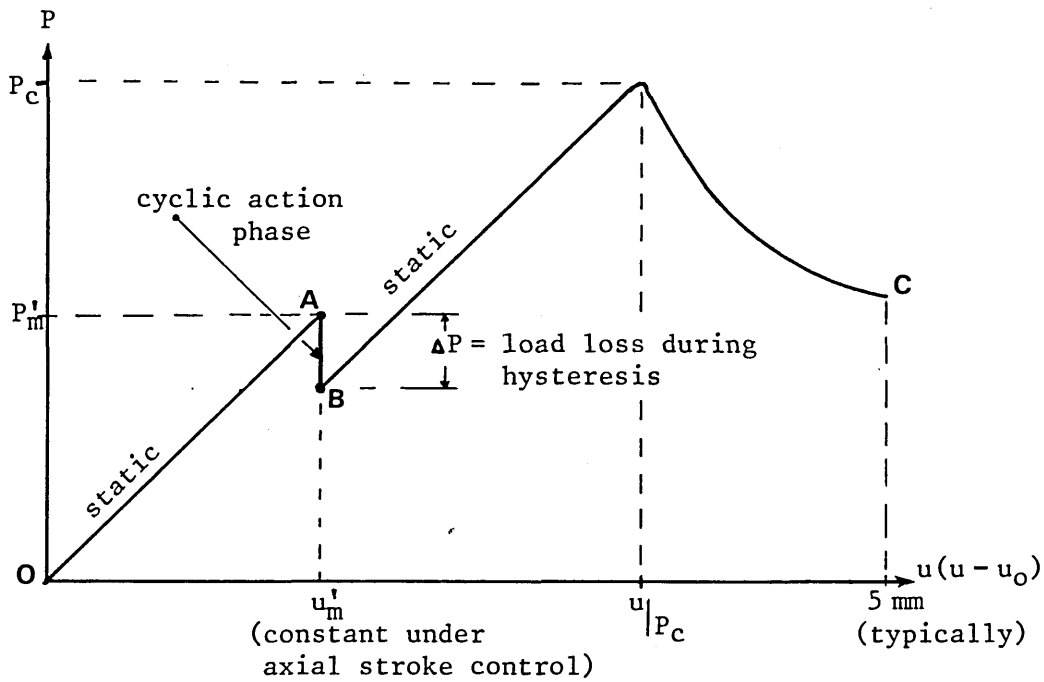
Figure 3.30 ; Southwell Plot - Strut Ref. 5S

3.7 CYCLIC STRUT TESTING - RESULTS

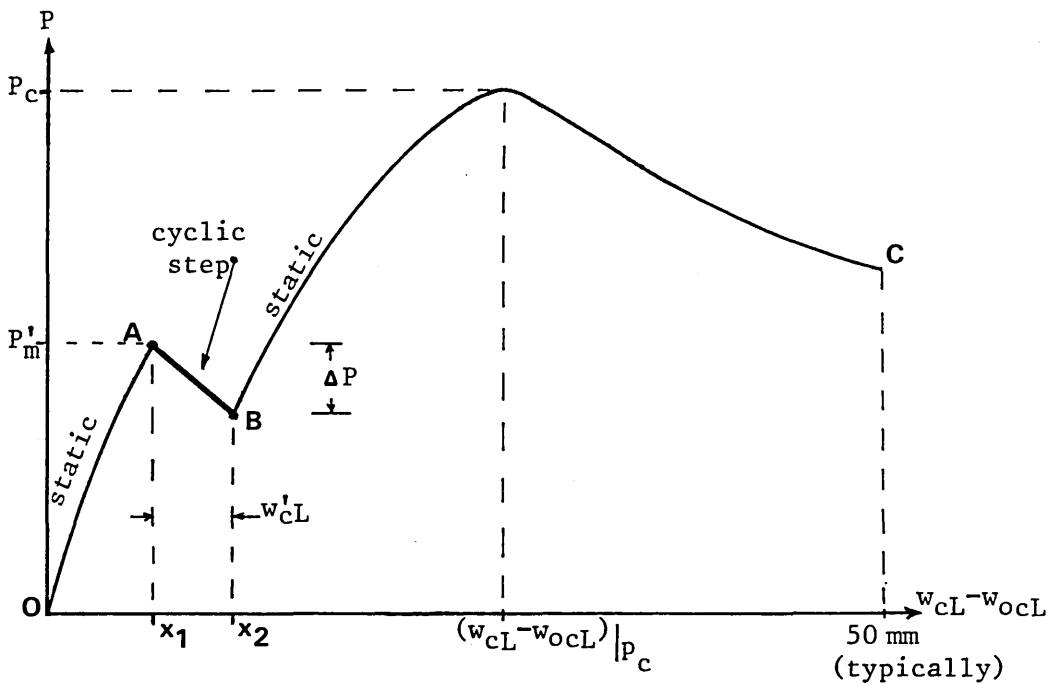
3.7.1 Pseudo-Static Parametric Response

Given that the primary objective of the research programme was to determine the effect of a pre-buckling cyclic phase of loading upon otherwise static strut performance, then the respective experimental data is considered in two parts. First, the pseudo-static characteristics are studied; these relate to assessment of the appropriate static parameters, the cyclic action phase being considered as an interface between the respective static regimes. The situation is illustrated in Fig 3.31 with statically monitored regimes OA and BC being interfaced with a linear locus AB, points A and B representing the statically defined start and stop limits of the cyclic action phase. Fig 3.31 is thereby deemed to illustrate the pseudo-static characteristics of the strut system. Study of the actual cyclic action phase is considered in Section 3.7.2. Strictly, Fig 3.31 could not have been produced 'earlier', due to the absence of appropriate experimental data despite an intensive literature search, note the Bibliography, this search including the use of computer-based international facilities.

Key details of the cyclic profiles employed with respect to the 27 mainstream tests (1C-27C) are given in Table 3.11. The 'unfactored' base symbol U denoting u_m^1 nominally corresponding to the ECCS limit state load, F denoting a Perry⁽⁶⁰⁾-type reduction from this to relate to service condition behaviour with u_m^1 nominally corresponding to 45kN; note Section 3.1. The necessity



(a) Generalised P vs u Locus



point A = (x_1, P'_m) : point B = $(x_2, (P'_m - \Delta P))$

or,

point A = $((w_{cL} - w_{ocL})|_{P'_m}, P'_m)$: point B = $((w_{cL} - w_{ocL})|_{P'_m + w'_{cL}}, (P'_m - \Delta P))$

(b) Generalised P vs $w_{cL} - w_{ocL}$

Figure 3.31 ; Cyclic Strut Studies - Pseudo - Static Considerations

Strut Ref.	Stroke Drive						Primary Monitored Response			Classification			
	u'_m (mm)		$\pm u_{am}$ (mm)		$\frac{u'_m}{u} P_c$		Duration (number of cycles)		P_m/P_c (%)		$\frac{w'_{cL}}{(w_{cL}-w_{ocL})} P_c$ (%)		
	F	U	F	U	F	U	F	U	F		U	F	U
1	1.19	1.96	0.25	0.45	0.45	0.75	25	25	45.1	75.6	1.3	2.3	
2	n/a	n/a	n/a	n/a	n/a	n/a	n/a	n/a	n/a	n/a	n/a	n/a	
3	1.29	1.96	0.35	0.35	0.54	0.73	250	750	54.1	77.0	1.5	0.0	
4	1.29	2.02	0.47	0.27	0.55	0.75	500	500	57.6	75.5	1.6	-0.1	
5	1.28	2.04	0.35	0.35	0.53	0.78	500	500	52.8	78.4	-0.5	0.1	
6	1.96	1.96	0.35	0.35	0.71	0.71	1000	1000	51.7	70.5	0.6	2.2	
7	1.28	1.96	0.35	0.35	0.53	0.71	1000	1000	56.0	70.5	-0.1	0.6	
8	1.28	1.96	0.35	0.35	0.54	0.71	1000	1000	51.0	70.5	-0.1	0.6	
9	1.29	1.96	0.35	0.35	0.50	0.71	1000	1000	52.0	76.4	3.1	-0.5	
10	1.28	2.03	0.36	0.35	0.52	0.75	250	750	66.0	76.4	3.0	-0.5	
11	1.28	1.96	0.35	0.35	0.67	0.75	1000	1000	55.1	73.2	1.2	-1.1	
12	1.97	1.96	0.35	0.35	0.55	0.73	1000	1000	54.3	81.7	1.3	0.5	
13	1.28	2.05	0.35	0.35	0.55	0.81	1000	500	69.5	73.3	-0.8	1.0	
14	1.29	2.03	0.35	0.25	0.54	0.76	1000	500	82.0	82.0	1.6	1.6	
15	1.96	1.96	0.35	0.35	0.55	0.74	1000	1000	92.7	92.7	4.4	4.4	
16	1.36	1.96	0.35	0.35	0.55	0.74	1000	1000	88.0	88.0	2.6	2.6	
17	2.05	2.05	0.47	0.47	0.83	0.83	1000	1000	n/a	n/a	n/a	n/a	
18	2.14	2.14	0.50	0.50	0.91	0.91	1000	1000	94.8	94.8	11.9	11.9	
19	2.05	2.05	0.61	0.61	0.87	0.87	1000	1000	94.9	94.9	16.3	16.3	
20	1.98	1.98	1.13	1.13	1.00	1.00	1000	1000	96.3	96.3	2.5	2.5	
21	1.90	1.90	1.00	1.00	0.95	0.95	1000	1000	94.8	94.8	6.9	2.2	
22	1.89	1.89	0.95	0.95	0.97	0.97	1000	1000	91.0	91.0	18.3	18.3	
23	2.27	2.27	0.61	0.61	0.93	0.93	1000	1000	98.2	98.2	37.9	37.9	
24	2.15	2.15	0.65	0.65	0.95	0.95	1000	1000					
25	1.51	1.51	0.81	0.81	0.90	0.90	1000	1000					
26	1.71	1.71	1.02	1.02	0.95	0.95	1000	1000					
27	1.80	1.80	1.00	1.00	0.97	0.97	1000	1000					

n/a = not applicable \$ = buckled during cyclic phase F = factored base U = unfactored base

Table 3.11 ; Cyclic Experimental Data

Note

The classifications 'quasi-cyclic' and 'formally cyclic' can be more clearly defined by reference to the time-dependent responses discussed in the next section (i.e. 3.7.2). 'Quasi-cyclic' cases involve load/transverse displacement loci which possess closed loop line hysteresis; see Fig 3.50, page 141. The overall hysteresis band-widths are stabilised and narrow with a corresponding cyclic step of either hardening or softening form. 'Formally cyclic' cases involve load/transverse displacement loci which possess finite area hysteresis loops; see Figs 3.51 - 3.54, pages 143 - 145. The associated overall hysteresis band-widths are non-stabilised, the corresponding cyclic steps displaying definitive softening-only characteristics throughout.

of inducing inelastic excursions requires high peak $u_m = u_{am} + u_m^i$ values as given by the specific limiting elastic considerations discussed in Section 3.6.1. Lower values of u_m relate to quasi-elastic hysteresis⁽⁵¹⁾ considerations. In Table 3.11, u_m is non-dimensionalised with respect to the corresponding axial displacement at buckling. Accordingly, cases 1C to 17C relate to quasi-elastic hysteresis behaviour, the remaining tests appertaining to primary inelastic considerations. Case 2C was earmarked for static testing on account of the low buckling load P_c achieved in case 2S, concern over the validity of that test demanding a further static assessment. (Low values for σ_y from stub tests 2SS and 2SC confirmed that constitutive 'weakness' induced this lower P_c behaviour.) Throughout the cyclic tests, frequency $f=1/16\text{Hz}$ ⁽⁴⁶⁾. Case 20C represents an upper bound on the programme, with buckling being induced during the cyclic action phase.

It is valid to consider tests upto 17C separately from those beyond given the action data for $u_m/u|_{P_c}$ - and the response data for $w_{CL}^i/(w_{CL}-w_{ocL})|_{P_c}$ where w_{CL}^i represents the increase in measured central displacement (over L) induced during the cyclic action phase; w_{CL}^i is herein termed the 'cyclic step'. The tabulated non-dimensionalised cyclic step is $\delta=L/2$ -transformation independent - note Section 3.5.1 and Fig 3.28. Tests upto 17C are termed 'quasi-cyclic' on account of the small, and variably-signed, cyclic step; those beyond are considered to exhibit a more substantial cyclic step and are thereby deemed to be 'cyclic-proper' or formally cyclic tests.

Cases 1C to 17C (less 2C) correspond to a cyclic action phase inducing quasi-elastic hysteresis in which constitutive impurities in the nominally linear elastic range of the material give rise to hysteresis or work loss in the supposedly fully reversible constitutive regime^(51,61). Importantly, however, the induced system changes can result in both cyclic hardening or softening according to experimental work on axial compression samples under reversed axial loading⁽⁶³⁾. The negative values of cyclic step obtained in cases 4C, 5C, 8C, 9C, 10C, 12C and 16C testify to the highly variable nature of the quasi-elastic hysteresis phenomenon, heightened, perhaps, by the imperfection sensitivity of the strut samples concerned. That is, the sensitivity could perhaps result in a 'positive' response to such action. However, as shown by the magnitude of the cyclic steps involved in cases 1C to 17C, the overall effect of cyclic action is small. Case 4C shows opposing effects with respect to the two cyclic phases involved.

Table 3.11 also gives details of the peak axial compression P_m induced during the cyclic action phase in terms of the ensuing post-cyclic action phase buckling load P_c . The demarcation between the quasi-cyclic and formally cyclic classifications is clearly shown. Table 3.12 gives an overview of all strut testing key data showing that in no instance other than the singular case 20C was a substantial loss in buckling load P_c reported due to pre-buckling cyclic action, the cyclic P_c being compared with its static partner's P_c . Even in the formally cyclic cases showing substantial cyclic hysteresis or cyclic step, note cases 21C, 22C, 26C and 27C, there was little variation between corresponding

Strut Ref.	λ/λ_1		w_{oc} (direct) (mm)		w_{oc} (interpolated) (mm)		e (mm)		P_c (kN)		$(w_{cL} - w_{ocL})/P_c$ (mm)		P_c/P_e		P_p/P_e	
	S	C	S	C	S	C	S	C	S	C	S	C	S	C	S	C
1	0.93	0.92	n/a	0.04	0.28	0.10	0.60	0.58	106.7	113.7	4.27	3.86	0.71	0.75	0.64	0.63
2*	0.77	0.78	n/a	0.07	0.34	0.43	0.08	0.10	78.4	84.6	3.49	1.86	0.54	0.58	0.48	0.49
3	0.94	0.93	n/a	0.30	0.67	0.56	0.74	0.64	104.8	105.3	4.77	5.41	0.70	0.71	0.65	0.64
4	s/t	0.98	s/t	0.36	s/t	0.63	s/t	0.42	s/t	106.0	s/t	5.64	s/t	s/t	s/t	0.67
5	0.94	0.97	0.14	0.67	0.19	0.44	0.37	0.01	106.4	107.1	4.56	5.03	0.72	0.73	0.64	0.67
6	0.89	0.93	n/a	0.26	0.13	0.37	0.73	0.36	115.1	116.5	2.01	2.71	0.76	0.80	0.60	0.64
7	0.94	0.94	0.24	n/a	0.33	0.31	0.09	0.31	109.3	110.3	3.22	4.28	0.70	0.72	0.65	0.65
8	0.91	0.91	0.17	0.30	0.44	0.55	0.26	0.37	112.2	102.9	1.78	5.10	0.74	0.69	0.62	0.62
9	1.01	1.01	n/a	n/a	0.22	0.48	0.79	0.59	104.5	113.7	5.84	2.78	0.74	0.76	0.71	0.68
10	0.96	0.98	0.20	n/a	1.01	1.08	0.41	0.57	106.8	111.0	3.53	3.37	0.70	0.74	0.67	0.68
11	0.82	0.78	0.24	0.23	0.45	0.31	0.27	0.05	78.1	85.7	3.33	2.20	0.53	0.58	0.49	0.49
12	0.98	0.98	n/a	n/a	0.62	0.30	0.62	0.72	112.5	112.7	3.20	3.95	0.75	0.74	0.69	0.68
13	0.97	1.04	0.10	0.08	0.59	0.67	0.76	0.51	107.8	105.3	4.95	5.32	0.70	0.79	0.67	0.73
14	1.01	0.94	0.30	n/a	0.97	0.66	0.74	0.82	106.2	106.9	4.73	4.42	0.72	0.71	0.71	0.65
15	0.91	0.91	n/a	n/a	0.23	0.28	0.55	0.79	112.5	111.9	3.89	4.23	0.73	0.73	0.62	0.62
16	n/a	0.78	n/a	0.03	n/a	0.21	n/a	0.36	n/a	84.3	n/a	1.54	n/a	n/a	n/a	0.49
17	1.02	1.01	0.52	n/a	0.84	0.60	0.23	0.29	100.6	101.2	5.27	6.19	0.75	0.74	0.71	0.70
18	0.99	1.00	0.66	0.42	0.89	0.63	1.18	0.69	94.7	90.6	7.47	9.21	0.69	0.67	0.68	0.69
19	0.96	0.96	0.11	n/a	0.49	0.13	0.13	0.55	97.7	100.1	5.93	5.38	0.73	0.74	0.66	0.66
20\$	0.88	0.88	0.12	n/a	0.16	0.15	0.26	0.34	109.6	86.3	4.47	20.38	0.62	0.49	0.60	0.60
21	0.88	0.89	0.61	0.23	0.95	0.24	0.45	0.36	110.4	117.1	4.34	2.85	0.62	0.67	0.59	0.60
22	0.85	0.84	n/a	n/a	0.43	0.09	0.72	0.50	107.6	111.7	3.38	2.72	0.62	0.64	0.56	0.57
23	1.01	1.01	0.15	n/a	0.40	0.40	0.34	0.39	98.1	92.4	5.08	8.47	0.80	0.76	0.70	0.69
24	1.02	1.02	0.20	0.21	0.56	0.42	0.71	0.50	96.3	91.8	6.37	8.05	0.80	0.75	0.69	0.70
25	0.87	0.89	n/a	0.27	0.22	0.41	0.60	0.42	74.0	77.0	4.06	3.95	0.63	0.64	0.58	0.59
26	0.84	0.84	0.17	0.37	0.59	0.24	0.58	0.26	116.6	114.5	3.71	3.69	0.57	0.57	0.56	0.57
27	0.84	0.85	n/a	n/a	0.25	0.26	0.49	0.51	117.0	114.0	2.75	4.77	0.58	0.58	0.56	0.58

* = first low result for P_c , therefore cyclic specimen tested in static mode

‡ = buckled during cyclic phase

S = static C = cyclic

n/a = not applicable s/t = spoilt test

‡ = buckled during cyclic phase

Table 3.12 ; Primary Experimental Data

strut case cyclic and static P_c values. Indeed, the former pair exhibit an increase in P_c over their respective static partners. This fact can be explained by reference to the appropriate imperfections, the 'cyclic' strut cases being initially less imperfect in both cases. It was precisely this sort of problem which led to the large number of tests undertaken.

Case 20C actually buckled during the cyclic action phase and, unsurprisingly, post cyclic action phase buckling load P_c suffered a drastic drop. Apart from this case, it appears that deformation was more susceptible to pre-buckling cyclic action than load carrying capacity itself. This consideration is limited by the fact that definitive control upon static/cyclic P_c correlation is not available, as discussed above, whilst the cyclic step is more readily assessed in terms of the cyclic test central transverse displacement at buckling. It is not assessed against the corresponding static buckling displacement, note Table 3.12.

Crucially, however, Tables 3.11 and 3.12 show that the key cases 21C, 22C, 26C and 27C can be seen to correspond to high peak inelastic excursions in struts possessing a relatively substantial inelastic range. It is considered that this represents the primary research finding, noting just how high a degree of inelastic incursion is required to cause problems for imperfection sensitive struts. For the prescribed values of frequency f and duration n_c , the CHS specimens employed display considerable resilience to pre-buckling cyclic action. It should also be recalled at this stage that although the specimens employed corresponded to being imperfection

sensitive, they were remarkably imperfection-free as shown in Table 3.12, remembering also the low level of residual stress present(32).

Supporting data to that given in Tables 3.11 and 3.12 is provided by that given in Table 3.13 where experimental buckling loads P_c are assessed against squash load P_s (stub test) and ECCS load P_p (36) (but $l = L/2$). It is considered that modified slenderness ratio λ_m , an important reference in the above finding, affords an excellent means of overall buckling classification taking on board as it does the relationships exhibited by P_c to elastic/ inelastic demarcation (' P_p '), elastic buckling (P_e and λ) and squash load (P_s) considerations. It should be noted that employing $l = L/2$ effectively doubles the ECCS load P_p , this effect being somewhat offset by the fact that η (36) is far in excess of the imperfections w_{oc} encountered herein as discussed in Section 3.5.1. The complex nature of the imperfection role in strut stability is emphasised by the nature of the w_{oc} , both direct and interpolated, e and w_{ocL} parameters. The number of cases in which a direct w_{oc} centred imperfection could not be determined is notable. This problem, detailed in Section 3.5.1, is 'masked' when pin-ended strut testing is employed; rarely are such conditions met in engineering practice and it is to be noted that studies into the nature of practical effective lengths are being conducted elsewhere(62).

The primary research finding propounded above is considered further in Fig 3.32. The central cyclic step displacement is duly

Strut Ref. Number	λ	w_{ocL} (mm)		P_c/P_s		P_p/P_c		Strut Ref. Number	λ	w_{ocL} (mm)		P_c/P_s		P_p/P_c	
		S	C	S	C	S	C			S	C	S	C	S	C
1	80	0.49(*)	0.14	0.84	0.88	0.90	0.84	15	80	0.28(*)	0.32(*)	0.89	0.88	0.85	0.85
2(**)	80	0.64(*)	0.61	0.92	0.92	0.89	0.84	16(**)	80	n/a	0.54	n/a	0.98	n/a	0.83
3	80	1.25(*)	1.25(*)	0.80	0.82	0.93	0.90	17	85	1.35	0.62(*)	0.72	0.73	0.95	0.95
4	80	s/t	s/t	s/t	0.75	s/t	0.96	18	85	1.60	1.17	0.71	0.68	0.99	1.02
5	80	0.34	0.34	0.83	0.79	0.89	0.92	19	85	0.64	0.50(*)	0.81	0.80	0.90	0.89
6	80	0.16(*)	0.16(*)	0.97	0.93	0.79	0.80	20 \$	75	0.28(*)	0.17(*)	0.81	0.63	0.97	1.22
7	80	0.55	0.55	0.80	0.81	0.93	0.90	21	75	1.54	0.66	0.82	0.86	0.95	0.90
8	80	0.63	0.63	0.90	0.84	0.84	0.90	22	75	0.53(*)	0.44(*)	0.87	0.90	0.90	0.89
9	80	0.18(*)	0.18(*)	0.72	0.73	0.96	0.90	23	90	0.61	0.54(*)	0.78	0.75	0.88	0.91
10	80	1.45	1.45	0.76	0.79	0.96	0.92	24	90	0.83	0.60	0.78	0.74	0.86	0.93
11(**)	80	0.69	0.69	0.88	0.95	0.92	0.84	25(**)	90	0.24(*)	0.74	0.81	0.81	0.92	0.92
12	80	0.86	0.86(*)	0.78	0.78	0.92	0.92	26	70	0.90	0.43	0.81	0.81	0.98	1.00
13	80	0.76	0.76	0.75	0.73	0.96	0.92	27	70	0.37(*)	0.29(*)	0.83	0.81	0.97	1.00
14	80	1.40	1.40	0.81	0.81	0.87	0.92								

(*) $w_{ocL} \neq w_{om}$ s/t=spoil test \$=buckled during cyclic phase

(**) low $\sigma_y/\sigma_0.2\%$ (<210N/mm²)

Table 3.13 ; Supporting Experimental Data

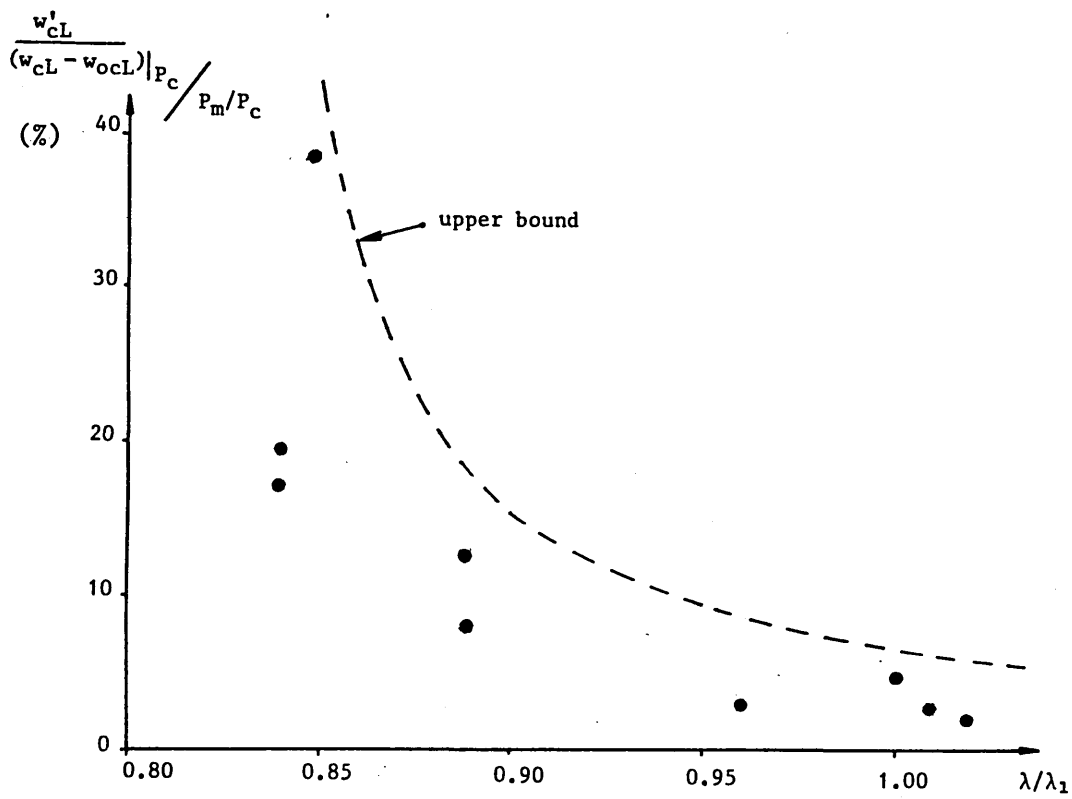


Figure 3.32 ; Cyclic Step / Peak Cyclic Load Ratio vs Modified Slenderness

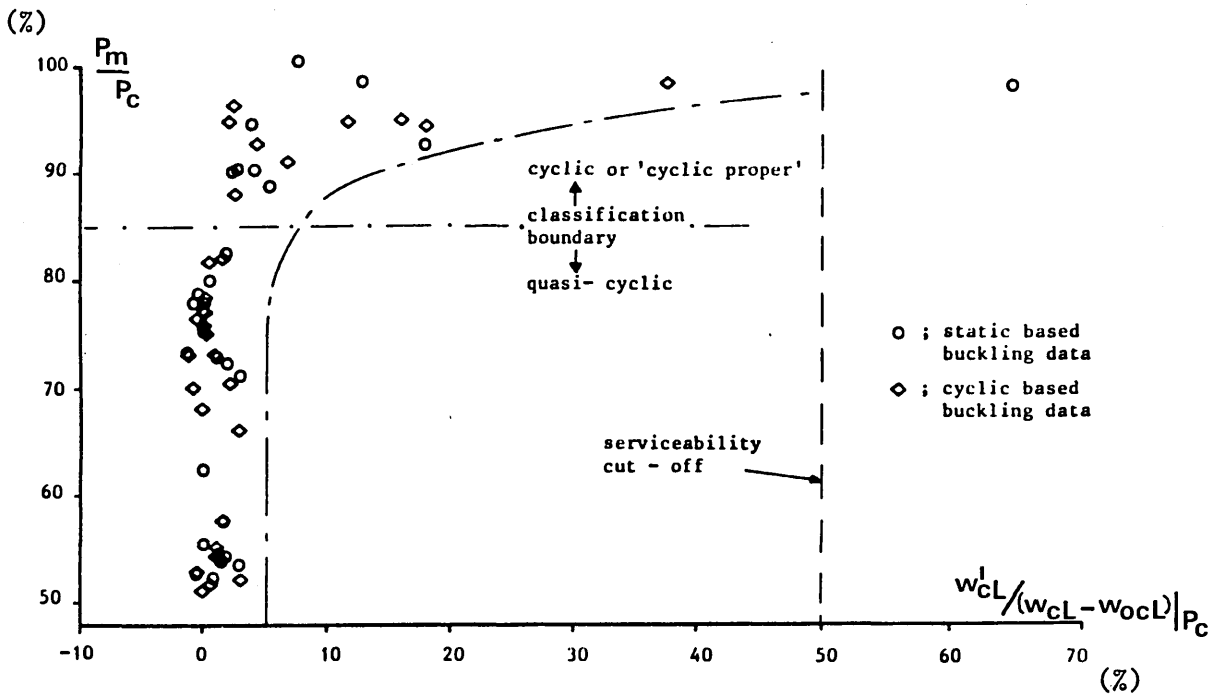


Figure 3.33 ; Peak Cyclic Load vs Cyclic Step Response

presented in terms of the peak inelastic cyclic load, both parameters being normalised to their respective buckling equivalents. As plotted against the equally embracing modified slenderness ratio, a concise visual presentation is afforded of the fact that cyclic amplification of initial imperfection effects is dependent upon the availability of substantial inelastic exposure. With respect to design considerations, the key relationship between cyclic step and peak cyclic loading P_m is given in Fig 3.33. The aforementioned classifications of quasi-cyclic and formally cyclic cases are denoted and P_m data is presented in terms of both the respective specimen P_c values (C and S). This attempts to overcome the variations between the corresponding static and cyclic strut partners' imperfections and to provide data appertaining to the appropriate static value, static values being the accepted medium in engineering practice. Fig 3.33 represents the research programme's primary finding in design terms and includes a suggested empirical locus with $w_{cL}' / (w_{cL} - w_{ocL}) = 5\%$ for $P_m / P_c \leq 0.75$ and

$$w_{cL}' / (w_{cL} - w_{ocL})|_{P_c} = (85.5 - 86.27P_m / P_c)^{-1} \quad (3.14)$$

for $P_m / P_c > 0.75$, noting the serviceability cut-off.

Figs 3.34 to 3.37 display computer graphic output for case 13C, typical of the quasi-cyclic batch; see Table 3.11. The cyclic effects are small with little load shedding - note ΔP in Fig 3.31. Two cyclic action phases were involved and the possibly surprising stiffening effects best displayed in Fig 3.34 are the

AXIAL LOAD vs. AXIAL DISPLACEMENT

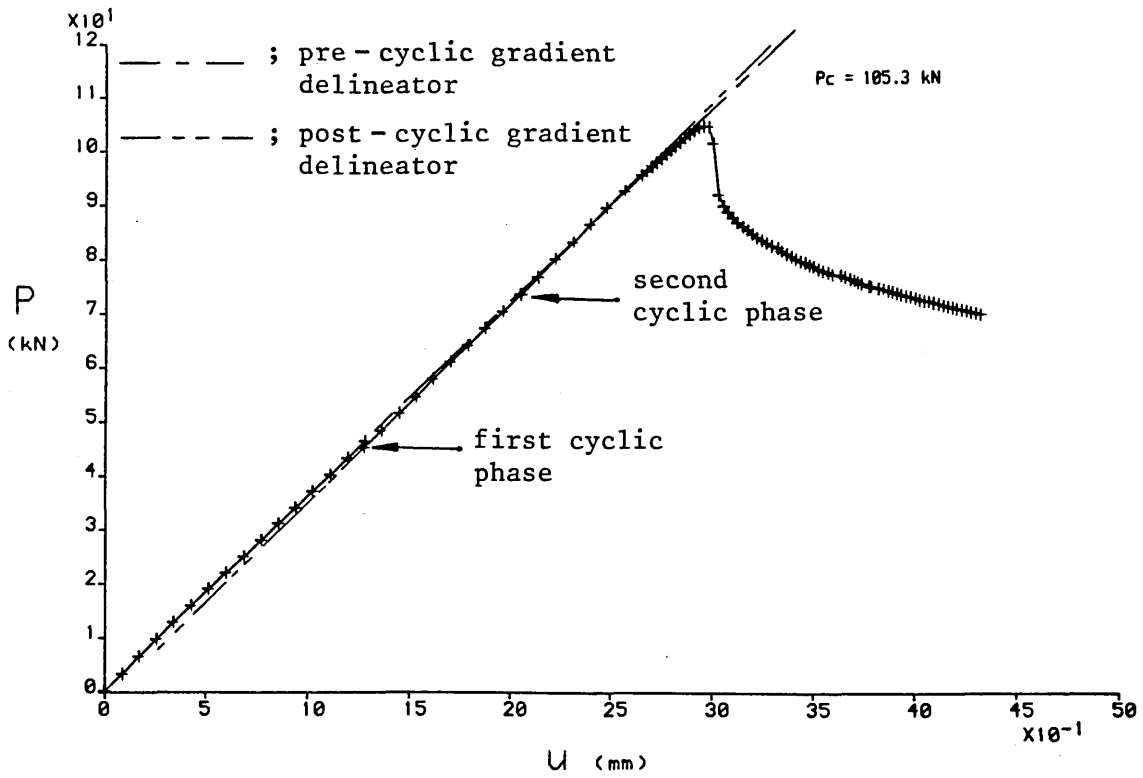


Figure 3.34 ; P vs u - Strut Ref. 13C

AXIAL LOAD vs. MID-SPAN RESULTANT LATERAL DISPLACEMENT

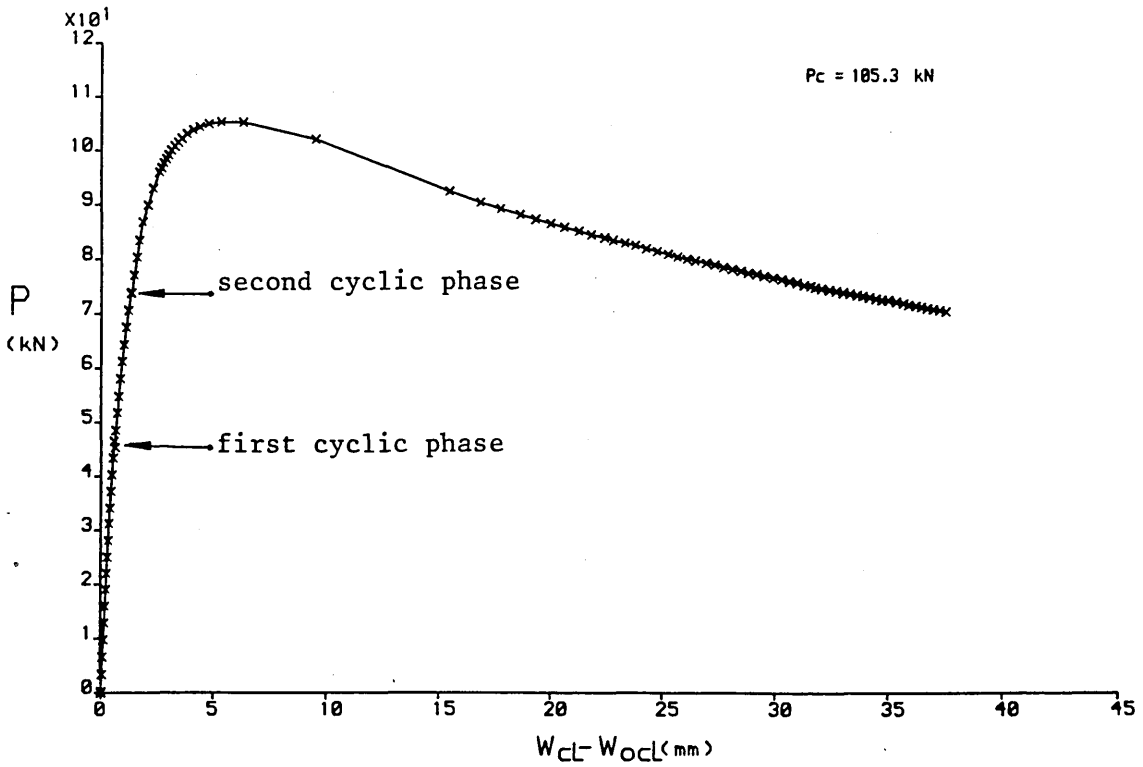


Figure 3.35 ; P vs $w_{CL} - w_{oCL}$ - Strut Ref. 13C

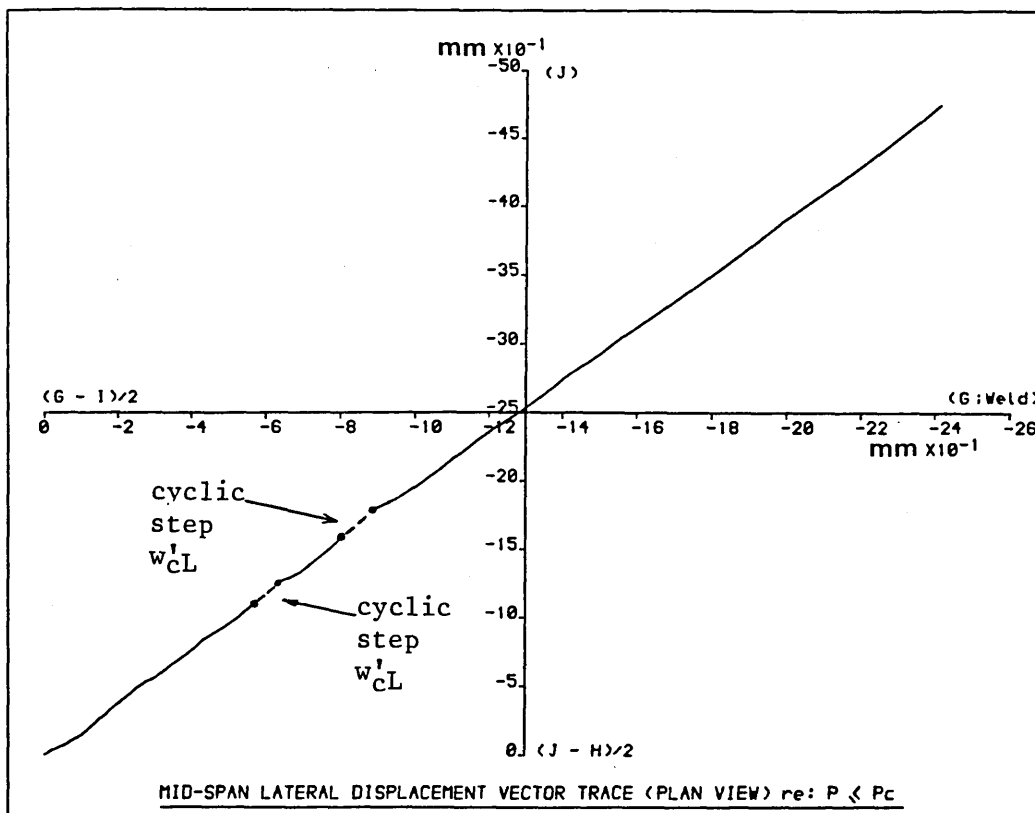


Figure 3.36 ; Vector Trace ($P < P_c$) - Strut Ref. 13C

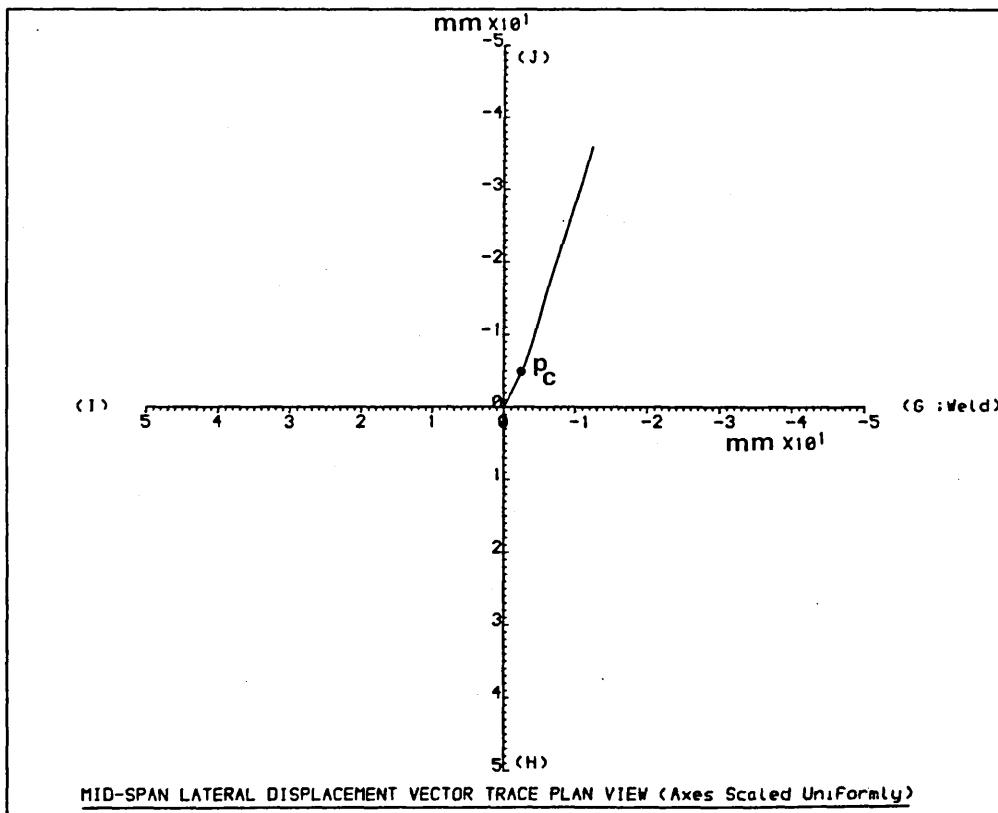


Figure 3.37 ; Vector Trace - Strut Ref. 13C

most notable feature, the axial stiffness, essentially E , being increased by approximately 3%. Figs 3.36 and 3.37 show the respective vector traces, these not being notably different from the static equivalents discussed in Section 3.6.1.

Figs 3.38 to 3.41 and 3.42 to 3.45 provide computer graphics output for cases 26C and 27C, typical of the formal cyclic batch displaying a significant cyclic step. In conjunction with this, load loss during the cyclic phase is more substantial than in the quasi-cyclic cases but still $\leq 10\% P_m'$. Figs 3.38 and 3.42 similarly display a larger than formerly increase in axial stiffness/ E of approximately 5%. It should perhaps be noted that in the quasi-cyclic cases, the change in stiffness compensates for the load loss ΔP in so much that in the vicinity of buckling, the post-cyclic locus crosses over the projection of the pre-cyclic path in the P vs u loci, see Fig 3.34. However, in the formal cyclic cases, see Figs 3.38 and 3.42, the increase in stiffness fails to 'claw back' in this manner. That is, increase in axial stiffness or E fails to overcome the inelastic increase in deformation as assessed by the associated cyclic step; note Figs 3.39 and 3.43. In all cited cyclic cases, note Figs 3.34, 3.35, 3.38, 3.39, 3.42 and 3.43, the buckling state is well-defined. The vector traces of Figs 3.40, 3.41, 3.44 and 3.45 are again of the essentially planar form displayed by their static and quasi-cyclic counterparts. This situation can be contrasted with the pre-buckling vector trace shown in Fig 3.46 which corresponds to case 19C. The cyclic step is associated with a distinct shift in the vector trace, although the post-cyclic phase path and the

AXIAL LOAD vs. AXIAL DISPLACEMENT

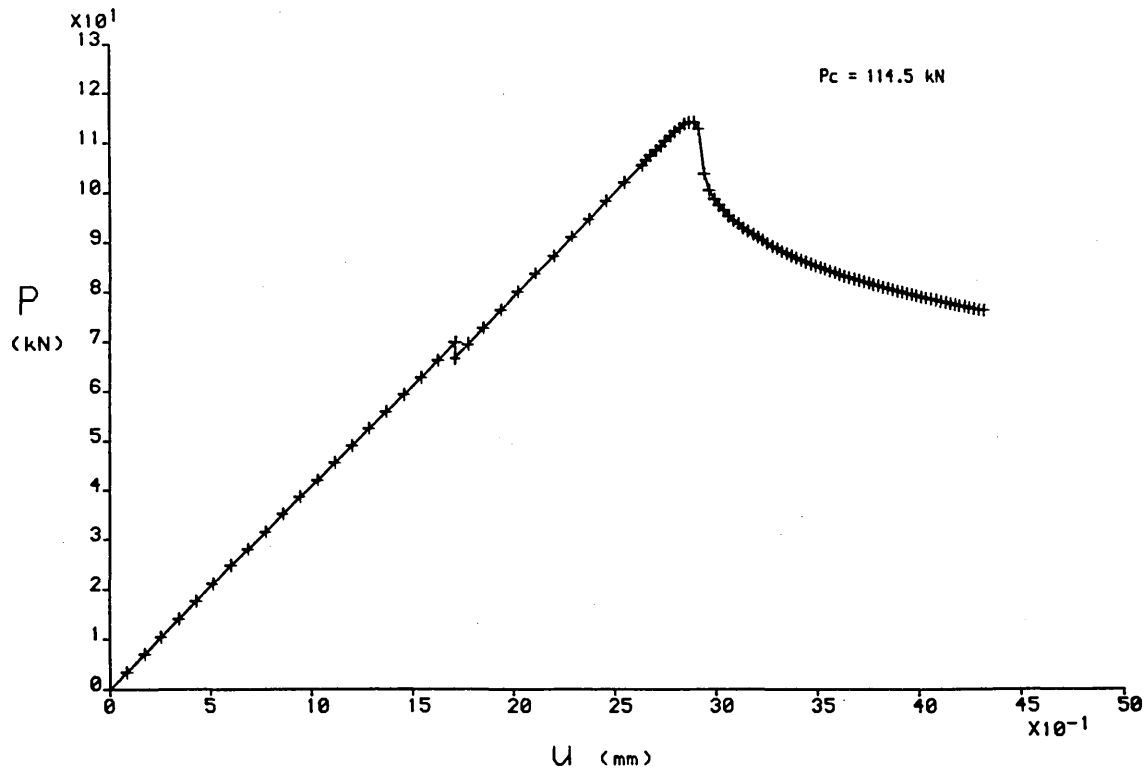


Figure 3.38 ; P vs u - Strut Ref. 26C

AXIAL LOAD vs. MID-SPAN RESULTANT LATERAL DISPLACEMENT

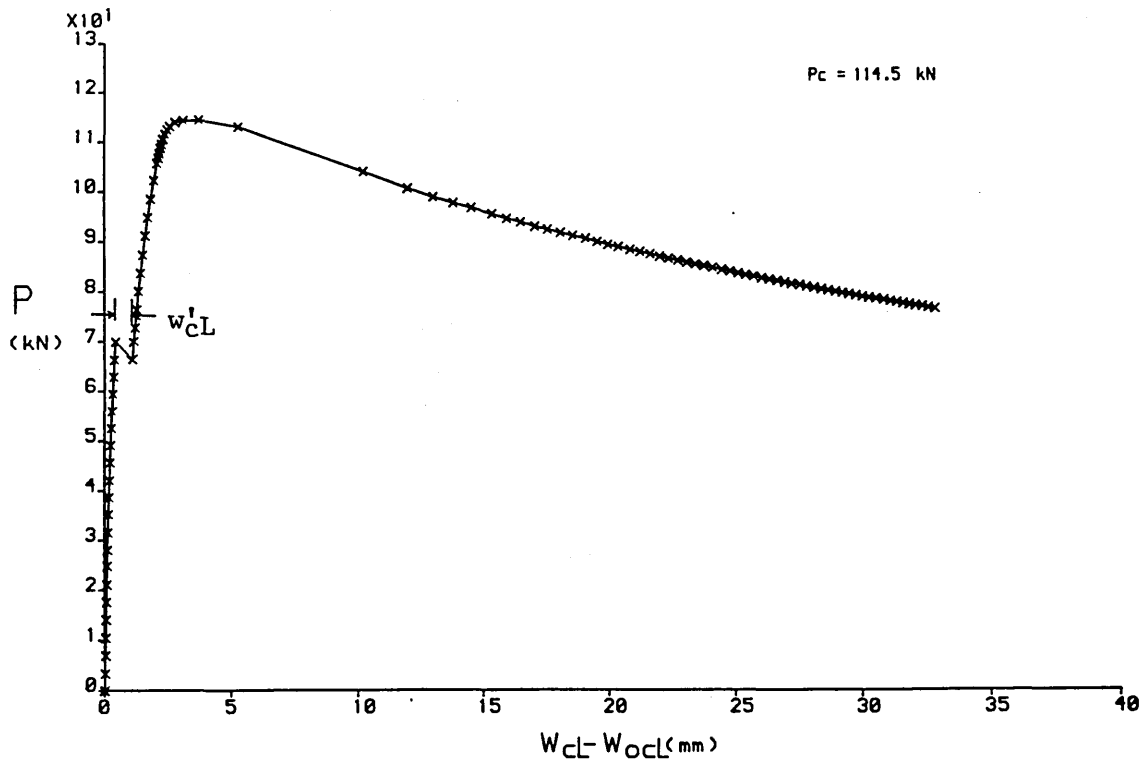


Figure 3.39 ; P vs $w_{cL} - w_{oC_L}$ - Strut Ref. 26C

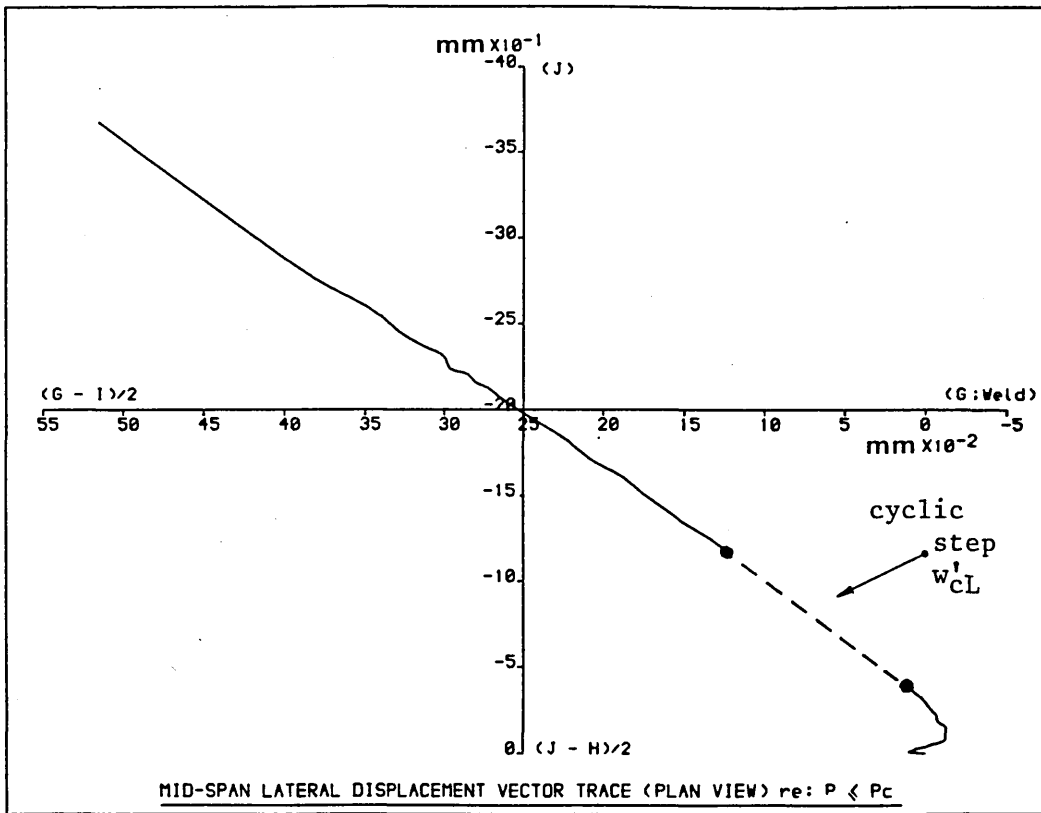


Figure 3.40 ; Vector Trace ($P \leq P_c$) - Strut Ref. 26C

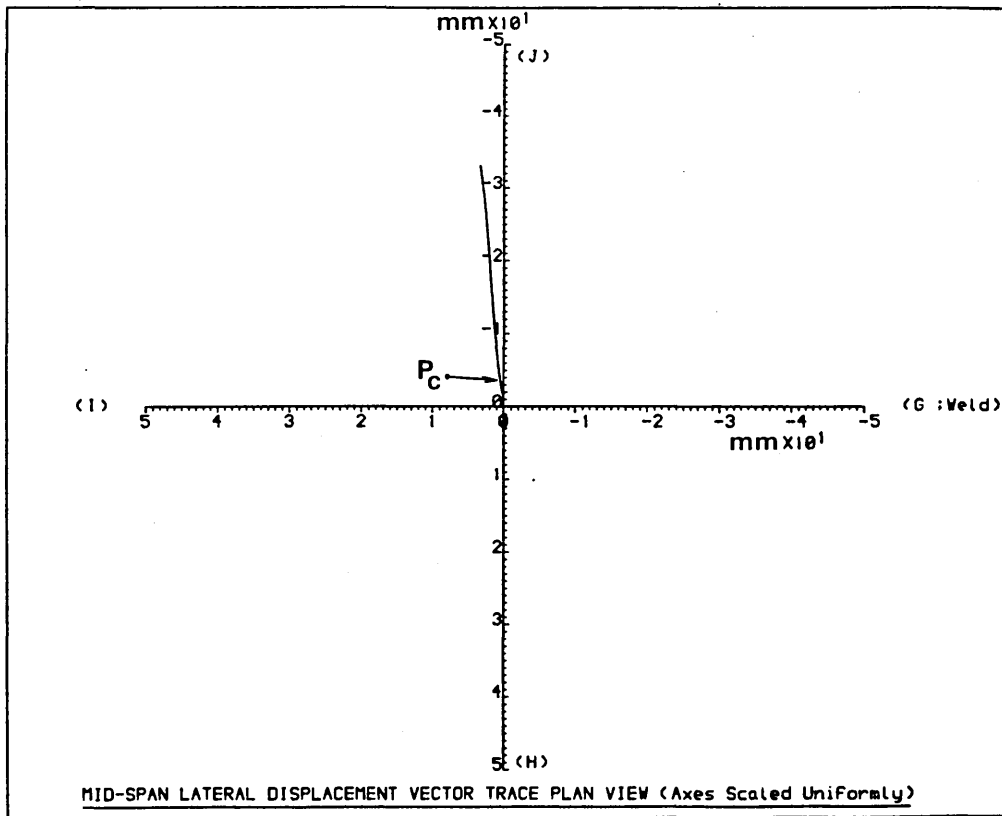


Figure 3.41 ; Vector Trace - Strut Ref. 26C

AXIAL LOAD vs. AXIAL DISPLACEMENT

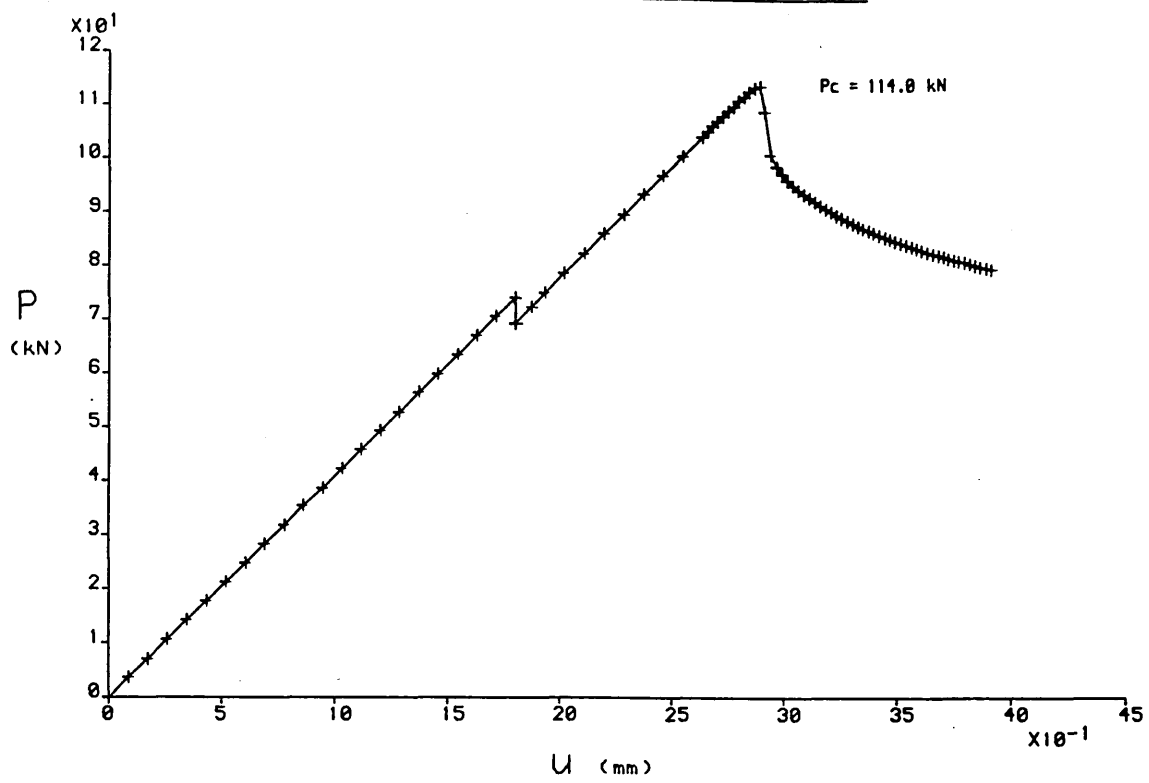


Figure 3.42 ; P vs u - Strut Ref. 27C

AXIAL LOAD vs. MID-SPAN RESULTANT LATERAL DISPLACEMENT

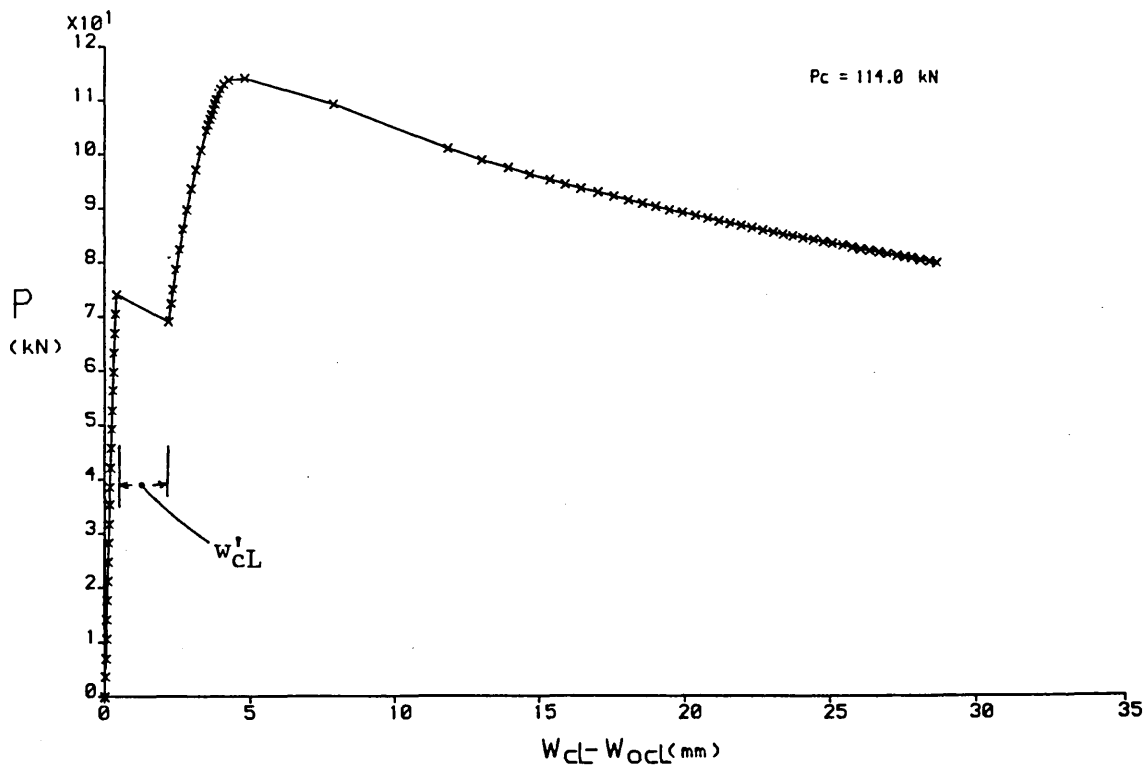


Figure 3.43 ; P vs $w_{cL} - w_{ocL}$ - Strut Ref. 27C

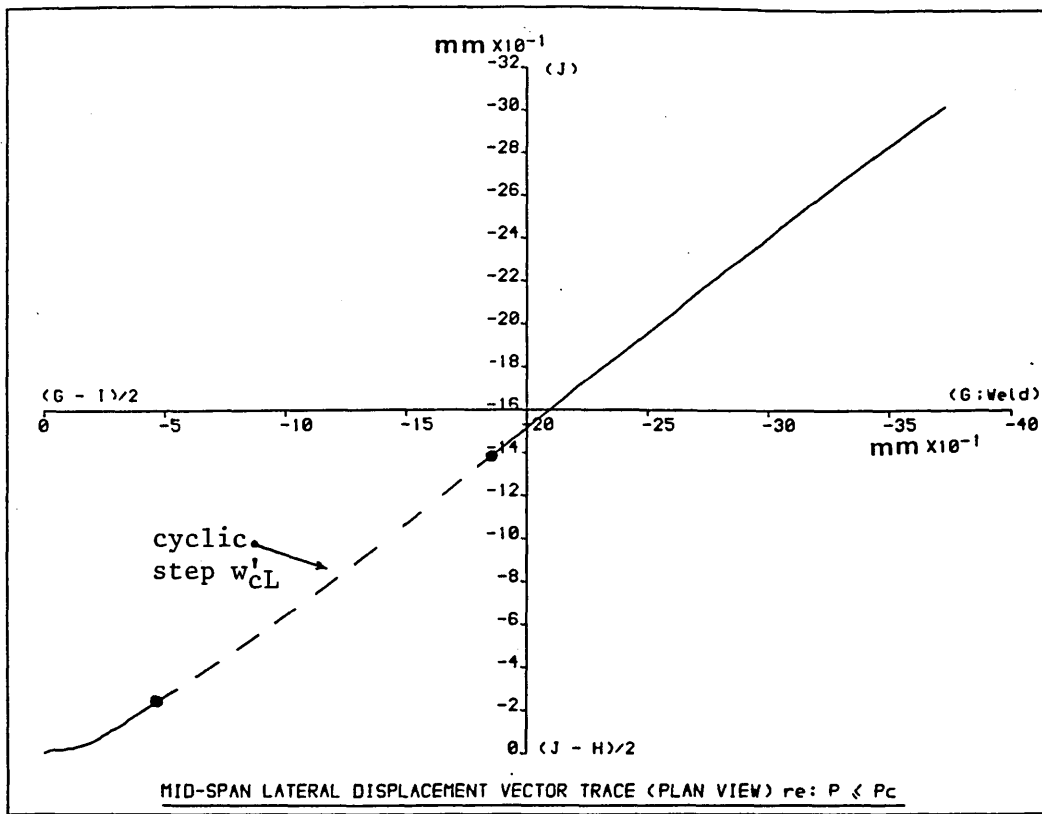


Figure 3.44 ; Vector Trace ($P < P_c$) - Strut Ref. 27C

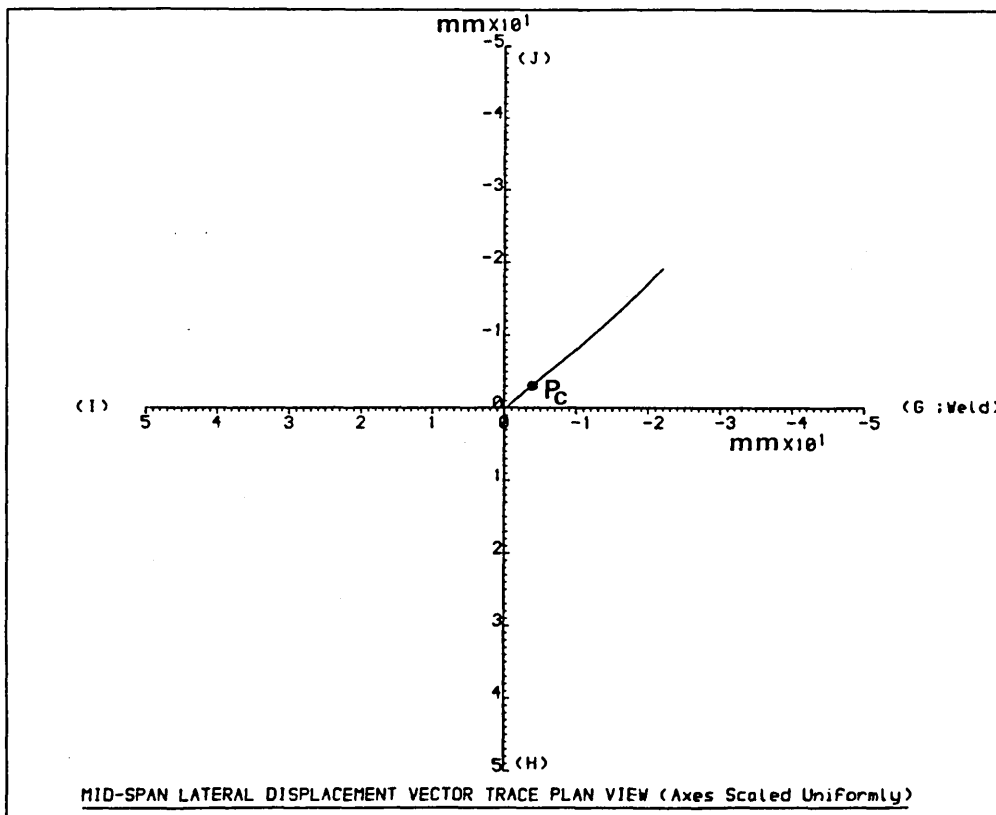


Figure 3.45 ; Vector Trace - Strut Ref. 27C

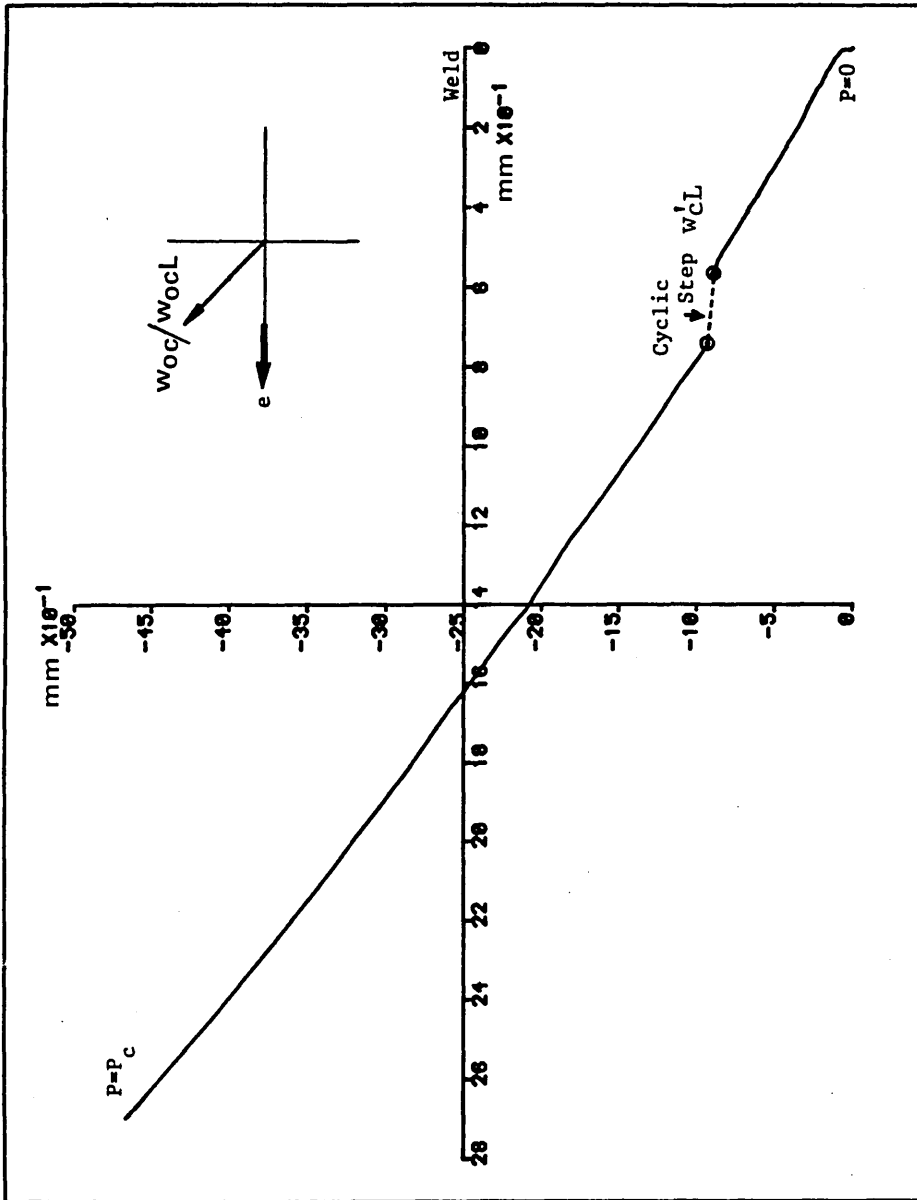


Figure 3.46 ; Vector Trace ($P \leq P_c$) - Strut Ref. 19C

displacement magnitudes involved are small. That is, the effect is small. Given the above parallelism, it is useful to recall the former arguments relating to buckling path orientation and monitored imperfections w_{ocL} and e given in Section 3.6.1. The apparent agreement between the orientations of w_{ocL} and the vector trace belies the fact that 19C was also a heavily corkscrewed case with no direct w_{oc} value being available; note Table 3.12 and the typical corkscrewed topology of Fig 3.11. Summarising, planarity of the vector trace can be disturbed by cyclic action, the orientation of the vector trace planarity remaining largely under the control of the complex initial imperfection interaction discussed in Section 3.6.1.

Finally, attention is drawn to case 20C wherein buckling was induced during the cyclic phase as denoted in Table 3.12 and illustrated in Figs 3.47 and 3.48. As is to be expected, given the nature of instability studies, the cyclic step and the cyclic phase load loss increase dramatically with respect to the other formal cyclic cases. Reference to Table 3.11 shows that a relative increase of 5% in $u_m/u|_{P_C}$, see cases 21C, 22C, 26C and 27C, produces a disproportionate increase in response as noted formerly; cases 20C and 21C share common λ_m . Recall that Figs 3.38 and 3.39, and Figs 3.42 and 3.43, show the respective characteristics for cases 26C and 27C with which Figs 3.47 and 3.48 should be compared. The post-cyclic action phase value of P_C is 20% below that of its static partner 20S, the only such registered case in the testing programme. This reduction suggests that imperfection sensitive struts only suffer drastic performance

AXIAL LOAD vs. AXIAL DISPLACEMENT

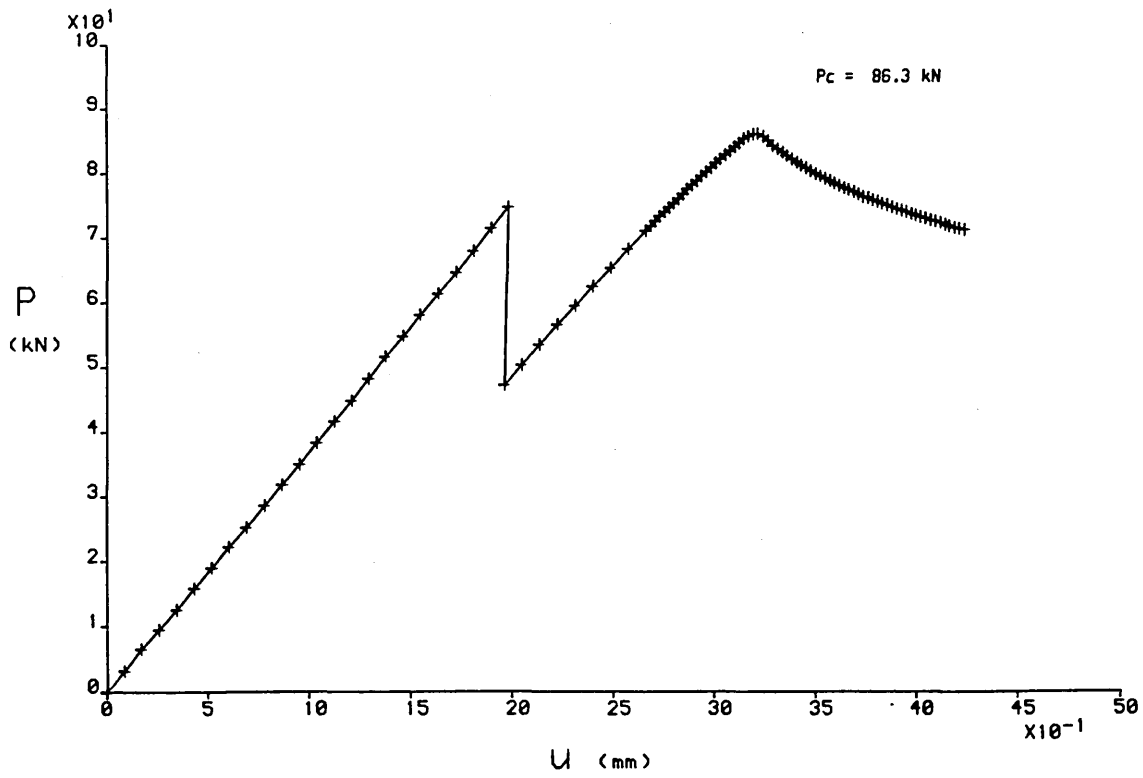


Figure 3.47 ; P vs u - Strut Ref. 20C

AXIAL LOAD vs. MID-SPAN RESULTANT LATERAL DISPLACEMENT

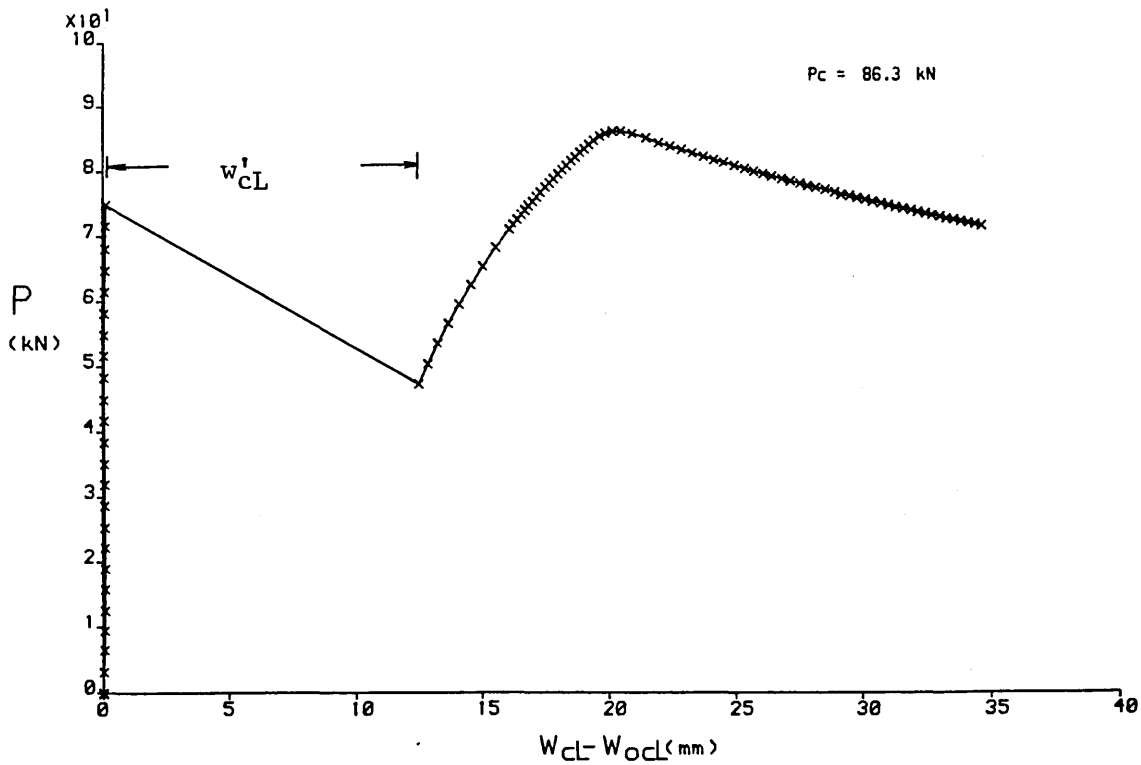


Figure 3.48 ; P vs $w_{cL} - w_{ocL}$ - Strut Ref. 20C

loss due to cyclic action if buckling is actually induced during the cyclic phase.

The nature of the struts' behaviour during the cyclic action phase is important. Response 'temporal rates' will govern the degree of validity possessed by an essentially static or pseudo-static analysis. Consideration will therefore now be given to the time-dependent aspects of the C-series tests.

3.7.2 Time-Dependent Parametric Response

Typical quasi-elastic hysteresis⁽⁵¹⁾ behaviour is illustrated in Figs 3.49 and 3.50 which relate to case 13C. These loci can be compared with those shown in Figs 3.34 and 3.35 which relate to static (only) paths. The hysteresis consists of closed loop lines⁽⁶³⁾ displaying cyclic stiffening. Cyclic phase exit paths are variably located within the hysteresis bounds. That is, the hysteresis lines are overwriting, oscillating within a band width established earlier in the cyclic phase; note cases with $n_c \neq 1000$ - P22 to P24, 1C, 13C and 14C (cf Tables 2.3, 3.11 and 3.12). This maximised band-width suggests that quasi-elastic hysteresis importantly involves effectively stabilised and narrow band-widths. The highly variable hysteresis behaviour signified by the dual signed cyclic steps of Table 3.11 is thereby fortunately 'bounded'. Pseudo-static interpretation would appear to be substantive.

Two types of hysteresis occur in the formally cyclic cases.

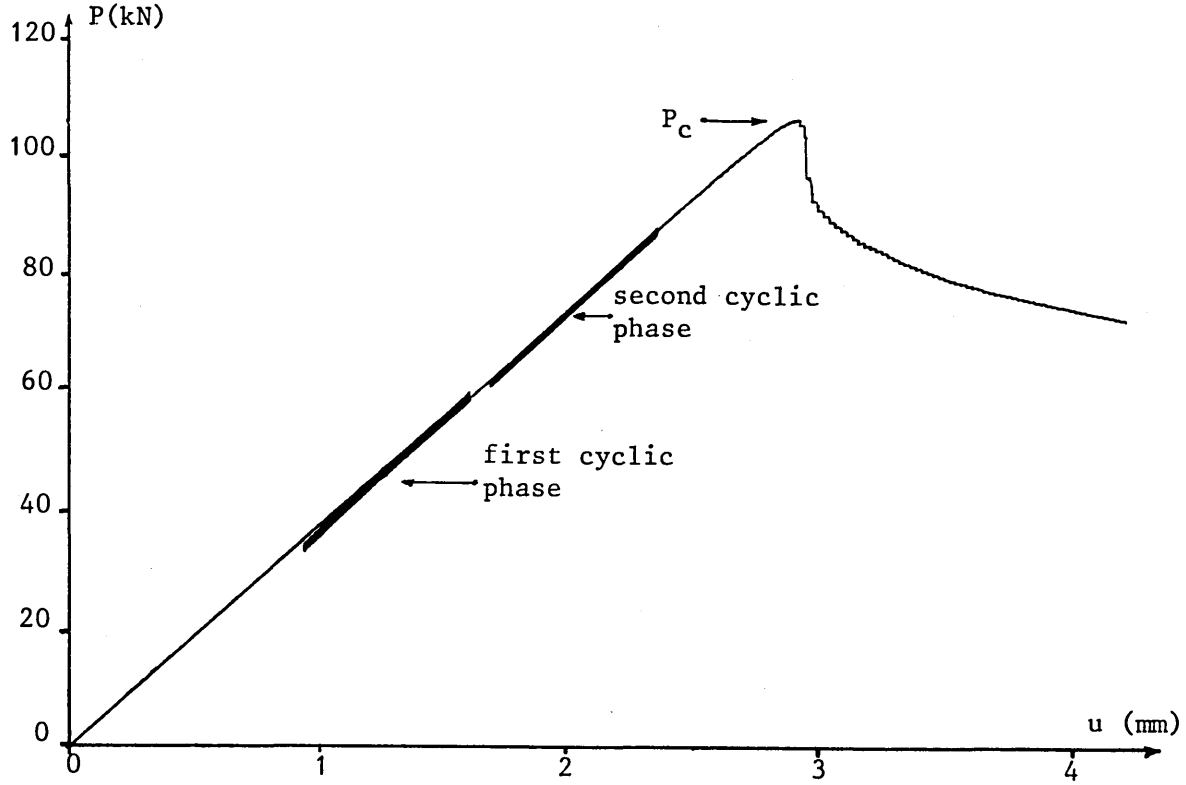


Figure 3.49 ; Quasi - Elastic Hysteresis : P vs u Trace - Strut Ref. 13C

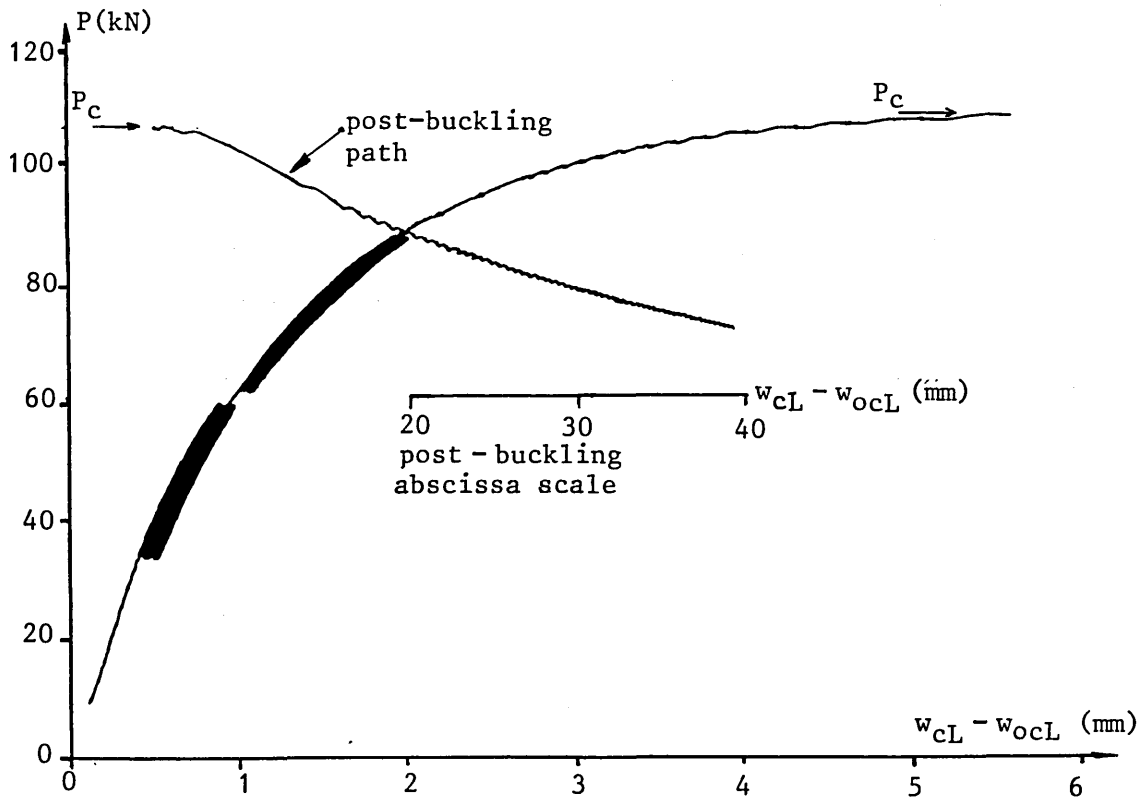


Figure 3.50 ; Quasi - Elastic Hysteresis : P vs $w_{cL} - w_{ocL}$ Trace - Strut Ref. 13C

Finite area⁽⁶⁴⁾ single band hysteresis occurs for cases showing a lesser cyclic step, ie those involving higher λ_m and/or lower u_m values. This is typified in Fig 3.51, case 19C, where a single basic loop is effectively traced out by all cycles. (It should be noted that the RV10 function generator is manually controlled and involves a gradual attainment of full amplitude over the first few cycles.) Again, stabilisation occurs well within 1000 cycles although the band-width is larger and of uniform 'sign' or 'sense' throughout. Multiple band hysteresis is illustrated in Fig 3.52 and relates to case 21C. This profile is typical of those cases involving higher values of cyclic step with lower values of modified slenderness ratio λ_m and higher values of peak cyclic displacement u_m . In this situation, discrete groups of individual hysteresis loops of finite area forward march, increasing the band-width. Figs 3.53 and 3.54 display similar hysteresis patterns with respect to cases 26C and 27C. Although there is a 'tightening' of the individual hysteresis loops with increasing cycles, cyclic creep deceleration^(64,65), there is, importantly, no cyclic creep stabilisation; incremental displacement is evident with each cycle. Any proposed pseudo-static modelling for these cases must include treatment of the cyclic step w_{cL}' . The above discussion has utilised P vs $w_{cL}-w_{ocL}$ loci; these display cyclic activity more distinctly than the corresponding P vs u loci. However, as shown in Figs 3.55 and 3.56, relating to cases 26C and 27C respectively, formally cyclic P vs u hysteresis differs from that associated with quasi-elastic hysteresis by being of uniform 'sense' or 'sign' (ie no cyclic hardening) throughout and by displaying substantially larger band-widths.

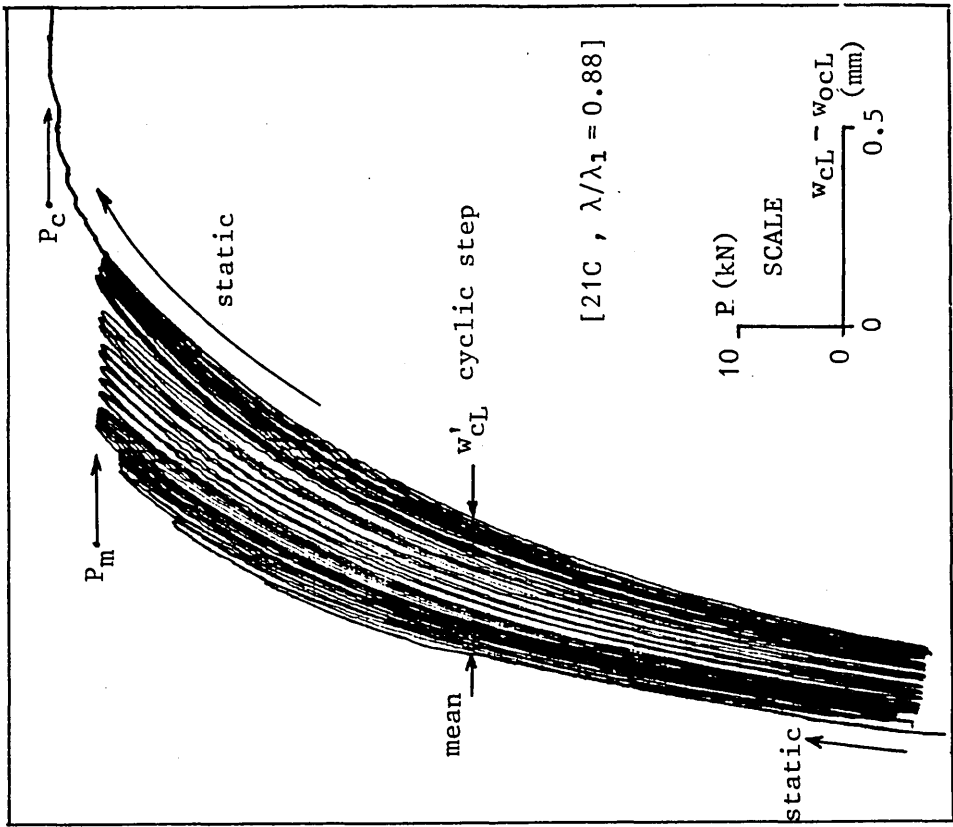


Figure 3.52 ; Multiple Band Hysteresis :
 P vs $w_{cL} - w_{ocL}$ Trace - Strut Ref. 21C

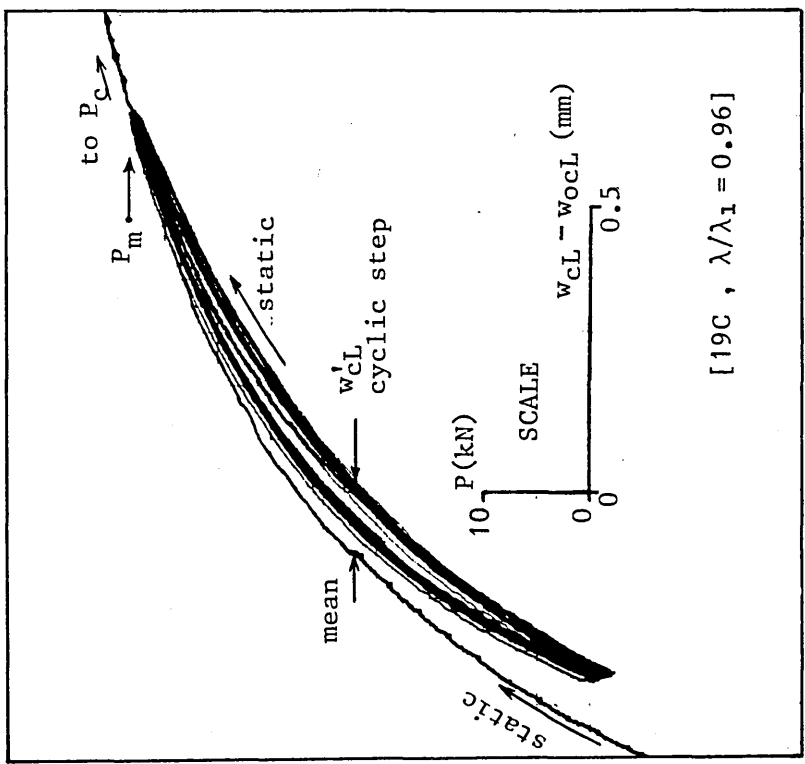


Figure 3.51 ; Single Band Hysteresis :
 P vs $w_{cL} - w_{ocL}$ Trace - Strut Ref. 19C

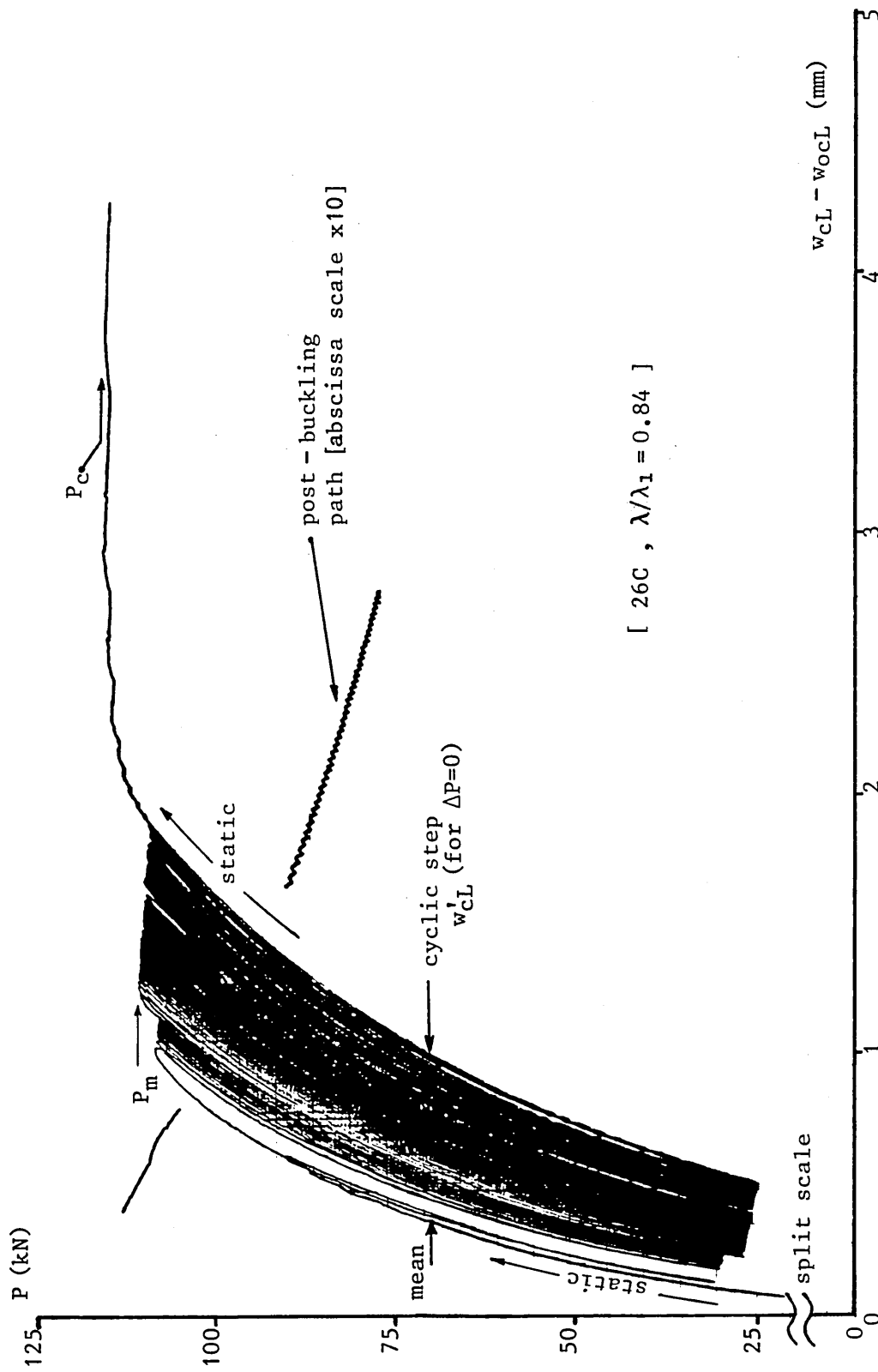


Figure 3.53 ; Cyclic Creep : P vs $w_{CL} - w_{ocL}$ Trace - Strut Ref. 26C

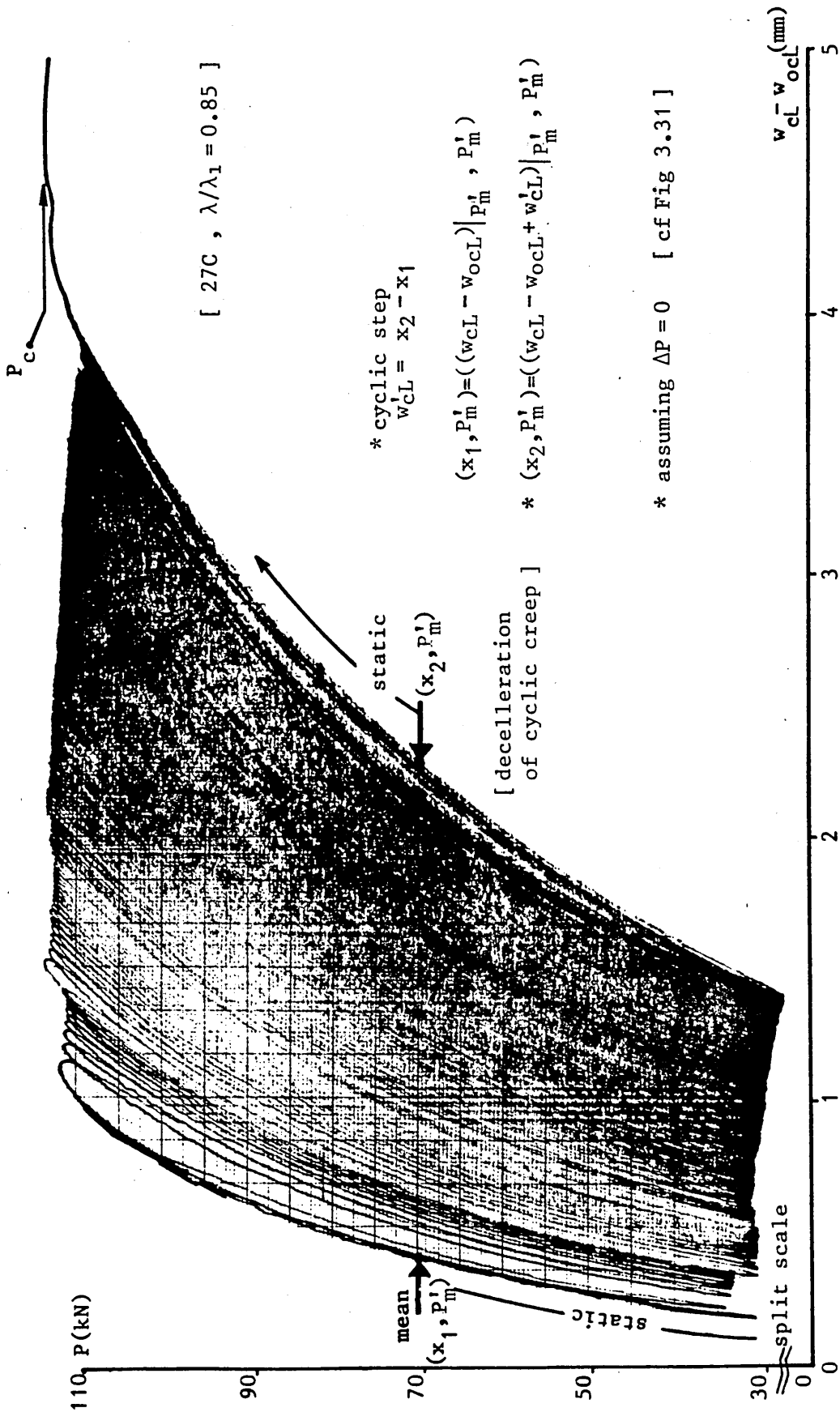


Figure 3.54 ; Cyclic Creep : P vs $w_{cL} - w_{ocL}$ Trace - Strut Ref. 27C

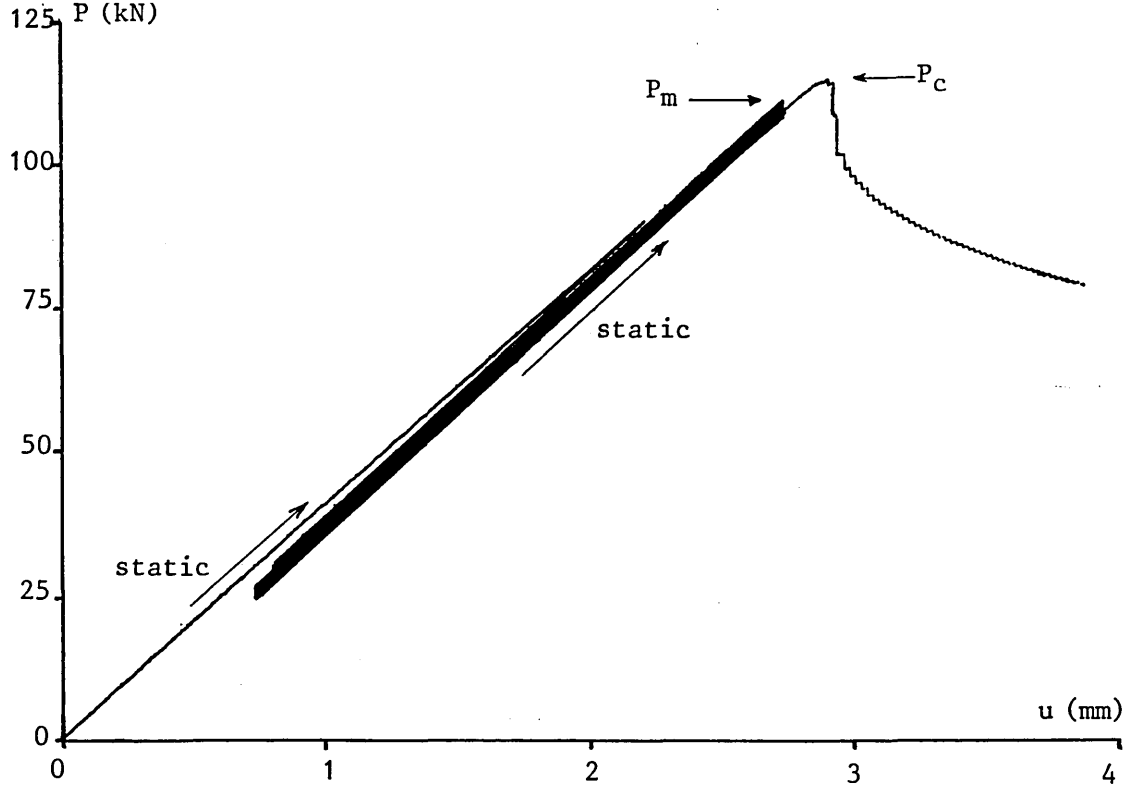


Figure 3.55 ; P vs u Hysteretic Trace - Strut Ref. 26C

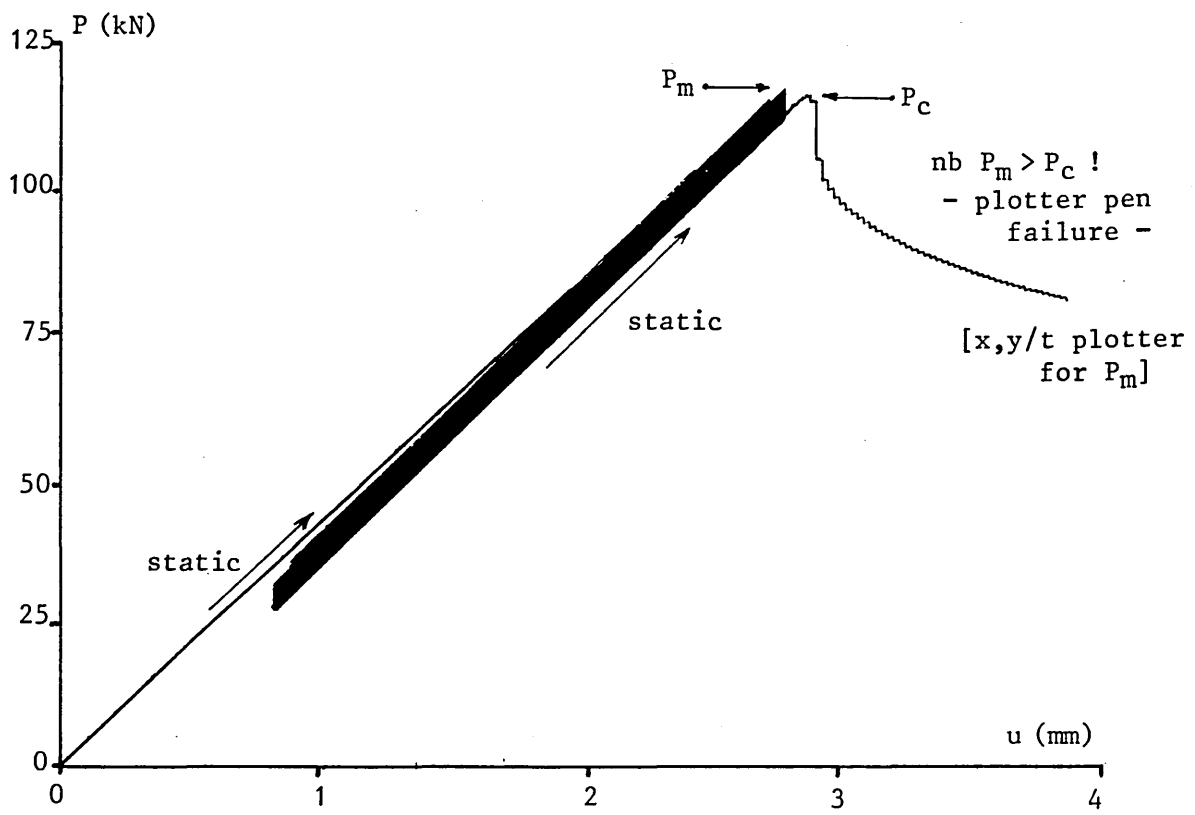


Figure 3.56 ; P vs u Hysteretic Trace - Strut Ref. 27C

Finally, Figs 3.57 and 3.58 respectively display the P vs u and P vs $w_{cL} - w_{ocL}$ loci relating to case 20C which buckled during the cyclic phase. Visually dramatic with P_m/P_c nominally equal to unity, P_c as defined does not exist, the singular behaviour represents an upper bound on the testing programme. Cyclic creep accelerates into the buckling state before deceleration occurs post-buckling. Given the subsequent degradation in performance, it appears that for imperfection sensitive struts to display catastrophic behaviour under short duration, low frequency cyclic action, pre-buckling displacement state must be 'local' to the buckling state.

3.7.3 Semi-Empirical Analyses - Southwell and Lundquist Plots

Given the usefulness of their application to the static strut studies, it was decided to attempt to employ the Southwell and Lundquist plots in the cyclic strut studies. The objective in each case was to obtain two distinct linear fit ranges of pre- and post-cyclic phase form which were parallel but offset. This implied no change in effective length due to loss of collet grip, but inelastic amplification of the initial lumped imperfection. It has been noted that a small increase in direct modulus E was incurred as a result of cyclic action and this will affect the parallelism factor.

With respect to the quasi-cyclic cases, however, the induced cyclic step w_{cL}' was so small that no effectively distinct pairs of linear fits could be obtained. Figs 3.59 and 3.60 show the

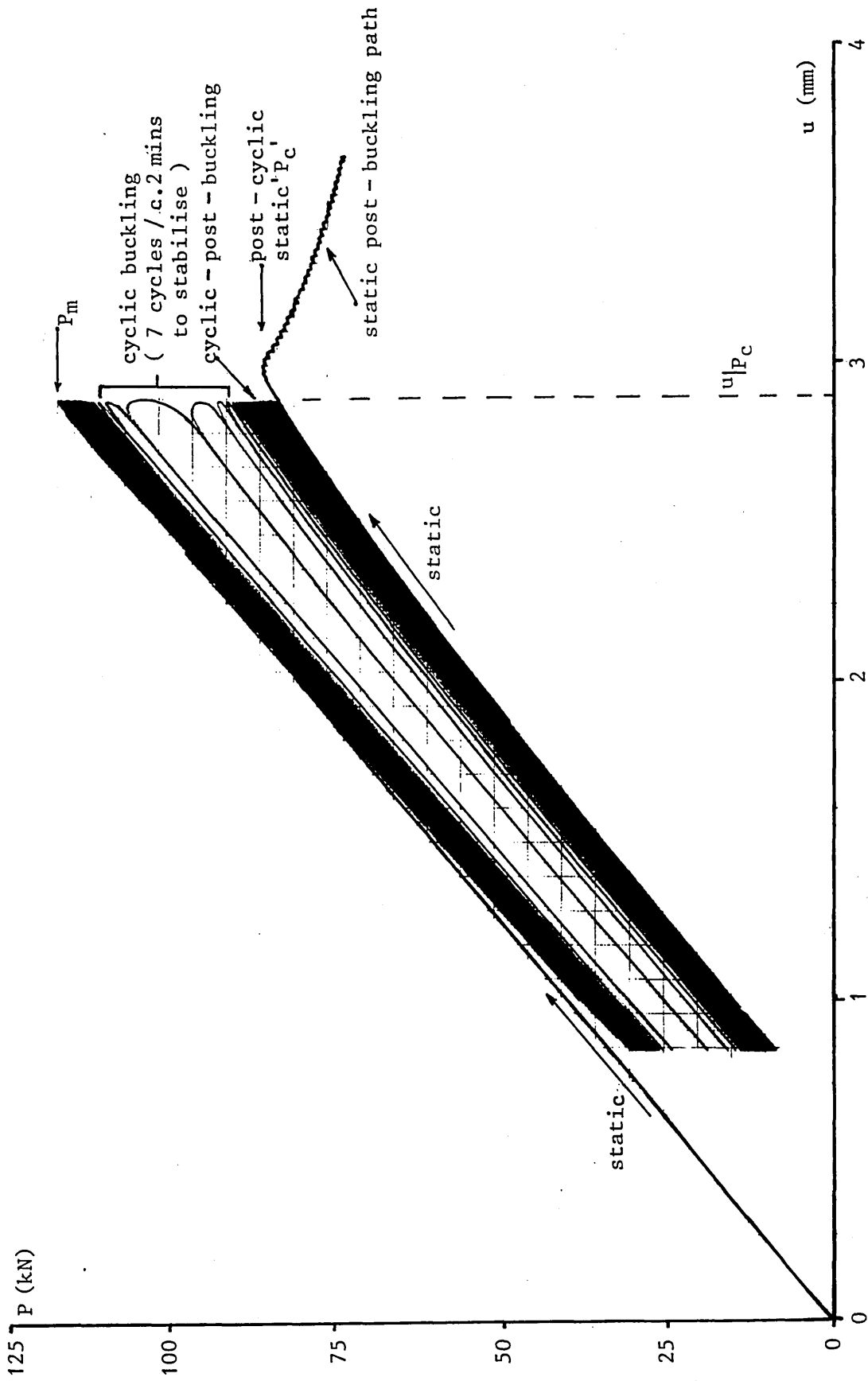


Figure 3.57 ; Cyclic Buckling : P vs u Hysteretic Trace - Strut Ref. 20C

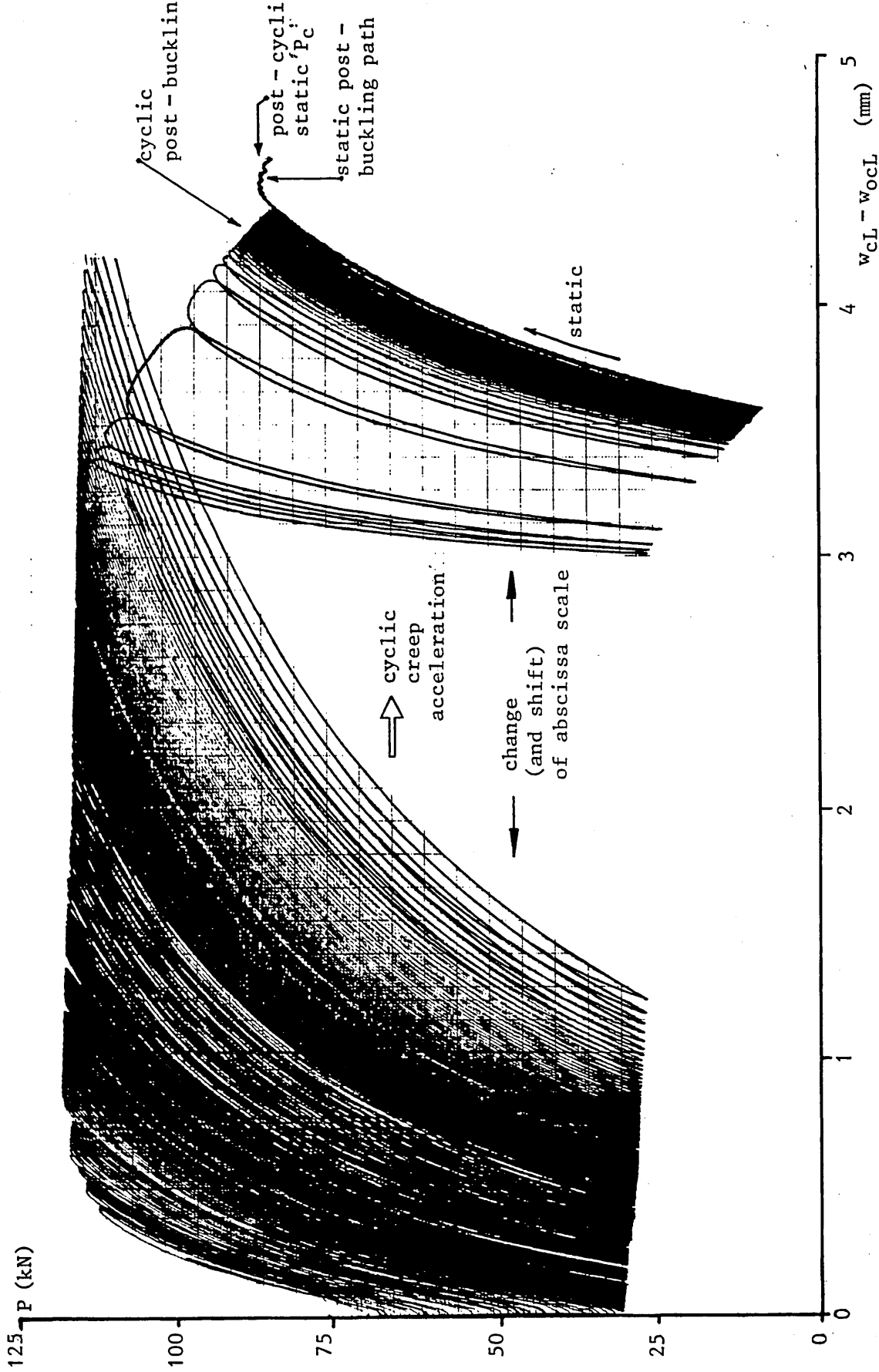


Figure 3.58 ; Cyclic Buckling : P vs $w_{cL} - w_{ocL}$ Hysteretic Trace - Strut Ref. 20C

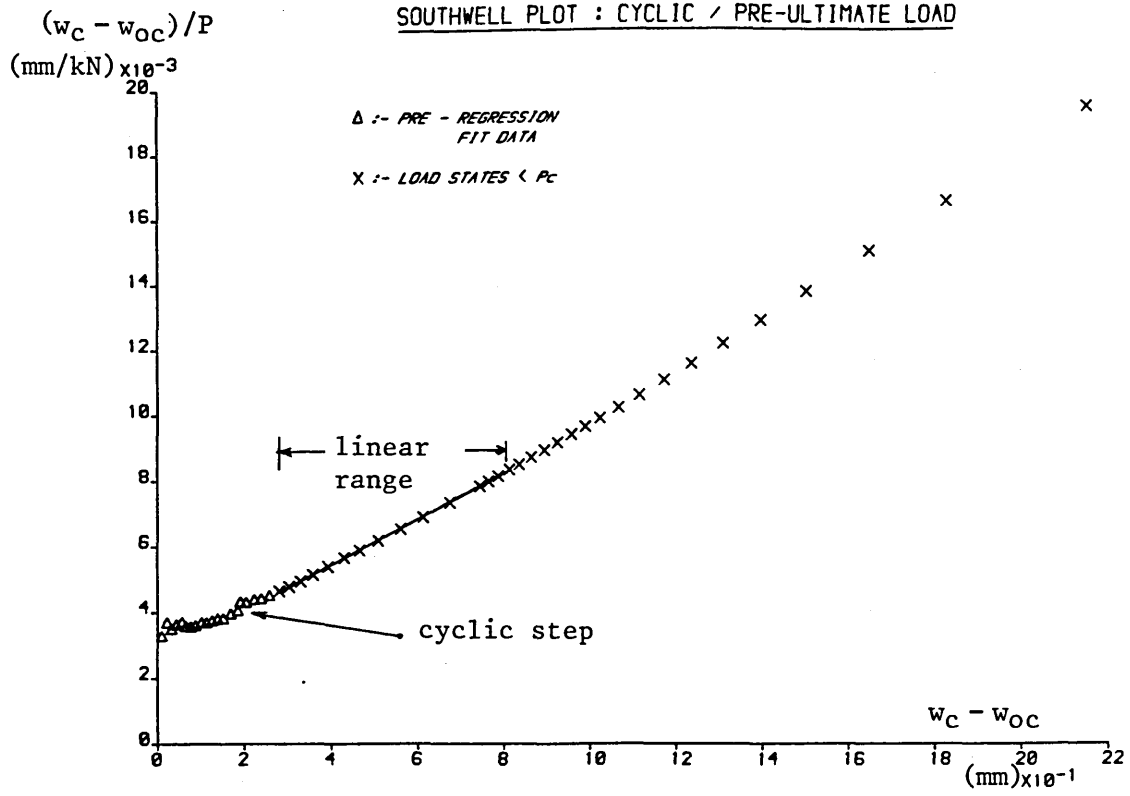


Figure 3.59 ; Southwell Plot - Strut Ref. 7C

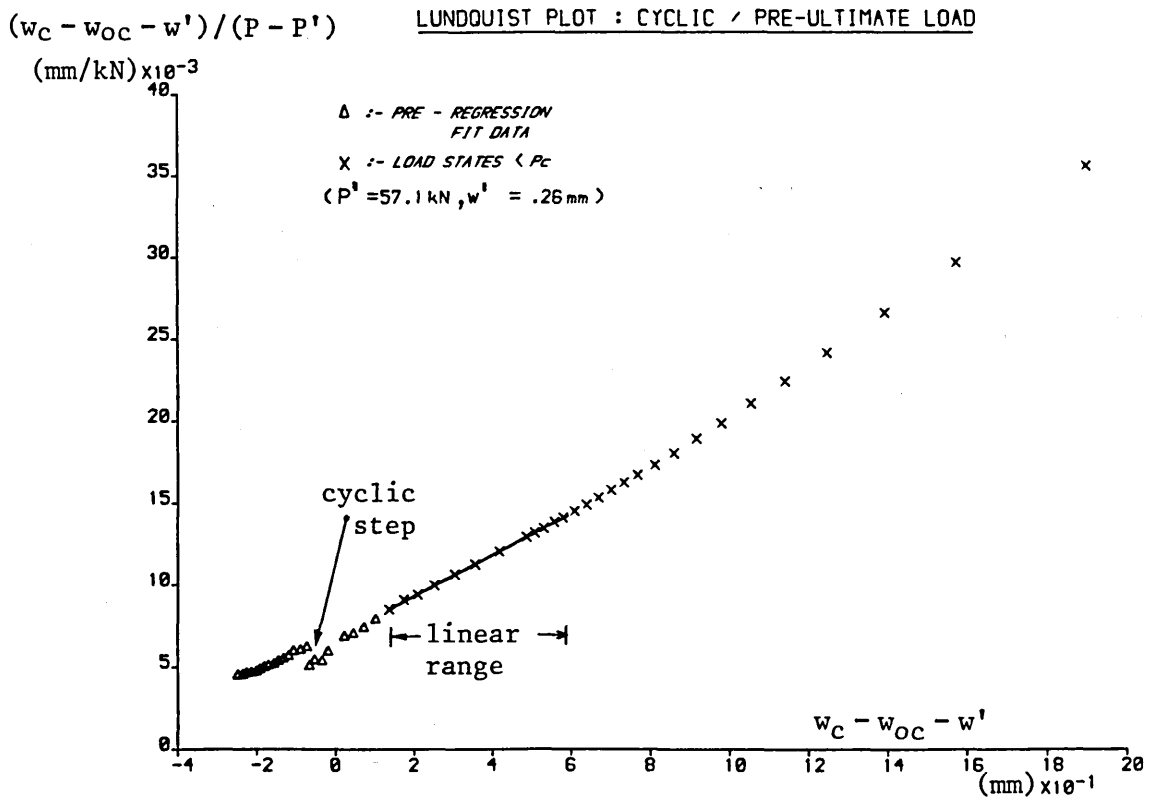


Figure 3.60 ; Lundquist Plot - Strut Ref. 7C

computer graphic plots for case 7C. The locations of the cyclic step within these plots are indicated and relate to a relatively low value of mean cyclic stroke. Their identity is partially masked by low load irregularities⁽⁵⁶⁾. In other cases, the linear fit range sometimes included the state corresponding to the cyclic step. Appropriate data for all quasi-cyclic tests is given in Table 3.14. All cases were effectively treated as static studies. Three cases failed to provide acceptable linear fit ranges; the low value of $P_c/P_e=0.58$ for case 11C is to be noted⁽⁵⁶⁾.

With respect to the formally cyclic cases, attempts to obtain viable pre- and post-cyclic action phase pairs of plots were reasonably successful as indicated in Table 3.15, the cases of inadmissibility being restricted to those with relatively low λ_m values. The respective effective length estimates show a consistent and small reduction for the post-cyclic values but these variations are in keeping with the above-mentioned increase in direct modulus (average of +5%). Cyclic plots for case 24C are exemplified in Fig 3.61, with the computer graphics appertaining to case 18C being displayed in Figs 3.62 and 3.63. The location of the cyclic step is clearly depicted throughout. In all cases available, there is a distinct increase in the initial lumped imperfection parameters a_{0s} and a_{0l} due to cyclic action. That is, the plots display, as denoted in Table 3.15, amplification of initial strut imperfections due to pre-buckling cyclic action.

Strut Ref.	Linear Fit Range (% of P_e)		Euler Data		w_{oc} Data (mm)	
	Southwell	Lundquist	l_s/l	l_1/l	a_{os}	a_{o1}
1C	60 - 73	60 - 73	1.06	1.07	0.21	0.11
§ 2C	n/a	n/a	n/a	n/a	n/a	n/a
3C	38 - 48	50 - 60	1.00	1.05	0.55	0.40
4C	49 - 59	51 - 59	1.01	1.05	0.75	0.54
5C	61 - 70	55 - 63	1.08	1.07	0.24	0.35
6C	59 - 77	60 - 77	1.07	1.07	0.05	0.05
7C	36 - 58	39 - 59	1.03	1.04	0.39	0.33
8C	50 - 63	40 - 58	1.03	1.05	0.70	0.52
9C	(*)	(*)	(*)	(*)	(*)	(*)
10C	(*)	(*)	(*)	(*)	(*)	(*)
11C	(*)	(*)	(*)	(*)	(*)	(*)
12C	51 - 63	60 - 70	1.02	1.07	0.35	0.10
13C	72 - 77	65 - 75	1.03	1.02	0.40	0.38
14C	39 - 53	55 - 64	1.04	1.08	0.36	0.25
15C	59 - 66	59 - 67	1.04	1.06	0.37	0.34
16C	37 - 49	31 - 48	1.01	1.08	0.44	0.24
17C	53 - 64	53 - 64	1.03	1.02	1.54	1.63

(*)=inadmissible ranges §=static test n/a=not applicable

Table 3.14; Quasi-Cyclic Struts - Southwell and Lundquist Plot Data

Strut Ref.	Linear Fit Range			Euler Data		w _{OC} Data	
	X = Pre-Cyclic Y = Post-Cyclic	Southwell (% of P _e)	Lundquist (% of P _e)	l _s /l	l ₁ /l	a _{OS} (mm)	a _{OL} (mm)
18	X	26 - 44	24 - 44	1.05	1.07	1.16	0.82
18	Y	47 - 55	47 - 55	1.03	1.03	1.54	1.63
19	X	41 - 50	22 - 48	1.05	1.09	0.42	0.33
19	Y	59 - 68	64 - 68	1.04	1.07	0.48	0.37
20	X	\$	\$	\$	\$	\$	\$
20	Y	\$	\$	\$	\$	\$	\$
21	X	34 - 41	n/a	1.02	n/a	0.19	n/a
21	Y	53 - 59	58 - 62	1.01	1.00	0.40	0.61
22	X	20 - 39	n/a	1.02	n/a	0.36	n/a
22	Y	56 - 60	54 - 60	1.00	0.95	0.68	0.25
23	X	39 - 56	39 - 56	1.03	1.07	0.65	0.42
23	Y	59 - 70	59 - 72	1.03	1.04	0.75	0.73
24	X	43 - 54	43 - 54	1.07	1.08	0.51	0.44
24	Y	62 - 75	62 - 73	1.06	1.06	0.60	0.75

samples 25 to 27 (incl.) are n/a

l = L/2

n/a = inadmissible ranges
\$ = buckled during cyclic phase

Table 3.15 ; Southwell and Lundquist Plot Data

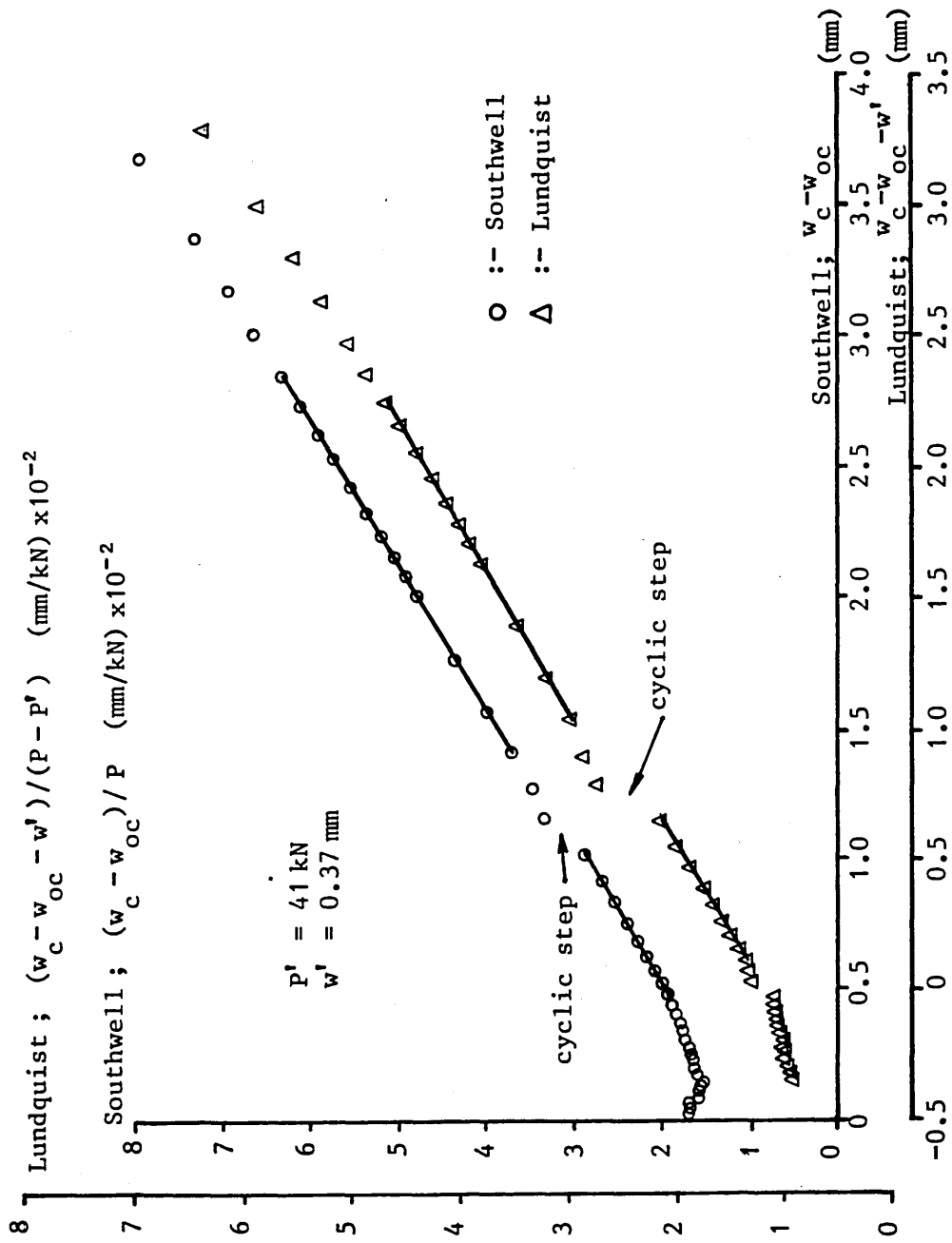


Figure 3.61 ; Southwell and Lundquist Plots - Strut Ref. 24C

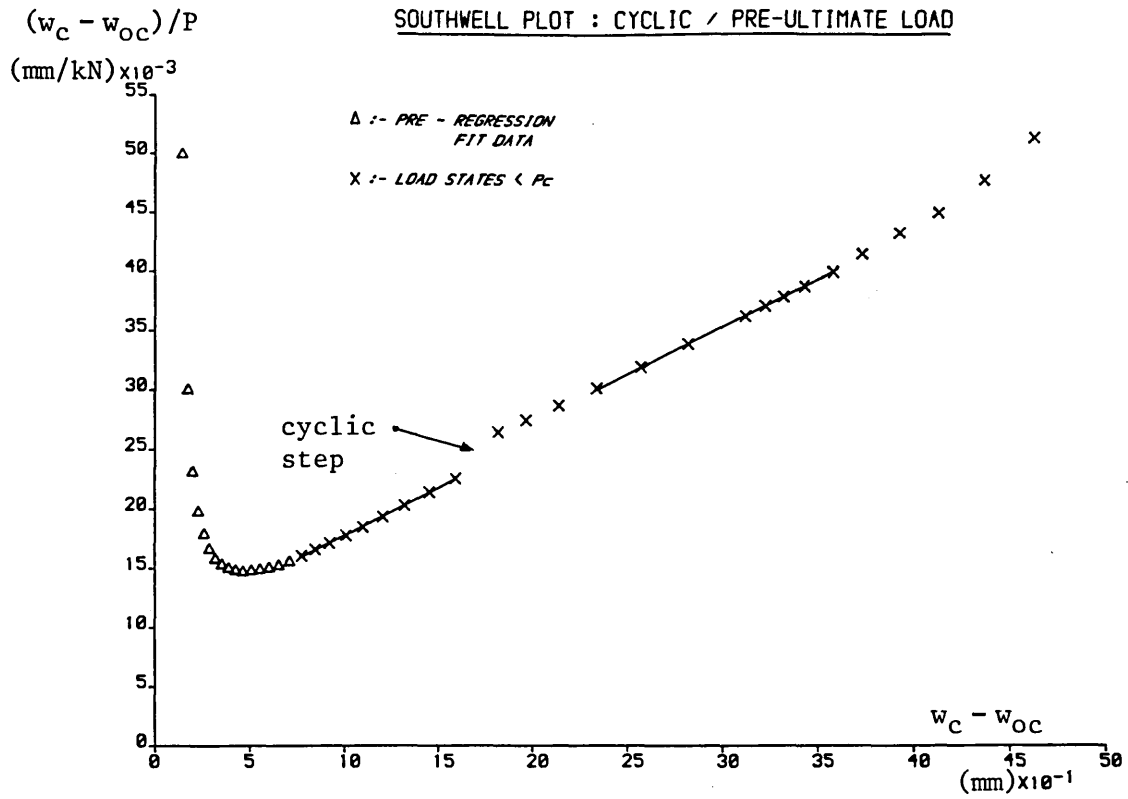


Figure 3.62 ; Southwell Plot - Strut Ref. 18C

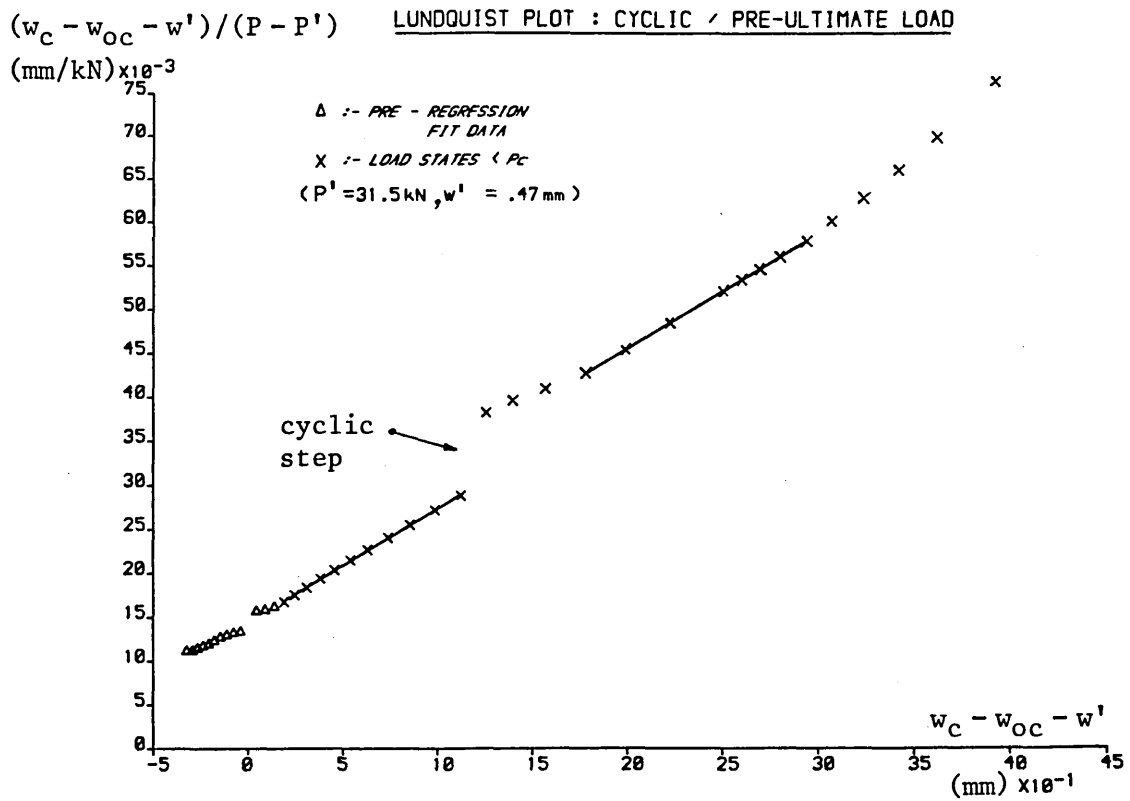


Figure 3.63 ; Lundquist Plot - Strut Ref. 18C

3.8 ADDITIONAL TESTS

3.8.1 Comments

Three series of additional stub and strut tests were conducted for purposes of data control. Six stub tests were undertaken using additional material to ascertain the effect of quasi-elastic hysteresis on structural specimens independent of stability considerations, ie low λ . Nine strut specimens were subjected to a 'section bending' process in order to investigate the static performance of the CHS specimens in the presence of larger imperfections - the high quality of the ESWR specimens employed having been specifically discussed. Use was made of facilities available in the South Yorkshire coalfield to achieve the necessary circular arc profile for the nine strut specimens - section bending is used to provide runway roofing. The cold-forming technique employed will not only generate larger initial curvatures but also set up residual stress leading to complex high order imperfections. Alternative control using highly imperfect struts was also achieved by re-testing, statically, six previously buckled specimens from the mainstream testing programme. However, as three of the specimens had previously been tested cyclically, additional control on fatigue and comparative cyclic/static assessment was also made available.

3.8.2 Cyclic Stub Test

Table 3.16 gives the key data appertaining to the six additional

Stub Ref	Mode	Pre-cyclic E (kN/mm ²)	Post-cyclic E (kN/mm ²)	ΔP (kN)	
1D	S	n/a	n/a	n/a	1D; $\sigma_y=305\text{N/mm}^2$ E=201kN/mm ²
2D	S	n/a	n/a	n/a	2D; $\sigma_y=294\text{N/mm}^2$ E=205kN/mm ²
1D	(a)	C	199	204	-0.3
	(b)	C	200	206	0.5
2D	(a)	C	204	212	2.5
	(b)	C	203	210	2.1

Table 3.16 ; Cyclic Stub Test Data

Strut Ref	λ / λ_1	w_{ocL} (mm)		P_c (kN)	P_c/P_B	
		Pinned w_{ocL}	Encastré w_{ocE}			
		28	(a)	0.98	5.33	2.48
	(b)	0.98	5.80	2.70	104.0	0.71
29	(a)	0.90	5.20	2.67	94.7	0.75
	(b)	0.91	8.47	4.27	90.6	0.72
30	(a)	0.98	9.67	4.63	94.2	0.63
	(b)	0.97	7.50	3.79	96.3	0.68
31	(a)	0.96	6.79	3.24	99.5	0.70
	(b)	0.97	8.06	3.89	95.2	0.67
32	(a)	0.87	7.37	3.62	75.7	0.80

P_c average = 95kN; P_c/P_B average = 0.67

Table 3.17 ; Synthetically Deformed Strut Test Data

Strut Ref	1R	2R	3R	4R	5R	6R	Average
Original Strut Ref	5S	10S	10C	13C	15S	15C	-
w_{ocE} (mm) encastré	18.8	26.4	18.1	20.9	27.9	23.6	22.6
P_c (kN)	70.6	61.1	71.1	65.3	59.4	58.2	64.3
Original P_c (kN)	106.4	106.8	111.0	105.3	112.5	111.9	109.4

Table 3.18 ; Retested Strut Test Data

stub tests conducted on CHS material cut from two further runs of steel, demarked 1 and 2 respectively. Tests 1D and 2D were purely static to establish appropriate E and σ_y /proof stress data; note Section 3.4.1. The cyclic action profiles implemented in the remaining four tests were constrained to maintain cyclic action wholly within the nominally linear elastic range. Figs 3.64 and 3.65 display typical behaviour. As shown in Table 3.16, the post-cyclic stiffness increases in accordance with the findings of Section 3.7.1, with the post-cyclic modulus E being clearly deemed to be the agent of this increase. Quasi-elastic hysteresis is a random phenomenon⁽⁵¹⁾ and this is borne out by the results obtained. The characteristics of the densely grouped line hysteresis displayed in Fig 3.64 are of similar form to those obtained in the quasi-cyclic strut tests, note also ΔP in Table 3.16, showing imperfection sensitivity and slenderness ratio are not of importance with respect to the random quasi-elastic hysteresis phenomenon.

3.8.3 Synthetically Curved Struts

Data appertaining to these static strut tests is given in Table 3.17. Strut Ref 32(a) overwrites case 16S as discussed in Section 3.2.2, the remaining samples being strut pairs from the denoted 7.5m section runs; for all cases, $\lambda=80$. Due to the larger geometric imperfections induced, correlation between the lathe-centre or pinned mode w_{ocL} data and the corresponding encastré mode data w_{ocE} is lost; note Section 3.5.1. These imperfection values are an order of magnitude higher than those of the

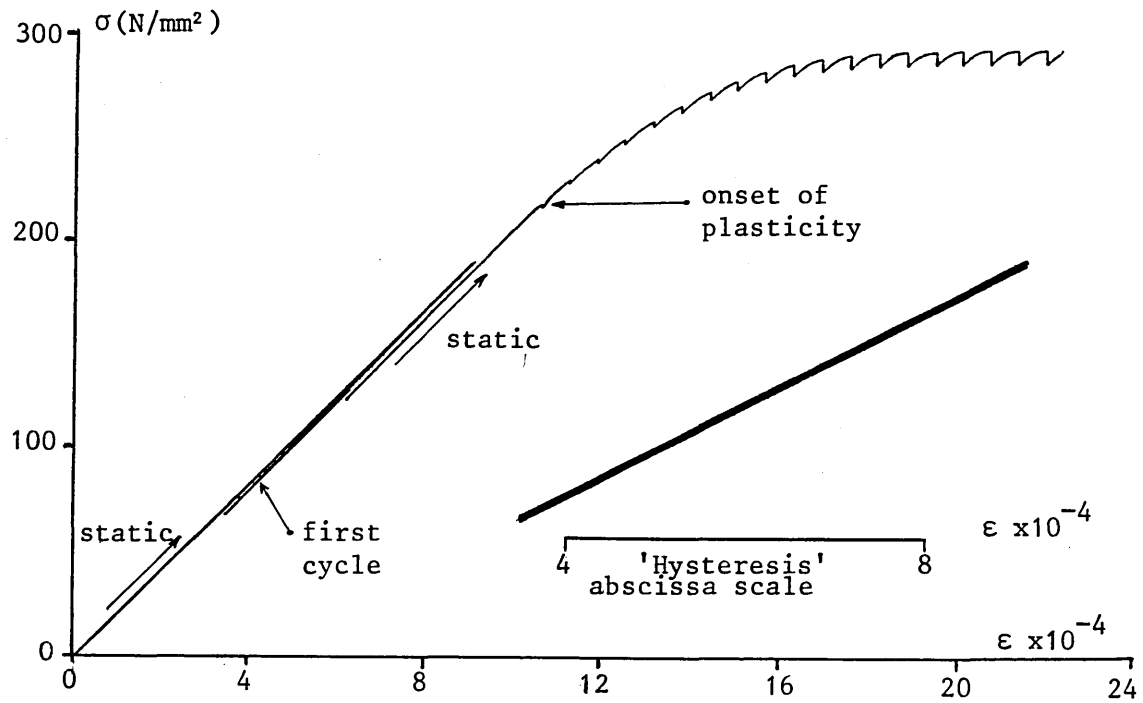


Figure 3.64 ; Cyclic Stub Test (Autographic) Output
- Stub Ref. 2D(a)

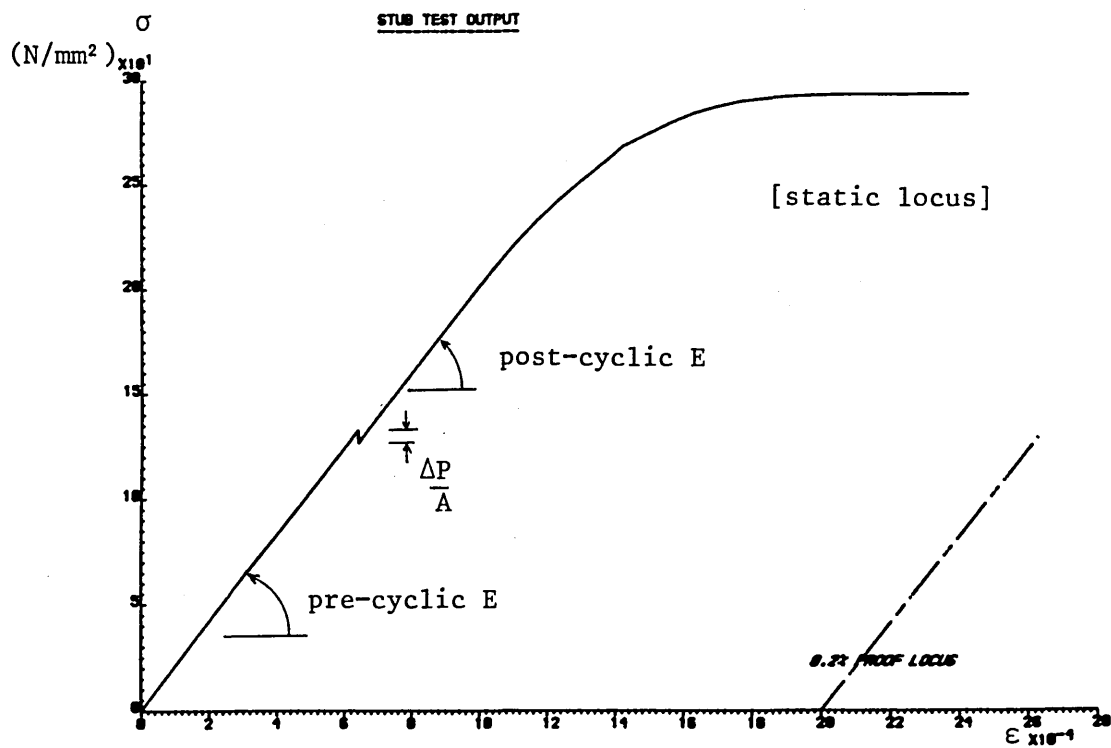


Figure 3.65 ; Cyclic Stub Test: Computer Graphic Output
- Stub Ref. 2D(a)

mainstream strut tests. Comparison with the average P_c/P_s value for the mainstream static strut tests with $\lambda=80$ shows an average reduction in P_c/P_s of some 20%; from 0.83 to 0.67, note Tables 3.12 and 3.13. Fig 3.66 shows a typical P vs $w_{cL}-w_{ocL}$ locus with apparently negative pre-buckling stiffness. Fig 3.67 shows the corresponding vector trace explaining this apparent anomaly, with planarity of the buckling path clearly invalid. The path is subject to a complex interaction of larger imperfections, noting particularly the implications of clamping a circular arc initial strut topology. It should be noted that P_c in case 32(a) is approximately 12% lower than the P_c of case 16C.

3.8.4 Re-Tested Struts

A final six static tests upon struts of a heavily imperfect form were undertaken using previously tested specimens. Key data is given in Table 3.18; note the large values of w_{ocE} recorded in comparison with those of Table 3.13. Reductions in buckling load of the order of 40% were obtained and lateral displacement at buckling increased significantly. The previously cyclically tested struts, as anticipated, showed no sign of fatigue having been induced due to the former cyclic action. The correspondence between the re-tested data for both the S and C type cases reinforce the finding that the quasi-elastic hysteresis associated with the quasi-cyclic tests does not significantly affect static strut performance. Fig 3.68 displays a typical re-test P vs $w_{cL}-w_{ocL}$ locus; the corresponding vector traces are planar as is to be expected given their re-tested nature.

AXIAL LOAD vs. MID-SPAN RESULTANT LATERAL DISPLACEMENT

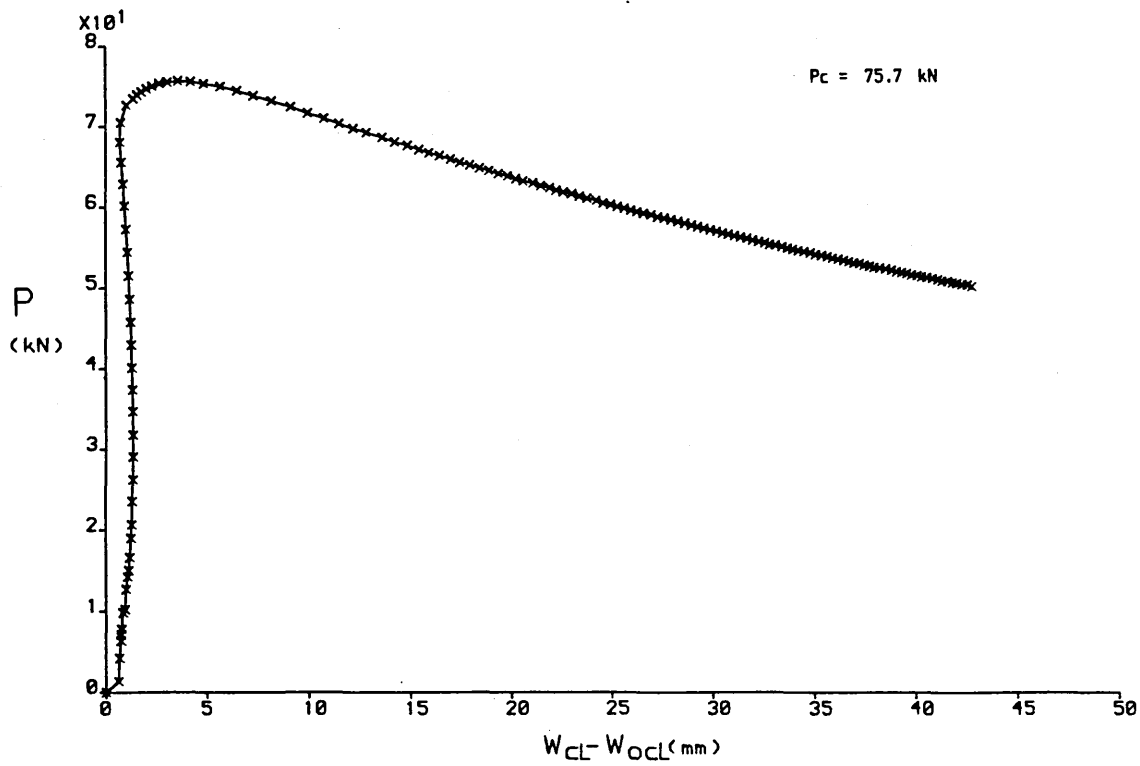


Figure 3.66 ; P vs $w_{cL} - w_{oCL}$ - Strut Ref. 32(a)

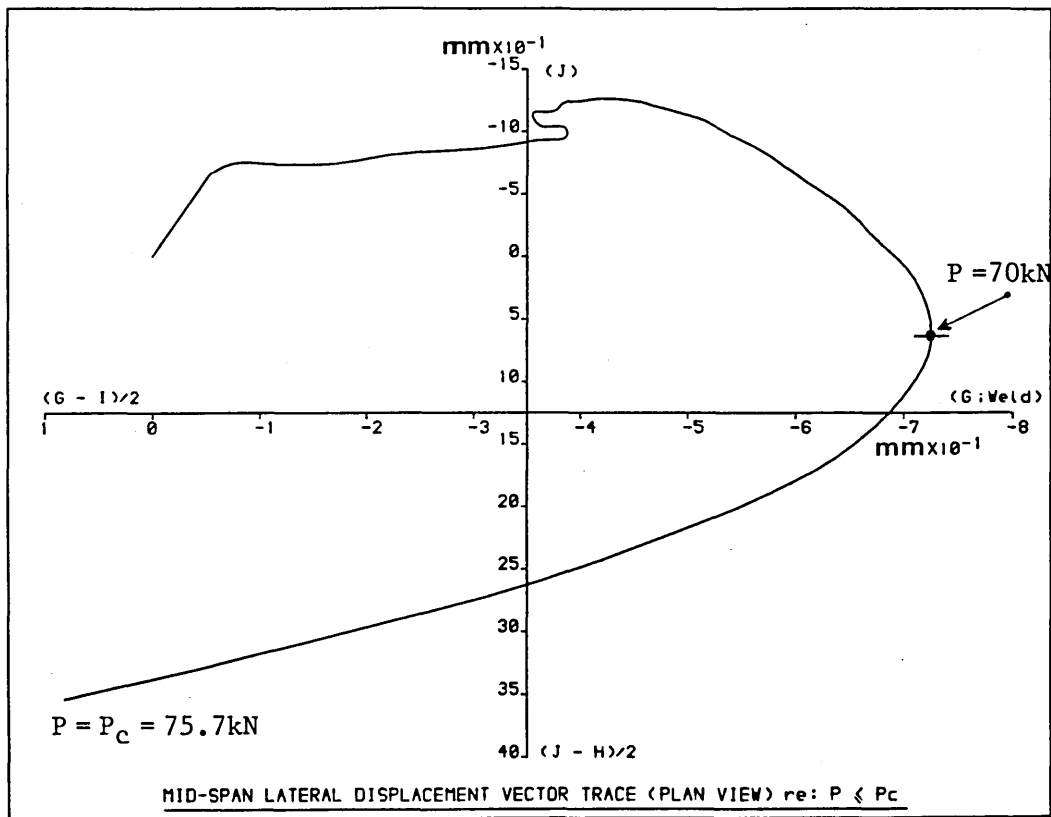


Figure 3.67 ; Vector Trace ($P \leq P_c$) - Strut Ref. 32(a)

AXIAL LOAD vs. MID-SPAN RESULTANT LATERAL DISPLACEMENT

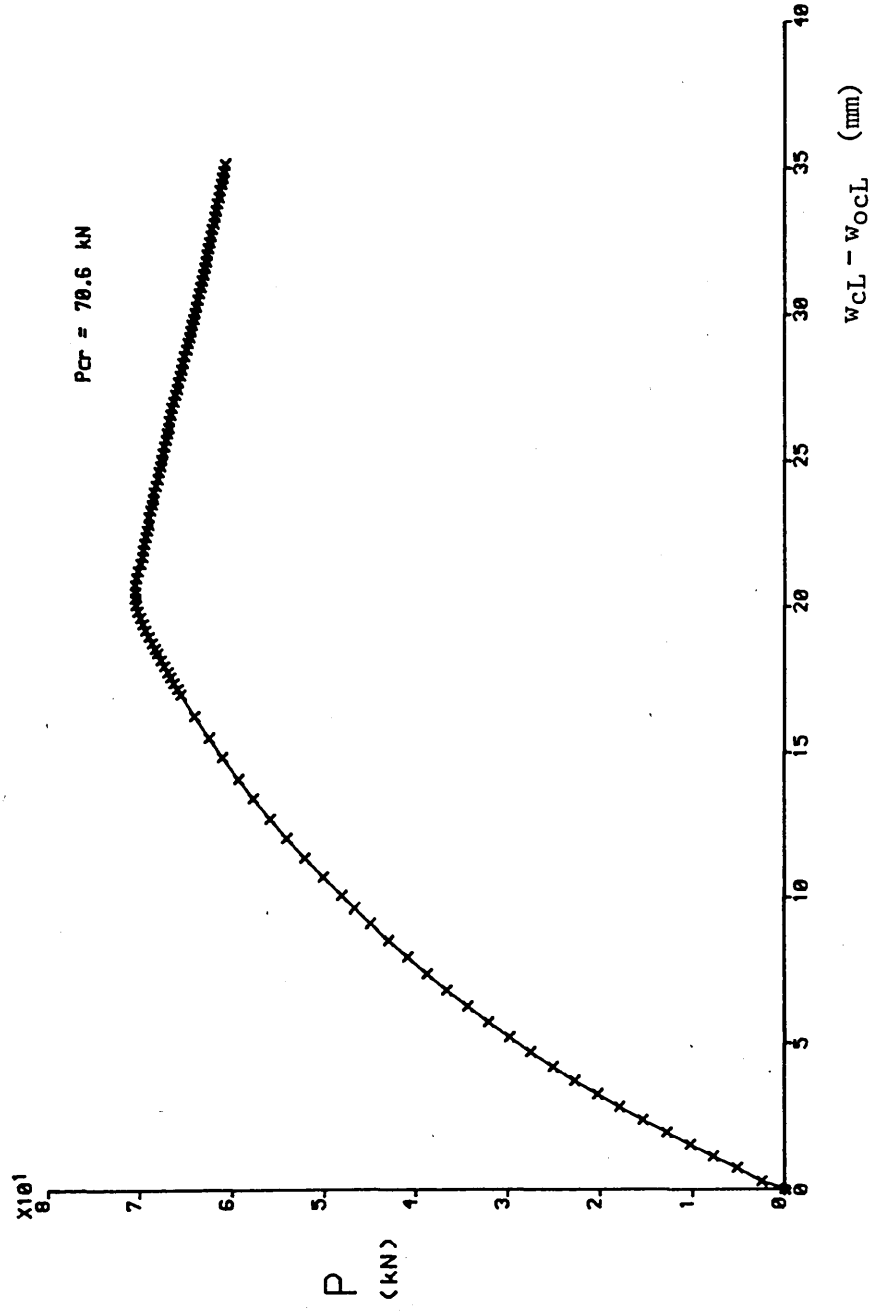


Figure 3.68 ; P vs $w_{CL} - w_{ocL}$ - Strut Ref. 1R

3.9 SUMMARY

The findings of in excess of 200 computer governed large scale tests have been presented and discussed. Further deliberation will follow the theoretical modelling set out in the next chapter. Key data has been summarised in Tables 3.11, 3.12 and 3.13 whilst primary findings are typified by Fig 3.33. A schedule of tests is given in Fig 3.69.

Considerations will now be given to a theoretical study with regard to which attention is drawn to the nature of the cyclic step (w_{cL}^1 or, with respect to $\ell=L/2$, w_c^1) and the fact that upto four different forms of identifying the initial out-of-straightness are available for each strut. Finally, the importance of λ_m values upon strut performance has been specifically recorded. This demands that particular attention be given to the matter of constitutive modelling.

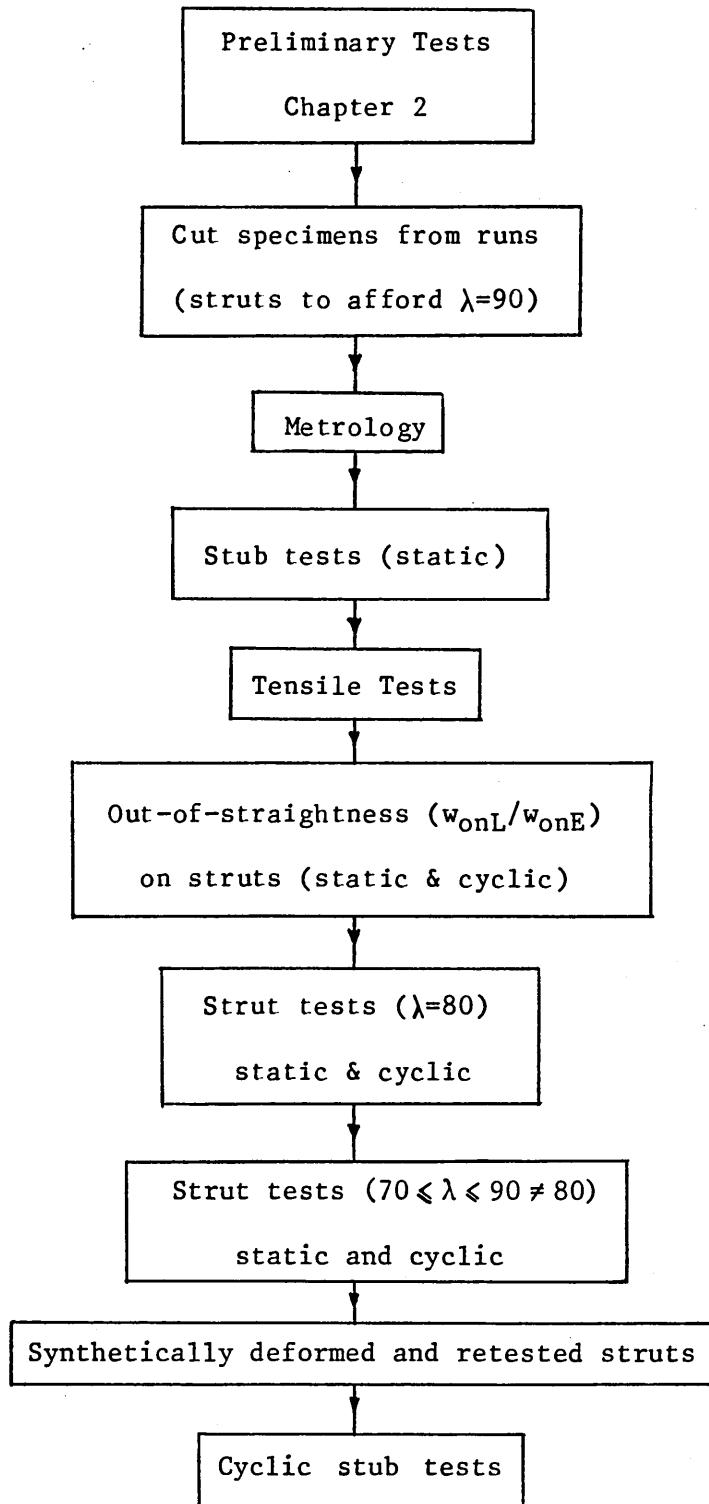


Figure 3.69 ; Schedule of Tests

CHAPTER 4

THEORETICAL STUDY

4.1 INTRODUCTION

Given the complexities associated with inelastic strut behaviour, their planar static analysis invariably involves numerical or approximate techniques. A variety of approaches have been established(35,66,67,68), with finite element(55,69) and tangent stiffness(70,71) studies being prominent amongst them. Constitutively, three phases of behaviour have been identified, the 'elastic', the 'primary plastic' and the 'secondary plastic' phases(72). The first phase relates to those zones of the strut which are only stressed in the elastic range, the second to those in which yielding occurs in the compressive fibres, whilst the 'secondary plastic' phase involves those zones of the strut in which yielding occurs in both tensile and compressive fibres. Strut analysis also involves their interaction, a task requiring considerable computational effort.

It is against this background that the present theoretical studies are set and the following decisions were taken with regard to their implementation. With the primary purpose being to analyse static strut behaviour subject to the effect of a phase of pre-buckling cyclic loading, a fully static model was to be initially produced. This static model was to involve the aforementioned three zone constitutive relationships. In an attempt to simplify

this involvement, a novel moment-thrust-curvature function, of central importance to the theoretical studies, was derived. Computational amenability was completed by employing a representative spring-link strut model approach^(3,35) Spring-link modelling as introduced in Section 1.4 provides an excellent research tool, enabling convenient and representative quantification of system parameters. System performance was to be couched in terms of virtual work^(73,74), and analysis was to be continued well into the post-buckling range.

Inclusion of cyclic effects was to be centred on representation of the cyclic step as exemplified in Fig 3.33 and Eqn (3.14). Experimentation had shown this to be the primary effect of a pre-buckling cyclic action phase and modelling the appropriate pseudo-static characteristics as delineated in Fig 3.31 was thereby deemed to afford sufficient definition of the problem. Concentration was placed upon flexural behaviour, this being considered to be the quintessential arbiter of buckling performance. End-shortening modelling was to be largely intuitive.

The model was to accommodate imperfections in the form of an initial central transverse displacement, data for this parameter being provided from the experimental programme in the form of w_{OC} -direct, w_{OC} -interpolated, a_{OS} (Southwell) and a_{O1} (Lundquist). The latter pair of parameters should provide for the correct planarity of action and inclusion of eccentricity of loading and residual stress (however small) effects. Upto four theoretical

models per strut case analysis are thereby provided for, case assessments being detailed following derivation of the model.

Theoretical studies are based upon an effective length $\ell (=L/2)$ and the necessary transformation for experimental flexural deformation data is carried out in accordance with the discussions of Section 3.5.1, see Eqn (3.10) for example, and Section 3.6.2, noting Fig 3.28 in particular. Essentially, all prototype flexural deformation parameters are halved with respect to model studies, confidence in the deemed experimental assumption of $\ell=L/2$ being provided by the effective length assessments given in Tables 3.10 and 3.14. The non-dimensionalised cyclic step ratio denoted in Eqn (3.14) is invariant. Resulting theoretical or model flexural deformation values are then doubled for use in theoretical/experimental assessment employing prototype loci.

Computer resident algorithms were employed throughout using 64-bit based routines for solution of the resultant non-linear expressions. Computer graphics were employed for parametric output and the appropriate files were interactively controlled to enable appropriately fine incrementation in the vicinity of the buckling state.

4.2 FORMAL STATIC MOMENT-THRUST-CURVATURE CONSTITUTIVE RELATIONSHIPS

An encastré CHS strut is illustrated in section and half-elevation, noting the relevant symmetry, in Figs 4.1(a) and (b)

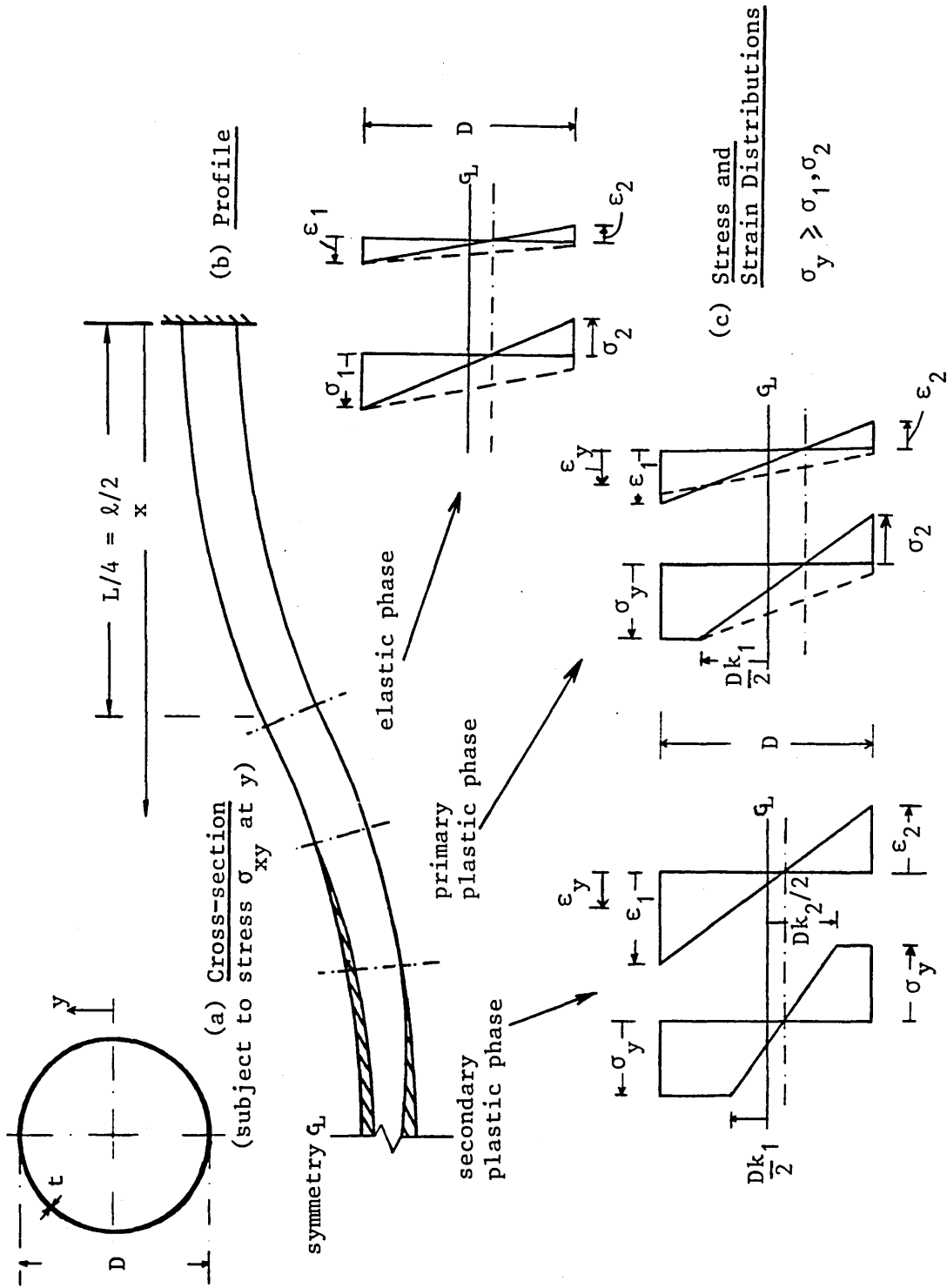


Figure 4.1 ; Three Phase Constitutive Topology

respectively. The appropriate three-phase constitutive topology⁽⁷²⁾ is shown in Fig 4.1(c) with ϵ_1 and ϵ_2 denoting the respective maximum compression and tensile direct strains, σ_1 and σ_2 the corresponding maximum elastic stresses and parameters k_1 and k_2 denoting non-dimensional elastic core delineators. Yield zones are hatched in the half-elevation profile. Idealised elasto-plastic behaviour is assumed, the stub test experimentation, noting Section 3.4.1 in particular, supporting this assumption overall.

General moment, thrust and curvature relationships at any centreline location are derived employing

$$P \equiv P_x = \int_A \sigma_{xy} \, dA \quad (4.1)$$

$$M \equiv M_x = \int_A \sigma_{xy} y \, dA \quad (4.2)$$

$$v \equiv v_x = (\epsilon_1 - \epsilon_2) / D \quad (4.3)$$

y denoting the spatial coordinate orthogonal to x . Eqns (4.1) to (4.3) are evaluated for each of the three phases, resulting in

$$P = AE (\epsilon_2 + vD/2) \quad (4.4)$$

$$M = EIv \quad (4.5)$$

$$v = (\epsilon_1 - \epsilon_2) / D \quad (4.6)$$

for the elastic phase

$$P = P_S + \frac{ED^2 t \nu}{2} [k_1 \cos^{-1}(k_1) - k_1 - (1-k_1^2)^{\frac{1}{2}}] \quad (4.7)$$

$$M = \frac{ED^3 t \nu}{8} [k_1 (1-k_1^2)^{\frac{1}{2}} + \cos^{-1}(-k_1)] \quad (4.8)$$

$$\nu = 2(\epsilon_y - \epsilon_2) / D(1+k_1) \quad (4.9)$$

for the primary plastic phase, and

$$\begin{aligned} P = & \frac{P_S}{\epsilon_y \pi} \left[\epsilon_y [\sin^{-1}(k_2) - \sin^{-1}(k_1)] \right. \\ & + \frac{\nu D}{2} - \epsilon_2 [(\sin^{-1}(k_1) + \sin^{-1}(k_2))] \\ & \left. + \frac{\nu D}{2} [(1-k_1^2)^{\frac{1}{2}} - (1-k_2^2)^{\frac{1}{2}}] \right] \quad (4.10) \end{aligned}$$

$$\begin{aligned} M = & \frac{2ED^2 t}{4} \left[(1-k_1^2)^{\frac{1}{2}} [\epsilon_y + \epsilon_2 - \frac{\nu D}{2}(1+k_1/2)] \right. \\ & + (1-k_2^2)^{\frac{1}{2}} [\epsilon_y - \epsilon_2 - \frac{\nu D}{2}(k_2/2 - 1)] \\ & \left. + \frac{\nu D}{4} [\sin^{-1}(k_1) + \sin^{-1}(k_2)] \right] \quad (4.11) \end{aligned}$$

$$\nu = 4\epsilon_y / D(k_1 + k_2) \quad (4.12)$$

for the secondary plastic phase.

The above are represented in graphical terms in Fig 4.2, the moment-thrust-curvature expressions being evaluated in terms of $n=P/P_S$ using an open form solution procedure⁽⁷⁵⁾. The dashed asymptotes relate to the respective plastic moments of resistance

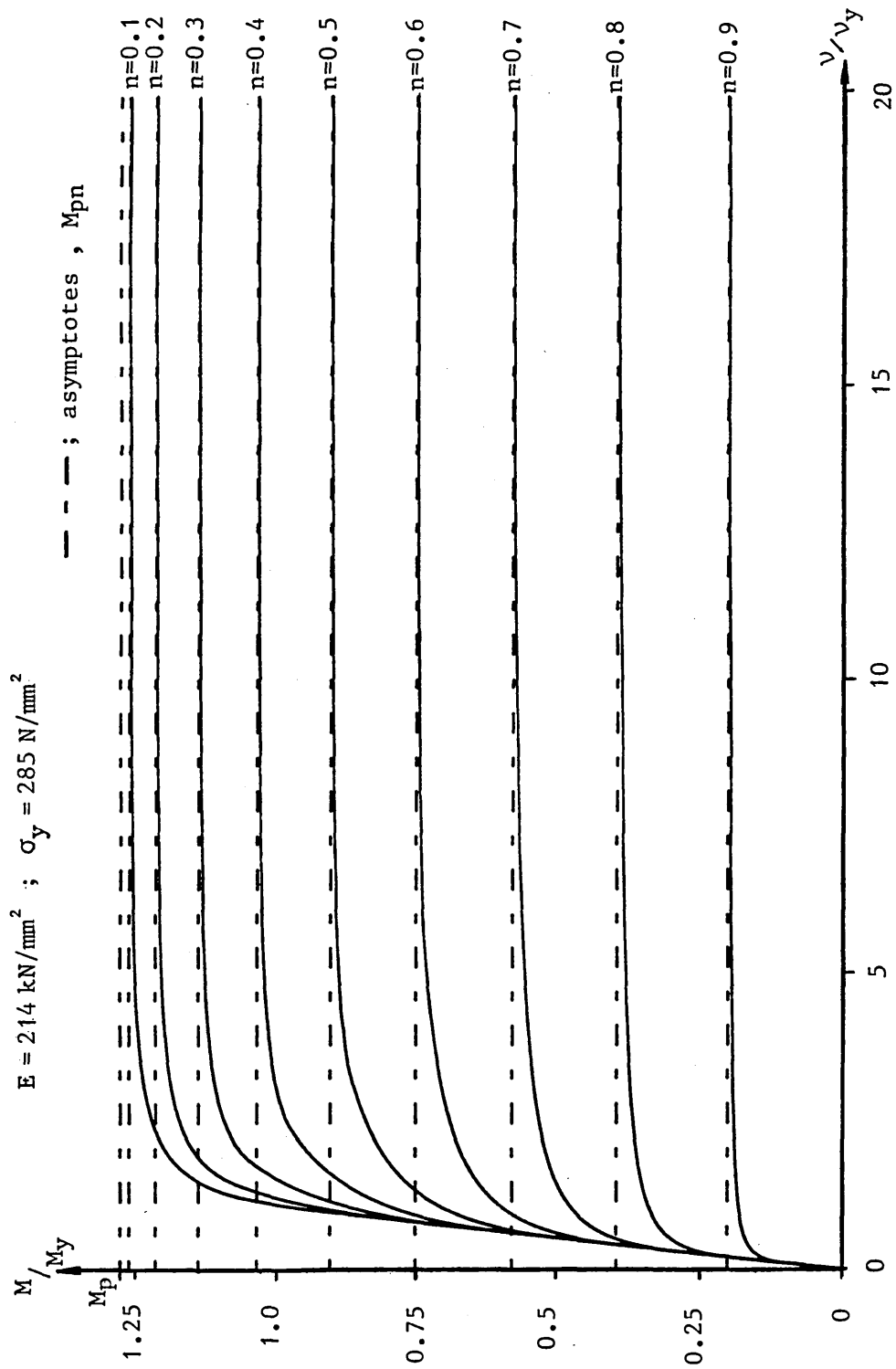


Figure 4.2 ; Formal M - P - v Contours

in the presence of axial thrust, M_{pn} , these asymptotes obeying

$$M_{pn} = M_p \cos(n\pi/2) \quad , \nu \rightarrow \infty \quad (4.13)$$

as required by the sectional geometry of Fig 4.1(a), M_p denoting the fully plastic moment. Fig 4.2 is presented in non-dimensional form, values being normalised to first yield moment M_y and curvature ν_y . Noting the complex natures of Eqns (4.7) to (4.12), then specific values for E and σ_y must be employed for Fig 4.2, the values actually employed therein being the respective average values obtained from the stub testing programme; see Section 3.4.1.

Eqns (4.4) to (4.12) relate to a complex stress-strain régime and are computationally unwieldy, particularly given the need to interface these three phases in accordance with the relevant governing system requirements.

4.3 NOVEL CONSTITUTIVE MODELLING

It was considered that the provision of a continuous moment-thrust-curvature function would do much to overcome the problems associated with implementation of the three-phase constitutive modelling. Previously published work relating to simplification of Eqns (4.4) to (4.12) has been restricted to the use of curve-fitting, with respect to loci of the form illustrated in Fig 4.2, involving the use of several piecewise connecting sub-functions^(76,77). Noting work elsewhere in the modelling of

non-conservative forces using exponential functions⁽⁷⁸⁾, a search for a suitable and unique moment-thrust-curvature expression was undertaken. Two primary constraints were placed upon the perceived function; first, initial behaviour must be in accordance with linear elastic characteristics and second, compliance with the asymptote behaviour denoted above must be present. The basic form of the function required was perceived to be of the form

$$M = M_{pn} (1 - e^{-f[M_{pn}, v]}) \quad (4.14)$$

and various attempts were undertaken to refine the modelling, conducted employing interactive computer graphics. This refinement resulted in acceptance of

$$M = M_p \cos(n\pi/2) \left(1 - e^{-[EIv / (M_p \cos(n\pi/2)) + c(1-n)v^2]} \right) \quad (4.15)$$

where $c = 123 \times 10^6 \text{ mm}^2$, a sectional constant. Eqn (4.15) is valid for $0 \leq n \leq 1$, and the performance is typified by Fig 4.3. The initial gradient of Eqn (4.15) with respect to the format of Fig 4.3 is given by $\partial M / \partial v = EI$ which accords with linear elastic theory. Asymptotes for all respective n are as required with $1/e^\infty = 0$ as v approaches ∞ . Eqn (4.15) is also capable of being conveniently normalised to first yield values of moment and curvature, with

$$M/M_y = r_s \cos(n\pi/2) \left(1 - e^{-[v(v_y r_s \cos(n\pi/2))^{-1} + c(1-n)v^2]} \right) \quad (4.16)$$

where $r_s = M_p / M_y$ denotes the respective shape factor.

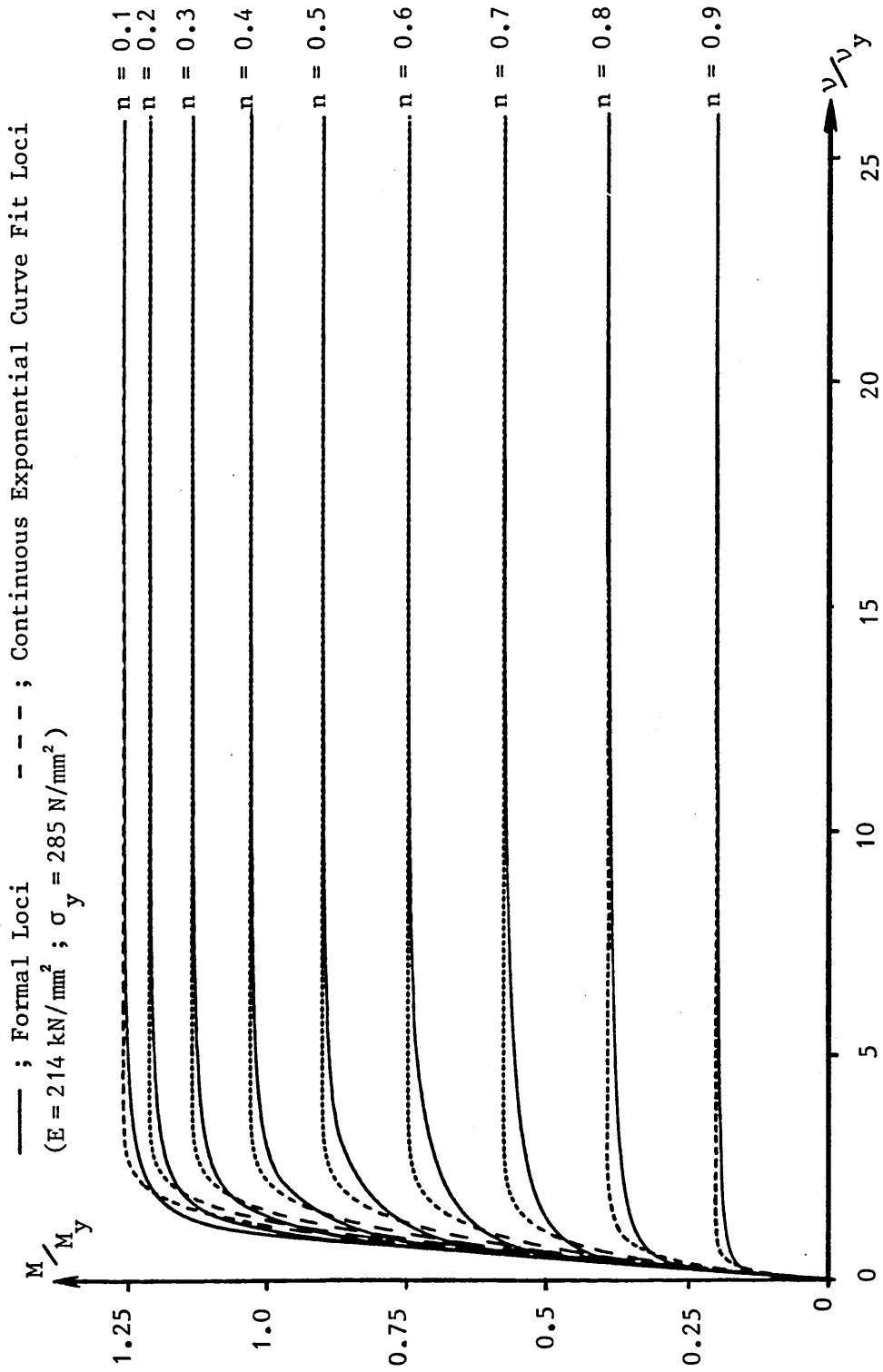


Figure 4.3 ; Formal M - P - v and Curve Fit Contours

The above formulation represents a unique and fully differentiable modelling of Eqns (4.4) to (4.12) and affords a computationally amenable format. Static strut modelling is now undertaken with a view to implementing the foregoing in a structural system of similarly accurate yet convenient form.

4.4 SPRING-LINK STRUT MODEL

Representative spring-link modelling was introduced in Section 1.4 with respect to elastic strut stability. Fig 4.4 illustrates a typical spring node i as displaced from an idealised zero datum state. The slopes of the adjacent links are given by θ_i and θ_{i-1} respectively, the angle through which the spring stiffness k_i works thereby being $\alpha_i = \theta_{i-1} - \theta_i$. Nodal v_i therefore takes the form

$$v_i = \alpha_i / [(\cos\theta_{i-1} + \cos\theta_i)\ell_i / 2] \approx \alpha_i / \ell_i = (\theta_{i-1} - \theta_i) / \ell_i \quad (4.17)$$

wherein the degree of system non-linearity is restricted⁽²⁴⁾. The spring moment M_i is given by

$$M_i = k_i \alpha_i \quad (4.18)$$

where spring stiffness $k_i = f(\alpha_i)$ for non-linear constitutive behaviour; see Eqn (4.15).

Fig 4.5 accordingly depicts a four-link strut model appertaining to an effective length ℓ with $k_1 = k_5 = 0$. The system is considered to be symmetrical, effectively possessing two degrees-of-freedom,

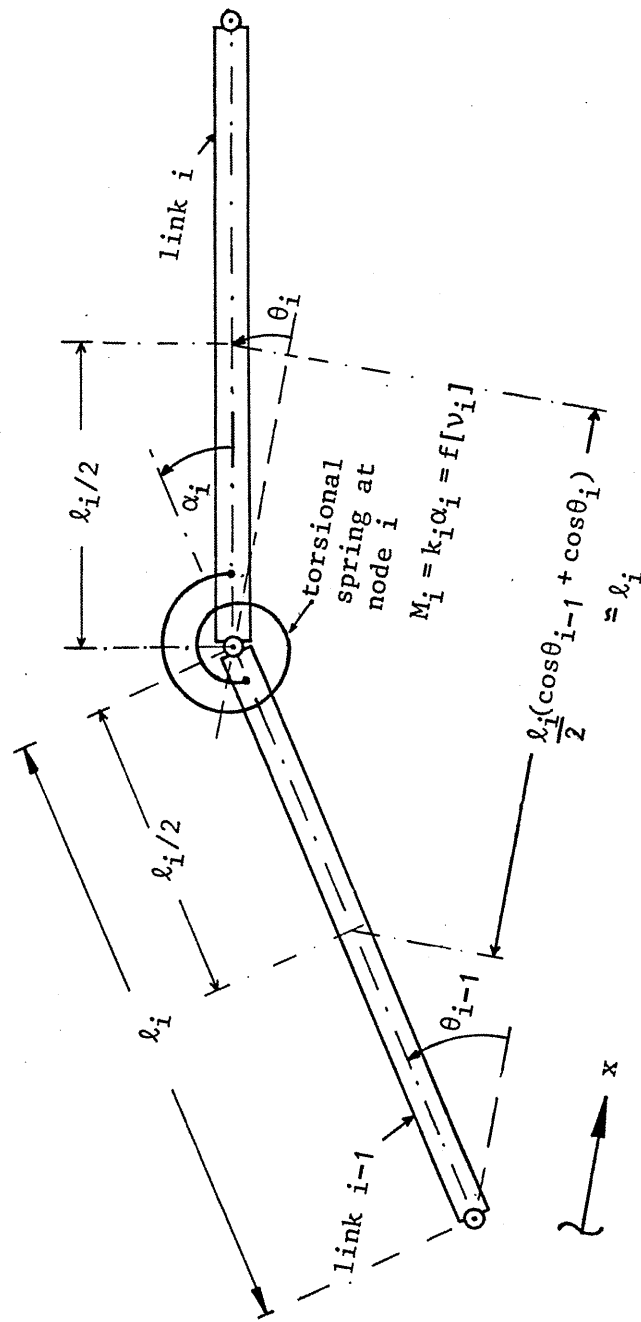


Figure 4.4 ; Typical Spring - Link Configuration

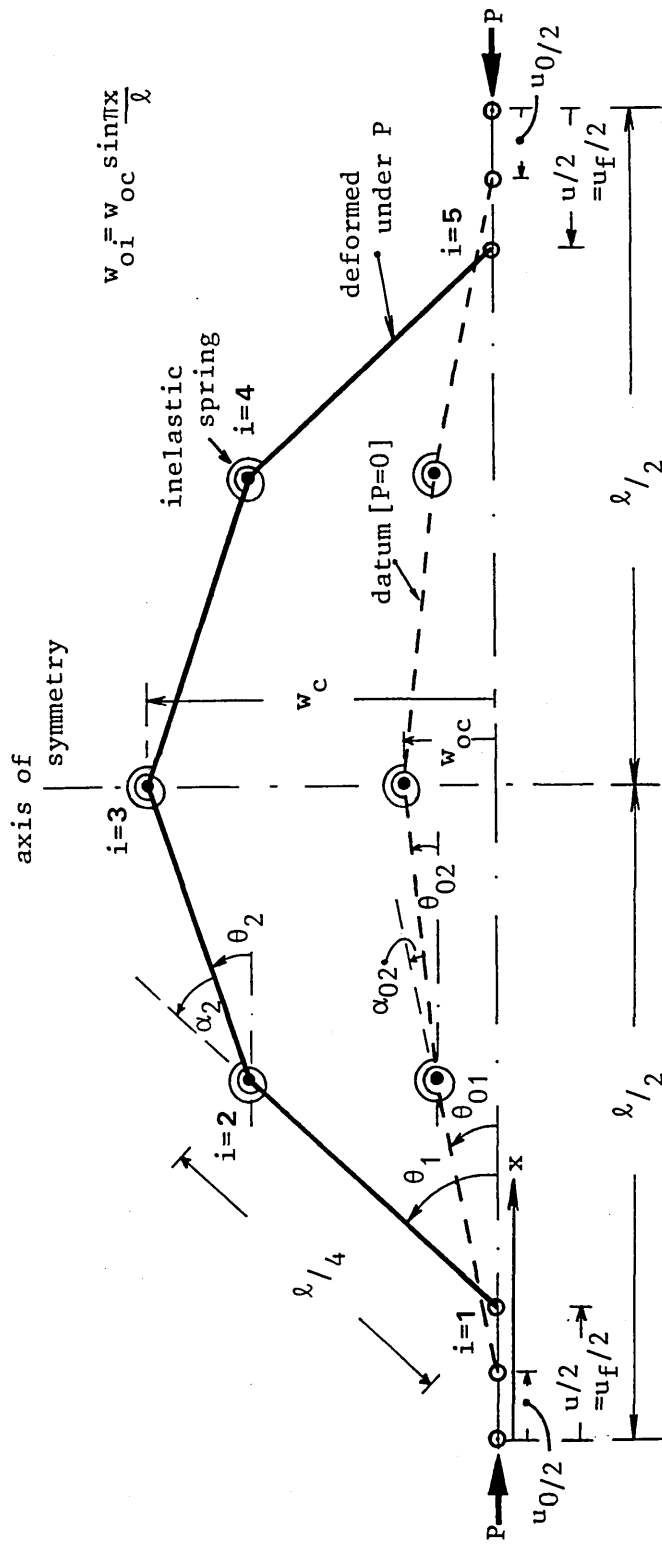


Figure 4.5 ; Theoretical Model

say θ_1 and θ_2 . Net central displacement is given by $w_c - w_{oc}$, noting the imperfect structural datum essentially defined by θ_{01} and θ_{02} . Values for these parameters are deduced from rigid body geometry, w_{oc} data obtained from the experimental programme and acceptance of an initial sinusoidal profile. The imperfect datum requires curvature v_i and moment M_i to become

$$v = (\alpha_i - \alpha_{0i}) / (\ell/4) = 4(\theta_{i-1} - \theta_{0(i-1)} - \theta_i + \theta_{0i}) / \ell \quad (4.19)$$

and

$$M_i = k_i (\alpha_i - \alpha_{0i}) \quad (4.20)$$

where k_i represents employment of Eqn (4.16) subject to the appropriate substitution of Eqn (4.19) for curvature $v = v_i$ and with $M_i = M$.

End shortening u neglects axial straining u_a , with flexural end shortening represented by u_f . Net end shortening is thereby formally written

$$u - u_0 = u_f - u_0 = \ell (\cos \theta_{01} - \cos \theta_1 + \cos \theta_{02} - \cos \theta_2) / 2 \quad (4.21)$$

as denoted in Fig 4.5. Axial modelling for imperfection sensitive struts must include axial strain effects and this feature is discussed in Section 4.9.

Eqn (4.16) subject to Eqns (4.19) and (4.20) thereby defines the strut model characteristics involved. The next section employs

the virtual work method to set up the necessary system equations.

4.5 ANALYTICAL VIRTUAL WORK FORMULATION

Denoting the internal virtual work by δU , then

$$\delta U = \sum_{i=2,3,4} [M_i \cdot \delta(\alpha_i - \alpha_{0i})] \quad (4.22)$$

The external virtual work, δW , takes the form

$$\delta W = P \delta(u_f - u_0) \quad (4.23)$$

For statics

$$\delta U = \delta W \quad (4.24)$$

Incorporating relationships established in Eqns (4.19) and (4.21), then Eqns (4.22) to (4.24) gives

$$\begin{aligned} & \sum_{i=2,3,4} [M_i \delta(\theta_{i-1} - \theta_{0(i-1)} - \theta_i + \theta_{0i})] \\ & = P \delta [\cos\theta_{01} - \cos\theta_1 + \cos\theta_{02} - \cos\theta_2] \end{aligned} \quad (4.25)$$

Substituting from Eqn (4.15), recalling $M=M_i$ and $v=v_i$, and employing $\delta U = (\partial U / \partial \theta_i) \delta \theta_i$ with $\delta W = (\partial W / \partial \theta_i) \delta \theta_i$ gives, for $i=1,2$ noting the symmetry in Fig 4.5

$$\begin{aligned}
& \frac{\partial}{\partial \theta_i} \left(\begin{array}{l} 2M_{pn} (\theta_1 - \theta_{01}) + e \\ - [2A(\theta_2 - \theta_{02}) + 4B(\theta_2 - \theta_{02})^2] \\ \cdot M_{pn} [A + 4B(\theta_2 - \theta_{02})]^{-1} \end{array} \right) \\
& + 2e \left(\begin{array}{l} - [A(\theta_1 - \theta_{01} - \theta_2 + \theta_{02}) + B(\theta_1 - \theta_{01} - \theta_2 + \theta_{02})^2] \\ \cdot M_{pn} [A + 2B(\theta_1 - \theta_{01} - \theta_2 + \theta_{02})]^{-1} \end{array} \right) \\
& = \frac{\partial}{\partial \theta_i} \left[\frac{P\ell}{2} (\cos \theta_{01} - \cos \theta_1 + \cos \theta_{02} - \cos \theta_2) \right] \quad (4.26)
\end{aligned}$$

where $A = 4EI/(\ell M_{pn})$ and $B = 16c(1-n)/\ell^2$. Differentiating affords

$$\sin \theta_1 + \sin \theta_2 = 4M_p \cos(n\pi/2) (1 - e^{-C}) / P\ell \quad (4.27)$$

and

$$\sin \theta_1 = 4M_p \cos(n\pi/2) (1 - e^{-D}) / P\ell \quad (4.28)$$

where

$$C = \frac{8EI(\theta_2 - \theta_{02})}{\ell M_p \cos(n\pi/2)} + \frac{4c(1-n)(\theta_2 - \theta_{02})^2}{(\ell/4)^2} \quad (4.29)$$

and

$$D = \frac{4EI(\theta_1 - \theta_2 - \theta_{01} + \theta_{02})}{M_p \ell \cos(n\pi/2)} + \frac{c(1-n)(\theta_1 - \theta_2 - \theta_{01} + \theta_{02})^2}{(\ell/4)^2} \quad (4.30)$$

Eqns (4.27) and (4.28) represent the pair of non-linear simultaneous equations which effectively govern the flexural system behaviour. Although highly non-linear, they provide an

extremely simple modelling procedure to the static strut problem, with only two equations covering the entire constitutive history. Whilst they can be applied directly to static case studies, their implementation with respect to struts subject to a pre-buckling cyclic action phase requires some further modelling development. This and the related matters of imperfection inclusion and solution algorithms are discussed in the following.

4.6 APPLICATION AND SOLUTION PROCEDURES

4.6.1 Static Studies

As noted above, the treatment of static strut studies requires only the provision of the appropriate data for use with Eqns (4.27) and (4.28). Case studies were undertaken for all static strut tests employing individual constitutive and geometric data. Most notable, perhaps, was the treatment of imperfections θ_{01} and θ_{02} . Data for w_{oc} , from which input values for θ_{01} and θ_{02} were deduced, was available in upto four forms per case, w_{oc} being provided by both direct and interpolated means as well as by a_{0s} and a_{0l} , the Southwell and Lundquist versions of w_{oc} respectively.

4.6.2 Cyclic Studies

Struts subjected to a pre-buckling cyclic action phase require the inclusion of an additional procedure to allow for the cyclic step $2w'_c (=w'_{cL})$, the appropriate transformations between displacement values based upon effective and nominal lengths being discussed

previously). Attention is also drawn to Fig 3.31(b).

Considering first the use of w_{oc} direct and interpolated data, then analysis for $0 < P < P'_m$, mean cyclic load P'_m being a prescribed system parameter, is conducted in the accepted static manner, together with determination of the respective equivalently fully static buckling load ' P_c ' and attendant central transverse displacement ' $(w_c - w_{oc})|_{P_c}$ '. The displacement at the P'_m state is then deemed to increase by cyclic step parameter w'_c , load loss due to hysteresis, note ΔP in Fig 3.31(b), being considered negligible. A new post-cyclic static state $(w_c - w_{oc} + w'_c)|_{P'_m, P'_m}$ is thereby established, the magnitude of w'_c being determined from Fig 3.33 or Eqn (3.14). The invariance of the non-dimensionalised cyclic step as delineated in Eqn (3.14) is to be recalled. Use of Fig 3.33 or Eqn (3.14) requires prescribed P_m and knowledge of the equivalently fully static values for ' P_c ' and ' $(w_c - w_{oc})|_{P_c}$ ' obtained as above.

The immediate objective now is to determine a new or revised value of initial imperfection ' w_{oc} ' that would generate a load-displacement locus that would pass, statically, through the above delineated post-cyclic static state $(w_c - w_{oc} + w'_c)|_{P'_m, P'_m}$. This static-type procedure was undertaken on an iterative trial-and-error basis, the revised value of initial imperfection being indicative of cyclic hysteresis amplification of initial strut imperfections. Once this amplified imperfection has been determined, a revised static analysis is conducted through to the post-buckling range in accordance with accepted procedures.

Finally, therefore, the overall pseudo-static modelling involves a static path based upon the respective initial imperfection for $0 \leq P \leq P_m'$, implementation of the cyclic step based upon the empirical design curve of Fig 3.33, followed by a second static analysis employing the appropriate cyclically revised imperfection through buckling for $P \geq P_m'$. This latter step provides the effective pseudo-static or post-cyclic buckling load associated with cyclic studies, P_c , together with the corresponding central transverse displacement. Referring to Fig 3.33, quasi-cyclic cases, note Table 3.11, employ the lower 5% cut-off value for the cyclic step. However, given the small values of cyclic step involved, a standard static analysis of the respective strut case is considered to be of sufficient accuracy.

With respect to employment of the lumped⁽⁵⁶⁾ Southwell and Lundquist imperfection parameters a_{0s} and a_{0l} , a different cyclic analysis procedure is utilised given the existence, where feasible, of distinct pairs of pre- and post-cyclic action phase values of a_{0s} and a_{0l} . Each cyclic strut case analysis consists of two static loci, one employing the pre-cyclic value of a_{0s} or a_{0l} , the other employing the corresponding post-cyclic value. For $0 \leq P \leq P_m'$, the former locus is valid, while the latter locus is valid for $P \geq P_m'$, the effective pseudo-static locus being completed by a transition line joining these two part-loci at $P = P_m'$. It is pertinent to note that for those cases of the Southwell and Lundquist plots in which only a post-cyclic linear fit range was available, see Table 3.15, the appropriate pseudo-static or post-cyclic buckling load P_c and its attendant central transverse

displacement remain accessible. For the quasi-cyclic cases, note Table 3.11, single static-type linear fit ranges were employed as denoted in Table 3.14, and, analytically, standard static strut procedures were followed in the manner described in the preceding section.

4.6.3 Non-Linear Solution Routine

Having established the means by which Eqns (4.27) and (4.28) were to be applied to the imperfection-sensitive static and cyclic case studies, the procedures by which the resulting expressions were actually evaluated can be considered. For computational convenience, Eqns (4.27) and (4.28) were actually rewritten in the form

$$\theta_1 = \sin^{-1} [(4M_p \cos(n\pi/2)(1-e^{-C})/P\ell) - \sin\theta_2] \quad (4.31)$$

and

$$0 = (1 - e^{-D}) - P\ell \sin\theta_1 / 4M_p \cos(n\pi/2) \quad (4.32)$$

recalling that C and D are given in Eqns (4.29) and (4.30) respectively. With only two equations to solve, an in-house solution procedure was established employing suitable tolerance values. The solution procedure consisted of prescribing $P(n)$, estimating θ_2 and determining the corresponding value of θ_1 from Eqn (4.31). The three values were substituted into Eqn (4.32) to provide a 'remainder' with respect to which θ_2 was re-estimated and a revised value of θ_1 obtained from Eqn (4.31), Eqn (4.32) again

acting as control. The procedure was repeated until a 'null' condition of $\pm 1 \times 10^{-9}$ was achieved. This procedure was adopted for all specified values of $P(n)$. For low values of $P(n)$, particularly small estimates of θ_2 were required corresponding to the pre-buckling path, with second roots defining the post-buckling path becoming acceptable as the load values of $P(n)$ increased. Fine incrementation was employed as $P(n)$ reached buckling, this being the state at which the two relevant roots become coincident. The foregoing procedure included provision for a cyclic step as necessary, transverse displacement being singularly increased at $P=P_m'$ in accordance with the principles established in Section 4.6.2.

Both numerical and graphical output were provided. The latter involved the merging of both the corresponding numerical and experimental data files for each case study. Initially, however, the performance of the model is exemplified in more generalised terms in the following section.

4.6.4 Static Strut Analysis, $\lambda_m=1$

Typical numerical modelling performance is typified in Fig 4.6 with $\lambda_m=1$ and constitutive data in accordance with BS 5950(36). For the quasi-idealised case ($w_{oc}=0$), the squash and critical loads are coincident and inelastic strut imperfection sensitivity is maximised. Imperfection loci corresponding to three arbitrary values of w_{oc} are also shown. Locus (a) employs an imperfection corresponding to case 18C ($\lambda_m=1$), thereby approximating to a

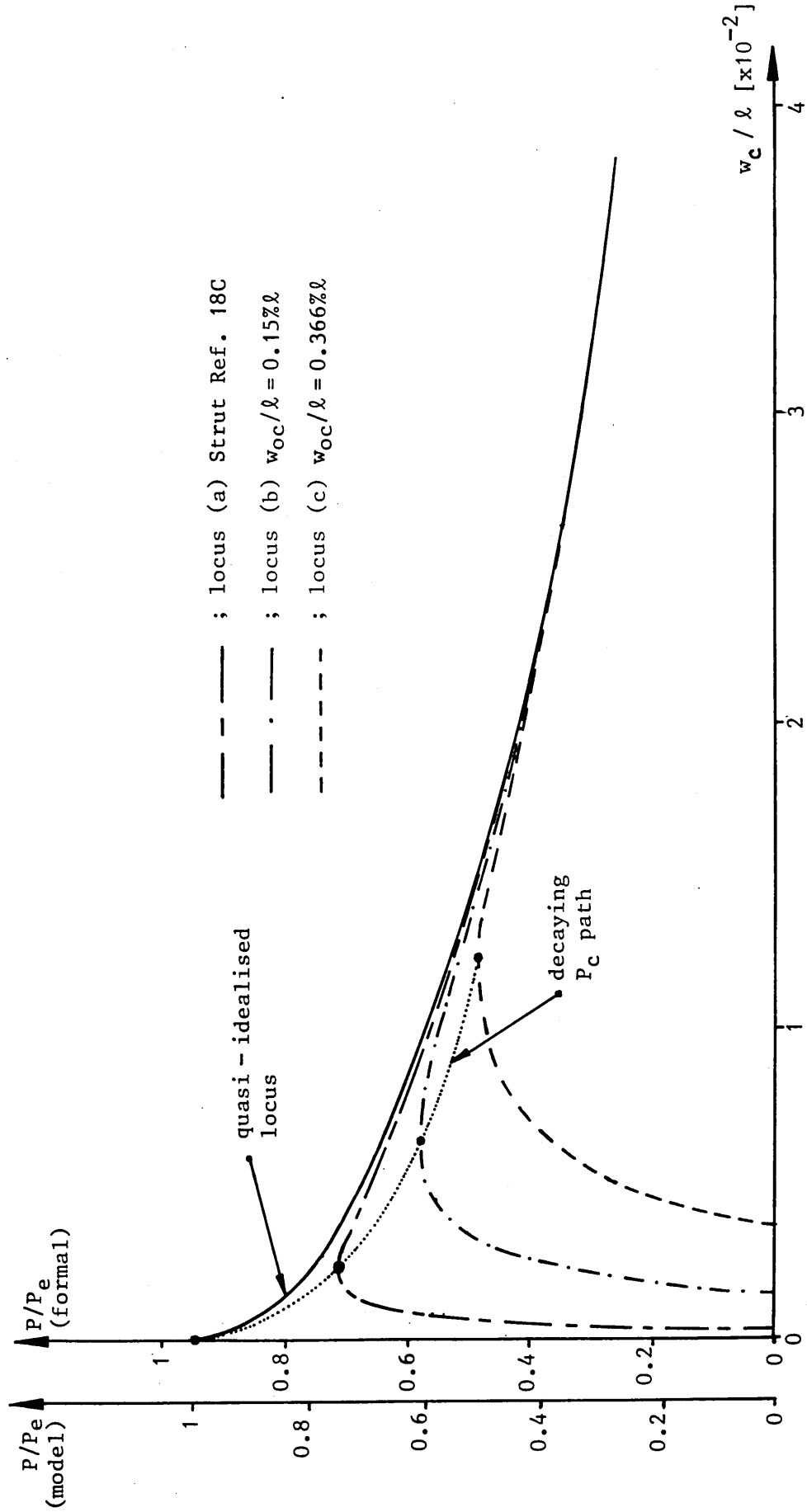


Figure 4.6 ; Quasi - Idealised and Imperfection Buckling Loci : $\lambda_m = 1$

specific experimental case study (nb E , σ_y and C specification). It is considered that the loci are consistent with established data and conducive to confidence in application of the model. The quasi-idealised locus acts as an 'envelope' to the appropriate imperfect loci.

4.7 CASE STUDIES; STATIC ANALYSES

Theoretical studies were undertaken for all mainstream static tests; see Table 3.12. Upto four analyses were possible in each case, these respectively employing the four different types of imperfection parameter w_{oc} -direct, w_{oc} -interpolated, a_{oS} -Southwell, and a_{o1} -Lundquist. Only w_{oc} -interpolated analyses were available for all static case studies. Figs 4.7 and 4.8 illustrate typical theoretical performance in terms of prototype or L-based values, with w_{oc} -direct type modelling showing well in both the 18S and 21S cases depicted; such w_{oc} -direct planar modelling was not available, however, in 10 of the 26 static strut cases denoted in Table 3.12.

Sample static strut modelling data is given in Table 4.1 with theoretical buckling loads being given in terms of the corresponding experimental value. The consistently lower bound nature of the Southwell-based results is most noteworthy. As denoted in Section 3.6.2, a_{oS} and a_{o1} data was available for most - 19 and 18 cases respectively - static strut cases. Given the 2 degrees-of-freedom analyses employed, the modelling data is considered to be particularly good. The majority of theoretical

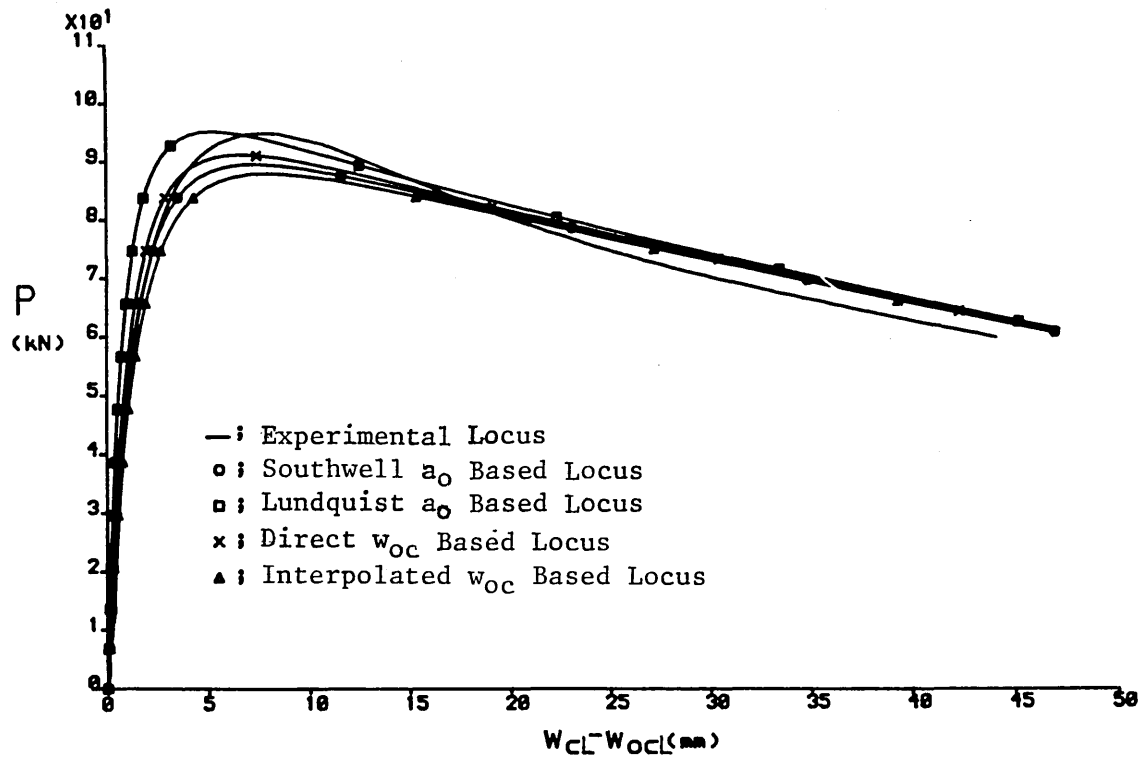


Figure 4.7 ; Case Study - Strut Ref. 18S

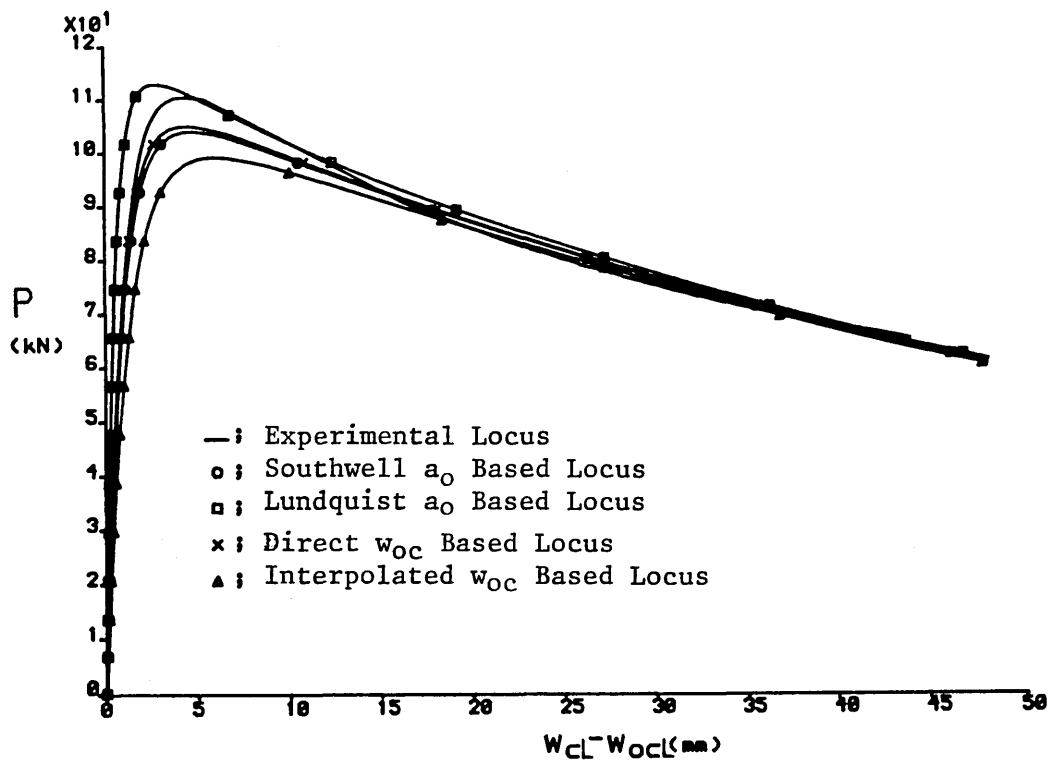


Figure 4.8 ; Case Study - Strut Ref. 21S

Strut	Theoretical Buckling Load (% of experimental value)			
	Southwell	Lundquist	Direct	Interpolated
3S	88.7	103.3	n/a	91.6
5S	89.9	102.4	102.4	99.6
9S	91.4	101.4	n/a	101.4
15S	92.4	100.0	n/a	94.7
17S	94.9	108.8	88.5	94.0
18S	95.9	100.8	96.7	92.9
20S	95.3	99.0	111.3	109.0
21S	94.2	101.9	95.6	90.1
22S	92.0	98.5	n/a	96.2
24S	96.6	91.4	96.1	86.2

n/a - not applicable

Table 4.1; Sample Static Strut Data - Theoretical Buckling
Load Assessment

Strut	Theoretical Buckling Load (% of experimental value)			
	Southwell	Lundquist	Direct	Interpolated
3C	91.7	95.4	96.9	91.4
4C	90.3	93.9	97.2	92.0
7C	93.4	94.7	n/a	95.7
8C	88.4	91.5	98.2	91.0
12C	94.6	104.9	n/a	96.3

n/a - not applicable

Table 4.2; Sample Quasi-Cyclic Strut Data - Theoretical
Buckling Load Assessment

static P_c values were of conservative form in keeping with Figs 4.7 and 4.8 and Table 4.1. Overall static modelling average values are summarised towards the end of this chapter. It is considered that the data trends illustrate satisfactory performance, with convergence to the appropriate experimental post-buckling path, wherein the effects of imperfections degenerate, being well displayed in Fig 4.8 .

4.8 CASE STUDIES; CYCLIC ANALYSES (PSEUDO-STATIC MODELLING)

Theoretical studies were conducted for all mainstream cyclic tests, note Table 3.12, with upto four analyses per case being available as noted in the previous section. Given the small and highly variable nature of the cyclic step involved in the quasi-cyclic cases, ie 1C to 17C, less 2C , it was deemed appropriate to treat these cases as effectively static, note Section 3.7. That is, with respect to the w_{oc} , direct and interpolated approaches, the 5% cut-off of Fig 3.33 was considered to be equivalent to a minimal effect as suggested in Section 4.6.2. Support for this interpretation is provided by an appropriate case-study. Also noted in that section was the fact that only single, static-type linear fit ranges were obtained in the respective Southwell and Lundquist plots; see Table 3.14. Accordingly, similarly static-type a_{0s} and a_{0l} analyses were also applied to the quasi-cyclic cases.

Table 4.2 contains sample theoretical modelling data appertaining to the quasi-cyclic studies. Values for buckling load are largely

conservative, typical of the 16 strut case-studies undertaken; overall average model values are considered in the summary of this chapter. The theoretical and experimental load-displacement loci for cases 3C and 7C are illustrated in Figs 4.9 and 4.10, no w_{oc} -direct analysis being available for the latter case; note Table 3.12. These loci display typical theoretical performance, employing static modelling. The performance is considered satisfactory, particularly given the loci shown in Fig 4.11 which incorporates a w_{oc} -direct analysis of case 3C, note Fig 4.9, which includes a 5% cyclic step with no cyclic load loss in accordance with the dictates of Fig 3.33. Whilst deformation characteristics are improved, buckling load estimates correspondingly suffer and, overall, little is considered to be effectively gained whilst computational effort is significantly increased. This is particularly so for case 3C as two distinct cyclic action phases were included, causing transverse displacement to be doubly augmented whilst the buckling load is doubly diminished. Given the highly variable nature of the cyclic step in the quasi-cyclic strut cases, note particularly the signs of $w'_{cL}/(w_{cL}-w_{ocL})|P_c$ in Table 3.11, there is a danger of over-conservatism in strictly adhering to the 5% cut-off rule of Fig 3.33.

The opportunity is taken in Fig 4.11 to clarify the 'equivalently fully static buckling load' referred to in Section 4.6.2. This load is denoted by P_{cs} and indicates that buckling load theoretically predicted from a fully static analysis with reference to struts suffering a cyclic action phase. Strictly,

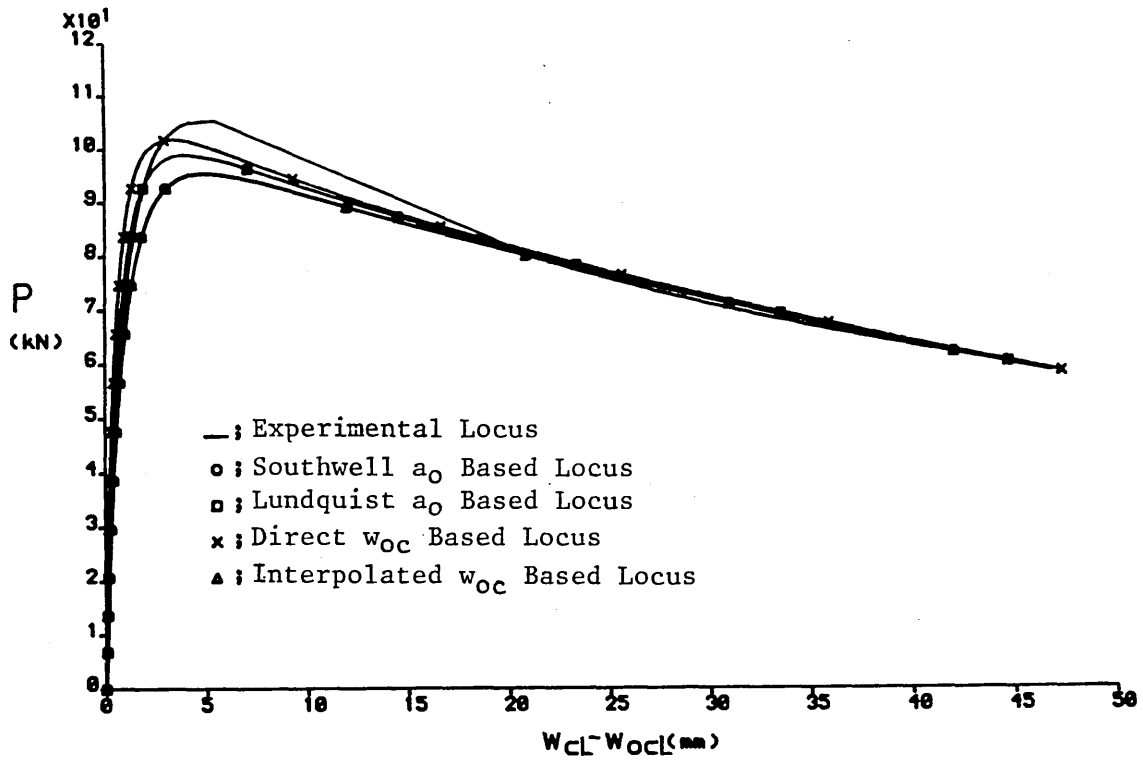


Figure 4.9 ; Case Study - Strut Ref. 3C

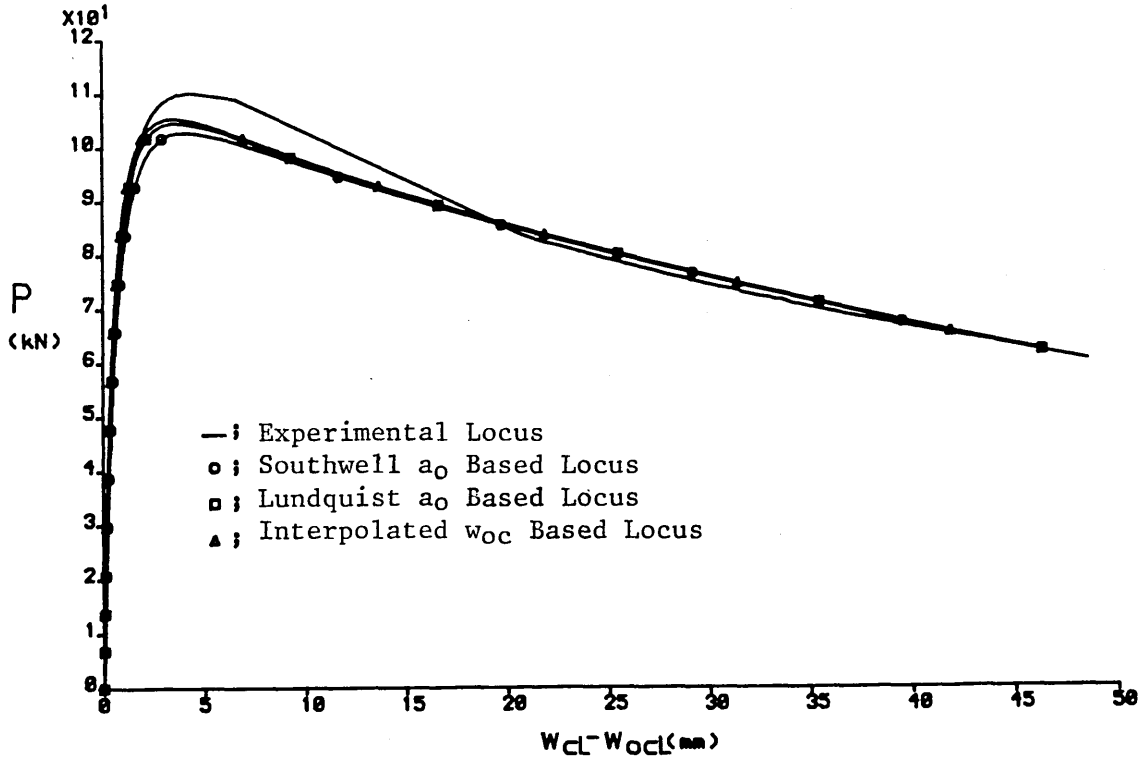


Figure 4.10 ; Case Study - Strut Ref. 7C

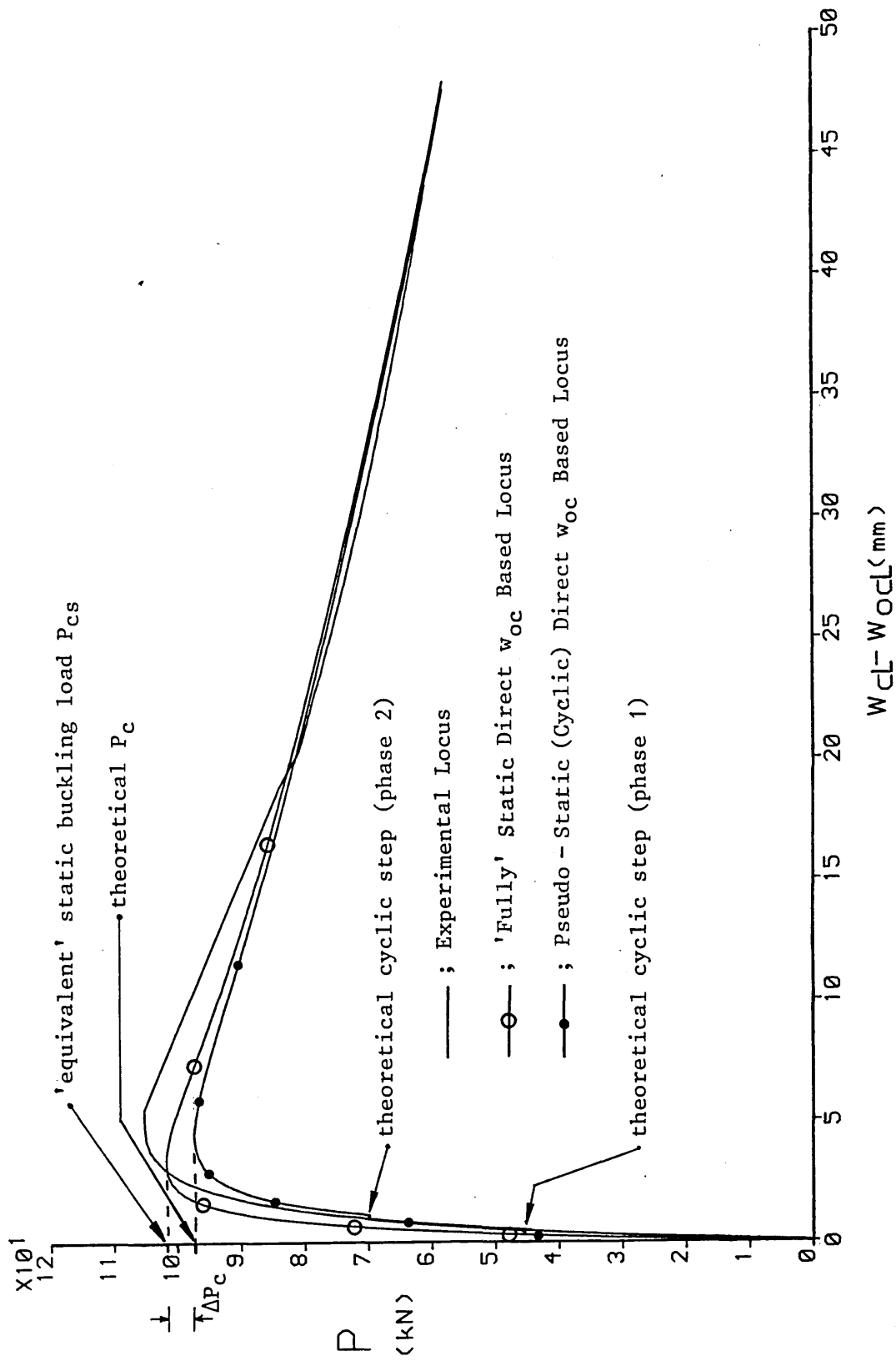


Figure 4.11 ; Case Study - Strut Ref. 3C

quasi-cyclic cases analysed in a static manner, see Figs 4.9 and 4.10 and Table 4.2, generate P_{CS} values.

With respect to the nine formally cyclic cases, 18C to 27C less 20C, the four analytical approaches were applied, as feasible, in accordance with the pseudo-static modelling procedure delineated in Section 4.6.2. Table 4.3 presents the appropriate theoretical buckling load values in terms of the respective experimental value. Given the central importance of these nine, ten including 20C, cases, the theoretical values appertaining to the corresponding static strut cases, note the previous section, are also included in Table 4.3 for comparison.

No theoretical study is made in the case of 20C as it relates to buckling being incurred during the cyclic action phase and is therefore beyond the sub-buckling cyclic action category. Despite the cyclic step being considered excessive with respect to serviceability requirements as denoted by the upper cut-off value in Fig 3.33, analysis for case 27C is included. Unsurprisingly, neither Southwell nor Lundquist plots were available for this case. Additionally, a_{0s} and a_{01} values were not available for cases 25C and 26C, these last three cases all possessing low λ_m but high u_m values; see Section 3.7.3 and Tables 3.11, 3.12 and 3.15. It is considered that the Southwell-based analytical values for P_c are of exemplary form, being consistently conservative throughout. The respective static and cyclic theoretical percentages show a relative decrease in accuracy overall in the cyclic cases. Given the greater degree of complexity involved,

Strut Ref.	P _C , Theoretical Buckling Load (% of Corresponding Experimental Value)											
	Direct			Interpolated			Southwell			Lundquist		
	S	C		S	C		S	C		S	C	
18	95.9	97.9		92.9	94.7		95.9	88.6		100.8		87.9
19	105.4	n/a		91.6	96.3		93.7	90.9		99.8		93.5
20	111.3	§		109.0	§		95.3	§		99.0		§
21	95.6	85.2		90.1	85.1		94.2	93.4		101.9		89.2
22	n/a	n/a		96.2	96.0		92.0	88.3		98.5		98.0
23	96.8	n/a		88.7	89.2		95.8	87.1		103.3		87.3
24	96.1	91.7		86.2	88.6		96.6	90.4		91.4		88.0
25	n/a	93.5		106.8	91.9		n/a	n/a		n/a		n/a
26	110.2	91.4		98.6	92.9		n/a	n/a		n/a		n/a
27	n/a	n/a		106.0	87.1		n/a	n/a		n/a		n/a
Average	102	92		97	* 91 **92		95	90		99		91

n/a = inadmissible range

§ = buckled during cyclic phase

S = static C = cyclic

* = including 27C, ** = excluding 27C (re serviceability 'cut-off' cf Fig 3.33)

Table 4.3; Theoretical Buckling Loads for Cyclic and Corresponding

Static Struts

this is to be expected. The average values given in Table 4.3 are considered satisfactory, particularly given the two degrees-of-freedom nature of the modelling.

Figs 4.12 to 4.17 illustrate typical load-displacement loci. The cyclic step, 'horizontally' modelled in the theoretical studies, is clearly depicted, with case 18C of Fig 4.12 providing for employment of all respective theoretical cyclic loci. General points to note include post-buckling convergence with the dramatic experimental buckling increment delaying this in Fig 4.13, the delightful Southwell-based locus of Fig 4.14, the ready availability of w_{OC} -interpolation loci and the problems associated with static-cyclic correlation as highlighted by the respective experimental loci in Figs 4.15 and 4.16, the former being apparently pathological whilst the latter case is thoroughly well-behaved. Fig 4.13 shows good w_{OC} -interpolated performance whilst the pre-buckling characteristics of the Southwell-based locus are exemplary. Fig 4.17 relates to case 27C which includes the largest cyclic step recorded - excluding case 20C - and modelling suffers accordingly although this case is deemed to exceed serviceability requirements as noted in Fig 3.33. It is considered that the theoretical pseudo-static interpretations employed provide for satisfactory modelling of the physical phenomena associated with the low cycle, low frequency inelastic hysteresis involved; see Sections 3.7.1 and 3.7.2. By employing upto four alternative imperfection values for each strut case, data trends, reflecting the above denoted statistical/empirical nature of strut design, are definitively established.

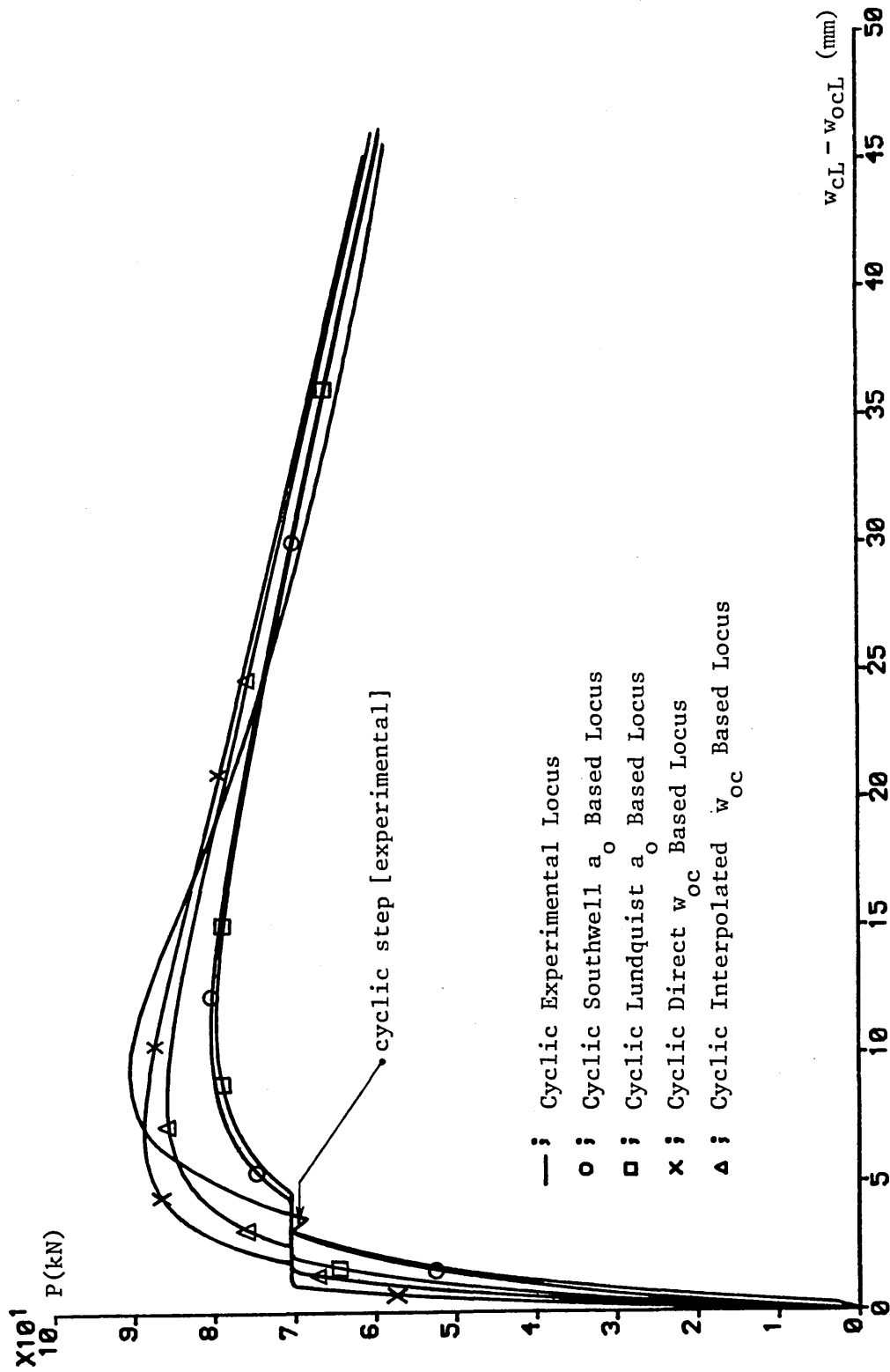


Figure 4.12 ; Case Study - Strut Ref. 18C

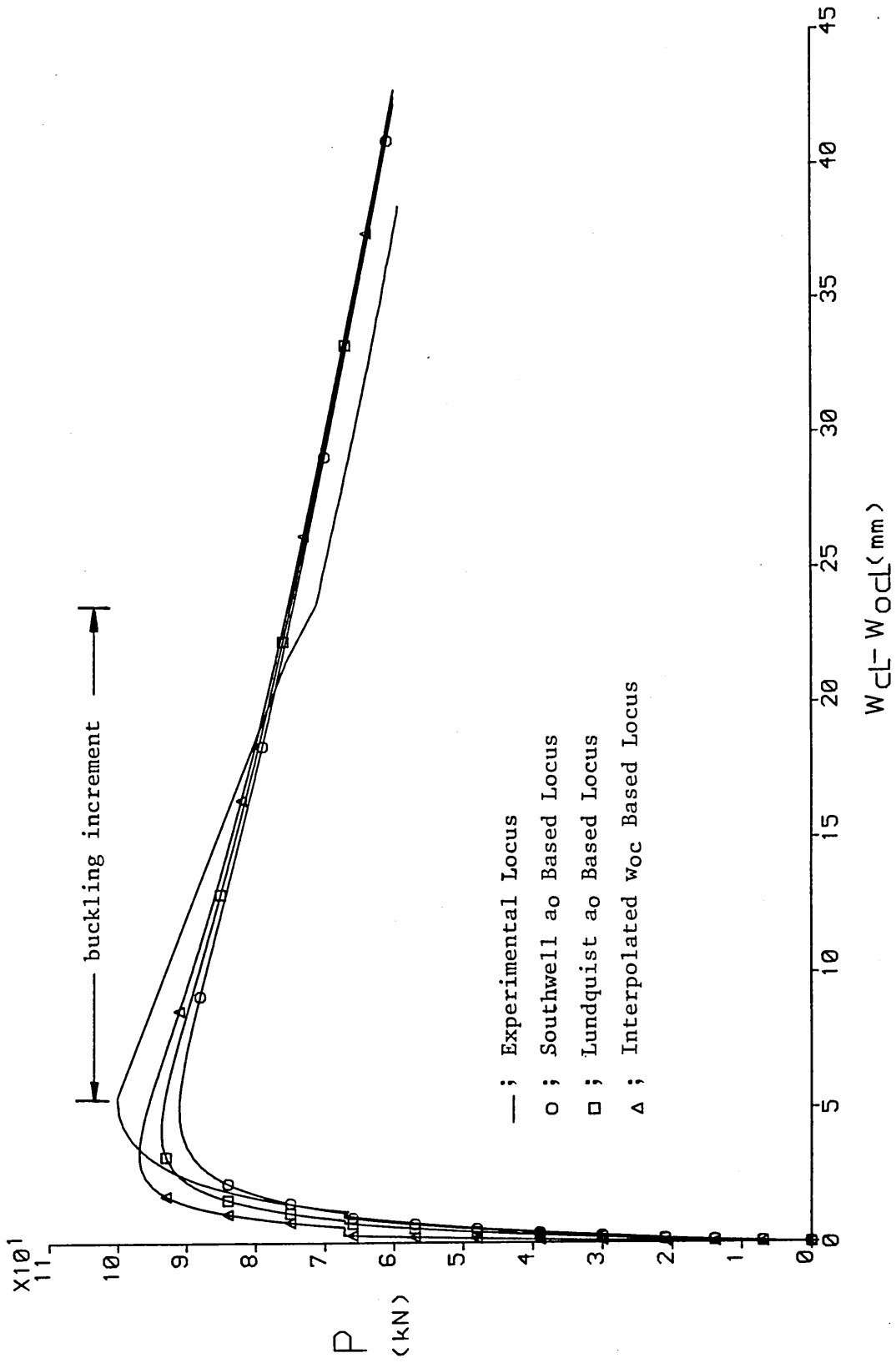


Figure 4.13 ; Case Study - Strut Ref. 19C

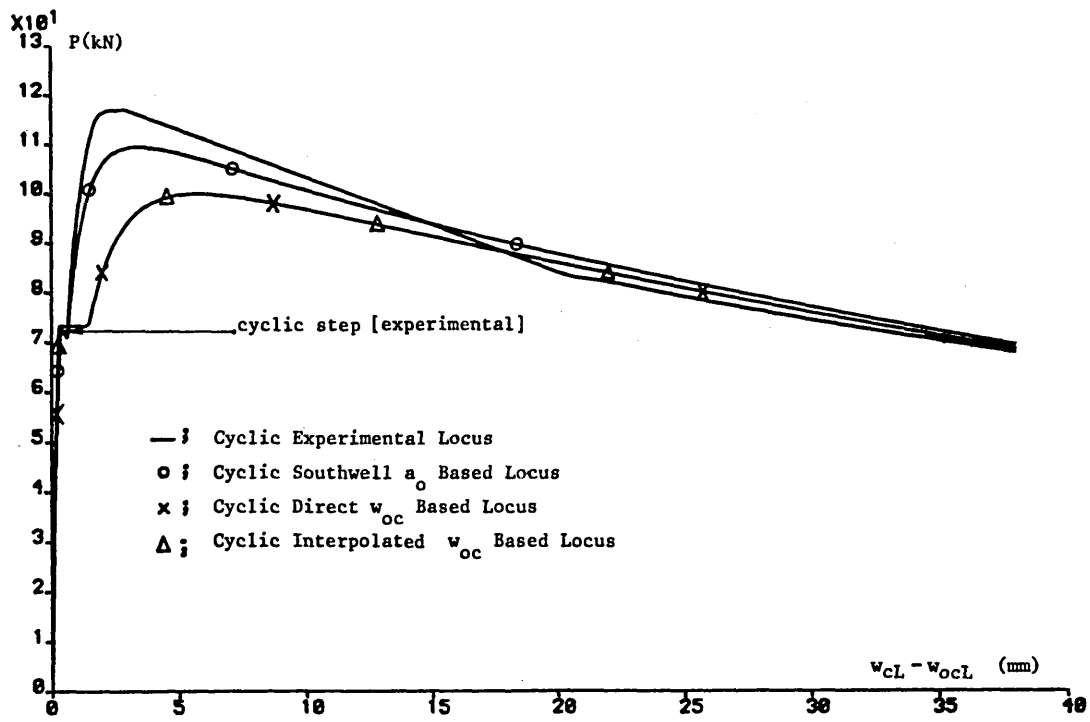


Figure 4.14 ; Case Study - Strut Ref. 21C

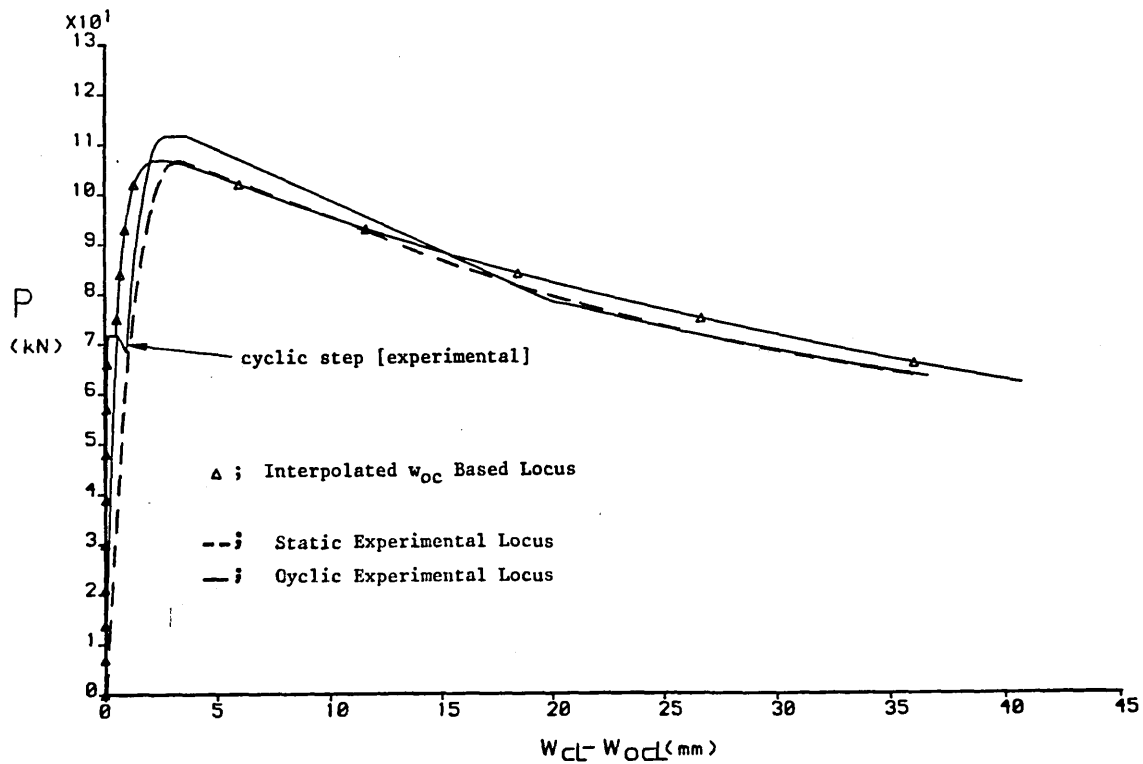


Figure 4.15 ; Case Study - Strut Ref. 22C

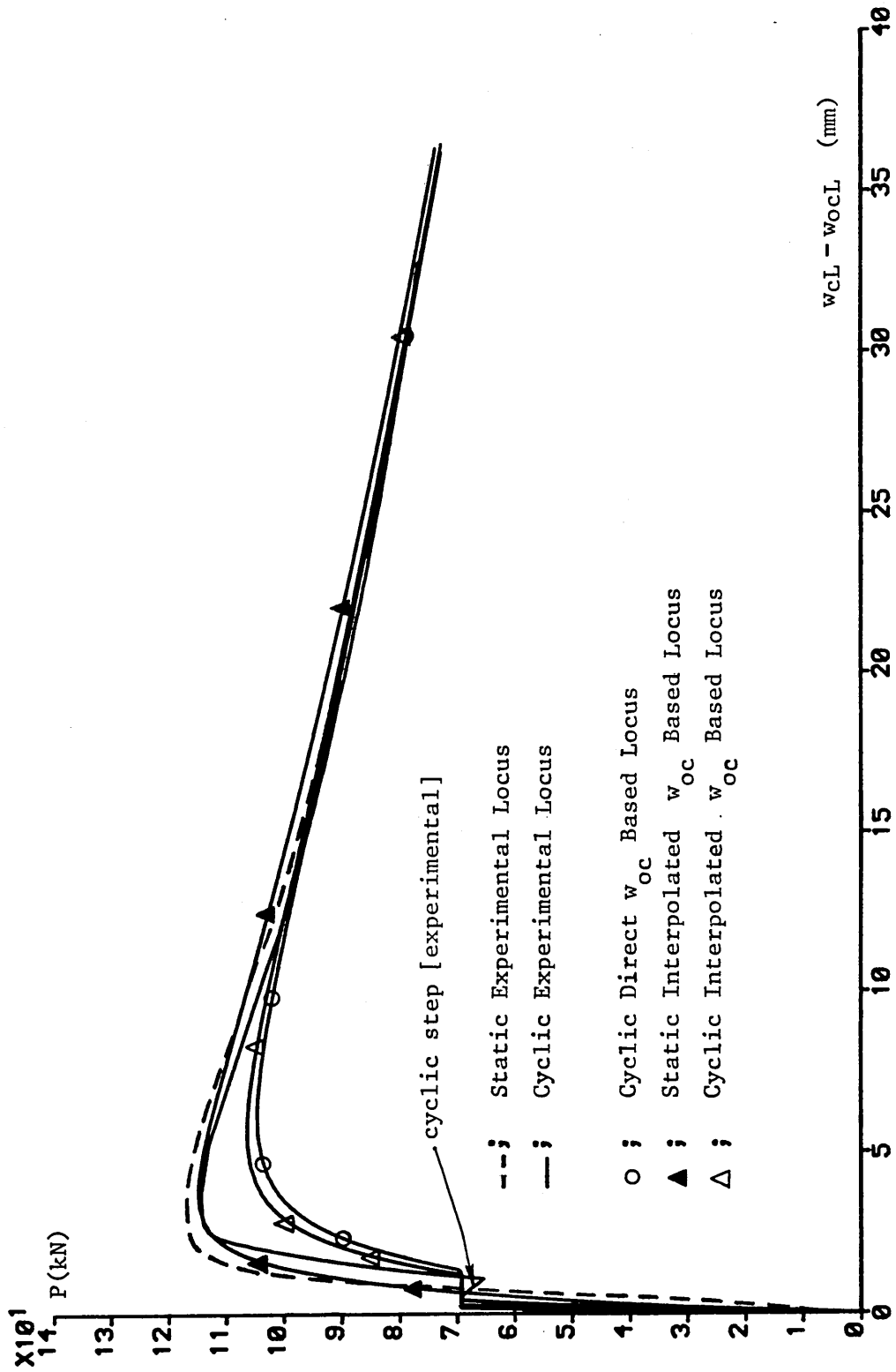


Figure 4.16 ; Case Study - Strut Ref. 26C

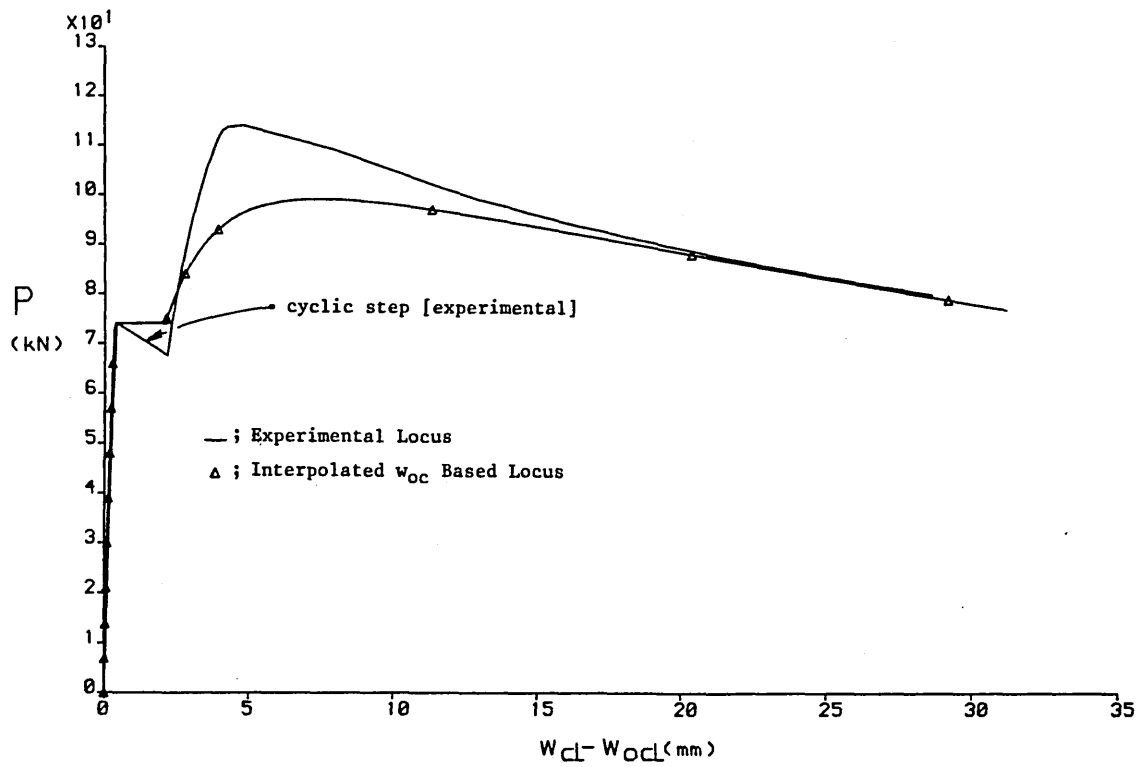


Figure 4.17 ; Case Study - Strut Ref. 27C

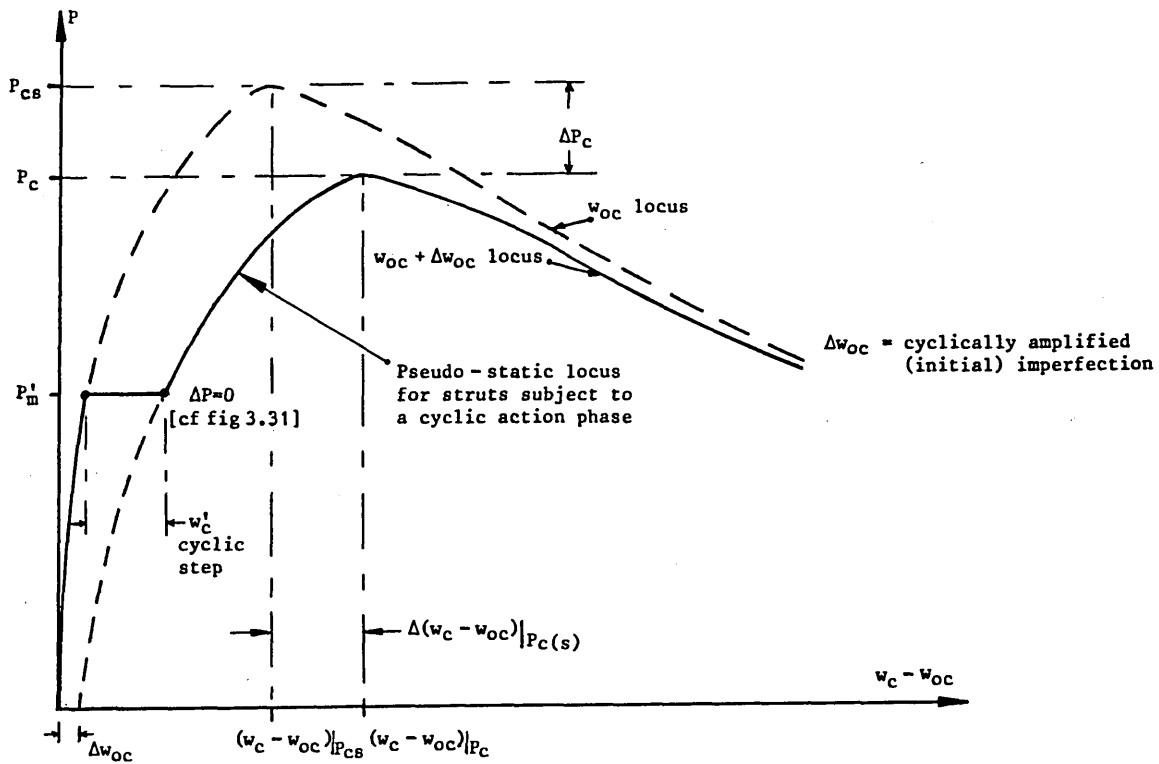


Figure 4.18 ; Pseudo - Static Model Characteristics

Finally, some assessment of static/cyclic correlation must be made. Matters regarding static/cyclic correlation or data control with respect to experimental buckling load P_c values are at the mercy of the complex interaction of the respective and highly variable prototype imperfections. Modelling within planar constraints on an individual basis is exceptionally difficult - hence the statistical basis of strut design(35,36). It is instructive to recall at this stage, however, that, as noted in Section 4.6.2 and Fig 4.11, the theoretical models themselves are quite capable of providing a degree of data control inasmuch as they can provide, in addition to the post-cyclic buckling load P_c , an equivalently fully static buckling load P_{cs} based only on the respective pre-cyclic or initial imperfection data in each case. Clearly, this latter value will be in excess of the defined post-cyclic P_c , this difference thereby highlighting the effect of a pre-buckling cyclic action phase upon initial strut imperfections.

This feature is clarified in Fig 4.18 which displays typical pseudo-static characteristics, this time in terms of model effective length $\ell=L/2$ parameters; note Fig 3.31 which is based on prototype L parameters. The appropriate pseudo-static locus is shown bold, consisting of the initial imperfection-based (w_{oc}) locus for $P \leq P'_m$, the cyclic step neglecting cyclic load loss ΔP , and the cyclically amplified imperfection ($w_{oc} + \Delta w_{oc}$) for $P > P'_m$. Additionally, the w_{oc} and $w_{oc} + \Delta w_{oc}$ loci are shown in their respective entireties by means of dashed curves. The equivalently fully static load P_{cs} is shown to be the theoretical buckling load

corresponding to the particular strut case if the strut were considered in purely static terms (ie; as in the case of the quasi-cyclic case studies). The corresponding loss in buckling load from P_{CS} to that theoretically predicted from the respective cyclic strut analysis, P_C , is denoted by ΔP_C . This term, effectively unobtainable experimentally due to the variability of imperfections between static/cyclic strut pairs as denoted in Table 3.12, thereby affords some consistent measure of cyclic action phase effects. Accordingly, Table 4.4 provides the appropriate data for the formally cyclic strut cases with cases 21C, 22C, 26C and 27C showing distinctly greater cyclically induced ΔP_C losses. This is in keeping with the experimental findings denoted in Section 3.7, these being the cases involving high u_m and low λ_m data. The less conservative data according to the Southwell and Lundquist approaches is due to the in-built safety tolerance of Fig 3.33/Equ (3.14) as employed in the other pair of approaches. The loss in buckling strength is upto the order of 10% of the anticipated static strut strength (P_{CS}) except in the exceptional 20C - buckling during cyclic loading - and 27C - excessive deformation breaching deemed serviceability limits - cases.

Fig 4.18 also shows the theoretical accompanying increase in central transverse displacement at buckling, $\Delta(w_C - w_{OC})|_{P_C(s)}$. Values appertaining to this effect are given in Table 4.5, the above denoted data trend being confirmed with cases 21C, 22C, 26C and 27C showing the most significant cyclically induced increase in buckling state displacement. Values for $\Delta(w_C - w_{OC})|_{P_C(s)}$ lie in

Strut Ref.	P _c /P _{cs} (%)				
	Direct	Interpolated	Southwell	Lundquist	Average
18C	93.9	94.9	95.9	90.9	93.9
19C	n/a	91.0	98.5	98.8	96.1
*20C	-	-	-	-	-
21C	86.4	86.6	93.3	n/a	88.8
22C	n/a	89.0	93.2	n/a	91.1
23C	n/a	89.0	98.3	93.9	93.7
24C	91.8	94.2	98.3	94.2	94.7
25C	93.8	93.7	n/a	n/a	93.8
26C	91.7	90.2	n/a	n/a	91.0
27C	n/a	83.2	n/a	n/a	83.2

* buckled during cyclic phase

Table 4.4; Post Cyclic Phase Buckling Loads, P_c, Expressed as a Percentage of Their Fully Equivalent Static Values, P_{cs}

Strut Ref.		w _{cL} - w _{ocL} /P _c (s) (mm)											
		Direct		Interpolated		Southwell		Lundquist		Average			
		ES	C	ES	C	ES	C	ES	C	ES	C		
18	5.0	6.46	6.43	7.95	9.26	10.94	7.53	11.31	7.1	9.2			
19	n/a	n/a	2.14	3.10	4.51	4.94	3.87	4.17	3.5	4.1			
20 *	-	-	-	-	-	-	-	-	-	-			
21	2.30	5.16	2.32	5.17	1.99	3.41	n/a	2.98	2.2	4.2			
22	n/a	n/a	0.92	2.38	2.75	4.35	n/a	2.65	1.8	3.1			
23	n/a	n/a	5.00	6.44	6.69	7.30	5.13	7.22	5.6	7.0			
24	3.51	5.05	5.31	7.06	6.00	6.58	5.46	7.56	5.1	6.6			
25	2.62	4.63	3.51	5.81	n/a	n/a	n/a	n/a	3.1	5.8			
26	2.75	6.37	1.98	5.20	n/a	n/a	n/a	n/a	2.4	5.8			
27	n/a	n/a	2.37	5.13	n/a	n/a	n/a	n/a	2.4	5.1			

* = buckled during cyclic phase

ES = fully equivalent static based values

C = cyclic based values

Table 4.5; Theoretical Fully Equivalent Static and Cyclic Buckling Displacements

the range 20% to 140%, the latter value predictably lying with case 27C.

The above static/cyclic correlations are consistent both in themselves and with the primary experimental findings. Data trends are definitive, both with respect to the four theoretical approaches employed as shown in Table 4.3 and to the individual strut case analyses as shown in Tables 4.4 and 4.5.

4.9 END-SHORTENING CONSIDERATIONS

Emphasis in this chapter has been properly placed upon the primary flexural characteristics of the strut system. Typically, strut tests were terminated when the central transverse displacement was of the order of 50mm, the corresponding end-shortening being an order of magnitude less, say 5mm, reflecting the above emphasis.

With cyclic action being of kinematic form in the experimental programme, ie u'_m is unchanged through the cyclic phase, the only cyclic effects upon the axial compression/end-shortening characteristics are load loss, note ΔP in Fig 3.31, and a slight post-cyclic increase in direct modulus E. Figs 3.14, 3.19 and 3.24 can be compared with Figs 3.34, 3.38 and 3.42, whilst Fig 3.47 shows the substantial load loss ΔP accompanying the singular case 20C; Fig 3.49 can be interpreted as displaying reasonably typical P vs u hysteresis in the context of a pseudo-static locus. Neglecting load loss ΔP led to the decision to treat both static and cyclic strut case axial compression/end-shortening

characteristics in a fully static sense.

Initially, therefore, end-shortening takes the form

$$u - u_0 = u_a + u_f - u_0 \quad (4.33)$$

which can be contrasted with Eqn (4.21) wherein u_a was neglected; this did not affect the flexural modelling adversely as the axial term $u_a = f(\theta_i)$, $i=1,2$ with respect to Eqn (4.26).

From the static strut strain gauge output, typified in Figs 3.16 and 3.21, it was observed that, overall, the respective four buckling state strains could be joined to the datum state by linear loci whose average gradient showed a reduction of the order of 7% with respect to the actual initial and common linear gradient involved; the pre-buckling strain gauge loci were substantially linear. The tensile studies reported in Section 3.4.2 showed an average reduction in direct modulus of the same order of magnitude with respect to the corresponding stub test data as noted in Table 3.5 and illustrated in Fig 3.9. Accordingly, noting Eqn (1.1), u_a is intuitively modelled with

$$u = PL / AE_{tt} \quad (4.34)$$

for $P < P_c$ where E_{tt} denotes employment of the tensile modulus value, whilst $u_f - u_0$ is obtained from Eqn (4.21). Eqn (4.33) is thereby non-linear though the linear axial term of Eqn (4.34)

predominates given the imperfection sensitive topologies involved ($\lambda_m \approx 1$) for $P \leq P_C$. The respective theoretical buckling load P_C was obtained for each strut case from the data trends established in the previous flexural studies. That is, in each strut case, that flexural analysis which provided the most accurate estimate of P_C as assessed against the appropriate experimental data was re-run using the average E_{tt} and σ_{ytt} values denoted in Table 3.5. Employing constitutive data consistent with the foregoing axial considerations gave a slightly revised value of model P_C , together with the respective flexural end-shortening values in accordance with Eqn (4.21).

Post-buckling modelling assumed the axial term u_a to be wholly inelastic with $u_a = u_a|_{P_C}$ for $u_a > u_a|_{P_C}$ the respective flexural component being obtained from the revised flexural analyses undertaken as noted above.

Typical axial compression/end-shortening modelling characteristics are illustrated in Figs 4.19 and 4.20 which relate to strut cases 20S and 21S. The substantially linear experimental pre-buckling paths are well replicated whilst the post-buckling characteristics are considered acceptable. The familiar problems associated with the sudden, immediately post-buckling load loss⁽⁵⁵⁾ are smoothed. The concomitant reversal of end-shortening in this vicinity is available theoretically only if elastic recoverability is accounted for; this was not considered to be an essential requirement of the study although a u-reversal partial recovery modelling showing the u-reversal effect is included in Fig 4.19

AXIAL LOAD vs. AXIAL DISPLACEMENT

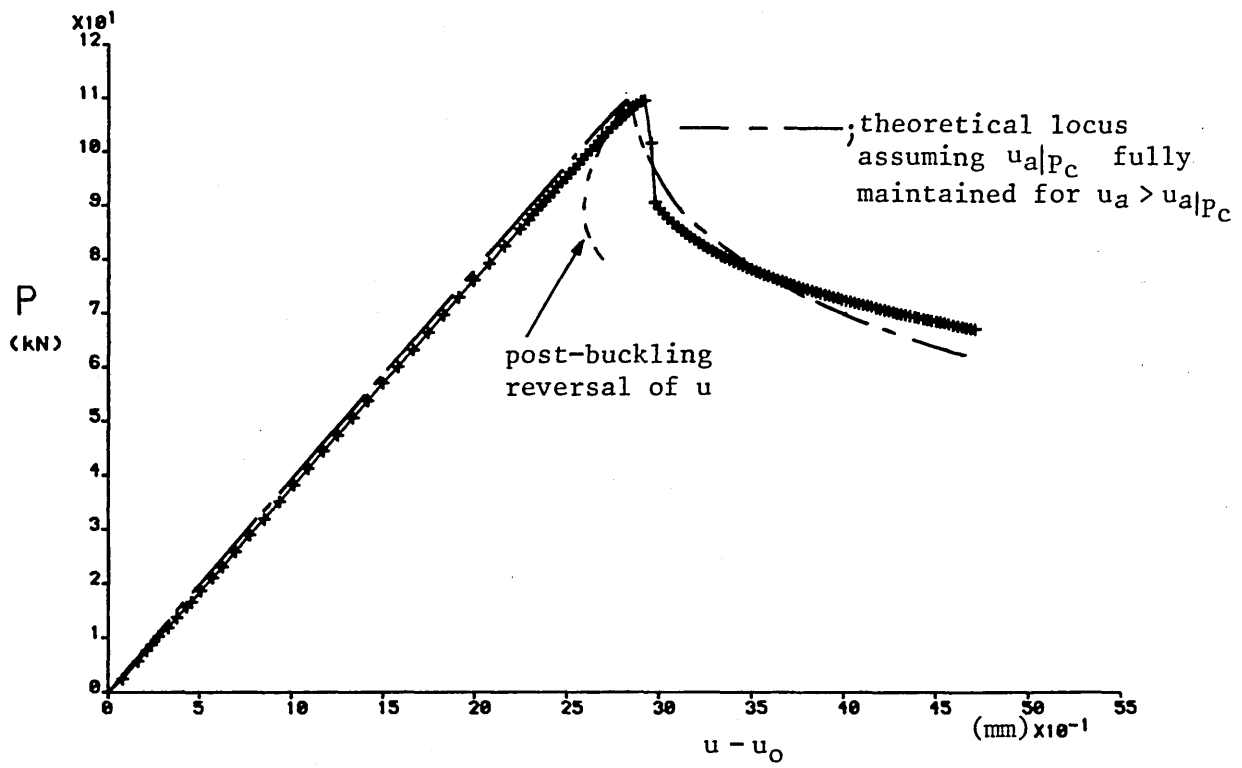


Figure 4.19 ; P vs $u - u_0$ Case Study - Strut Ref. 20S

AXIAL LOAD vs. AXIAL DISPLACEMENT

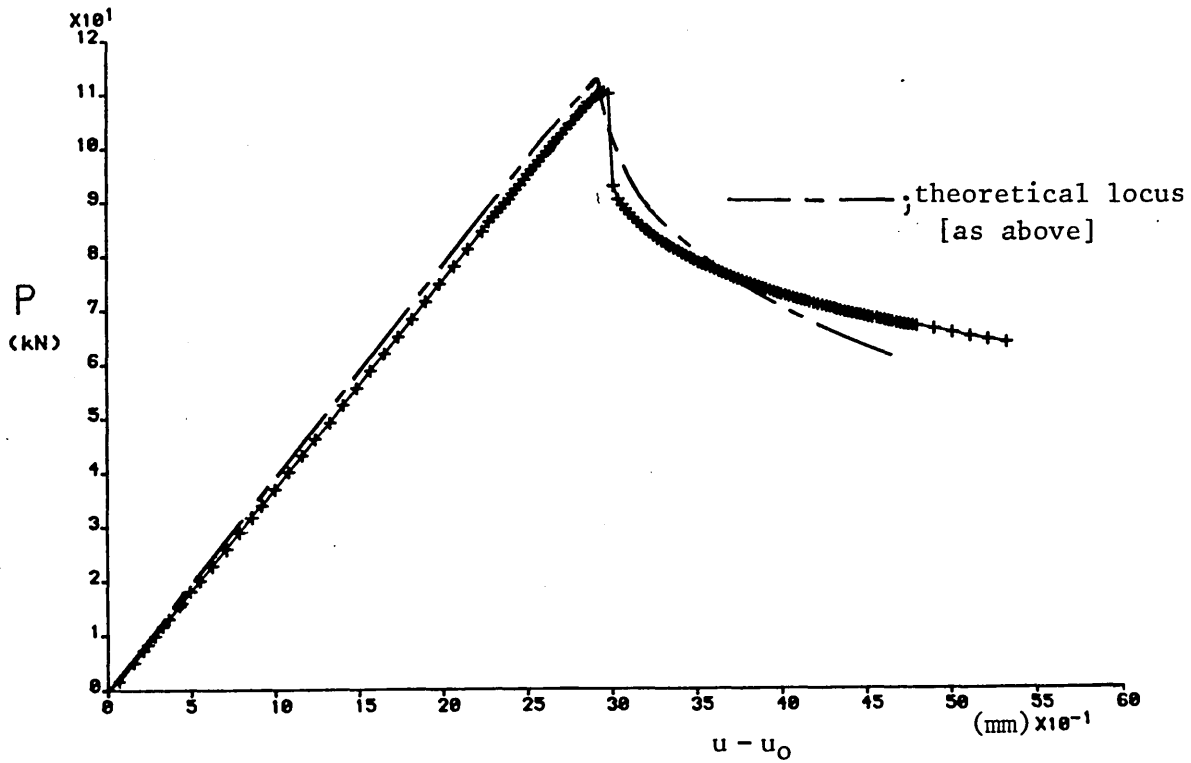


Figure 4.20 ; P vs $u - u_0$ Case Study - Strut Ref. 21S

for completeness.

4.10 SUMMARY

No fewer than 156 flexural case analyses of the static and cyclic configurations were undertaken, with overall buckling load performances summarised in Table 4.6. The data appears to be highly acceptable, particularly given the relative simplicity of Eqns (4.31) and (4.32). Clearly, the employment of additional spring-links in the strut modelling illustrated in Fig 4.5 would improve model performance, especially in the formally cyclic cases which tend to exhibit over-stiff pre-buckling paths, but this was not considered to be necessary given the quality of modelling obtained.

Table 4.6 shows a relative deterioration of modelling characteristics to exist in all four approaches with respect to the inclusion of cyclic action effects. Noting the increased problem complexity due to this inclusion, this is to be expected and the least accurate modelling, that of the cyclic Southwell-based studies, is still within 10% of the experimental average. Further, it is considered that this is offset by the fact that the Southwell-based studies were consistently conservative throughout the respective 36 case studies. All four theoretical approaches attract confidence with the Lundquist standard deviations being remarkably consistent. All four approaches possess individual attributes, note the general applicability of the novelly-defined w_{oc} -interpolated data whilst

Classification	No. off Exptl. Spec.'s	Direct		Interpolated		Southwell		Lundquist	
		(%)	No.	(%)	No.	(%)	No.	(%)	No.
Static	26	100 (s=6.5)	16	94 (s=6.7)	26	96 (s=4.9)	19	101 (s=4.2)	18
Quasi - Cyclic	16	97 (s=5.7)	9	91 (s=4.1)	16	94 (s=2.9)	13	96 (s=4.3)	13
Cyclic	9(*)	92 (s=4.6)	5	92(s=3.6) 91(s=4.0)	8(\$) 9(Ψ)	90 (s=2.3)	6	91 (s=4.3)	6

(*) = excluding strut Ref. 20C: buckled during cyclic phase (\$) = excluding 27C [cf Table 4.3]
 (Ψ) = including 27C

Table 4.6; Average Theoretical Buckling Loads ;
 Given as Percentages of Their Corresponding
 Experimental Buckling Loads

the w_{oc} -direct approach possesses the intrinsic advantage of employing the rawest form of experimental data. Additional significance is gained by the consistency of the overall data trends, with static/cyclic strut correlation being made available.

Of crucial importance to the flexural model is the novel moment-thrust-curvature expression delineated in Eqn (4.16). It is the sophistication of this expression that enables effective modelling to be undertaken with only two degrees-of-freedom. It is not uncommon for equivalent finite element studies to employ as many as 20 non-linear elements(55).

End-shortening characteristics assumed a lesser role in the study. This was considered to be reasonable given the overriding importance herein of the cyclic action phase effects. Employing stroke-displacement loading in the experimental study resulted in the flexural cyclic step assuming a primary role in the research programme. The empirical inclusion of this cyclic step, employing either the data of Fig 3.33 or of paired Southwell/Lundquist plots, represents a novel interpretation of the problem allowing for satisfactory pseudo-static modelling. This is in keeping with the essentially static-based design approach to structural steelwork practice(36).

CHAPTER 5

DISCUSSION

5.1 INTRODUCTION

The primary objective of the research programme was to assess the effects of a pre-buckling cyclic action phase upon otherwise static strut behaviour. Strut topologies were in the imperfection sensitive range, $\lambda_m=1$, and effective amplification of initial strut imperfections due to cyclic hysteresis was sought. The cyclic phase consisted of low frequency, low duration cyclic hysteresis action. Effort was concentrated upon a frequency of 1/16Hz and a duration of 1000 cycles. Action thereby lay between fatigue⁽⁵²⁾ and incremental plasticity^(10,79,80). It should be noted that 1000 cycles involving substantial inelastic excursions can represent a long time in terms of service life⁽⁸¹⁾ despite the low duration classification in strictly 'cyclic action' terms.

Attempts to set up experimental static/cyclic performance correlation were constricted by the variability and complex interaction of practical strut imperfections. That is, despite struts being tested as static/cyclic pairs cut from the same run of steel CHS as supplied, and despite the sizeable supporting constitutive and geometric testing programmes which provided for individual strut data, the respective pairs of static and cyclic strut specimens remained subject to the statistical variations encountered in strut imperfections. Fig 4.15 shows case 22C to

possess a greater buckling load than its static counterpart 22S, whilst Fig 4.16 shows the more consistent relationship for cases 26C and 26S which exhibit a decrease in buckling strength under cyclic action. This apparent anomaly can be explained by the former pair involving an initially more imperfect static specimen. The w_{oc} data of Table 3.12 only forms part of the reason; localised eccentricity data e is also involved together with the effects of residual stresses, although these are small in the sections employed⁽³²⁾ herein. The complexity of imperfection effects is further compounded by their interaction. Attempts to assess this problem included the use of imperfection monitoring together with the apparently novel vector trace inclusion. The latter showed that even initially corkscrewed struts buckled in a planar manner, but that this plane was virtually impossible to predict a priori; note the e/w_{oc} orientations superposed on the vector traces depicted in Sections 3.6.1 and 3.7.1. Southwell and Lundquist plot techniques were useful in dealing with this matter, affording empirical buckling plane oriented lumped imperfections which resulted in the static/cyclic correlations given in Tables 4.4 and 4.5.

Over 200 large scale computer governed tests were undertaken including 52 mainstream strut tests. The extensive experimental data base generated provided for data control over the statistically highly volatile results obtained. Empiricism forms a prominent aspect of instability studies⁽⁴⁴⁾. Digital computer incorporation was crucial and whilst it could be argued that more modern column testing machines than the basic Schenck system

employed herein now provide for automatic computerised data output, it has to be recalled that mainframe 32/64-bit accuracy was employed in the numerical and graphical output; see Section 2.4.

Theoretical studies employed a basic spring-link representative model in conjunction with novel moment-thrust-curvature analysis and a novel imperfection inclusion. The latter refers to the four w_{oc} -direct, w_{oc} -interpolated, a_{os} -Southwell and a_{o1} -Lundquist initial imperfection data sets. The data trends established between the four approaches employed both in terms of the approaches themselves - see Tables 4.1, 4.2 and 4.3 - and in terms of each formally cyclic strut case per se - see Tables 4.4 and 4.5 in the context of Table 3.11 - are definitive in supporting the modelling interpretations presented. Table 4.6 gives an overview of the 155 strut analyses undertaken - 156 including 27C-; the resulting pseudo-static modelling being graphically illustrated in Sections 4.7 to 4.9. Fig 4.6 elegantly relates the modelling to established theory(3,35).

It remains to set the research programme findings in the context of design practice. To this end, the following sections attempt to condense the substantial data provided in Chapters 3 and 4 into appropriate form. Throughout the experimental programme, data control over the various aspects involved has been considered imperative. This philosophy has also been applied to the theoretical modelling throughout which empiricism is a necessary inclusion. Modelling for pre-buckling cyclic action in strut

studies is now available.

5.2 STATIC-CYCLIC CORRELATION

5.2.1 Experimental Considerations; Data Control

Provision of individual strut geometric and constitutive data, discussed particularly in Sections 3.2.3, 3.4.1 and 3.4.2, was itself subject to data control. Two means of assessing specimen cross-sectional areas were employed whilst tensile tests served as control on the problems associated with stub specimen end-bulging - see Plates 10 and 11. Initial out-of-straightness measurements, discussed in Section 3.5.1, were undertaken in encastré and lathe-centred (pinned) modes, which revealed the complexities involved. Central values were not necessarily the respective maxima and corkscrewed topologies, note Fig 3.11, were invariably encountered. The struts were of good quality inasmuch as they were well within the 0.2%L requirement⁽⁴⁷⁾; this factor is considered further in Section 5.3. Histograms relating to the numerous coarse constitutive and geometric data were given in Figs 3.3, 3.4, 3.5, 3.10, and 3.12. Further, localised eccentricity readings were taken, importantly showing the weld to be a primary parameter in its evaluation; see Section 3.5.2. Whilst the residual stresses due to welding are largely removed from the EWSR steel, the additional wall thickness in the weld vicinity is not. The eccentricity values were importantly shown to be of the same order of magnitude as the out-of-straightness data; the overall high quality of the steel tubing must be

reiterated, however. Perhaps the most crucial observation with respect to this data, apart from the obvious one concerning the necessary provision of specific support data for strut testing assessment purposes, was that this 'high quality' was deemed to offset the imperfection sensitivity associated with struts possessing $\lambda_m \approx 1$.

The struts were tested in a doubly encastré mode, a feature of particular note. This involved employment of the most practically attainable form of end condition and one whose performance could be readily assessed - pins can seize under high compression loading - and provided for a more direct relationship with practical design conditions. This feature relates to the fact that pinned-end conditions are rarely encountered in design practice and necessitated that effective length, a primary parameter in strut design, be assessed from observation. That is, the experimental convenience of employing $\ell=L$ is at some cost in engineering practicality. Practical effective length assessment is presently a contentious issue in itself(62). The corollary was, however, the necessity of undertaking the model ℓ /prototype L transformations, based upon $\ell=L/2$, identified in Figs 3.13 and 3.28. An off-shoot of this transformation was the derivation of w_{OC} -interpolated data, providing for a guaranteed imperfection parameter, in all strut cases, suited to analytical employment.

Assessment of effective length $\ell=L/2$ was undertaken in two ways. Post-test observation of the specimen in-situ corroborated maintenance of end fixity throughout the strut testing programme.

Further, computer-resident Southwell and Lundquist plots, in interactive graphics mode, were employed to assess effective lengths (and provide for lumped imperfection parameters a_{0S} and a_{0L} respectively). Initially employed in the static strut series in an established manner, note Table 3.10 and Figs 3.29 and 3.30, they were then employed with confidence in the cyclic strut cases, note Tables 3.14 and 3.15 together with Figs 3.59 to 3.63. This was itself a novel procedure. It is useful to note that the average ℓ_S/ℓ ratio for all suitable static strut tests (19/26), quasi-cyclic strut tests (13/16) and cyclic strut tests with respect to the pre-cyclic behaviour (6/9) is 1.04; the Lundquist equivalent is 1.05 giving good correlation. Noting the previously mentioned tensile testing control upon stub test data and the resulting 7% overestimate of direct modulus E - see Table 3.5 - then the above values can be adjusted with

$$P_e / P_{es} = (E_{tt} / \ell^2) / (E / \ell_S^2) \quad (5.1)$$

ie

$$P_e / P_{es} = 0.93 (\ell_S / \ell)^2 \quad (5.2)$$

For $\ell=L/2$, $P_e=P_{es}$, then

$$\ell_S / \ell = (0.93)^{-\frac{1}{2}} \quad (5.3)$$

ie

$$\ell_S / \ell = 1.04 \quad (5.4)$$

which implies remarkably accurate $\ell=L/2$ provision. Noting the a_{0S} -Southwell and a_{0L} -Lundquist based analyses employed in Chapter 4 and discussed further in the following section, then the

Southwell and Lundquist techniques can be seen to have been of major importance to the research programme. Additionally, the a_{0s} and a_{0l} parameters served as control on the negligibility of residual stresses - note also the 'retested' struts discussed shortly - in EWSR sections and on the imperfection interaction involved.

It is also considered that the central transverse deflection vector traces, liberally illustrated in Sections 3.6.1 and 3.7.1, possess a degree of novelty, similar diagrams not having been located in reference material. Planarity of buckling deformation, even for corkscrewed struts, has been shown; this planarity is hardly disturbed by the inclusion of a cyclic action phase - note Figs 3.44 and 3.46 in particular. Validity of planar modelling was supported. The vector trace data was confirmed by the strain gauge readings throughout. Confidence in avoidance of machine interference in the form of eccentric loading additional to that associated with weld effects being incurred, was shown with buckling planes being dispersed in diverse orientations.

Strut testing was oriented about the cyclic cases 1C-27C, static strut tests being primarily undertaken for the purposes of data control and design code⁽³⁶⁾ relevance; in design practice, only static limit state loads are explicitly available. Case 20C, in which buckling was deliberately incurred during the cyclic action phase, formed an upper bound to the cyclic testing programme. Testing was centred on $n_c=1000$ cycles, control for this being presented by testing struts with cyclic ranges varying between

50-1500 cycles. Primary system parameters were deemed to be modified slenderness ratio λ_m , peak cyclic displacement u_m and cyclic step w'_c (or w'_{cL}). Under axial displacement control, some small cyclic load loss ΔP resulted from hysteresis, but w_c remains the prominent (and kinematic) response parameter. Peak cyclic load P_m was found to be of the form

$$P_m / P_c \quad \overset{\infty}{\text{approximately}} \quad u_m / u|_{P_c} \quad (5.5)$$

corroboration for this approximate proportionality coming from the substantially linear P-u loci distributed through Sections 3.6.1 and 3.7.1.

A major finding of the research programme was the demarcation between the so-called quasi-cyclic and formally cyclic cases. The former involve quasi-elastic hysteresis⁽⁶¹⁾ wherein cyclic action occurs within the nominally elastic range - this range was ascertained from the strain gauge readings as exemplified on page 112. Material impurities give rise to highly variable but relatively small cyclic effects. Both cyclic hardening and softening can occur. Static interpretation is deemed sufficient. The formally cyclic cases, however, afford only cyclic softening and a pronounced cyclic step; peak inelastic excursions were of the order of $u_m / u|_{P_c} = 0.91$ to 1.0.

Whilst the static strut tests failed to provide for direct static/cyclic strut data control - this was never anticipated - it served to provide the appropriate static strut data trend. The cyclic

tests thereby showed the specimens to be resilient to significant load loss except when inelastic behaviour was incurred in the close proximity of the 'static' buckling state. Strut transverse deformations were another matter, however, with serviceability considerations being deemed to have been breached in the more extreme cases - ie; cases 20C and 27C. The primary experimental finding was that significant degradation in strut performance due to pre-buckling cyclic action was associated with those cases involving high peak stroke u_m in conjunction with struts possessing a low modified slenderness ratio. This situation maximises the degree of inelastic excursion available; see Section 3.7, all important strut testing data being summarised in Tables 3.11, 3.12 and 3.13. Cases 20C and 27C indicate that catastrophic buckling load loss is limited to cases involving $P_m = P_c$.

Experimentally, little loss in buckling strength appears to occur due to pre-buckling cyclic action; this is matched by the negligible load loss incurred during cyclic action - note ΔP in Fig 3.31. Similarly matched but in the opposing sense, cyclic step w_{CL}^1 and the increase in transverse buckling displacement due to cyclic action are more pronounced with respect to the formally cyclic cases. Figures 3.32 and 3.33 present the above-noted primary findings in concise form; they are considered further in Section 5.3. Noting the small loss in buckling strength incurred due to cyclic action and given the design code's⁽³⁶⁾ orientation about static load values, then Fig 3.33 includes both the respective cyclic-based and static-based P_c data. Figs 5.1 to 5.3 extend this reasoning with all 52 cases of mainstream strut data

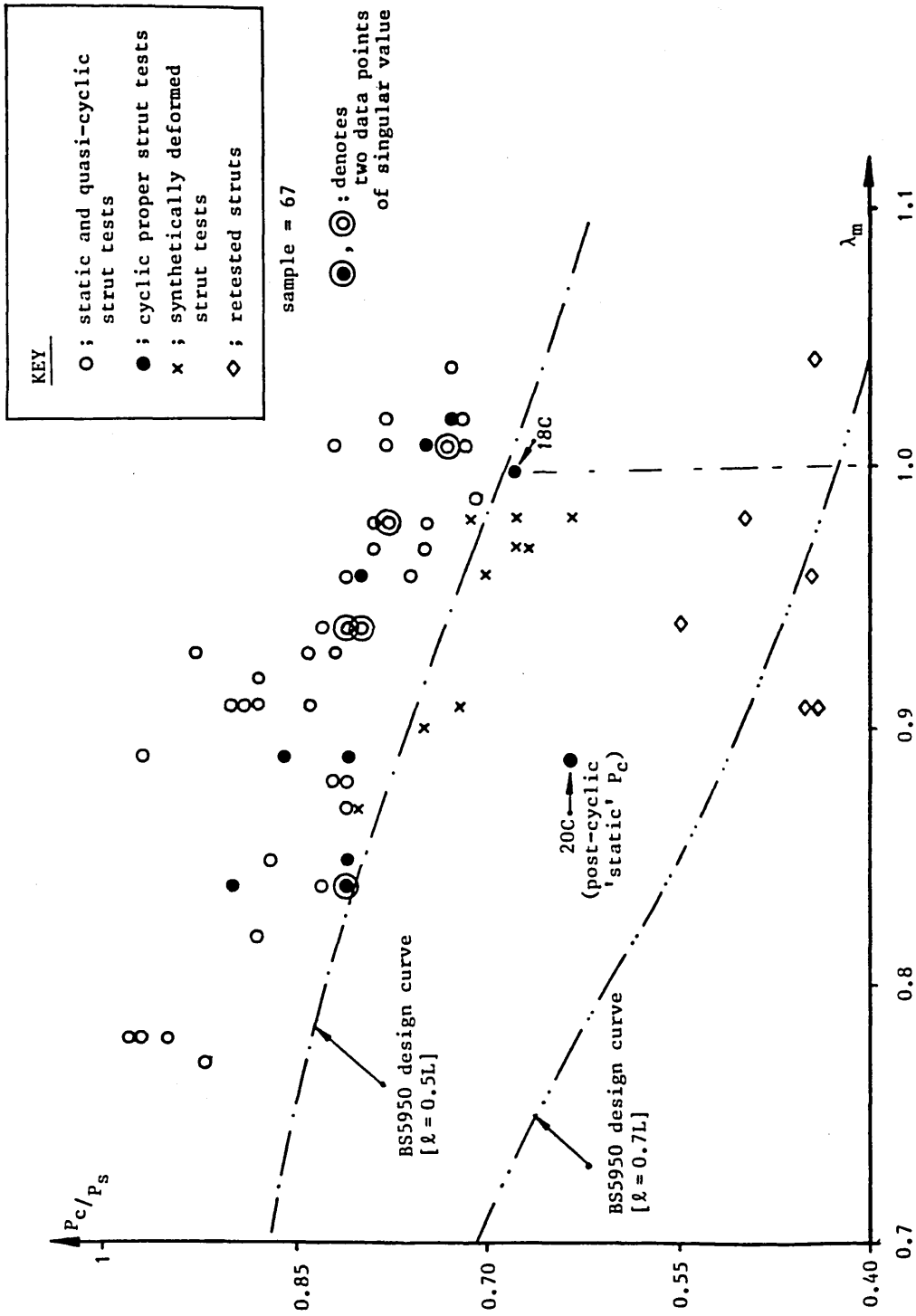


Figure 5.1 ; Normalised Experimental Buckling Loads vs λ_m

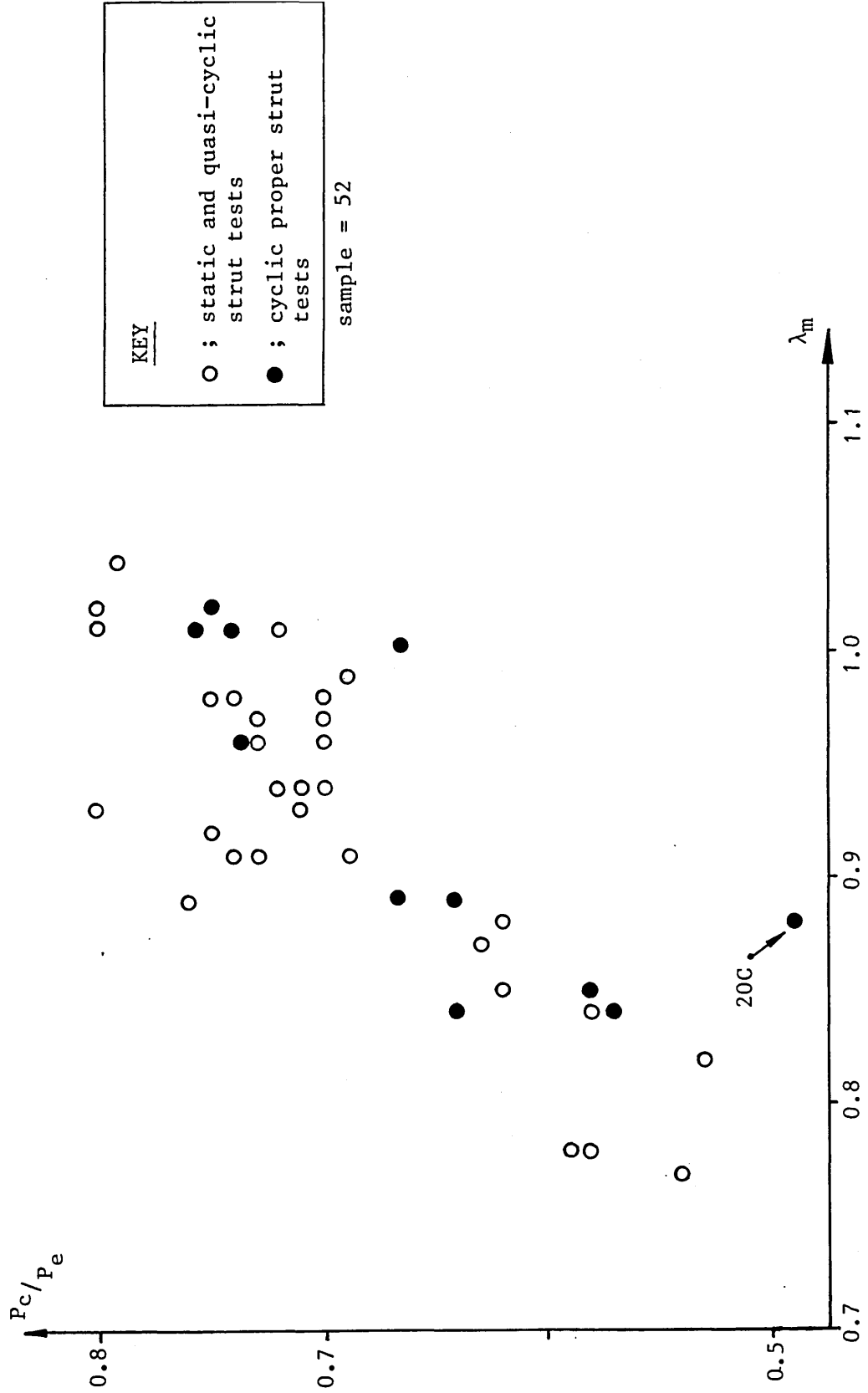


Figure 5.2 ; Non - Dimensionalised [P_e] Experimental Buckling Loads vs λ_m

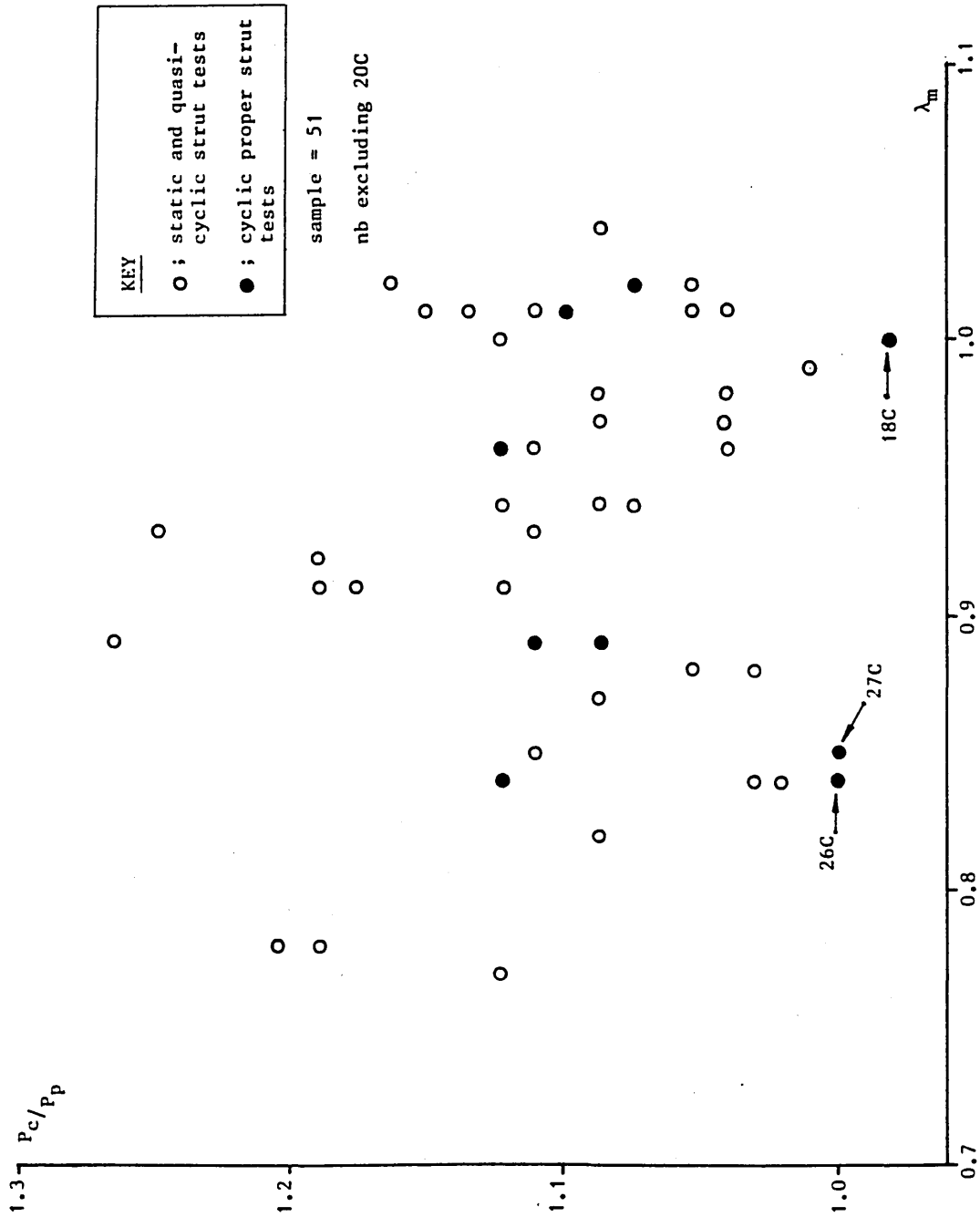


Figure 5.3 ; Non - Dimensionalised [P_p] Experimental Buckling Loads vs λ_m

referred to in the presentations of P_c in terms of P_s , P_e and P_p [note Eqn (1.4)] against λ_m . Fig 5.1, which additionally includes re-test and synthetically deformed strut test data, shows most mainstream strut P_c values to be just lower bounded by the respective ECCS curve(36) with $\lambda=L/2$. Case 20C clearly falls below the design (L/2) curve due to the extreme cyclic action involved; case 18C also breaches the design (note below) locus. All P_s data is deduced from individual constitutive and geometric values, however. Further, the location $\lambda_m=0.93$ relates to a slenderness ratio of 80 using code values of $\sigma_y=275\text{N/mm}^2$ and $E=205\text{kN/mm}^2$. At this state, the code effectively provides for a w_{oc} of $0.104\% \lambda(35,36)$ which is well in excess of the order of experimental w_{oc} values recorded - see page 100. That is, the cyclic action effects are offset by the high quality of the strut specimens provided by BSC. Further, most experimental constitutive data exceeds the corresponding code values, hence, the P_c/P_s data values are generally lower than if design P_s data had been employed.

Fig 5.2 shows the cyclic cases again towards the unsafe region of the appropriate data trend, with experimental values increasing towards P_e as modified slenderness ratio increases. Accepting that the design P_p locus of Fig 1.4, although nominally based on elastic theory(35), is a lower bound to experimental buckling data, then the critical or P_e locus will be approached by experimental data in the manner shown in Fig 5.2. Fig 5.3 accordingly shows the lower bound provided by P_p to the experimental data, in this instance individual constitutive data being employed in the P_p evaluations which implies $P_c/P_p=1$ affords

conservatism with respect to design values. The one case - case 20C is omitted in view of its singular nature - involving $P_c/P_p < 1$, case 18C, will not therefore actually lie below a P_p locus employing design code data as shown in Fig 5.1. Case 18C possesses only moderate imperfections but subscribes to $\lambda_m = 1$, generating maximum imperfection sensitivity - note Fig 4.6. Fig 5.3 most clearly shows cases 26C and 27C to be close to design limits. The design implications of Figs 5.1 to 5.3 are considered in Section 5.3.

Using the cyclic stub tests as control, the quasi-cyclic and formally cyclic cases showed post-cyclic phase increases in direct modulus E of the orders of 3% and 5% respectively. These increases occurred immediately cyclic action was initiated, note the time-dependent characteristics illustrated in Section 3.7.2. The quasi-cyclic cases involved this increase succeeding in 'clawing back' any hysteresis generated additional displacement; see Fig 3.34. It is suggested that the lack of significant buckling load loss due to pre-buckling cyclic action relates to this enhanced E effect, with cyclic work-hardening providing for some further saving in buckling load loss.

The Southwell and Lundquist plot techniques were employed in a novel manner in the case of the formally cyclic tests with respective pre- and post- loci being produced as shown in Table 3.15 and Figs 3.61-3.63. This data is effectively the Southwell and Lundquist equivalent to that provided in Fig 3.33. As noted in Section 3.7.3 and recalling Eqns (5.1)-(5.4), this post-cyclic

E shift results in the data provided in Table 3.15 with respect to post-cyclic effective length assessment being superior to the apparent trend illustrated. Incorporating both tensile moduli and post-cyclic moduli effects, then

$$\begin{aligned} & [(\ell_s \text{ or } \ell_1 / \ell)_{\text{pre-cyclic}}] / [(\ell_s \text{ or } \ell_1 / \ell)_{\text{post-cyclic}}] \\ & = (0.98 / 0.93)^{\frac{1}{2}} = 1.03 \quad (5.6) \end{aligned}$$

That is, the anticipated post/pre cyclic ratio for effective length assessment should be 1.03 for $\ell=L/2$ throughout; significantly this is in keeping with Table 3.15.

Most effort has been centred on the provision of pseudo-static data employing highly accurate digital monitoring. The cyclic action phase behaviour, however, showed two distinct patterns in keeping with the established quasi-cyclic and formally cyclic classifications. Quasi-cyclic action involved quasi-elastic hysteresis⁽⁶³⁾ displaying closed loop lines - see Fig 3.50 - with random exit paths. Formally cyclic cases displayed finite area loops⁽⁶⁴⁾, with forward marching multiple band finite area loops⁽⁶⁵⁾ being obtained in the more significant cyclic effect cases of 21C, 22C, 26C and 27C; note Figs 3.51-3.54. This latter type of hysteresis is not unrelated to incremental plasticity⁽¹⁰⁾, with cyclic creep displayed amidst a decelerating but non-stabilised cyclic profile. Case 20C singularly involved creep acceleration as is to be expected from intuition; note Figs 3.57 and 3.58. The cases involving lack of cyclic creep stabilisation - cases 21C, 22C, 26C and 27C - imply that pseudo-static considerations will be directly affected for $n_c > 1000$ cycles.

The re-tested struts served to show that fatigue was not a problem in the mainstream cyclic strut tests. A 40% loss in buckling strength upon static re-testing was found with highly planar buckling behaviour being appropriately dictated in the re-tested configuration. The synthetically deformed struts also showed the effects of larger imperfections with buckling strength typically 20% down on the mainstream strut values. Highly non-planar buckling action was observed, see Figs 3.66 and 3.67, due to the conflict between the prescribed circular arc initial free body profile and the reverse curvature initial doubly-encasté testing mode. Both re-tested and synthetically deformed strut cases are shown in Fig 5.1 to clearly breach design criteria ($\lambda=L/2$), both types failing to meet the 0.2%L BS requirement for initial out-of-straightness⁽⁴⁷⁾. Interestingly, case 20C, which suffered buckling during the cyclic action phase, shows up well in Fig 5.1 as compared with the retest data.

Finally, some mention must be made of problems encountered in the experimental programme. No fewer than three servo-valves were required through the programme due to mechanical failure of the system. Impurities of micron size in the oil led to this succession of problems. One such failure in turn led to static test 4S being spoilt due to the Schenck machine suffering vibration in the vicinity of the buckling state. This dramatic occurrence was never repeated and served to prove the validity of computer controlled shut-down procedure as noted on page 44. Test 27C involved plotter pen failure - note Fig 3.56 - readings for P_m being obtained from x,y/t plotter data (note Appendix). Data from

the plotters was subject to less stringent tolerances as denoted in Table 2.4 and values of P_m/P_c are subject to this factor. Cyclic tests took approximately four hours to complete, with unavoidable 'electronic drift' being associated with time-dependent monitoring.

5.2.2 Pseudo-Static Modelling

Pseudo-static modelling provides for an analytical assessment of the effect of a pre-buckling cyclic action phase upon otherwise static strut behaviour. In those more extreme cyclic cases involving non-stabilised cyclic creep - see Figs 3.52-3.54 - care must be taken with respect to the total number of cycles involved; otherwise, fatigue governs this factor⁽⁵²⁾. The pathological case 20C relates to a singular phenomenon and breaches the 'sub-buckling' constraint of this research study.

The basic analytical vehicle was the two degrees-of-freedom spring-link model depicted in Fig 4.5. Used in conjunction with the novel moment-thrust-curvature expression of Eqn (4.16) and the four types of initial imperfection experimentally provided, a large data base relating to the 51 mainstream strut tests (ie 52 less 20C) has been established. Overall experimental/theoretical correlation is considered to be good, with a concise overview given in Table 4.6. Improved theoretical modelling could be readily achieved by the incorporation of additional spring-links as previously noted. This would detract, however, from the computational amenability available from use of Eqns (4.31) and

(4.32). Typical static strut analysis can involve using 20 finite elements⁽⁵⁵⁾; the (static) modelling provided herein is not considered to be inferior.

Static strut analysis provided a testing ground for the four 'methods', see Figs 4.7 and 4.8. The four static data trends provided were closely followed in the cyclic analyses as shown by Tables 4.1-4.3 and 4.6. Whilst the quasi-cyclic cases were fully statically modelled as illustrated in Figs 4.9 and 4.10 (but note Fig 4.11), the formally cyclic cases - those cases involving cyclic softening and a distinct cyclic step - were modelled in accordance with Fig 3.33 with respect to the w_{OC} -direct and w_{OC} -interpolated data.

The equivalent a_{oS} -Southwell and a_{o1} -Lundquist approaches were separately modelled employing a novel 'paired linear fit' procedure. This afforded a distinct form of cyclic analysis and thereby provides for data control. Whilst, overall, most theoretical buckling load values were conservative, Southwell-based values were conservative throughout. Indeed, as employed herein, the Southwell and Lundquist techniques form truly catalytic interfaces between experimentation and theory. The additional computational effort required in the Lundquist approach has not shown any dramatic improvement upon the Southwell⁽⁵⁶⁾ method. The major limitation of both methods was that their applicability was limited, particularly with respect to the more significant formally cyclic cases 21C, 22C, 26C and 27C. In these cases, the low λ_m /high u_m configuration mitigated against these

two semi-graphical approaches. It is these four cases that relate to the most significant cyclic action phase effects recorded and the unavailability of Southwell-based and Lundquist-based models is a major limitation.

Fortunately, however, the w_{OC} -interpolated model was always applicable, ensuring modelling availability for all such problems by an approach which can be assessed by the use of three other approaches in the majority of cases. Modelling employing coarse experimental data - ie w_{OC} -direct - was the least available approach but possessed the attraction of employing the most fundamental type of imperfection. Figs 5.4-5.7 exhibit each method's P_c data trend for all strut cases in the manner of the experimental equivalent presented in Fig 5.1 and with which they can be compared. Essentially they show the same data trends but with conservative estimates of P_c showing greater violation of the design locus ($\lambda=L/2$). The increased conservatism noted for the formally cyclic cases in Table 4.6 results in a clearer demarcation between these and the remaining strut cases in Figs 5.4-5.7. This particular trend will be specifically considered in Section 5.3 as a matter of some import. It must be recalled that most data points would rise relative to the design curve if design values rather than individual strut values were employed in the evaluation of squash load P_s ; similarly the code's $\lambda=0.7L$ restriction should be noted⁽³⁶⁾.

Figs 4.12-4.17 illustrate typical modelling performance with respect to the formally cyclic cases, clearly the most complex

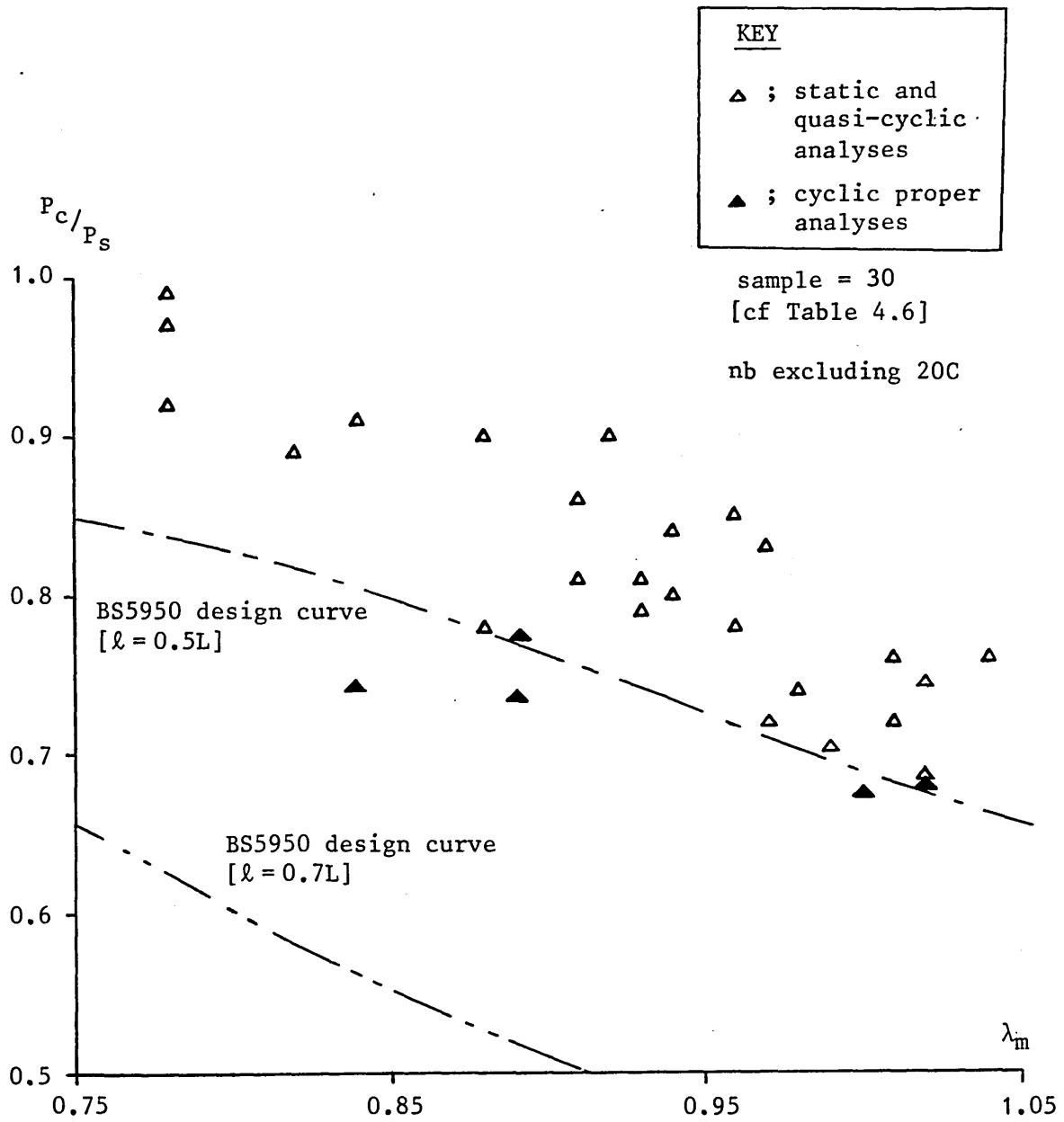


Figure 5.4 ; Normalised Theoretical Buckling Loads Based on Direct w_{oc} Values vs λ_m

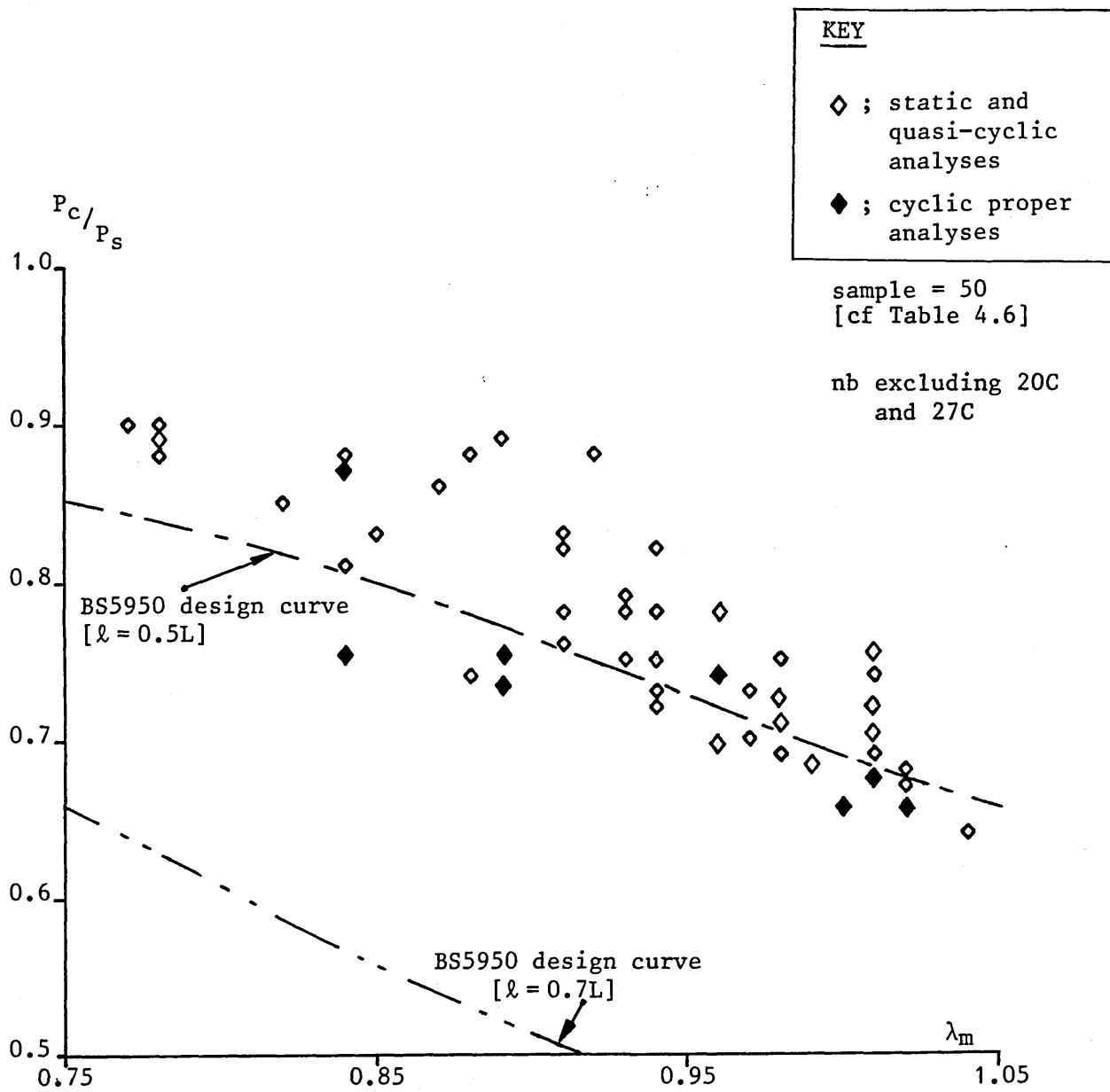


Figure 5.5 ; Normalised Theoretical Buckling Loads Based on Interpolated w_{OC} Values vs λ_m

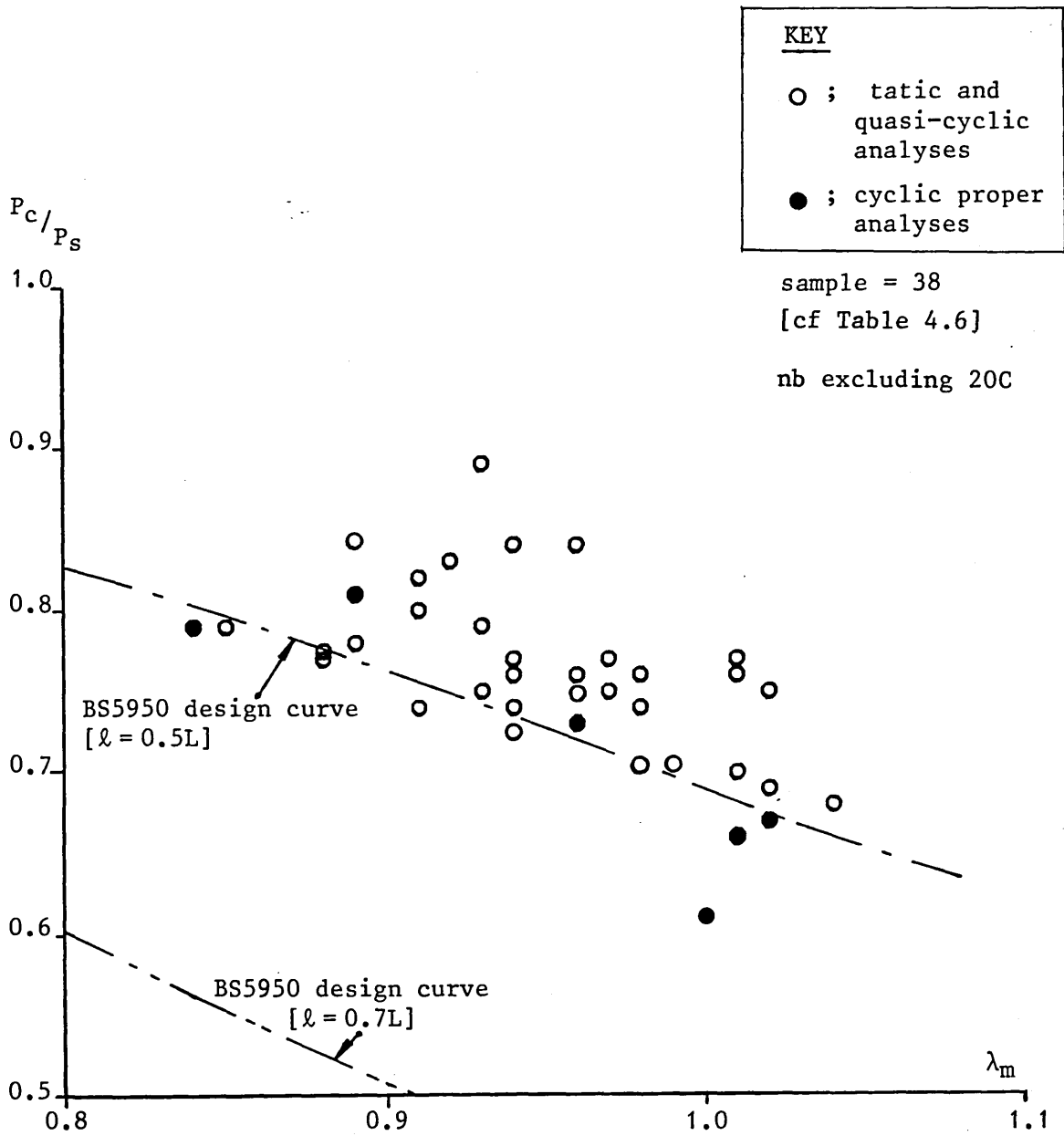


Figure 5.6 ; Normalised Theoretical Buckling Loads Based on Southwell a_{OS} Values vs λ_m

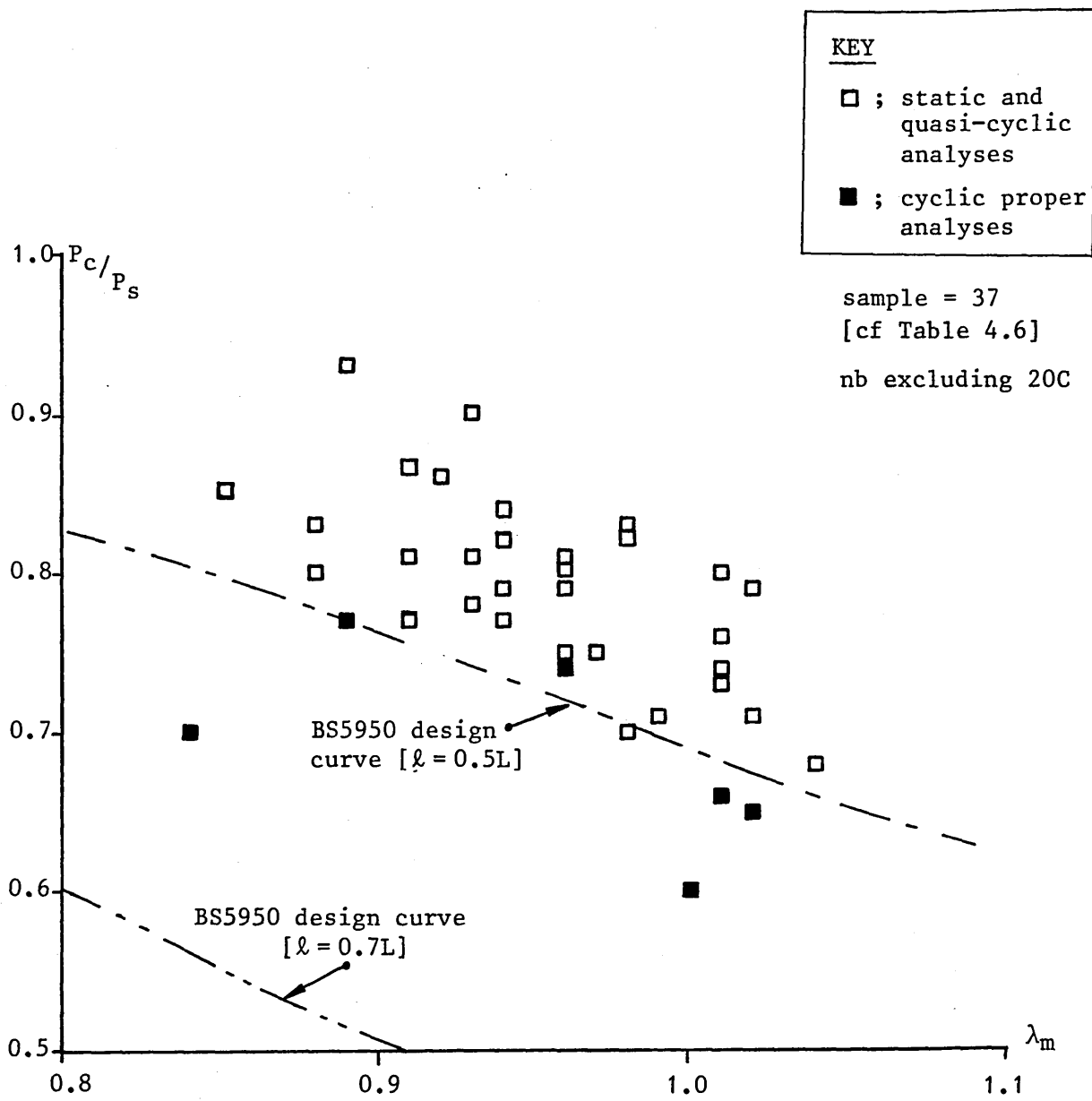


Figure 5.7 ; Normalised Theoretical Buckling Loads Based on Lundquist a_{01} Values vs λ_m

strut testing configuration involved. Perhaps the four approaches are a little over-stiff in their pre-cyclic action phase characteristics, but not Figs 4.14 and 4.17; this situation could be resolved by including additional spring-link units within the model if required.

An important feature of the theoretical study was the provision of a means of assessing static/cyclic strut correlation with respect to the associated buckling load loss ΔP_c and the corresponding increase in central transverse displacement at buckling, see Fig 4.18. Theoretical assessment is not so subject to the rules of imperfection sensitivity as direct experimentation but is obviously more restricted in appeal. The data trends provided, however, are consistent in themselves, note Tables 4.4 and 4.5, and afford the only alternative to the acquisition (and testing) of 'identical' pairs of struts. The theoretical trend is one of buckling displacement increasing more notably than buckling strength decreases - that serviceability considerations are more crucial than concern with loss of load carrying capacity except in the most severe of cases (ie 20C). This is totally in keeping with the experimental findings and, taken together with the rest of the theoretical findings discussed in the foregoing, suggests insight into the physical phenomenon has been gained.

End-shortening characteristics have been considered to a lesser extent than the transverse-flexural. Support for this came from the orders of deformation magnitude involved and the displacement controlled nature of the cyclic action applied. Neglecting cyclic

action phase load loss ΔP (not to be confused with ΔP_c above) simplified modelling without significant loss of accuracy and effectively demanded that the transverse displacement cyclic step, w_c' or w_{cL}' , be the primary response parameter - recall Table 3.11. [Response parameter P_m was virtually linear in terms of action u_m as noted in Eqn (5.5)].

5.3 DESIGN IMPLICATIONS

It is now apposite to suggest the means by which the experimental and theoretical studies summarised in the previous section could be incorporated into design practice; Figs 5.1-5.7 have been produced with this in mind. They show quite clearly that strict adherence to the maximum code value of $\ell = 0.7L$ would apparently cater for the type of cyclic action considered herein⁽³⁶⁾. Against this, however, is the fact that laboratory control implies that relationship to practice is more valid upon the basis $\ell = L/2$; it is effective length ℓ that is crucial. This factor suggests that cyclic action can lead to minimal safety tolerances if design practice employs only static criteria. Given that no British Standard relates to stub testing, the matter of employing such data in Figs 5.1-5.7 with respect to all coordinate axes again suggests that cyclic action effects require careful treatment before formal design rules could be drawn.

Further, the high quality of the specimens provided by BSC cushions the effects of cyclic action due to the inherent out-of-straightness being far less than that provided for by the design

code(36). That is, the borderline nature of the static interpretations shown in Figs 5.1-5.7 is subject to a considerable leeway in imperfection provision, with less perfect but still code-acceptable struts showing a more critical data trend. This feature is supported by the performance of the synthetically-deformed and re-tested data shown in Fig 5.1, and by the w_{oc} -direct, w_{oc} -interpolated, a_{os} -Southwell and a_{o1} -Lundquist data trends displayed in Fig 5.8. Strictly, only the w_{oc} -direct data is applicable with respect to code considerations and the high quality of the struts is clearly shown. Recall that the re-tested and synthetically-deformed struts breached the 0.2%L initial out-of-straightness requirement(47).

A design procedure in which explicit account is taken of the cyclic effects is thereby proposed as follows;

- (i) Establish static strut buckling load P_p in accordance with present design practice(36).
- (ii) Establish a fully static P vs w_c-w_{oc} [or $w_{cL}-w_{ocL}$ with $\ell=f(L)$ as required] analysis in accordance with Eqns (4.31) and (4.32) employing an imperfection w_{oc} based upon the code's η parameter(35). This affords P_{CS} and $(w_c-w_{oc})|_{P_{CS}}$ - note Fig 4.18.
- (iii) From prescribed data for mean and peak cyclic axial displacements u'_m and u_m respectively (or u'_m and u_{am} , say), undertake a cyclic strut analysis in accordance with the

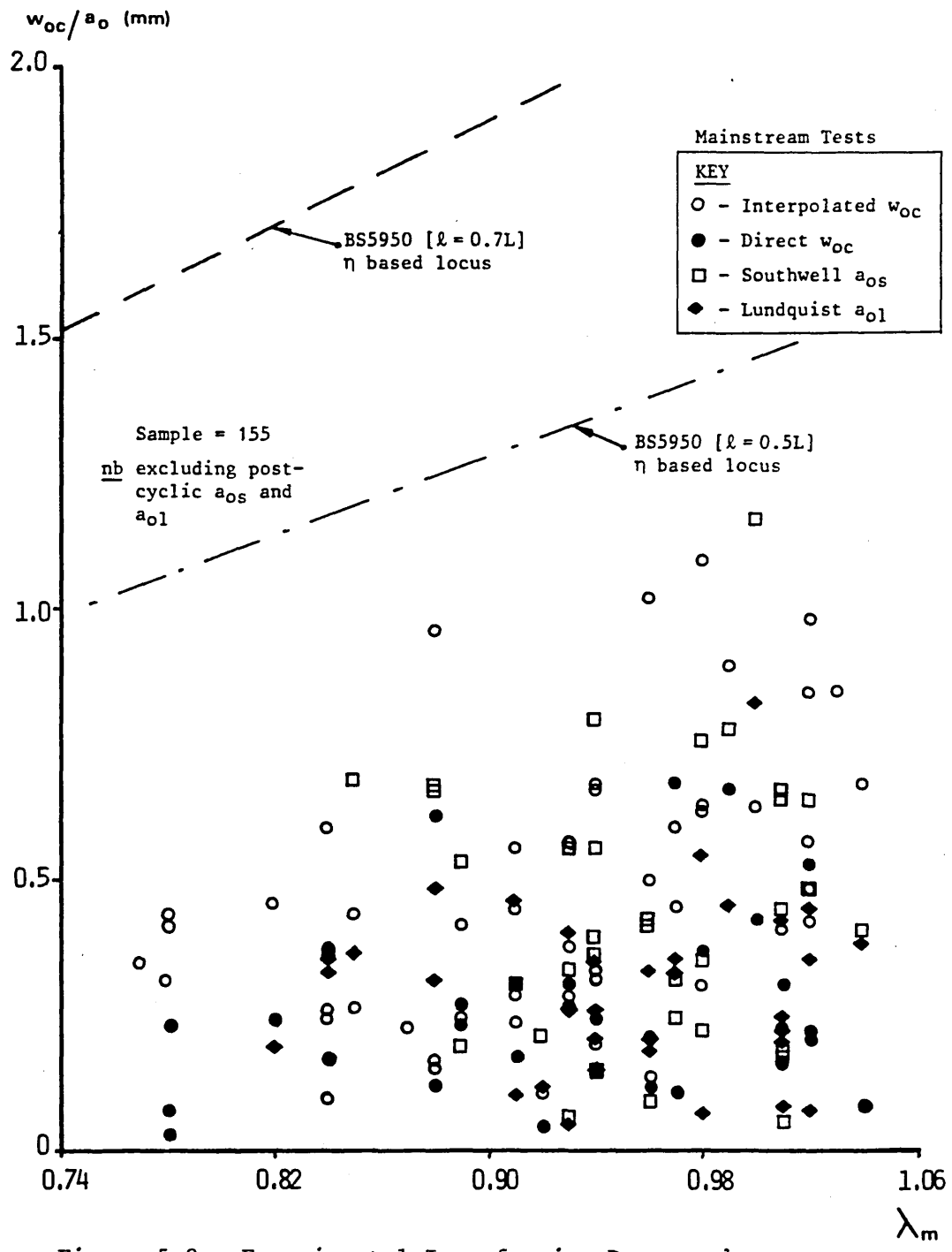


Figure 5.8 ; Experimental Imperfection Data vs λ_m

procedure established in Section 4.6.2, incorporating the employment of Fig 3.33 to define the respective cyclic step (recall the abscissa of Fig 3.33 is effective length transformation independent). With respect to this figure, peak cyclic load P_m is determined from u_m , noting Eqn (5.5), whilst ' P_c ' can take the form of P_p - note Fig 5.3 - as determined in (i) above. Initially, take $(w_c - w_{oc})|_{P_c} = (w_c - w_{oc})|_{P_{CS}}$. Note that prescribed values for P'_m and P_m would serve as alternatives to provision of u'_m and u_m respectively.

- (iv) A formal cyclic analysis in accordance with Section 4.6.2 can now be completed - note Figs 3.31(L) and 4.18(l).
- (v) Having established the increase in transverse central displacement at buckling, steps (iii) and (iv) can be revised to employ $(w_c - w_{oc})|_{P_c}$ in determination of the cyclic step - note (iii) above. This iteration is due to the fact that post-cyclic action phase values for P_c cannot be known a priori and that P_{CS} is effectively experimentally unattainable - note Section 5.2.2.
- (vi) Resultant values for post-cyclic action phase for P_c can be checked against P_p whilst $(w_c - w_{oc})|_{P_c}$ can be assessed against serviceability requirements.

Fig 3.33 thereby serves as a design chart; note Eqn (3.14). Further, a nomogram-type approach which would serve to quickly

estimate cyclic effects is available by combining Figs 3.32 and 3.33. Initially Fig 3.32 is redrafted as Fig 5.9 to include appropriate static buckling data - ie experimental buckling loads and lateral displacements for strut cases 18S-27S, less 20S - in the manner employed in Fig 3.33 and elsewhere. The upper bound locus is evaluated to be of the form

$$[w'_c / (w_c - w_{oc})]_{P_c} / (P_m / P_c) = \lambda_m (84\lambda_m - 69.76)^{-1} \quad (5.7)$$

Combining Eqns (5.7) and (3.14) affords

$$\lambda_m [85.5 (P_m / P_c) - 86.27 (P_m / P_c)^2] = (84\lambda_m - 69.76) \quad (5.8)$$

which, given input of λ_m and P_c gives an upper bound for tolerable P_m - ie peak cyclic load - values. The transformation independent nature of the non-dimensionalised cyclic step term is reiterated and care with respect to the 5% lower cut-off limit oriented about the quasi-cyclic cases must be exercised in the employment of Eqn (5.8).

5.4 SUMMARY

Whilst the data of Figs 5.1-5.7 suggest that present static design criteria could serve to accommodate pre-buckling cyclic action effects in terms of buckling load estimates, the tolerances are very tight and not conducive to confidence. The research programme has shown serviceability considerations, in the form of enhanced strut deformations being set up due to the effective

[λ or L based]

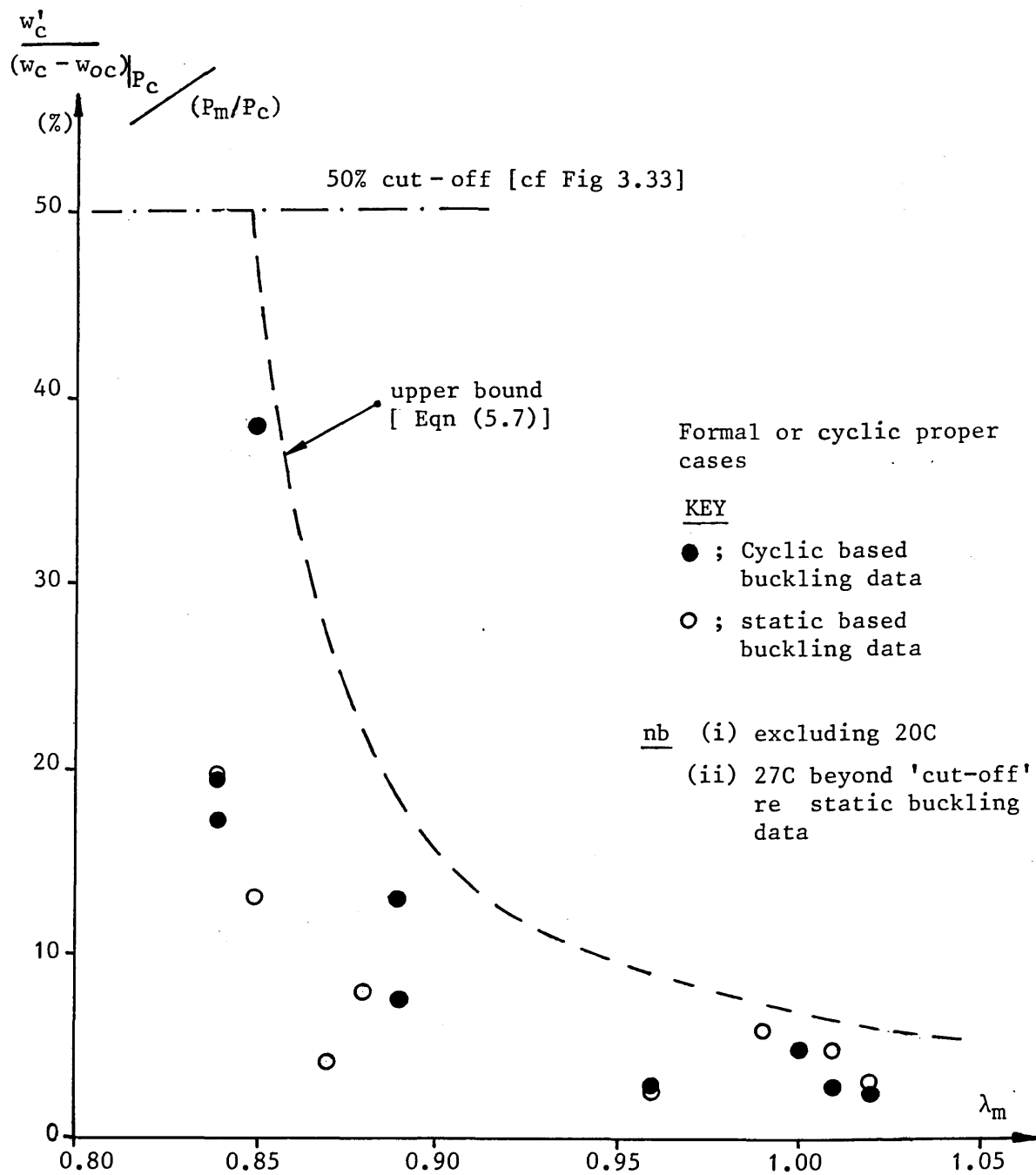


Figure 5.9 ; Non - Dimensionalised Cyclic Step Parameter vs λ_m

amplification of initial imperfections by cyclic action, to be more critical. Indeed, between statics and fatigue there is a range of limiting criteria to be established(82) with many serviceability problems encountered in practice being possibly due to sub-fatigue cyclic action(37).

The foregoing design discussions are produced in the context of the frequency, duration and specimen section (CHS) specifications considered herein. The principles involved, however, are generally applicable. Further, it is considered that the a_{0S} -Southwell and a_{01} -Lundquist type studies serve primarily as excellent research tools with possible scope in non-destructive testing work. Their inclusion in design procedures is not considered to be feasible in the short-term.

Relationships between the inelastic cyclic studies contained herein and established plasticity theorems exist. Whilst alternating plasticity(9,10) is not relevant due to the absence of net tension(82), the formally cyclic cases exhibit hysteresis reminiscent of incremental plasticity(9,10). Finally, it should be appreciated that there is no shakedown limit for struts(80); note the absence of cyclic creep stabilisation in all but those cases involving effectively nominal cyclic action.

CHAPTER 6

CONCLUSIONS

6.1 PRIMARY ASSESSMENTS

No structural loading is truly static and the research programme has sought to provide insight into the mechanics associated with imperfection sensitive strut behaviour under sub-fatigue and sub-buckling cyclic loading conditions. Substantial experimental and theoretical data and the corresponding data trends have been provided. A complex problem has been experimentally and theoretically studied and design practice interpretations have been presented. Key original findings are summarised below.

Inelastic imperfection sensitive struts possessing a relatively low modified slenderness ratio and subject to a pre-buckling cyclic action phase involving substantial peak inelastic excursions of low frequency suffer an effective amplification of their initial imperfections. Serviceability conditions are of particular concern, loss in post-cyclic buckling strength only becoming notable when buckling is initially induced during the cyclic action phase.

A range of cyclic profiles employing common values of frequency and duration has been applied to a variety of imperfection sensitive struts possessing a specific sectional form. Structural response has been classified into quasi-cyclic and formally cyclic

categories. Response to a cyclic action phase has been assessed in terms of the increase in central transverse displacement incurred during this phase - the cyclic step.

Theoretical studies involved the derivation of a novel moment-thrust-curvature relationship of fully differentiable form applicable to the entire constitutive range of the material concerned. The underlying analytical philosophy is fully capable of being exploited in other areas of structural engineering. The computational convenience afforded by the inclusion of this relationship cannot be underestimated, removing, as it does, the need for careful interfacing of the various constitutive zones involved through the body of the respective structural form.

It should perhaps be noted that the crucial strut cases involved incursion of substantial peak cyclic inelastic excursions. One thousand such cycles can relate to a significant period of service life in practice. Seismic studies are a case wherein significant inelastic excursions could be readily incurred whilst the frequency/duration specification employed refers typically to, say, a twenty year wave in offshore studies. With particular respect to struts, then it is considered that the absence of net tension mitigates against fatigue failure.

6.2 ASSOCIATED FACTORS

The Southwell and Lundquist plot techniques have been employed in a multi-role manner involving novelty of application in the case

of the formally cyclic studies. Employed as experimental effective length controls and as lumped, buckling plane-oriented imperfections in the theoretical studies, the techniques afforded a powerful experimental/theoretical interface. The Southwell and Lundquist plot techniques are powerful research tools and the relative success in their provision of essentially parallel but offset pre- and post-cyclic action phase linear fit loci was of major importance to the research programme both in terms of the novelty of application involved and the practical support afforded.

It is also considered that the employment of central transverse displacement vector traces provided a novel means of buckling path assessment. The validity of planar modelling, despite the presence of highly variable although relatively small imperfections, was clearly established for most strut cases. Importantly, however, the synthetically deformed strut experimentation findings serve as a control on this general assumption.

The experimental programme itself was extensive. The statistical problems associated with strut performance demanded that a large number of strut tests and supporting experimentation be undertaken. An exercise in project management, the manipulation of the large data sets involved was particularly demanding. In retrospect, some reduction in the number of supporting geometric and stub tests could have been made. The histograms provided, however, have been especially useful in engendering confidence in

the overall experimental data determined. Direct, hands-on experience of not only undertaking the actual tests but also of assisting in the establishment of the large scale testing system itself is considered to have been most useful; accuracy and physical 'feel' were obtained through engineering effort.

The research programme would have been impossible without considerable recourse to the digital computer. Computer applications were made with respect to experimental monitoring and control, involving a variety of specialist machines. Theoretical studies were interfaced with graphical experimental output data automatically. Typical strut test numerical output data and a listing of the graphical and numerical strut data interpretation computer programme are included in the Appendix for inspection.

6.3 SUGGESTIONS FOR FURTHER WORK

Most obviously, alternative frequencies, durations and forcing functions could be employed with respect to the cyclic action phase to extend the present data base. A variety of different structural sections could be tested for similar ends. Perhaps the testing of lighter gauge, cold formed sections would yield more notable responses. The whole question of the treatment of sub-fatigue but non-static structural loading would appear to require further attention.

APPENDIX I

PUBLICATIONS

I(A) Reference (24)

Taylor, N. and Hirst, P. Regarding Flexural Curvature. Proceedings of the Institution of Civil Engineers, 2, 77, TN 424, 1984.

I(B) Reference (59)

Taylor, N. and Hirst, P. Computerised Large Scale Strut Testing - Interaction Between Experimental and Numerical Models. Proceedings of the Third International Conference on Computational Methods and Experimental Measurement, 1, Porto Carras, 1986, Sept.

I(C) Reference (82)

Hirst, P. and Taylor, N. Strut Behaviour Subject to Pre-Buckling Cyclic Loading. Applied Solid Mechanics - 2, Strathclyde University, 1987, Apr.

SYNOPSIS OF TECHNICAL NOTE 424

Regarding flexural curvature

N. TAYLOR, BTech, MSc, PhD*

P. HIRST, BSc†

The theory of Simple Bending is one of the most important aspects of any undergraduate syllabus appertaining to Civil Engineering. Crucial to the study of flexure is the moment-curvature expression. It appears to the Authors, however, that the manner in which most texts on the subject derive this expression is at least tautological; at worst, it appears misleading. Presented herein is a consistent approach to this matter which, although not original, would not seem to be widely appreciated by authorities at large.

2. The well-established Bernoulli-Euler assumptions enable the derivation of the moment-curvature relationship

$$M/EI = 1/R \quad (1)$$

where M is the bending moment, EI represents the flexural rigidity of the section and R is the radius of curvature. The flexural inextensibility of the centroidal or neutral axis gives rise to the presence of flexural end-shortening terms \bar{u} and $\delta\bar{u}$. These are physical quantities which are important in the understanding of structural behaviour. All essential information is denoted in Fig. 1.

3. A typical element of beam δx is deformed from location PQ to P'Q'. Curvature is given by

$$v = 1/R = d\theta/dx \quad (2)$$

With

$$\sin \theta = dw/dx \quad (3)$$

then

$$v = \frac{d^2w}{dx^2} \left[1 - \left(\frac{dw}{dx} \right)^2 \right]^{-1/2} \quad (4)$$

Flexural end-shortening is given by

$$\bar{u} = \frac{1}{2} \int_0^x \left(\frac{dw}{dx} \right)^2 dx \quad (5)$$

The full manuscript of the Paper can be seen in the Institution Library.

* Senior Lecturer in Structural Engineering, Department of Civil Engineering, Sheffield City Polytechnic.

† Research Assistant, Department of Civil Engineering, Sheffield City Polytechnic.

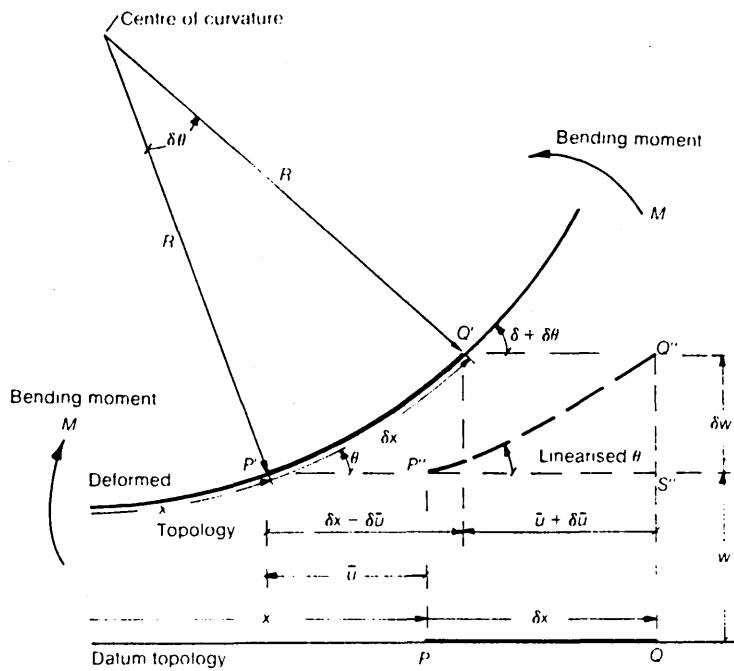


Fig. 1. Curvature topology

4. Accepted undergraduate texts, however, employ

$$\tan \theta = dw/dx \quad (6)$$

which generates

$$v = \frac{d^2w}{dx^2} \left[1 + \left(\frac{dw}{dx} \right)^2 \right]^{-3/2} \quad (7)$$

This is only acceptable if (i) linearization, denoted by arc P''Q'', is accepted a priori with

$$\bar{u} = \delta \bar{u} = 0 \quad (8)$$

or (ii) flexural end-shortening is compensated for by secondary effects (e.g. axial straining).

5. Condition (i) simply implies tautology; condition (ii) is rarely met in practice. The former approach is widely employed in finite deformation studies. Its consistency surely demands a revision of the accepted approach to this matter.

APPENDIX I(B)

COMPUTATIONAL METHODS CONFERENCE 1986 459

Computerised Large Scale Strut Testing – Interaction Between Experimental and Numerical Models

N. Taylor, P. Hirst

Department of Civil Engineering, Sheffield Polytechnic, U.K.

ABSTRACT

Noting the importance of structural imperfections with regard to strut studies, herein presented is a means of back-ending an experimental programme with a numerical modelling procedure in order that enhanced imperfection data is made available for use with predictive theoretical techniques. Lundquist and Southwell plot procedures are used to generate lumped imperfection parameters from the experimental data which also serves to check their validity. Sample comparative theoretical findings are made which illustrate the latent potential of the respective plot procedures with regard to the non-destructive testing of struts.

INTRODUCTION

A recently completed strut testing programme, employing a Schenck 250 Tonne column testing machine subject to in-house developed micro- and mini-computer control and monitoring, has provided a substantial data base involving the findings of in excess of 200 computer governed strut, stub and imperfection tests – note Plates 1 and 2. The strut elements have been subject to encastré end conditions and consist of 48.3mm diameter by 3.2 mm wall thickness, EWSR Grade 43 CHS sections. Effort has been centred about the modified slenderness ratio of unity, important because of its service practicality and imperfection sensitivity (Trahair, 1977); nominal strut length is therefore approximately 2.5 m.

The objective is to assess the rationale of imperfections with a view to providing a novel yet simple strut modelling procedure. Crucial to this is the incorporation of semi-graphical procedures to act as interpretative adjuncts to the established experimental data base. Deterministic procedures are essential given the statistical nature of imperfection studies (Ciria 1977; Lui and Chen 1983). Brevity



Plate 1; 250 Tonne Testing Machine

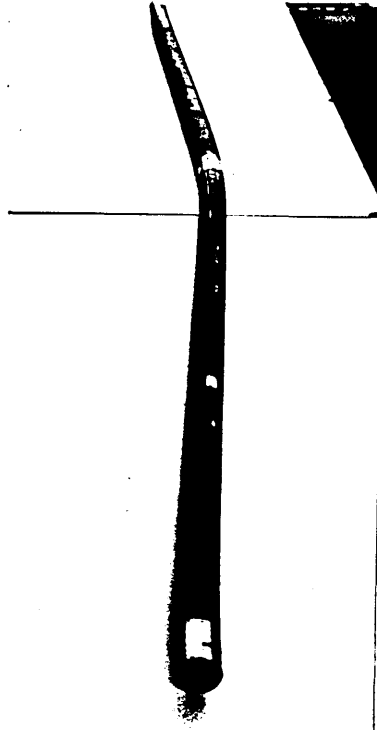


Plate 2; Buckled Specimen (partial recovery)

demands attention be focussed on a group of 14 strut tests; the findings are typical, however, of the larger sample (72).

EXPERIMENTAL PROGRAMME

Employing offcuts, a stub test (Tall, 1976) was carried out for each strut experiment undertaken in order to provide individual direct modulus and yield/proof stress data. Constitutive response ranged between the typical yield and roundhouse loci depicted in Fig.1, most loci being of slightly rounded, quasi-yielding form. Histograms for direct modulus E and yield/proof stress σ_y values are given in Fig.2. With variations from the mean of up to -13% and -33% respectively, determination of individual constitutive data can be seen to be of considerable importance (Ciria, 1977).

Regarding imperfection assessment, wall thickness measurements were taken using further offcuts as indicated in Fig.3(a); these relate to eccentricity of loading \bar{e} (Ellinas et al, 1984). Seven-point initial out-of-straightness imperfection measurements were taken, prior to testing, for each strut specimen as noted in Fig.3(b). These showed non-planar initial topologies extant throughout (corkscrew). Viable initial central displacement values w_{0c} based on an effective length of $\ell = L/2$ were thereby not always available with

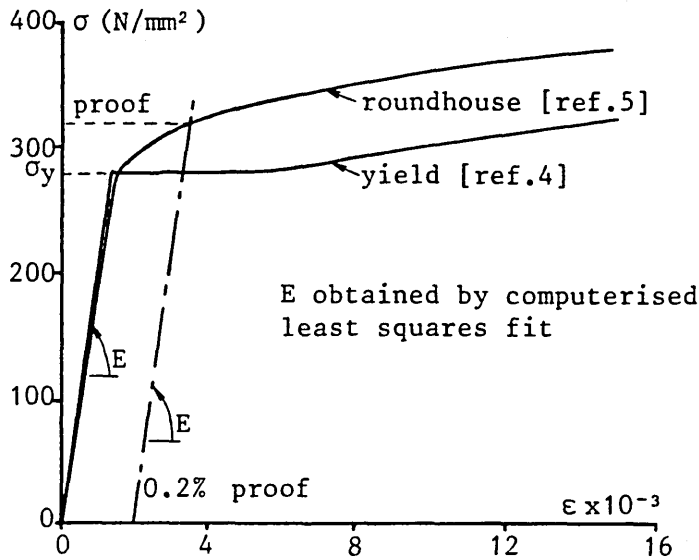


Figure 1; Stub Constitutive Loci

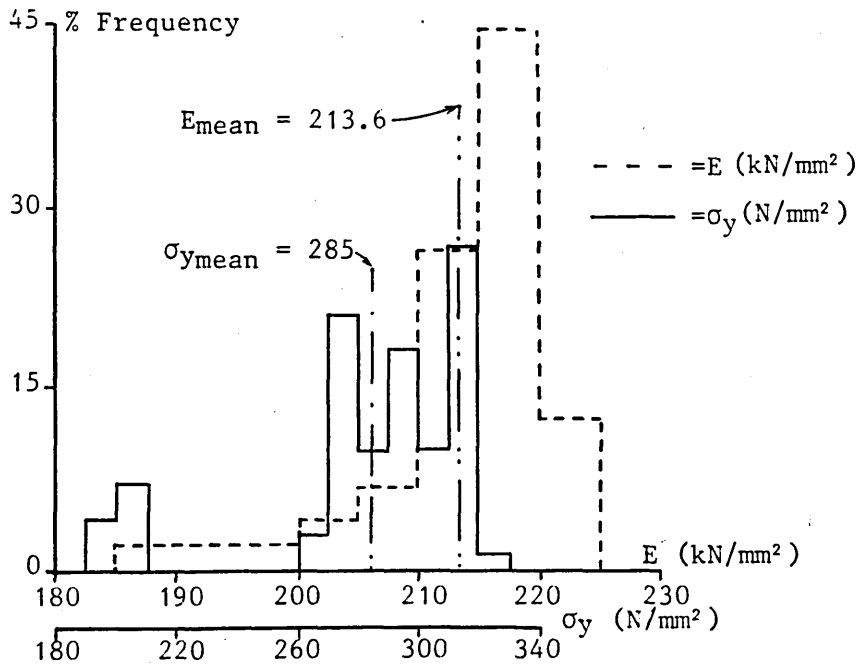


Figure 2; Direct Modulus and Yield/Proof Stress Histograms

non-central values being non-coplanar with, and often exceeding, the central reading. However, the struts were relatively straight, being well within the standard 0.2%L tolerance (BS 4848, 1975) and the accepted value of 0.1%L (Johnston, 1977). Values of $\bar{\epsilon}$ and w_{oc} are given in Table 1; importantly, they are of the same order of magnitude.

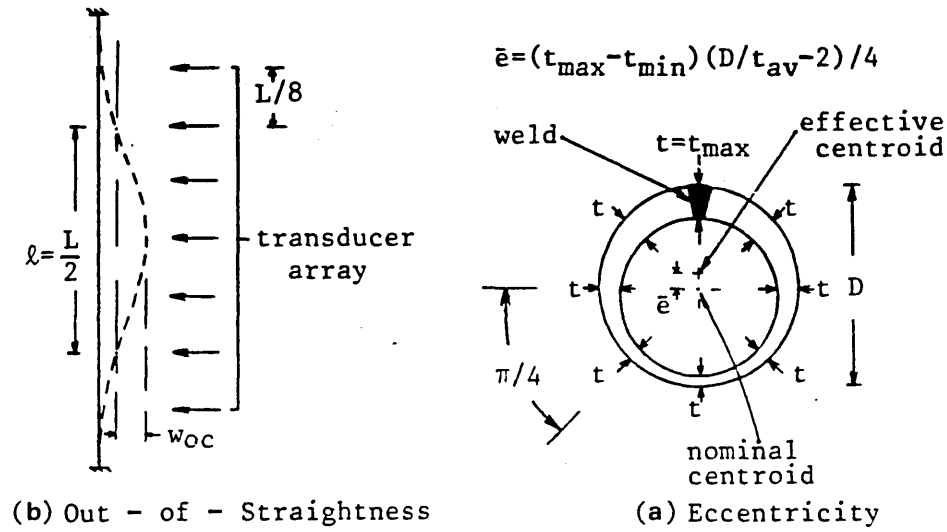


Figure 3; Imperfection Monitoring

Table 1; Experimental Data

Strut Ref.	λ/λ_1	w_{oc} (mm)	\bar{e} (mm)	P_s/P_e	P_c/P_e	P_p/P_e
1	0.94	n/a	0.74	0.88	0.70	0.65
2	0.94	0.14	0.37	0.87	0.72	0.64
3	1.01	n/a	0.79	1.03	0.74	0.71
4	0.91	n/a	0.55	0.82	0.73	0.62
5	1.02	0.52	0.23	1.04	0.75	0.71
6	0.99	0.66	1.18	0.97	0.69	0.68
7	0.88	0.12	0.26	0.77	0.62	0.60
8	0.88	0.61	0.45	0.76	0.62	0.59
9	0.85	n/a	0.72	0.71	0.62	0.56
10	0.93	0.30	0.64	0.87	0.71	0.64
11	0.98	0.36	0.42	0.94	0.70	0.67
12	0.94	n/a	0.31	0.89	0.72	0.65
13	0.91	0.30	0.37	0.82	0.69	0.62
14	0.98	n/a	0.72	0.95	0.74	0.68

Residual stresses were not considered in view of their relative unimportance in such hot rolled sections (Stamenkovic and Gardner, 1983).

Regarding the strut testing itself, the range of modified

slenderness ratios λ/λ_1 employed are also given in Table 1, with

$$\lambda/\lambda_1 = (\ell/r)(\sigma_y/\pi^2 E)^{1/2} \quad (1)$$

where r denotes the radius of gyration; this normalised ratio takes explicit account of the respective constitutive properties. As with the stub tests, deformation controlled loading was used throughout and key experimental findings are included in Table 1. Values of squash load P_s (stub test) and buckling load P_c are given in non-dimensionalised form with respect to the Euler critical load $P_e = \pi^2 EI/\ell^2$, I denoting second moment of area. Corresponding values of the modified Perry load P_p (BS 5950, 1985) are also included. The correlation between λ/λ_1 and P_s/P_e indicates accuracy in the testing procedure. Full equilibrium path output is discussed later, whilst, noting the above comments on imperfections, consideration is now given to the effective incorporation of such data within a theoretical model.

SOUTHWELL AND LUNDQUIST PLOTS

The basis for the Southwell plot technique and its related derivatives is well established (Attard, 1983; Leicester, 1970; Spencer and Walker, 1975). The governing equations of the Southwell and Lundquist plots take the form

$$(w_c - w_{oc})/P = (w_c - w_{oc})/P_{es} + a_{os}/P_{es} \quad (2)$$

and

$$(w_c - w_{oc} - w')/(P - P') = (w_c - w_{oc} - w')/(P_{el} - P') + a_{ol}/(P_{el} - P') \quad (3)$$

where w_c denotes the central displacement under elastic load P , P' and w' denote the elastic 'pivot' state, and P_{es} , a_{os} and P_{el} , a_{ol} delineate the Southwell and Lundquist estimates of the critical load and initial central displacement respectively. The Lundquist 'pivot' attempts to mitigate low load non-linearities.

Importantly, the a_{os} and a_{ol} parameters can be considered as lumped or effective imperfections taking account, when applied to practical struts, of not only w_{oc} but also eccentricity \bar{e} , residual stress and initial corkscrew effects (Croll and Walker, 1972). By comparing the P_{es} and P_{el} values with the critical load P_e , for which definitive E and $I(t)$ data exists, the viability of the a_{os} and a_{ol} values can be calibrated. That is, herein, the plot techniques are employed to lump all imperfections, which experimentation shows to be diverse and complex in form, into a format suited for use with predictive planar models, their viability being assessed by reference to experimental data (P_{es} , P_{el} vs. $P_e[\ell]$).

EXPERIMENTAL-NUMERICAL INTERACTION

In accordance with the above, Fig.4 depicts a typical pair of

Southwell and Lundquist plots, appropriate data being given for all specimens in Table 2. The respective linear interpolation employs a computerised least squares fit, the ranges of which can be seen to be extensive (Spencer and Walker, 1972) and within the elastic Perry limit (BS 5950, 1985), important features given the substantial inelastic

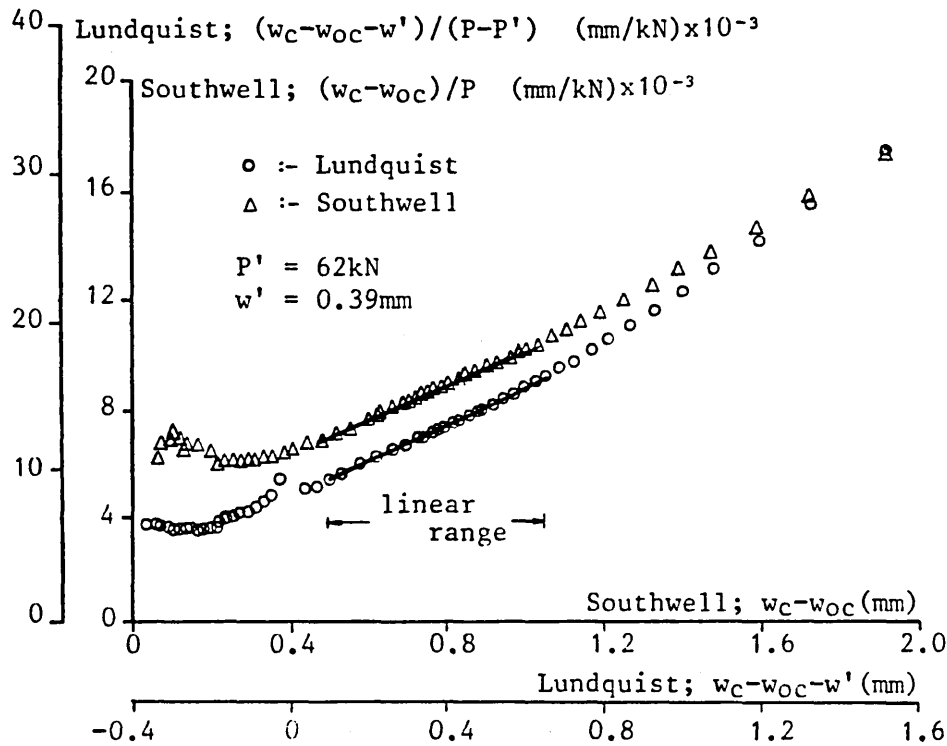


Figure 4; Southwell and Lundquist Plots , Strut Ref. 8

Table 2; Southwell and Lundquist Plot Data

Strut Ref.	Fit Range (% of P_e)		Euler Data (% of P_e)		w_{oc} Data (mm)	
	Southwell	Lundquist	P_{es}	P_{e1}	a_{os}	a_{o1}
1	55 - 62	52 - 60	103.2	88.5	0.79	0.18
2	58 - 67	50 - 67	96.8	87.3	0.55	0.14
3	59 - 67	50 - 67	102.3	93.6	0.66	0.22
4	53 - 61	53 - 61	98.0	86.1	0.30	0.10
5	57 - 66	57 - 70	97.2	85.9	0.48	0.07
6	38 - 55	44 - 57	91.5	83.2	0.77	0.45
7	36 - 50	39 - 52	98.6	89.8	0.67	0.48
8	38 - 54	38 - 54	95.2	82.7	0.66	0.32
9	37 - 51	46 - 55	97.3	84.1	0.68	0.36
10	38 - 48	50 - 61	99.7	92.2	0.55	0.40
11	49 - 60	51 - 60	97.6	90.7	0.75	0.54
12	42 - 58	46 - 58	94.3	91.4	0.39	0.43
13	52 - 62	45 - 55	93.7	91.1	0.70	0.52
14	53 - 62	61 - 69	96.7	85.5	0.35	0.10

range of the struts involved - note λ/λ_1 and P_p/P_e ratios in Table 1. On the basis that $\ell = L/2$ is not actually prescribed, then the respective average Southwell and Lundquist values for effective length are within 1% and 6% of this assumed relationship. This generates confidence in the experimentation and is consistent with acceptance of a_{0s} and a_{01} as effective or lumped imperfection parameters. The salient features of a theoretical planar strut model for which such parameters are well-suited will now be briefly considered.

THEORETICAL MODELLING

A constitutively and kinematically non-linear spring-link model is illustrated in Fig.5. The 2^oF modelling takes account of three-zone inelasticity (Chen, 1971; Snyder and Lip Seng, 1968) and, whilst being highly non-linear, generates computationally amenable expressions. A quasi-potential energy approach is employed with

$$V = \sum_{\text{springs}} \left(\int M d\theta \right) - P(u-u_0) \quad (4)$$

where V denotes the quasi-energy, M and θ the spring bending moment and rotation respectively, and $(u-u_0)$ defines the effective flexural end shortening. Applying the statics criterion $\delta V/\delta \theta_i$ for $i=1,2$ results in

$$\sin\theta_1 + \sin\theta_2 = M_p \cos(n\pi/2) (1 - e^{-k}) / P\ell \quad (5)$$

and

$$\sin\theta_1 = M_p \cos(n\pi/2) (1 - e^{-m}) / P\ell \quad (6)$$

where

$$k = \frac{2EI(\theta_2 - \theta_{02}) + 4800(1-n)(\theta_2 - \theta_{02})^2}{M_p \ell \cos(n\pi/2)} \quad (7)$$

and

$$m = \frac{EI(\theta_1 - \theta_2 - \theta_{01} + \theta_{02}) + 1200(1-n)(\theta_1 - \theta_2 - \theta_{01} + \theta_{02})^2}{M_p \ell \cos(n\pi/2)} \quad (8)$$

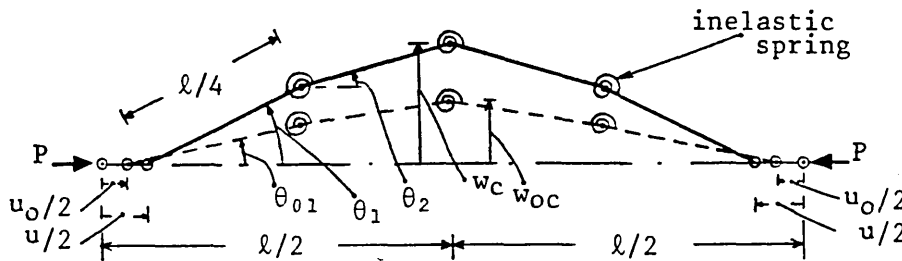
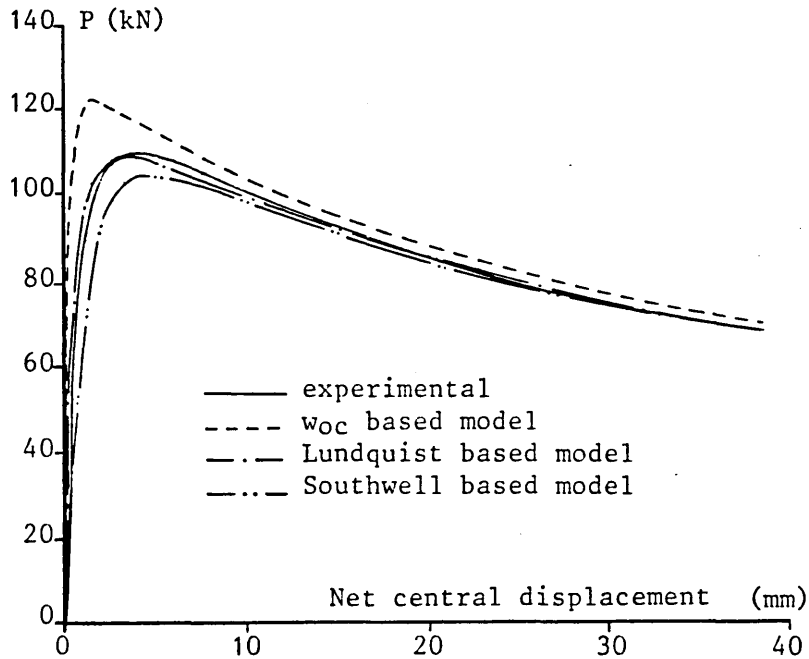
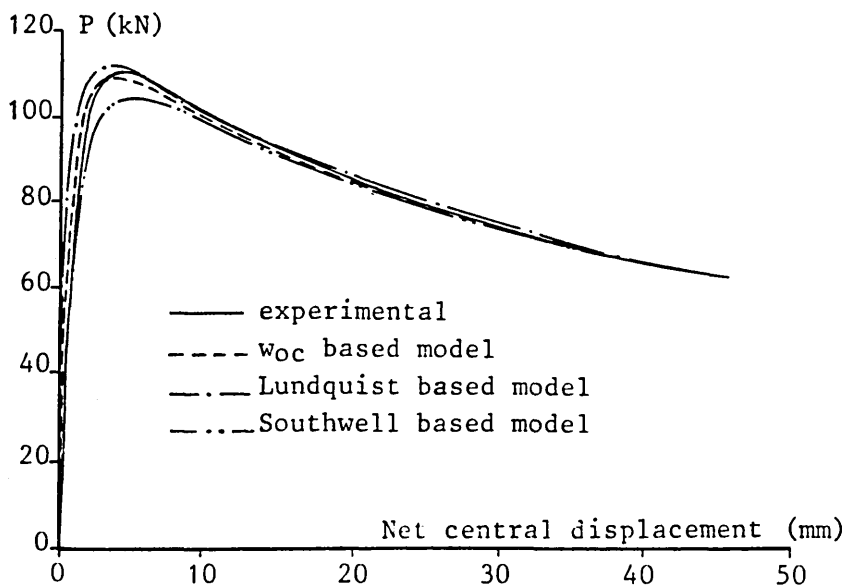


Figure 5; Theoretical Model

where M_p denotes the full plastic moment, $n=P/P_s$ and $\theta_i-\theta_{0i}$ is the net slope, $i=1,2$. Typical solutions obtained employing a_{0s} , a_{0l} and direct w_{oc} data respectively are given in terms of P vs. w_c loci in Fig.6 together with the associated experimental curves. Corresponding values for the set of buckling loads P_c are given in terms of the appropriate experimental values in Table 3. Noting both Fig.6 and Table



(a) Strut Ref. 7



(b) Strut Ref. 8

Figure 6; Action - Response Loci

Table 3; Theoretical Buckling Load Assessment

Strut Ref.	Theoretical Buckling Load (% of P_c)		
	Southwell	Lundquist	Direct
1	88.7	103.3	n/a
2	89.8	102.4	102.4
3	91.4	101.4	n/a
4	92.4	100.0	n/a
5	94.9	108.8	88.5
6	95.9	100.8	97.7
7	95.3	99.0	112.3
8	94.2	101.9	98.7
9	92.0	98.5	n/a
10	92.1	95.4	99.7
11	90.3	93.9	97.2
12	93.4	94.7	n/a
13	88.4	91.5	98.2
14	94.6	104.9	n/a
Av.	92.4	99.8	99.3*

* Restricted Applicability

3, it is considered that the Lundquist technique affords a highly attractive approach to experimental imperfection interpretation.

CONCLUSIONS

The Southwell and Lundquist plots offer a viable catalytic interface between experimental and theoretical or predictive studies. Their application in the non-destructive testing assessment of in-service struts should be considered. Their ability to interpret effective length, given the developing studies on end condition effects, is of particular note.

ACKNOWLEDGEMENT

Material support for the testing programme has been gratefully received from BSC (Tubes Division), Corby, UK.

NOMENCLATURE

E	direct modulus
I	second moment of area
L	nominal length
M, M_p	bending moments
P	load ($n=P/P_s$)
P_c, P_e, P_p, P_s	buckling, Euler, Perry and squash loads
P_{es}, P_{el}	Southwell and Lundquist P_e values
P', w'	Lundquist pivot state
V	quasi-potential energy
a_{os}, a_{ol}	Southwell and Lundquist imperfections

\bar{e}	eccentricity
l	effective length
r	radius of gyration
t	wall thickness
$u-u_0$	effective end shortening
w_c, w_{oc}	transverse central deformations
ϵ	strain
$\theta, \theta_i, \theta_{oi}$	slope; $i=1,2$
λ/λ_1	modified slenderness ratio ($=1$ for $P_e=P_s$)
σ, σ_y	stress; yield/proof stress

BIBLIOGRAPHY

- Attard, M.M. (1983). Extrapolation Techniques for Buckling Loads. *Jnl. Struct. Eng.*, ASCE, 109, 4, 926-935.
- British Standards Institution. (1975) Hot-rolled structural steel sections, Part 2: Hollow sections. BSI, London, BS 4848, Part 2.
- British Standards Institution. (1985). Structural use of steelwork in building, Part 1: Code of practice for design in simple and continuous construction; hot rolled sections. BSI, London, BS 5950, Part 1.
- Chen, W.F. (1971). Further Studies of Inelastic Beam - Column Problem. *Jnl. Struct. Div.*, ASCE, 97, ST2, 529-544.
- Ciria Report 63. (1977). Rationalisation of safety and serviceability factors in structural codes, Ciria, London.
- Croll, J.G.A. and Walker, A.C. (1972). Elements of Structural Stability. Macmillan Press, London.
- Ellinas, C.P. et al. (1984). Buckling of Offshore Structures. Granada Publishing, London.
- Johnstone, B.G. (1977). Third SSRC Guide with Column Design Applications. *Jnl. Struct. Div.*, ASCE, 103, ST7, 1359-1376.
- Leicester, R.H. (1970). Southwell Plot for Beam-Columns. *Jnl. Eng. Mechs. Div.*, ASCE, 96, EM6, 945-965.
- Lui, E.M. and Chen, W.F. (1983). Extrapolation of H-columns with small end restraints. *Struct. Eng.*, 61B, 1, 17-26.
- Snyder, J.S. and Lip-Seng, L. (1968). Buckling of Elastic-Plastic Tubular Columns. *Jnl. Struct. Div.*, ASCE, 94, ST1, 153-173.
- Spencer, H.H. and Walker, A.C. (1975). Critique of Southwell Plots with Proposals for Alternative Methods. *Jnl. Expt. Mechs.*, 15, 8, 303-310.
- Stamenkovic, A. and Gardner, M.J. (1983). Effect of Residual Stresses on the Column Behaviour of Hot-Finished Steel Structural Sections. *Proc. Instn. Civ. Engrs.*, Part 2, 75, 599-616.
- Trahair, N.S. (1977). The Behaviour and Design of Steel Structures. Chapman and Hall, London.

STRUT BEHAVIOUR SUBJECT TO PRE-BUCKLING CYCLIC LOADING

PAUL HIRST & NEIL TAYLOR
Department of Civil Engineering
Sheffield Polytechnic
Sheffield S1 1WB, UK

ABSTRACT

Amplification of the effects of an initial imperfection due to pre-buckling cyclic hysteresis is considered with respect to a range of imperfection-sensitive struts. The findings of a recently-completed large scale strut testing programme involving application of a variety of cyclic profiles are herein discussed. These cyclic profiles simulate excursions from nominally static loading and are bounded by constraining the axial load to remain compressive and of sub-buckling magnitude throughout. Imperfections were monitored and supporting static strut and stub tests undertaken for comparative assessment purposes. Testing was implemented under axial displacement control in conjunction with encastré end conditions. Circular hollow section specimens were employed, lengths being centred on a modified slenderness ratio of unity.

Findings indicate that serviceability degradation attends low cycle plastic excursions, the peak axial displacement/compression incurred during these excursions being the dominating influence. An empirical design chart is provided to this effect. A two degrees-of-freedom spring-link representative model which describes static strut behaviour as modified by the presence of a prescribed phase of cyclic action is derived for predictive purposes. Effective experimental-theoretical correlation is obtained.

1. INTRODUCTION

Little inquiry appears to have been made regarding the effect the incidence of low cycle excursions of pre- or sub-buckling form has upon the otherwise static performance of a strut. This would seem somewhat arbitrary given the importance of imperfections upon strut behaviour and the possibility of interaction occurring between these two phenomena, noting also that purely static loading cannot be guaranteed in practice. Study has therefore been undertaken to identify the primary features of static strut behaviour as modified by the presence of a phase or phases of low frequency, low duration pre-buckling cyclic action.

Investigation has been centred about the modified slenderness ratio of unity, important because of its service practicality and inelastic imperfection sensitivity (1). Circular hollow sections (CHS) have served for testing purposes. Cyclic action phases, involving a variety of profiles, have been introduced at static axial compressions corresponding to either the factored or unfactored ECCS service load (2). The axial displacement accompanying this compression is maintained as the mean cyclic axial displacement, with some load relaxation being associated with inelastic response (3). Excursions into the inelastic range of the material that incur hysteresis loops displaying the characteristic of cyclic creep (3) are of primary concern as these will tend to amplify the effect of any initial imperfection. Serviceability considerations are then made with respect to static strut performance, through to buckling, upon exit from the cyclic loading phase.

Given the foregoing, a recently completed strut testing programme, employing a 250 Tonne column testing machine subject to in-house developed micro- and mini-computer control and monitoring, has provided an appropriate and substantial data base involving the findings of in excess of one hundred computer governed strut, stub (4) and imperfection tests. Complementary predictive theoretical studies employ a representative spring-link model which utilises a novel fully differentiable and integrable moment-thrust-curvature expression capable of describing elastic, inelastic and plastic static behaviour. Whilst initial static behaviour is considered in largely established terms, post-cyclic loading phase static behaviour is modelled on the basis that an amplified initial imperfection has been effectively incurred during the cyclic phase. Definition of this amplified initial imperfection is made in terms of the amount of cyclic creep or 'cyclic step' incurred, use being made of an empirical design chart obtained from the experimental studies.

2. NOTATION

E	direct modulus
I	second moment of area
L	nominal length
M, M_i , M_p , M_y	bending moments
P	compressive load ($n=P/P_S$)
P_C , P_e , P_p , P_S	buckling, Euler, 'Perry' and squash loads
P_{es} , P_{el}	Southwell and Lundquist Euler estimates

P_m, P_m^i	maximum cyclic load, initial mean cyclic load
P', w'	Lundquist pivot state
R	section outer radius
$\delta U, \delta W$	internal and external virtual work functions
a_{os}, a_{ol}	Southwell and Lundquist imperfections
c	exponential constant
e	eccentricity
f	frequency
k_i	section constants; $i=1,2$
ℓ, ℓ_s, ℓ_1	effective lengths
r	radius of gyration
t	wall thickness
$u-u_0$	effective end shortening
u_a	half cyclic amplitude
u_m^i	mean cyclic stroke
w_c, w_{oc}	transverse central deformations
w_c^i	cyclic step
x, y, t'	independent coordinates
$\epsilon, \epsilon_i, \epsilon_y$	strain; yield/proof strain
$\theta, \theta_i, \theta_{oi}$	slope; $i=1,2$
λ/λ_1	modified slenderness ratio ($=1$ for $P_e=P_s$)
σ, σ_y	stress; yield/proof stress
$v; v_y$	curvature; first yield curvature

3. EXPERIMENTAL PROGRAMME

3.1 Test Specimens

All tests were conducted on EWSR Grade 43 CHS 48.3mm diameter by 3.2mm wall thickness specimens. Sections were supplied in 7m runs by BSC (Corby). Struts were subject to encastré end conditions giving an effective length $\ell=L/2$, where L denotes the nominal length, in both the elastic and inelastic behavioural regimes. Tests were undertaken on inelastically imperfection sensitive struts typically possessing modified slenderness ratios λ/λ_1 in the vicinity of unity where

$$\lambda/\lambda_1 = (\ell/r)(\sigma_y/\pi^2 E)^{\frac{1}{2}} \quad (1)$$

with r denoting radius of gyration, σ_y the appropriate yield or proof stress and E the corresponding direct modulus. Strut specimens were thereby approximately 2.5m in length, enabling two specimens of equal length and thereby possessing a common ECCS service load (2) to be cut from each 7m run of section as supplied. One specimen to be tested statically, the other to be additionally subjected to a cyclic loading phase centred upon some specified pre-buckling static state. This static/cyclic correlation provides for some degree of control over the experimental cyclic data, further control being sought by the large number of tests undertaken - see Table 1. This degree of control was considered essential given the statistical basis of strut design.

Further, employing offcuts from the 7m runs provided, stub tests (4) were carried out on specimens approximately 200mm in length to provide individual yield/proof stress and direct modulus data relating to each

static and cyclic strut test undertaken. The normalised ratio given in eqn 1 utilises this data explicitly with regard to strut specimen definition. Additional offcut material was used for wall thickness and outer diameter assessment enabling evaluation of the corresponding eccentricity of loading incurred in the static and cyclic strut tests (5).

3.2 Static Tests

Strut, stub and imperfection experimentation was carried out on a Schenck servo-hydraulic testing machine, see Plate 1, modified to operate under computer control (RML380Z) and digital monitoring (DEC1104). All testing was carried out under axial displacement control. To meet BS1610 requirements (6), a 225kN load cell was incorporated, and the testing machine's crosshead was pulled back with a pre-stress in excess of the maximum specimen loading in order to obviate adverse effects - particularly during cyclic loading, note later.

For stub test purposes, the crosshead was lowered and accurately formed loading platens incorporated in the machine (4). Constitutive response ranged between the typical yield and roundhouse loci depicted in Figure 1, most loci being of slightly rounded, quasi-yielding form. Histograms for direct modulus E and yield/proof stress σ_y values are given in Figure 2. With variations from the mean of up to -13% and -33% respectively, determination of individual constitutive data can be seen to be of considerable importance (7). It is to be noted that residual stresses were not explicitly considered in view of their relative unimportance in such hot rolled sections (8); stub test data - note Figure 1 - largely supports this view, relatively few full roundhouse curves being incurred.

Strut testing was conducted employing encastré end conditions, the modified slenderness ratios involved being given in Table 1. Taper-lock collets, possessing a clamping action which intensifies with increasing axial loading, were utilised to implement these conditions. The employment, discussed later, of the Southwell and Lundquist plot techniques (9)(10)(11) enabled a check to be made upon the effective length assessment - see Plate 2. Prior to actual testing, out-of-straightness measurements were taken. Each specimen was rotated through 360° and readings taken by seven transversely mounted transducers evenly distributed along the strut's length (9). These readings showed non-planar or corkscrew initial topologies extant throughout. Viable initial central displacement values w_{oc} based on an effective central length of $\ell=L/2$ - ie w_{oc} represents the difference between the central and averaged quarter-point transducer readings - were thereby not always available with non-central values being non-coplanar with, and often exceeding, the central reading. However, the struts were relatively straight, being well within the standard $0.2\%L$ tolerance (12) and the accepted value of $0.1\%L$ (13). Values of loading eccentricity e , determined from sectional geometry assessment (5) as noted previously, and w_{oc} are given in Table 1; importantly, these imperfections of form are of the the same order of magnitude. Two values for w_{oc} are given in Table 1; direct or viable readings, as defined above, are given where applicable. An 'interpolated' value is also given, this being derived by using a cosine curve possessing an unprescribed amplitude to define an initial shape and equating the volume of revolution swept out upon

rotation of this curve about the centreline with that similarly swept out on the basis of the appropriate seven transducer readings. The values of central initial displacement or amplitude thereby obtained are halved to relate to the same central effective length $\ell=L/2$ employed in defining the direct w_{OC} value.

Typically, each static strut test involved the acquisition of some 2000 discrete data items employing 150 quasi-static ramped axial stroke increments. Emphasis was placed upon experimental accuracy with tests being far longer in the preparation than the actual execution. Tests were conducted well into the post-buckling range and key static experimental data is summarised in Table 1, further details being available elsewhere (9). Values of buckling load P_C are given both in explicit and in non-dimensionalised form with respect to the appropriate Euler critical load $P_e = \pi^2 EA / (\ell/r)^2$, A denoting cross-sectional area. Evaluation of P_e is made using individual strut material and geometric properties. Corresponding values of the unfactored modified Perry/ECCS load P_p (2) are also included in terms of P_p/P_e ; for consistency, P_p is similarly evaluated employing individual test data with, additionally, $\ell=0.5L \neq 0.7L$ (2) given the experimental specification (note later). As-measured transverse central displacement values (w_c) corresponding to the onset of buckling are given in view of serviceability requirements. Respective squash load $P_s = \sigma_y A$ data is available from $\lambda/\lambda_1 = (P_s/P_e)^{1/2}$.

3.3 Cyclic Tests

With stub and imperfection data established a priori, cyclic strut tests commenced with a static procedure upto an axial displacement u_m^i which corresponded to some prescribed axial compression. This compression, denoted by P_m^i , took the form of the respective factored or unfactored ($P_m^i = P_p$) ECCS load, typically in the vicinity of 45kN and 70kN respectively. The former value relates to conditions in practice, the latter effectively guarantees inelastic response during the cyclic action phase.

Cyclic action was applied in the form of a sinusoidal forcing function

$$u = u_m^i + u_a \sin(2\pi f t') \quad (2)$$

where u denotes total axial displacement at any time t' such that u is compressive for all t' , u_a represents half-amplitude and f the appropriate frequency. Throughout, f was maintained at 1/16Hz, a typical offshore value, obviating inertial and resonance effects. Following attainment of u_m^i , cyclic action was instituted under axial displacement control in accordance with eqn 2. Monitoring was undertaken using x, y and $x, y/t$ analogue plotters, key data being the peak axial displacement $u_m^i + u_a$ and the peak axial compression P_m , with $P_m < P_C$ throughout. Cyclic action phase durations were again based on offshore values and generally consisted of 1000 cycles. It should be noted that fatigue failure per se was not being sought (14). A range of amplitudes $2u_a$ were investigated, some struts being subjected to two distinct cyclic action phases. Key details of the cyclic profiles employed and primary responses obtained are given in Table 2, data entries being identified by F for cyclic action phases based on the factored ECCS load, and by U for those based on the unfactored ECCS load.

Values of axial displacement u_m' , axial compression and central transverse displacement were digitally recorded upon emergence from the cyclic action phase. Whilst u_m' was invariably unchanged, as required, from its corresponding pre-cyclic value and load relaxation was negligible, distinct increases in central transverse displacement occurred in specific test cases. This increase in displacement due to cyclic creep (3) is identified by w_c' and represents the aforementioned cyclic step. Upon completion of the prescribed number of cycles, automatic static control was accordingly re-implemented. In most tests, this involved taking the strut statically through buckling, which occurred at an axial displacement of $u|_{P_c}$, to some limiting displacement state. In the remaining tests, a second cyclic action phase was instituted prior to the static buckling procedure being implemented. This cyclic phase was necessarily based on the appropriate unfactored ECCS load.

Values of the ensuing buckling load P_c and the corresponding central transverse displacement $w_c|_{P_c}$ are given in Table 1, whilst values of peak cyclic load P_m and cyclic step w_c' are expressed as percentages of these parameters in Table 2. These percentages, together with those corresponding to the use of the appropriate static test values for P_c and $w_c|_{P_c}$, included for control purposes, are graphically represented in Figure 3. Two classifications are indicated; those strut tests involving a small cyclic step $w_c' \leq 4\% w_c|_{P_c}$ are deemed to be of only 'quasi-cyclic' form - except for Strut Refs 19, 23 and 24 - whilst the remaining strut tests are termed cyclic or 'cyclic proper'. Together with the data in Table 2, Figure 3 indicates that the latter set corresponds to those cases involving substantial peak plastic excursions as shown by the respective values of $(u_m' + u_a)/u|_{P_c}$ (controlled) or P_m/P_c (monitored) - note Strut Refs 19, 23 and 24. A suggested empirical design locus is superposed in Figure 3 accordingly, with $w_c'/w_c|_{P_c} = 5\%$ for $P_m/P_c \leq 0.75$, corresponding values for $P_m/P_c > 0.75$ being obtained from

$$w_c'/w_c|_{P_c} = (85.5 - 86.27P_m/P_c)^{-1} \quad (3)$$

It is to be noted that the load carrying capacity of the struts - ie the buckling load P_c - is relatively insensitive to cyclic action of the form prescribed as indicated in Table 1.

Experimental axial load/central transverse displacement loci typifying the cyclic tests are given in Figures 4 to 6 which also display corresponding theoretical loci later discussed. These loci represent static paths, the cyclic step being simply represented by a transition line joining the coordinates $w_c - w_{oc}|_{P_m'}$, P_m' and $w_c - w_{oc}|_{P_m' + w_c'}$, P_m' ; they appertain to static strut behaviour as modified by the presence of a prescribed phase of pre-buckling cyclic action. Figure 6 additionally shows the appropriate (fully) static experimental and theoretical loci for comparative purposes, these loci relating to the statically tested 'partner' (Strut Ref 26).

Hysteresis displaying cyclic creep through the cyclic step w_c' is typified in Figure 7. Both load relaxation and cyclic creep deceleration (3), that is a 'tightening' of the individual hysteresis loops as cyclic creep increases, are displayed; it is important to note

that no stabilization of creep deceleration is reached, indicative of the interaction between the cyclic step and the imperfection sensitivity of the struts concerned. Alternative hysteresis profiles are given schematically in Figure 7. Type 7(a) relates to those quasi-cyclic tests involving relatively low peak axial compressions, P_m being incurred during the cyclic action phase or phases. This form of profile is termed quasi-elastic hysteresis (14) and is of variable but small effect upon strut performance. Local plastic inclusions and material imperfections induce, in the presence of cyclic action, effects which can either enhance or detract from strut stiffness with randomly located exit paths being recorded as hysteresis reversed and oscillated to a highly variable extent. Type 7(b) relates to those quasi-cyclic tests involving higher values of P_m and to Strut Refs 19, 23 and 24. Path stabilization occurs in the latter three cases, the random and complex nature of strut imperfections being held responsible for the apparently contrary behaviour involved. This feature is illustrated in Figure 8 which shows a 'plan view' of the path described by the central transverse displacement (Strut Ref 19). The cyclic step is to be noted as are the directions of measured imperfections w_{oc} and e . The apparent coincidence between the path's direction and that of w_{oc} belies the fact that Figure 8 relates to a corkscrew-type initial strut topology, note Table 1. Further, despite the weld dictating the direction of e for each strut involved in the testing programme, w_c path directions encompassed all four quadrants; this additionally indicates independence of the specimen from testing machine interference, however.

It should perhaps be noted that Strut Ref 20 relates to a cyclic test which resulted in buckling occurring during the cyclic action phase and thereby represents an upper bound to the cyclic testing programme with $(u'_m + u_a) / |u|_{P_c} = 1$ - note Table 2.

3.4 Southwell and Lundquist Plots

The basis for the Southwell plot technique and its related derivatives is well established (11,15). The governing equations of the Southwell and Lundquist plots take the form

$$(w_c - w_{oc}) / P = (w_c - w_{oc}) / P_{es} + a_{os} / P_{es} \quad (4)$$

and

$$(w_c - w_{oc} - w') / (P - P') = (w_c - w_{oc} - w') / (P_{el} - P') + a_{ol} / (P_{el} - P') \quad (5)$$

where $w_c - w_{oc}$ denotes net central transverse displacement under elastic load P , P' and w' denote the elastic 'pivot' state, and P_{es} , a_{os} and P_{el} , a_{ol} delineate the Southwell and Lundquist estimates of the critical load and initial central displacement respectively. The Lundquist 'pivot' attempts to mitigate low load non-linearities. Displacement values are again based on a centrally located effective length.

Importantly, the a_{os} and a_{ol} parameters can be considered as lumped or effective imperfections taking account, when applied to practical struts, of not only w_{oc} but also eccentricity e and residual stress effects (10). Further, given the availability of definitive material data (E, A, r, t), Southwell and Lundquist effective length estimates, ℓ_s and ℓ_l respectively, can be derived and employed to assess the deemed experimental value ($\ell = L/2$). Given the performance of these techniques

in the corresponding static studies wherein unique linear plots were obtained through both the elastic and inelastic behavioural regimes (9), it was determined to employ them with respect to the cyclic tests. Pre- and post-cyclic phase linear loci were sought, ideally the respective paths being parallel, P_e remains constant, but offset, indicating an increased initial imperfection (a_{0s} , a_{0l}). Appropriate data is given in Table 3 with respect to the cyclic (proper) cases. The fit ranges are considered adequate with the effective length estimates confirming confidence in the experimental value of $L/2$. Further, a significant number of viable pairs of bi-linear paths were obtained, typified by Figure 9, affording pre- and post-cyclic action phase values of a_{0s} and a_{0l} for inclusion in the planar theoretical modelling to which attention is now turned.

4. THEORETICAL MODELLING

Recalling that the primary objective is to determine static strut behaviour as modified by the presence of a prescribed phase of cyclic action, then theoretical modelling is to be undertaken employing a static strut model capable of describing the pre- and post-cyclic action phases, incorporation of the cyclic step w'_c being made by means of a simple transition locus for $P=P'_m$. That is, the post-cyclic static modelling will need to be capable of defining an artificial initial imperfection described in terms of w'_c .

A constitutively and kinematically non-linear representative spring-link model is illustrated in Figure 10; accepting symmetry, this possesses two degrees-of-freedom, θ_1 and θ_2 . The springs need to be able to model elastic, inelastic and plastic constitutive behaviour. A well-established three-zone constitutive strut topology is depicted in Figure 11 (16,17); this topology leads to complex governing equations typified by the moment-thrust-curvature loci given in Figure 12 which employ the non-dimensional compression parameter $n=P/P_s$. Simplification of these relationships is undertaken employing a curve fitting procedure (18) with respect to these loci based on the expression

$$M = M_p \cos(n\pi/2) \left[1 - e^{-\left[EIV/(M_p \cos(n\pi/2)) + c(1-n)v^2 \right]} \right] \quad (6)$$

where M and v denote general bending moment and curvature respectively, $I=Ar^2$, M_p denotes the plastic moment and c is a sectional constant - $c = 123.10^6 \text{mm}^2$ herein. Eqn 6 is applicable to all constitutive regimes for all n and, importantly, is continuous, differentiable and formally integrable, thereby lending itself to ease of manipulation. Eqn 6 is employed to define the spring characteristics of the analytical model with spring moment $M_1=M$ and spring curvature $v_1=4(\theta_{i-1}-\theta_i)/l=v$.

With δU and δW denoting the internal and external virtual work functions respectively, then

$$\delta U = \delta W \quad (7)$$

so that, for the model topology shown in Figure 10

$$\sum_{i=1,5} (M_i \delta\theta_i) = P \delta u \quad (8)$$

where end-shortening $u=f(\theta_i)$. Incorporating eqn 6 and applying $\delta\theta=(\partial\theta/\partial\theta_i)\delta\theta_i$ where $\theta=f(\theta_i)$ with respect to eqn 7, then, noting imperfections θ_{0i} and u_0 , eqn 8 affords, taking account of symmetry

$$\frac{\partial}{\partial\theta_i} \left(M_p \cos(n\pi/2) \left[2(\theta_1 - \theta_{01}) + \frac{-[2A(\theta_2 - \theta_{02}) + 4B(\theta_2 - \theta_{02})^2]}{A + 4B(\theta_2 - \theta_{02})} \right. \right. \\ \left. \left. + \frac{-[A(\theta_1 - \theta_{01} - \theta_2 + \theta_{02}) + B(\theta_1 - \theta_{01} - \theta_2 + \theta_{02})^2]}{A + 2B(\theta_1 - \theta_{01} - \theta_2 + \theta_{02})} \right] \right) \\ = \frac{\partial}{\partial\theta_i} \left[\frac{P\ell}{2} (\cos\theta_{01} - \cos\theta_1 + \cos\theta_{02} - \cos\theta_2) \right] \quad (9)$$

where $A=4EI/[\ell M_p \cos(n\pi/2)]$ and $B=16c(1-n)/\ell^2$, for $i=1,2$. Differentially operating on eqn 9 affords

$$\sin\theta_1 + \sin\theta_2 = 4M_p \cos(n\pi/2) (1 - e^{-C}) / P\ell \quad (10)$$

and

$$\sin\theta_1 = 4M_p \cos(n\pi/2) (1 - e^{-D}) / P\ell \quad (11)$$

where

$$C = \frac{8EI(\theta_2 - \theta_{02})}{\ell M_p \cos(n\pi/2)} + \frac{4c(1-n)(\theta_2 - \theta_{02})^2}{(\ell/4)^2} \quad (12)$$

and

$$D = \frac{4EI(\theta_1 - \theta_{01} - \theta_2 + \theta_{02})}{M_p \ell \cos(n\pi/2)} + \frac{c(1-n)(\theta_1 - \theta_{01} - \theta_2 + \theta_{02})^2}{(\ell/4)^2} \quad (13)$$

System solutions employing eqns 10 and 11 are initially determined by specifying $P(n)$, estimating θ_2 and determining the respective value of θ_1 . Revised estimates for θ_2 are made until a null condition is achieved. In addition to the input of individual strut case data,

values for θ_{01} and θ_{02} are determined from input w_{oc} values and acceptance of an initial sine profile. Upto four analytical case studies per strut specimen are available, alternatively employing direct w_{oc} , interpolated w_{oc} , Southwell a_{os} and Lundquist a_{o1} initial imperfection data respectively for w_{oc} as specified in Figure 10.

Employing the Southwell and Lundquist imperfection values, then two static analyses are carried out in each case, one employing the initial or pre-cyclic action phase imperfection values for a_{os} and a_{o1} and a second, P'_m being prescribed, employing post-cyclic values. The effective behavioural path consists of the former locus for $P \leq P'_m$ and the latter for $P \geq P'_m$, these being joined with a transition line $P = P'_m$ representing the cyclic step w'_c . Employing either the direct or interpolated w_{oc} values, an initial static analysis is carried out for $P \leq P'_m$ together with determination of the buckling parameters P_c and $w_c | P_c$. Given the relative insensitivity of P_c to the prescribed low cycle, low frequency cyclic actions involved, the respective cyclic step w'_c was determined using eqn 3 or the 5% cut-off value as appropriate - note Figure 3 also - on the basis of P_m/P_c employing the static P_c value determined above. An additional iterative procedure is now required in order to determine a revised or enhanced value of 'initial' imperfection w_{oc} such that the ensuing static analysis load-net displacement path passes through the state location $(w_c + w'_c) | P'_m, P'_m$ where $w_c | P'_m$ denotes the immediately pre-cyclic value of the net central transverse displacement. Upon securing this revised imperfection, the overall strut behaviour is obtained from the initial static analysis for $P \leq P'_m$, and from the corresponding static analysis employing the revised or enhanced w_{oc} value for $P \geq P'_m$; a transition line at $P = P'_m$ again completes the appropriate locus. Cases involving more than one cyclic action phase require similar but repeated application of the foregoing techniques.

Typical analytical solutions for the respective $P-w_c$ loci are given in Figures 4-6, Figure 6 also including static loci for comparison, whilst Table 4 gives all feasible theoretical P_c values for the cyclic (proper) set of tests together with those of their static counterparts. Values of w_c are interpreted in terms of $L=2\lambda$ - ie are doubled - when referring to the physical prototype.

5. DISCUSSION

For the range of variables employed, it is apparent from Table 1 that strut deformation is more susceptible to cyclic action than the load carrying capacity itself. Table 2 indicates that substantial inelastic straining is required before any notable degradation in structural performance is incurred due to pre-buckling cyclic action; Figure 3 presents an appropriate design chart. Imperfection variation between static and cyclic partners inhibits individual case assessment, and relatively large numbers of tests were undertaken to enhance data control. Importantly, Strut Ref 1 serves to show how quasi-elastic and closed loop hysteresis can involve cyclic steps which reduce upon continued excitation.

Cyclic amplification of initial imperfections involves open hysteresis

loops suffering progressive cyclic creep (3) as typified in Figure 7. This phenomenon incurs characteristics associated with incremental plasticity, there being no shakedown limit (19) for struts. Between statics and fatigue (typically $\leq 10^8$ cycles, with 'low cycle' fatigue $\leq 10^4$ cycles) there is a range of limiting criteria to be established (20), with many serviceability problems in practice being possibly due to cyclic action (21). Figure 3 is produced with these factors in mind.

The theoretical studies afford computationally amenable modelling of a complex problem. Figures 4 to 6 indicate effective conservative load-deformation characteristics are provided, with Tables 4 and 5 affording definitive data trends. The models could readily be refined by the incorporation of additional spring-links, with formal cyclic action modelling a possibility (22). The Southwell and Lundquist techniques proved to be very useful in providing simple means of treating the complexities of imperfection assessment, the respective effective length evaluations providing additional benefits.

6. CONCLUSIONS

Cyclic amplification of initial strut imperfections has been studied for a specified range of parameters and design guidance in the form of cyclic step data and associated buckling performance has been established. Strut deformation has been shown to be susceptible to low cycle, low frequency plastic excursions exhibiting substantial but sub-buckling compression peaks. With the absence of net tension possibly offsetting the associated imperfection sensitivity concerned, and, given the well-formed nature of the sections employed, the findings indicate that higher frequencies and greater, but sub-fatigue, cyclic durations should be considered. Different section types are likely to exhibit varying degrees of response to pre-buckling cyclic action with lighter gauge, cold-formed sections of perhaps particular interest.

7. ACKNOWLEDGEMENT

Material support received from BSC (Corby, UK) is gratefully acknowledged.

8. REFERENCES

- (1) Trahair, N S: "The behaviour and design of steel structures", Chapman and Hall, London, 1977.
- (2) British Standards Institution: "Structural use of steelwork in building, Part 1: Code of practice for design in simple and

- continuous construction; hot rolled sections", BSI, London, BS 5950, Part 1, 1985.
- (3) Sandor, I S: "Fundamentals of cyclic stress and strain", The University of Wisconsin Press, Wisconsin, 1972.
 - (4) Tall, L: "Stub column test procedure", Document X-282-61, Laboratory Report No 220A, Lehigh University, Bethlehem Pa, 1961.
 - (5) Ellinas, C P et al: "Buckling of offshore structures", Granada Publishing, London, 1984.
 - (6) British Standards Institution: "Materials testing machines and force verification equipment", Parts 1 and 2, BSI, London, BS 1610, 1985.
 - (7) Ciria Report 63: "Rationalisation of safety and serviceability factors in structural codes", Ciria, London, 1977.
 - (8) Stamenkovic, A and Gardner, M J: "Effect of residual stresses on the column behaviour of hot-finished steel structural sections", Proc Instn Civ Engrs, Part 2, 75, 1983, 599-616.
 - (9) Taylor, N and Hirst P B: "Computerised large scale strut testing - Interaction between experimental and numerical models", Proc of the Third Int Conf on Comp Meths and Exptl Meas, 1, Porto Carras, September, 1986, 459-468.
 - (10) Croll, J G A and Walker, A C: "Elements of structural stability", Macmillan Press, London, 1972.
 - (11) Spencer, H H and Walker, A C: "Critique of Southwell plots with proposals for alternative methods", Jnl Exptl Mechs, 15, 8, 1975, 303-310.
 - (12) British Standards Institution: "Hot-rolled structural steel sections, Part 2: Hollow sections", BSI, London, BS 4848, Part 2, 1975.
 - (13) Johnstone, B G: "Third SSRC guide with column design Applications", Jnl Struct Div, ASCE, 103, ST7, 1975, 1359-1376.
 - (14) Wood, W A: "The study of metal structures and their mechanical properties", Pergamon Press, New York, 1971.
 - (15) Attard, M M: "Extrapolation techniques for buckling loads", Jnl Struct Eng, ASCE, 109, 4, 1983, 926-935.
 - (16) Chen, W F: "Further studies of inelastic beam-column problem", Jnl Struct Div, ASCE, 97, ST2, 1971, 529-544.
 - (17) Snyder, J S and Lip-Seng, L: "Buckling of elastic-plastic tubular columns", Jnl Struct Div, ASCE, 94, ST1, 1968, 153-173.
 - (18) Taylor, N and Gan, A B: "Refined modelling for the lateral buckling of submarine pipelines", J Construct Steel Res, 6, 2, 1986, 143-162.
 - (19) Frederick, C O: "Shakedown of a rectangular beam under combined loading", CEGB, RD/B/N663, Berkeley Nuclear Laboratories, 1966.
 - (20) Bjorhovde, R: "Research needs in stability of metal structures", Jnl Struct Div, ASCE, 106, ST12, 1980, 2425-2442.
 - (21) Constrado/Instn of Struct Engrs: "Structural use of steelwork in building; Introduction to BS5950 Part 1", Constrado/Instn of Struct Engrs, 1986.
 - (22) Mulcahy, T M and Shoemaker, E M: "Column instabilities caused by cyclic loading", Int Jnl Solids and Structures, 6, 1970.

Strut Ref.	λ/λ_1		w_{oc} (direct) (mm)		w_{oc} (interpolated) (mm)		e (mm)		P_c (kN)		w_c/P_c (mm)		P_c/P_e		P_p/P_e	
	S	C	S	C	S	C	S	C	S	C	S	C	S	C	S	C
1	0.93	0.92	n/a	0.04	0.28	0.10	0.60	0.58	106.7	113.7	4.27	3.86	0.71	0.75	0.64	0.63
2*	0.77	0.78	n/a	0.07	0.34	0.43	0.08	0.10	78.4	84.6	3.49	1.86	0.54	0.58	0.48	0.49
3	0.94	0.93	n/a	0.30	0.67	0.56	0.74	0.64	104.8	105.3	4.77	5.41	0.70	0.71	0.65	0.64
4	s/t	0.98	s/t	0.36	s/t	0.63	s/t	0.42	s/t	106.0	s/t	5.64	s/t	0.70	s/t	0.67
5	0.94	0.97	0.14	0.67	0.19	0.44	0.37	0.01	106.4	107.1	4.56	5.03	0.72	0.73	0.64	0.67
6	0.89	0.93	n/a	0.26	0.13	0.37	0.73	0.36	115.1	116.5	2.01	2.71	0.76	0.80	0.60	0.64
7	0.94	0.94	0.24	n/a	0.33	0.31	0.09	0.31	109.3	110.3	3.22	4.28	0.70	0.72	0.65	0.65
8	0.91	0.91	0.17	0.30	0.44	0.55	0.26	0.37	112.2	102.9	1.78	5.10	0.74	0.69	0.62	0.62
9	1.01	1.01	n/a	n/a	0.22	0.48	0.79	0.59	104.5	113.7	5.84	2.78	0.74	0.76	0.71	0.68
10	0.96	0.98	0.20	n/a	1.01	1.08	0.41	0.57	106.8	111.0	3.53	3.37	0.70	0.74	0.67	0.68
11	0.82	0.78	0.24	0.23	0.45	0.31	0.27	0.05	78.1	85.7	3.33	2.20	0.53	0.58	0.49	0.49
12	0.98	0.98	n/a	n/a	0.62	0.30	0.62	0.72	112.5	112.7	3.20	3.95	0.75	0.74	0.69	0.68
13	0.97	1.04	0.10	0.08	0.59	0.67	0.76	0.51	107.8	105.3	4.95	5.32	0.70	0.79	0.67	0.73
14	1.01	0.94	0.30	n/a	0.97	0.66	0.74	0.82	106.2	106.9	4.73	4.42	0.82	0.71	0.71	0.65
15	0.91	0.91	n/a	n/a	0.23	0.28	0.55	0.79	112.5	111.9	3.89	4.23	0.73	0.73	0.62	0.62
16	n/a	0.78	n/a	0.03	n/a	0.21	n/a	0.36	n/a	84.3	n/a	1.54	n/a	0.59	n/a	0.49
17	1.02	1.01	0.52	n/a	0.84	0.60	0.23	0.29	100.6	101.2	5.27	6.19	0.75	0.74	0.71	0.70
18	0.99	1.00	0.66	0.42	0.89	0.63	1.18	0.69	94.7	90.6	7.47	9.21	0.69	0.67	0.68	0.69
19	0.96	0.96	0.11	n/a	0.49	0.13	0.13	0.55	97.7	100.1	5.93	5.38	0.73	0.74	0.66	0.66
20§	0.88	0.88	0.12	n/a	0.16	0.15	0.26	0.34	109.6	86.3	4.47	20.38	0.62	0.49	0.60	0.60
21	0.88	0.89	0.61	0.23	0.95	0.24	0.45	0.36	110.4	117.1	4.34	2.85	0.62	0.67	0.59	0.60
22	0.85	0.84	n/a	n/a	0.43	0.09	0.72	0.50	107.6	111.7	3.38	2.72	0.62	0.64	0.56	0.57
23	1.01	1.01	0.15	n/a	0.40	0.40	0.34	0.39	98.1	92.4	5.08	8.47	0.80	0.76	0.70	0.69
24	1.02	1.02	0.20	0.21	0.56	0.42	0.71	0.50	96.3	91.8	6.37	8.05	0.80	0.75	0.69	0.70
25	0.87	0.89	n/a	0.27	0.41	0.60	0.42	74.0	77.0	4.06	3.95	0.63	0.64	0.58	0.59	
26	0.84	0.84	0.17	0.37	0.59	0.24	0.58	0.26	116.6	114.5	3.71	3.69	0.57	0.57	0.56	0.57
27	0.84	0.85	n/a	n/a	0.25	0.26	0.49	0.51	117.0	114.0	2.75	4.77	0.58	0.58	0.56	0.58

n/a = not applicable s/t = spoilt test § = buckled during cyclic phase * = first low result for P_c , therefore cyclic specimen tested in static mode
S = static C = cyclic

Table 1 ; Primary Experimental Data

Strut Ref.	Stroke Drive								Primary Monitored Response				Classification	
	u'_m (mm)		$\pm u_a$ (mm)		$\frac{u'_m + u_a}{u'_m/P_c}$		Duration (number of cycles)		P_m/P_c (X)		$\frac{w'_s}{w_c/P_c}$ (X)			
	F	U	F	U	F	U	F	U	F	U	F	U		
1	1.19	1.96	0.25	0.45	0.45	0.75	25	25	45.1	75.6	1.3	2.3	Quasi-Cyclic	
2	n/a	n/a	n/a	n/a	n/a	n/a	n/a	n/a	n/a	n/a	n/a	n/a		
3	1.29	1.96	0.35	0.35	0.54	0.73	250	750	54.1	77.0	1.5	0.0		
4	1.29	2.02	0.47	0.27	0.55	0.75	500	500	57.6	75.5	1.6	-0.1		
5	1.28	2.04	0.35	0.35	0.53	0.78	500	500	52.8	78.4	-0.5	0.1		
6		1.96		0.35		0.71		1000			70.5			2.2
7	1.28		0.35		0.53		1000		51.7		0.6			
8	1.28		0.35		0.54		1000		56.0		-0.1			
9	1.29		0.35		0.50		1000		51.0		-0.1			
10	1.28	2.03	0.36	0.35	0.52	0.75	250	750	52.0	76.4	3.1	-0.5		
11	1.28		0.35		0.67		1000		66.0		3.0			
12		1.97		0.35		0.73		1000		73.2		-1.1		
13	1.28	2.05	0.35	0.35	0.55	0.81	1000	500	55.1	81.7	1.2	0.5		
14	1.29	2.03	0.35	0.25	0.54	0.76	1000	500	54.3	74.8	1.3	0.1		
15		1.96		0.35		0.74		1000		73.3		1.0		
16	1.36		0.35		0.55		1000		69.5		-0.8			
17		2.05		0.47		0.83		1000		82.0		1.6		
18		2.14		0.50		0.91		1000		92.7		4.4		
19		2.05		0.61		0.87		1000		88.0		2.6		
20§		1.98		1.13		1.00		1000		n/a	n/a	n/a		
21		1.90		1.00		0.95		1000		94.8		11.9		
22		1.89		0.95		0.97		1000		94.9		16.3		
23		2.27		0.61		0.93		1000		96.3		2.5		
24		2.15		0.65		0.95		1000		94.8		2.2		
25	1.51		0.81		0.90		1000		91.0		6.9			
26		1.71		1.02		0.95		1000		94.3		18.3		
27		1.80		1.00		0.97		1000		98.2		37.9		

n/a = not applicable § = buckled during cyclic phase F = factored base U = unfactored base

Table 2 ; Cyclic Experimental Data

Strut Ref.	Linear Fit Range			Euler Data		w _{oc} Data	
	X = Pre-Cyclic Y = Post-Cyclic	Southwell (% of P _e)	Lundquist (% of P _e)	ℓ _s /ℓ	ℓ _l /ℓ	a _{os} (mm)	a _{ol} (mm)
18	X	39 - 41	8 - 27	1.05	1.07	1.16	0.82
18	Y	53 - 64	53 - 64	1.03	1.03	1.54	1.63
19	X	41 - 50	22 - 48	1.05	1.09	0.42	0.33
19	Y	59 - 68	64 - 68	1.04	1.07	0.48	0.37
20	X	§	§	§	§	§	§
20	Y	§	§	§	§	§	§
21	X	34 - 41	n/a	1.02	n/a	0.19	n/a
21	Y	53 - 59	58 - 62	1.01	1.00	0.40	0.61
22	X	20 - 39	n/a	1.02	n/a	0.36	n/a
22	Y	56 - 60	54 - 60	1.00	0.95	0.68	0.25
23	X	39 - 56	39 - 56	1.03	1.07	0.65	0.42
23	Y	59 - 70	59 - 72	1.03	1.04	0.75	0.73
24	X	43 - 54	21 - 48	1.07	1.08	0.51	0.44
24	Y	62 - 73	66 - 73	1.06	1.06	0.60	0.75

samples 25 to 27 (incl.) are n/a

n/a = inadmissible ranges

ℓ = L/2

§ = buckled during cyclic phase

Table 3 ; Southwell and Lundquist Plot Data

Strut Ref.	P _c , Theoretical Buckling Load (% of Experimental Value)							
	Direct		Interpolated		Southwell		Lundquist	
	S	C	S	C	S	C	S	C
18	96.6	97.9	92.9	94.7	95.9	88.6	100.8	87.9
19	105.4	n/a	91.6	96.3	93.7	90.9	99.8	93.5
20	111.3	§	109.0	§	95.3	§	99.0	§
21	95.6	85.2	90.1	85.1	94.2	93.4	101.9	89.2
22	n/a	n/a	96.2	96.0	92.0	88.3	98.5	98.0
23	96.8	n/a	88.7	89.2	95.8	87.1	103.3	87.3
24	96.1	91.7	86.2	88.6	96.6	90.4	91.4	88.0
25	n/a	93.5	106.8	91.9	n/a	n/a	n/a	n/a
26	110.2	91.4	98.6	92.9	n/a	n/a	n/a	n/a
27	n/a	n/a	106.0	n/a	n/a	n/a	n/a	n/a

n/a = inadmissible ranges

§ = buckled during cyclic phase

S = static C = cyclic

Table 4 ; Theoretical Buckling Loads for Cyclic and Corresponding Static Struts

Classification	No. off Exptl. Spec's	Direct (%)		Interpolated (%)		Southwell (%)		Lundquist (%)	
		(%)	No.	(%)	No.	(%)	No.	(%)	No.
Static	26	100 (s=6.5)	16	94 (s=6.7)	26	96 (s=4.9)	19	101 (s=4.2)	18
Quasi - Cyclic	16	97 (s=5.7)	9	91 (s=4.1)	16	94 (s=2.9)	11	96 (s=4.3)	12
Cyclic	9 *	92 (s=4.6)	5	92 (s=3.6)	8	90 (s=2.3)	6	91 (s=4.3)	6

* = excluding strut (ref. 20) ; buckled during cyclic phase

s = standard deviation

Table 5 ; Average Theoretical Buckling Loads : Given as Percentages of Their Corresponding Experimental Buckling Loads

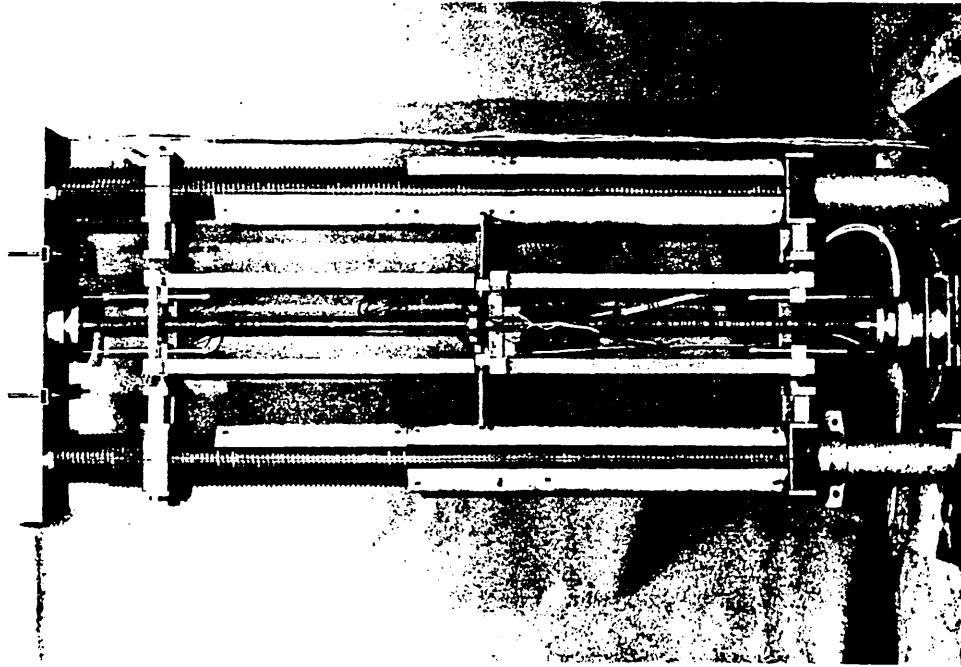


Plate 1; 250 Tonne Schenck testing machine

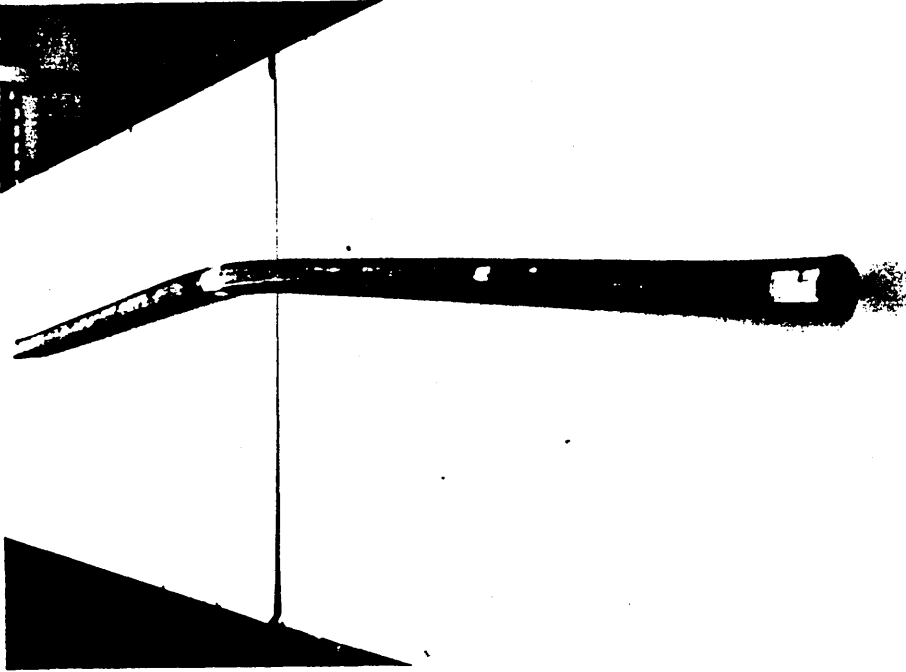


Plate 2; Buckled specimen (partial recovery)

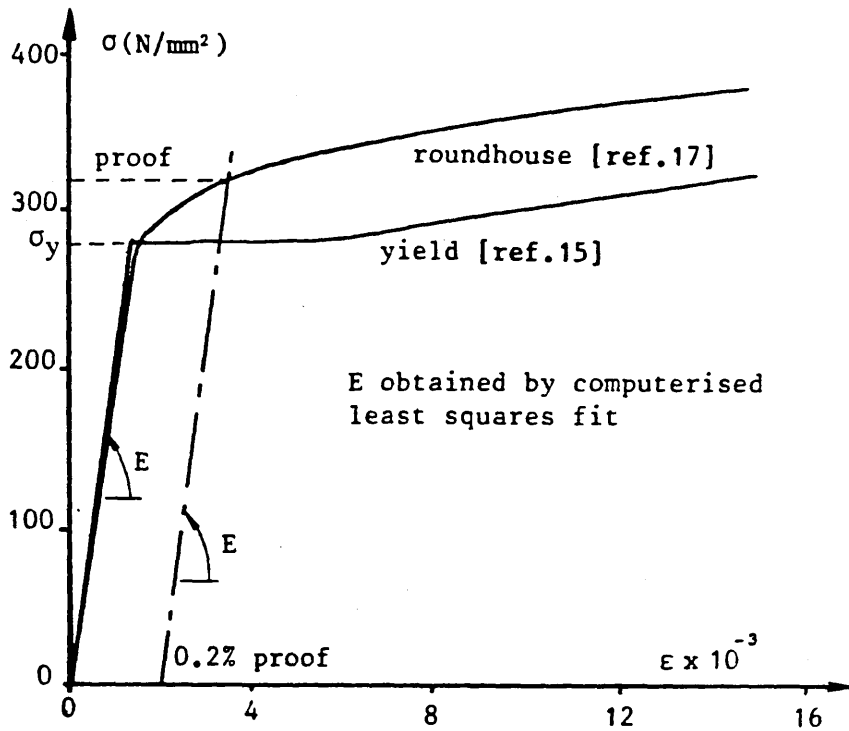


Figure 1 ; Stub Constitutive Loci

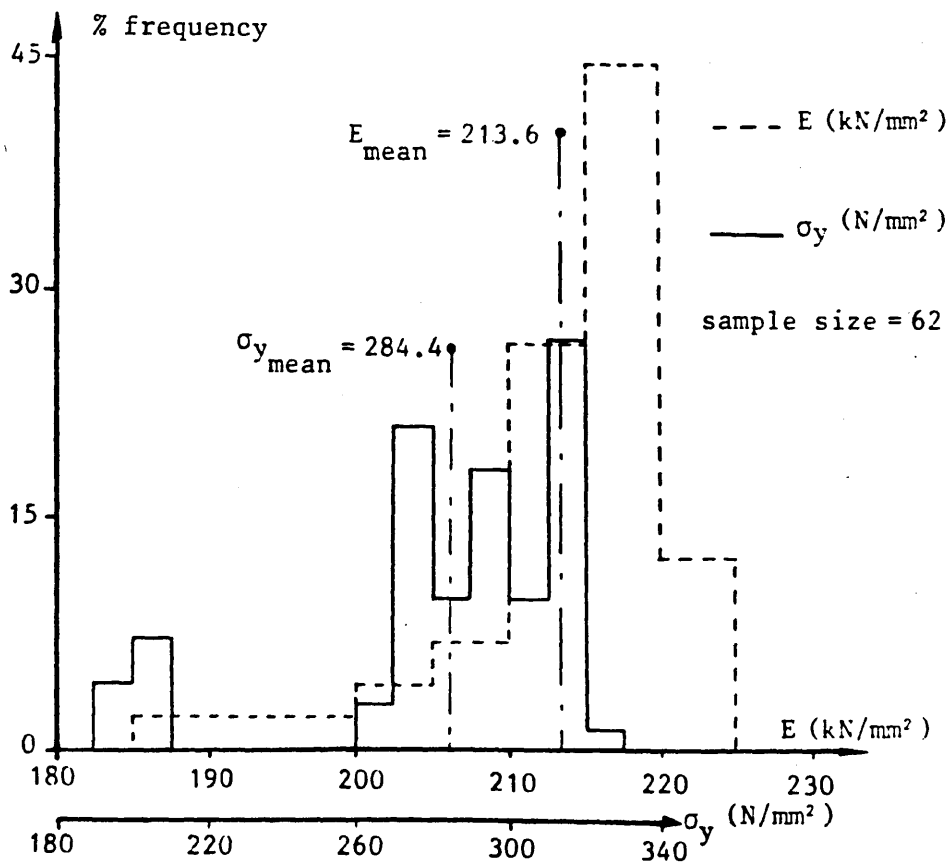


Figure 2 ;Direct Modulus and Yield/Proof Stress Histograms

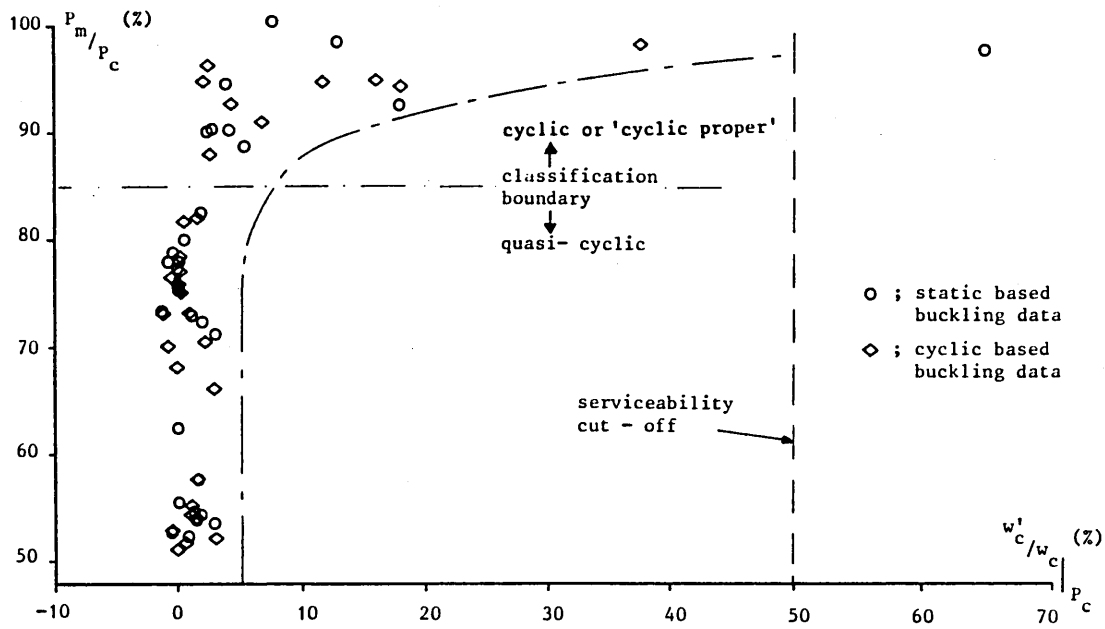


Figure 3 ; Peak Cyclic Load vs Cyclic Step Response

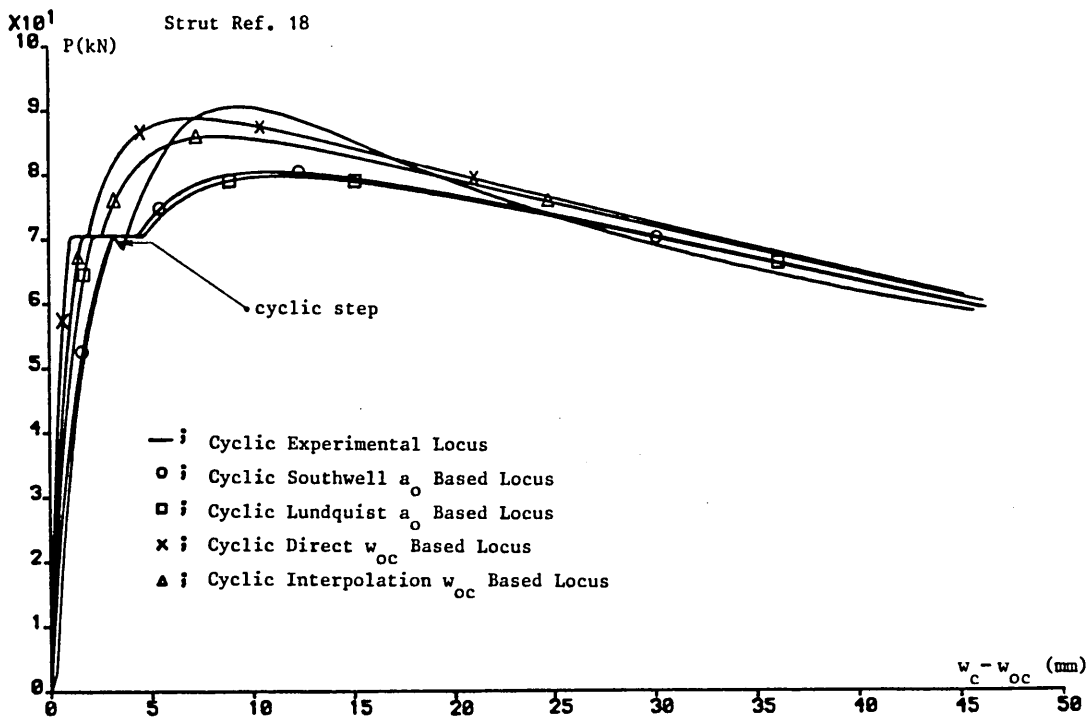


Figure 4 ; Axial Load vs Central Resultant Lateral Displacement

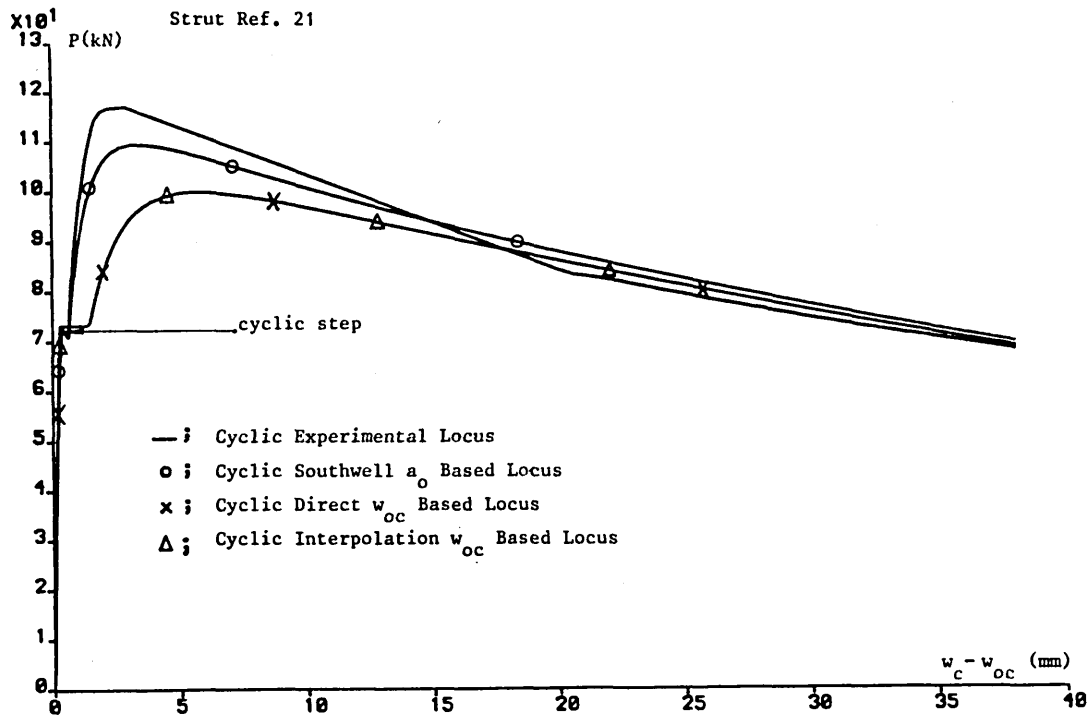


Figure 5 ; Axial Load vs Central Resultant Lateral Displacement

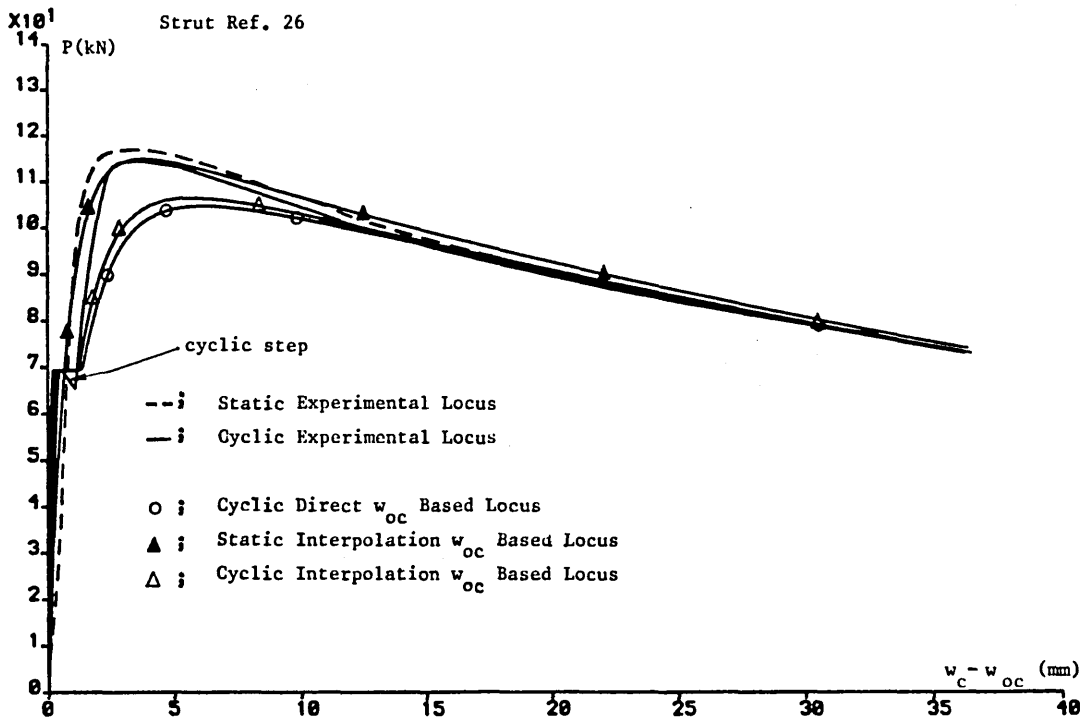


Figure 6 ; Axial Load vs Central Resultant Lateral Displacement

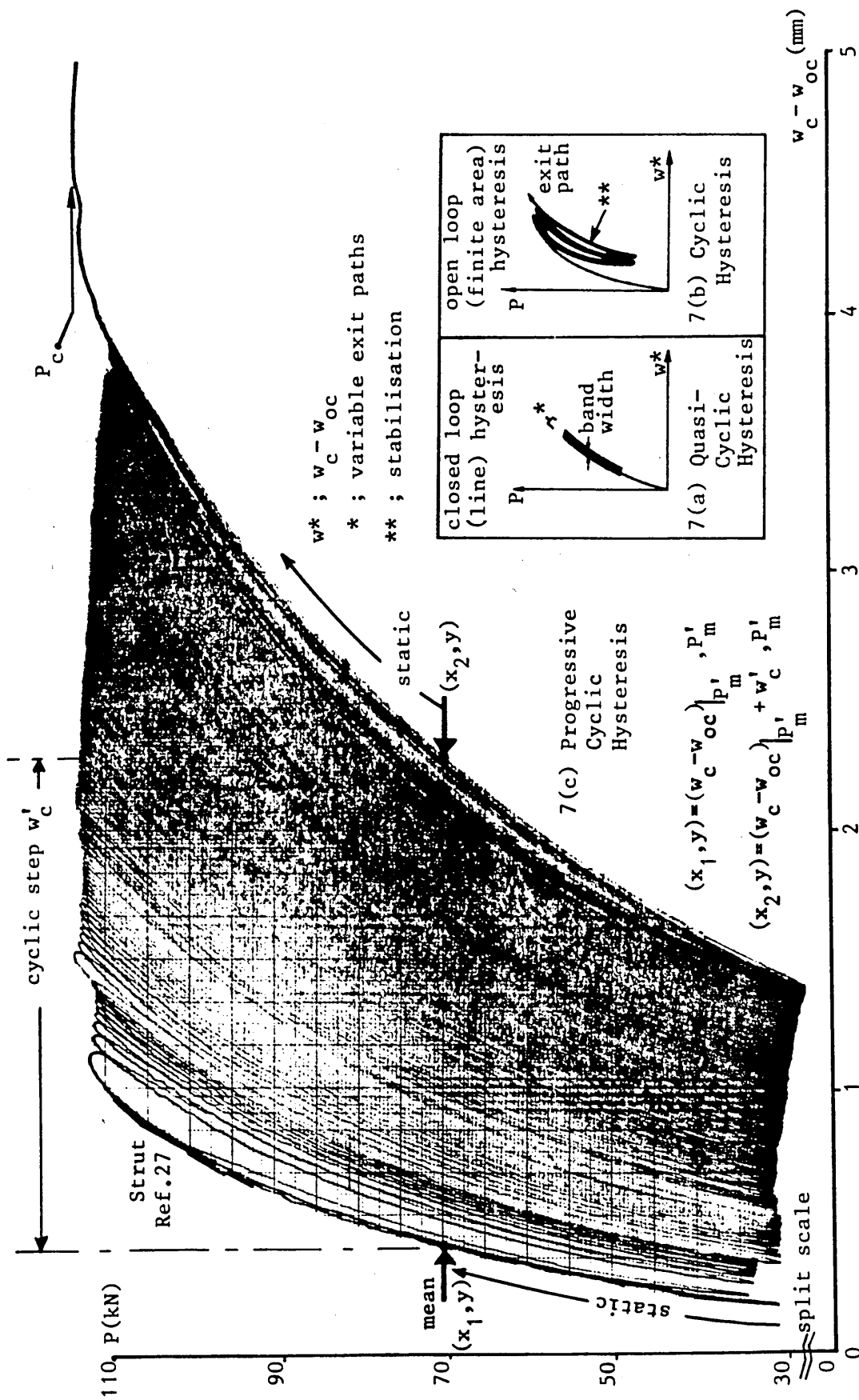


Figure 7 ; Hysteresis Assimilation

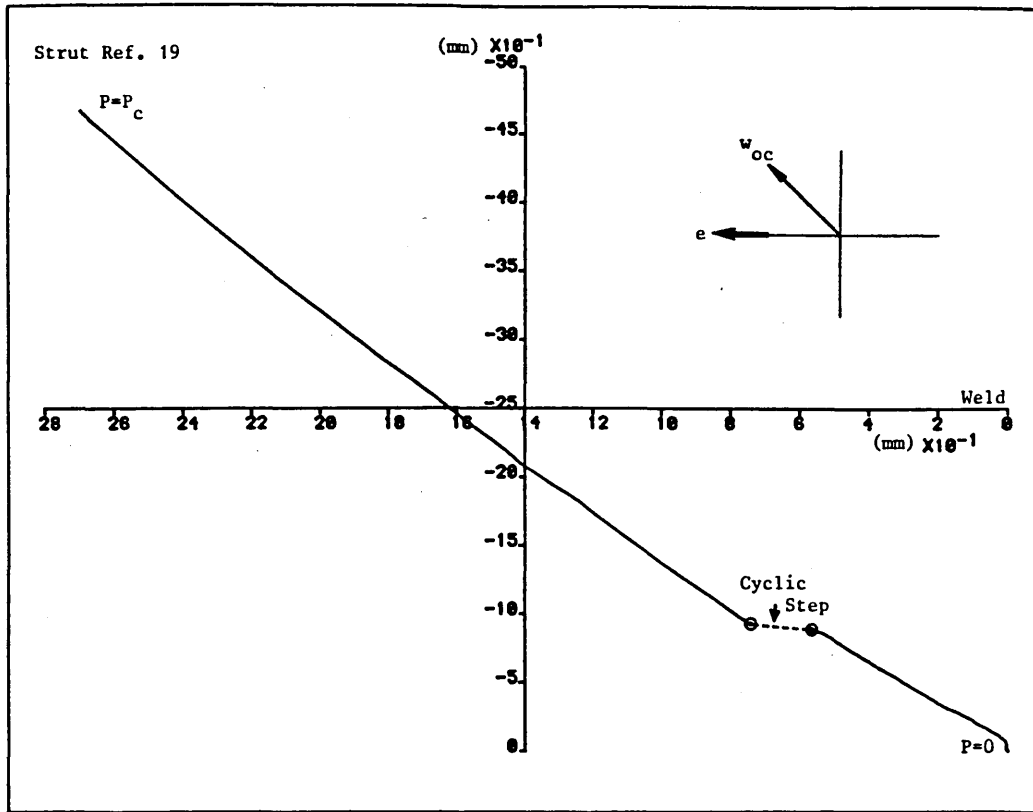


Figure 8 ; Net Central Resultant Lateral Displacement Vector Trace Plan View

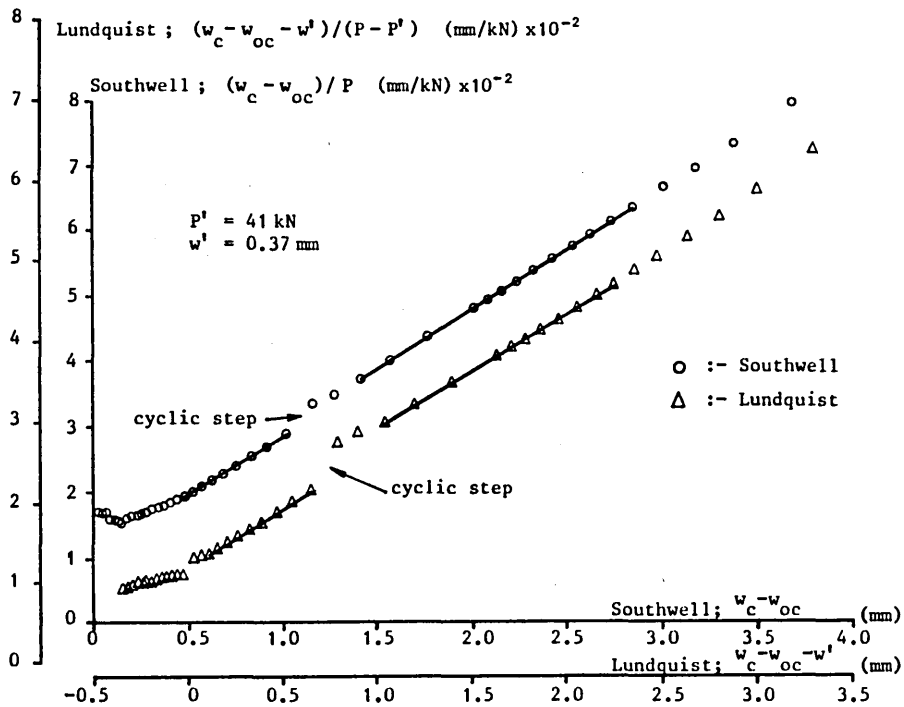


Figure 9 ; Swallowtail and Lundquist Plots (Strut Ref.24)

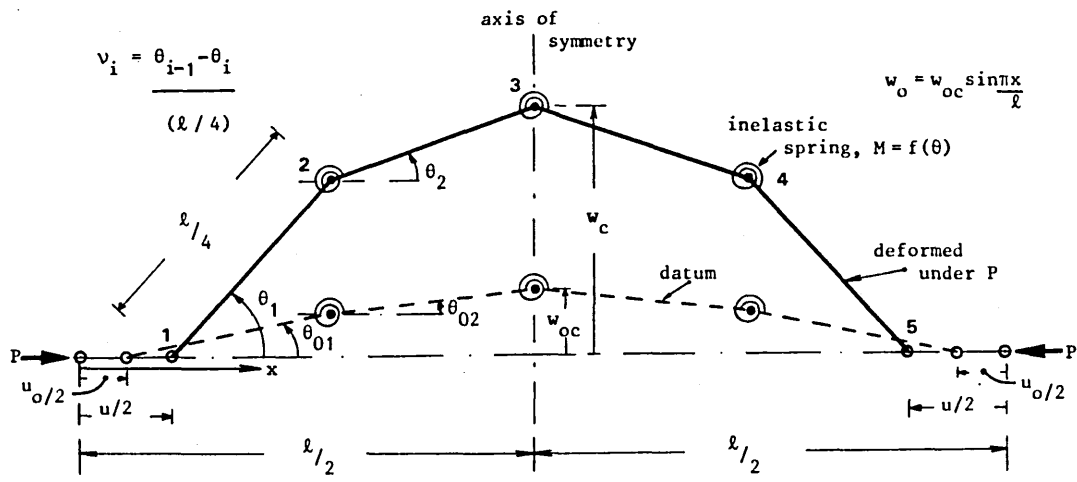


Figure 10 ; Theoretical Model

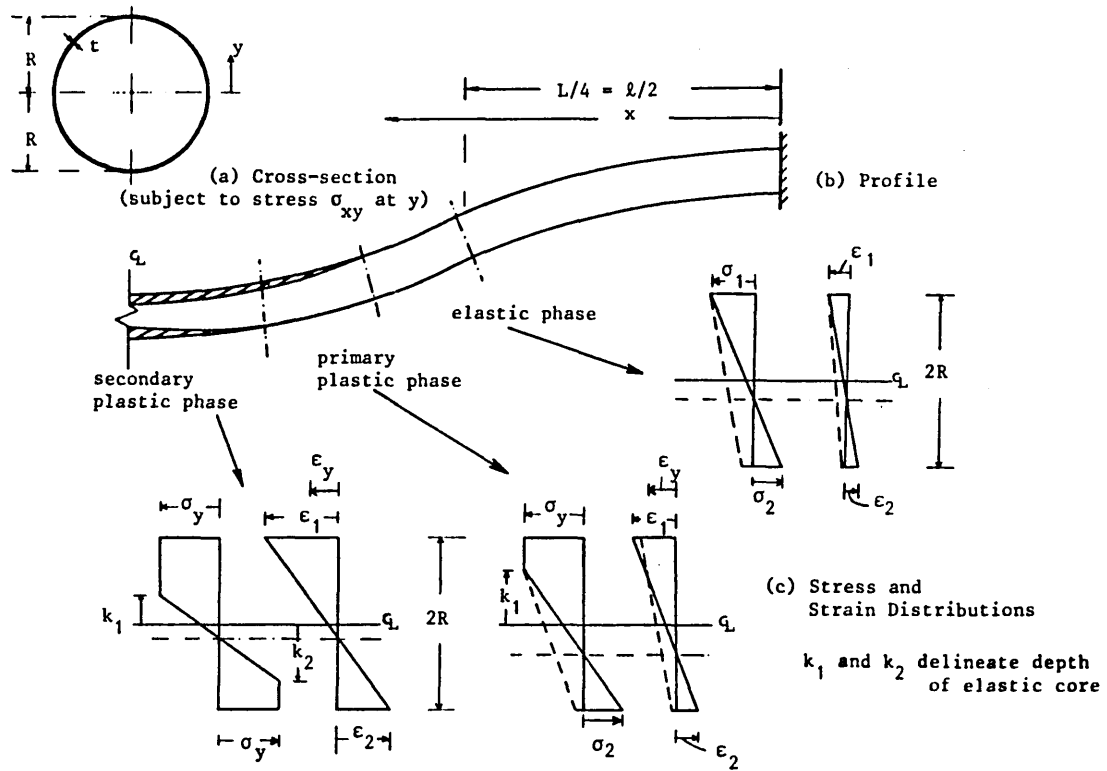


Figure 11 ; Three Phase Constitutive Topology

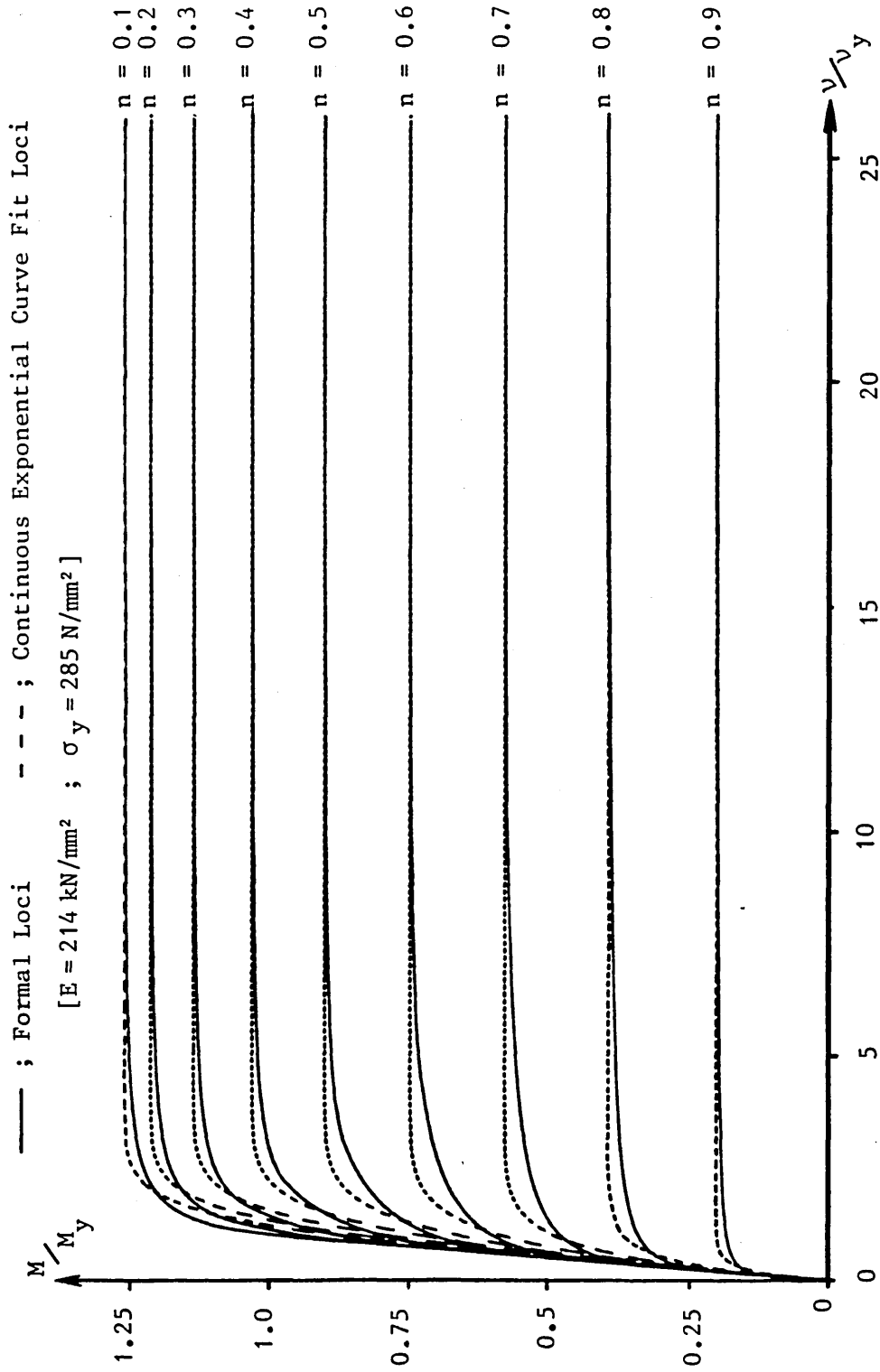


Figure 12 ; Formal M - P - v and Curve Fit Contours

APPENDIX II

TYPICAL NUMERICAL OUTPUT

FILE: JEANCAL OUTPUT A
 DATE: 09JUL1987 AT 14:09:54 HRS

(a) ; increment number
 (b) - (e) ; ϵ_n (n = 1,4) [$\mu\epsilon$]
 (f) ; u - u₀ [mm]
 (g) ; P [kN]
 (h) ; w_c - w_{oc} [mm]

STRUT REFERENCE = 20S

LOAD ST.	STRAIN1	STRAIN2	STRAIN3	STRAIN4	AX.DPLT.	LOAD	LAT.DPLT
(a)	(b)	(c)	(d)	(e)	(f)	(g)	(h)
0	2.	-10.	-11.	-9.	0.000	0.000	0.002
1	-35.	-34.	-37.	-32.	0.080	2.408	0.076
2	-73.	-68.	-73.	-64.	0.167	5.693	0.096
3	-93.	-86.	-91.	-83.	0.212	7.628	0.136
4	-105.	-96.	-103.	-93.	0.237	8.662	0.189
5	-123.	-108.	-122.	-110.	0.277	10.215	0.246
6	-141.	-126.	-137.	-122.	0.329	11.790	0.286
7	-163.	-146.	-158.	-142.	0.377	13.702	0.325
8	-186.	-166.	-178.	-157.	0.432	15.682	0.341
9	-195.	-177.	-188.	-170.	0.457	16.560	0.314
10	-215.	-198.	-210.	-191.	0.509	18.630	0.310
11	-241.	-222.	-235.	-213.	0.570	21.015	0.320
12	-263.	-242.	-260.	-238.	0.625	23.017	0.319
13	-294.	-272.	-287.	-266.	0.695	25.829	0.329
14	-326.	-301.	-318.	-295.	0.772	28.934	0.355
15	-359.	-332.	-351.	-326.	0.852	31.882	0.376
16	-394.	-363.	-388.	-358.	0.932	35.055	0.405
17	-427.	-393.	-423.	-390.	1.010	38.115	0.434
18	-460.	-422.	-453.	-418.	1.089	41.175	0.461
19	-495.	-454.	-489.	-452.	1.172	44.393	0.492
20	-527.	-483.	-525.	-482.	1.249	47.363	0.529
21	-563.	-515.	-562.	-515.	1.330	50.603	0.570
22	-597.	-544.	-595.	-544.	1.412	53.730	0.614
23	-635.	-575.	-632.	-575.	1.495	57.015	0.660
24	-666.	-603.	-665.	-605.	1.577	60.053	0.710
25	-702.	-632.	-702.	-635.	1.659	63.203	0.766
26	-739.	-662.	-740.	-668.	1.740	66.420	0.827
27	-777.	-694.	-780.	-704.	1.825	69.705	0.892
28	-814.	-723.	-817.	-731.	1.907	72.990	0.963
29	-851.	-751.	-854.	-763.	1.989	76.140	1.038
30	-886.	-779.	-889.	-791.	2.072	79.223	1.116
31	-926.	-808.	-931.	-823.	2.155	82.508	1.203
32	-962.	-836.	-967.	-850.	2.240	85.658	1.296
33	-982.	-850.	-990.	-866.	2.285	87.323	1.350
34	-995.	-858.	-1001.	-871.	2.307	88.313	1.382
35	-1003.	-864.	-1012.	-882.	2.330	89.190	1.411
36	-1014.	-872.	-1022.	-888.	2.354	90.068	1.443
37	-1023.	-877.	-1031.	-896.	2.372	90.788	1.466

38	-1035.	-885.	-1042.	-902.	2.395	91.733	1.503
39	-1044.	-891.	-1055.	-912.	2.419	92.453	1.536
40	-1057.	-901.	-1069.	-921.	2.437	93.510	1.569
41	-1068.	-908.	-1081.	-931.	2.464	94.388	1.609
42	-1077.	-914.	-1088.	-935.	2.485	95.153	1.646
43	-1090.	-920.	-1102.	-943.	2.509	96.143	1.699
44	-1100.	-926.	-1112.	-949.	2.530	96.885	1.733
45	-1112.	-932.	-1126.	-957.	2.555	97.763	1.777
46	-1124.	-940.	-1139.	-966.	2.575	98.663	1.824
47	-1136.	-943.	-1150.	-972.	2.597	99.518	1.875

LOAD ST. STRAIN1 STRAIN2 STRAIN3 STRAIN4 AX.DPLT. LOAD LAT.DPLT

48	-1147.	-950.	-1162.	-981.	2.624	100.395	1.934
49	-1160.	-954.	-1176.	-984.	2.645	101.228	2.006
50	-1172.	-959.	-1189.	-992.	2.665	102.083	2.069
51	-1186.	-964.	-1204.	-997.	2.685	102.960	2.146
52	-1198.	-967.	-1216.	-1003.	2.710	103.680	2.224
53	-1213.	-968.	-1232.	-1009.	2.734	104.603	2.326
54	-1230.	-973.	-1251.	-1014.	2.759	105.413	2.432
55	-1243.	-972.	-1267.	-1015.	2.779	106.110	2.558
56	-1263.	-974.	-1291.	-1022.	2.802	106.943	2.707
57	-1280.	-972.	-1311.	-1022.	2.825	107.595	2.875
58	-1302.	-967.	-1340.	-1022.	2.849	108.405	3.109
59	-1327.	-960.	-1372.	-1020.	2.870	108.855	3.379
60	-1354.	-944.	-1416.	-1016.	2.895	109.485	3.753
61	-1411.	-906.	-1502.	-994.	2.914	109.620	4.527
62	-1713.	-633.	-2040.	-857.	2.949	101.768	9.956
63	-2583.	-137.	-2846.	-679.	2.969	90.720	15.478
64	-2682.	-87.	-2941.	-663.	2.994	89.505	16.323
65	-2759.	-45.	-3021.	-651.	3.017	88.628	17.011
66	-2837.	-1.	-3105.	-637.	3.040	87.773	17.719
67	-2907.	36.	-3175.	-626.	3.067	86.918	18.331
68	-2972.	67.	-3242.	-618.	3.092	86.220	18.891
69	-3032.	99.	-3306.	-606.	3.114	85.568	19.424
70	-3093.	127.	-3370.	-600.	3.137	84.938	19.969
71	-3149.	159.	-3430.	-593.	3.159	84.330	20.442
72	-3207.	183.	-3490.	-582.	3.184	83.790	20.942
73	-3258.	210.	-3544.	-575.	3.207	83.228	21.398
74	-3312.	234.	-3600.	-572.	3.232	82.733	21.860
75	-3365.	261.	-3656.	-562.	3.254	82.238	22.329
76	-3417.	283.	-3705.	-558.	3.279	81.720	22.743
77	-3468.	308.	-3757.	-551.	3.302	81.293	23.177
78	-3515.	324.	-3803.	-550.	3.327	80.820	23.544
79	-3558.	343.	-3846.	-544.	3.347	80.528	23.926
80	-3607.	366.	-3891.	-539.	3.372	80.145	24.295
81	-3655.	387.	-3934.	-535.	3.395	79.718	24.677
82	-3700.	407.	-3979.	-531.	3.419	79.358	25.048
83	-3745.	424.	-4021.	-527.	3.442	78.998	25.413
84	-3789.	444.	-4059.	-523.	3.467	78.615	25.750
85	-3835.	462.	-4104.	-519.	3.490	78.323	26.137
86	-3877.	482.	-4136.	-515.	3.514	77.918	26.467
87	-3915.	497.	-4168.	-514.	3.535	77.648	26.796
88	-3955.	514.	-4203.	-511.	3.559	77.310	27.109
89	-3997.	533.	-4236.	-506.	3.582	77.085	27.474

90	-4036.	549.	-4272.	-504.	3.607	76.725	27.801
91	-4076.	565.	-4304.	-501.	3.630	76.433	28.142
92	-4109.	583.	-4335.	-500.	3.655	76.140	28.460
93	-4143.	595.	-4367.	-497.	3.677	75.870	28.761
94	-4177.	612.	-4401.	-497.	3.700	75.600	29.060
95	-4206.	623.	-4432.	-494.	3.722	75.353	29.359

LOAD ST.	STRAIN1	STRAIN2	STRAIN3	STRAIN4	AX.DPLT.	LOAD	LAT.DPLT
----------	---------	---------	---------	---------	----------	------	----------

96	-4241.	638.	-4464.	-494.	3.747	75.083	29.670
97	-4272.	651.	-4499.	-496.	3.770	74.835	29.960
98	-4305.	667.	-4533.	-493.	3.794	74.610	30.258
99	-4334.	678.	-4565.	-494.	3.819	74.363	30.548
100	-4366.	696.	-4603.	-489.	3.842	74.115	30.859
101	-4393.	708.	-4633.	-489.	3.864	73.845	31.127
102	-4421.	721.	-4667.	-486.	3.890	73.620	31.394
103	-4452.	732.	-4698.	-485.	3.912	73.418	31.669
104	-4481.	745.	-4737.	-486.	3.935	73.193	31.948
105	-4508.	759.	-4771.	-484.	3.959	72.990	32.241
106	-4541.	769.	-4805.	-485.	3.980	72.743	32.512
107	-4563.	780.	-4835.	-485.	4.005	72.518	32.740
108	-4594.	796.	-4877.	-481.	4.029	72.360	33.038
109	-4622.	807.	-4910.	-479.	4.052	72.135	33.287
110	-4649.	817.	-4942.	-482.	4.075	71.910	33.524
111	-4673.	829.	-4972.	-481.	4.099	71.730	33.745
112	-4702.	843.	-5010.	-476.	4.122	71.573	34.023
113	-4733.	853.	-5047.	-476.	4.145	71.415	34.296
114	-4763.	865.	-5087.	-476.	4.169	71.190	34.557
115	-4791.	877.	-5121.	-476.	4.192	70.988	34.803
116	-4821.	887.	-5159.	-475.	4.217	70.808	35.067
117	-4849.	899.	-5199.	-475.	4.240	70.605	35.323
118	-4881.	910.	-5236.	-477.	4.264	70.425	35.585
119	-4907.	923.	-5273.	-476.	4.284	70.178	35.806
120	-4936.	932.	-5311.	-479.	4.307	70.043	36.055
121	-4963.	945.	-5346.	-476.	4.330	69.863	36.289
122	-4991.	957.	-5381.	-474.	4.355	69.705	36.541
123	-5019.	969.	-5418.	-472.	4.382	69.503	36.785
124	-5047.	982.	-5456.	-472.	4.402	69.345	37.031
125	-5075.	994.	-5493.	-473.	4.429	69.165	37.269
126	-5098.	1003.	-5529.	-471.	4.450	68.963	37.479
127	-5125.	1017.	-5566.	-473.	4.472	68.828	37.720
128	-5150.	1026.	-5601.	-472.	4.499	68.648	37.949
129	-5175.	1038.	-5634.	-467.	4.520	68.490	38.164
130	-5204.	1050.	-5673.	-468.	4.542	68.355	38.415
131	-5234.	1060.	-5716.	-465.	4.565	68.198	38.672
132	-5258.	1075.	-5755.	-464.	4.590	67.995	38.897
133	-5284.	1085.	-5791.	-467.	4.614	67.815	39.115
134	-5309.	1095.	-5826.	-465.	4.639	67.658	39.333
135	-5336.	1107.	-5859.	-464.	4.660	67.455	39.550

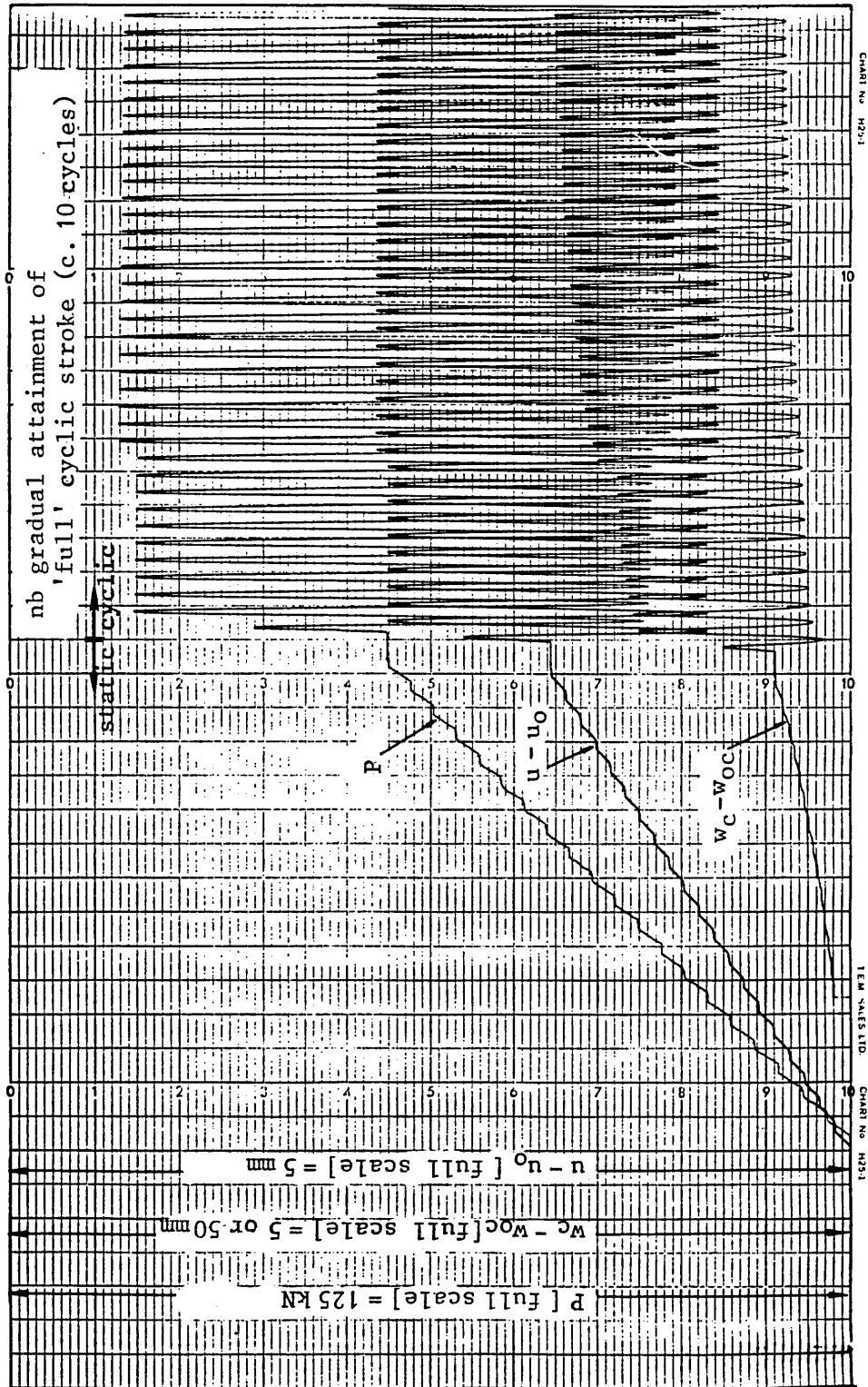
APPENDIX III

TYPICAL $x,y/t$ OUTPUT

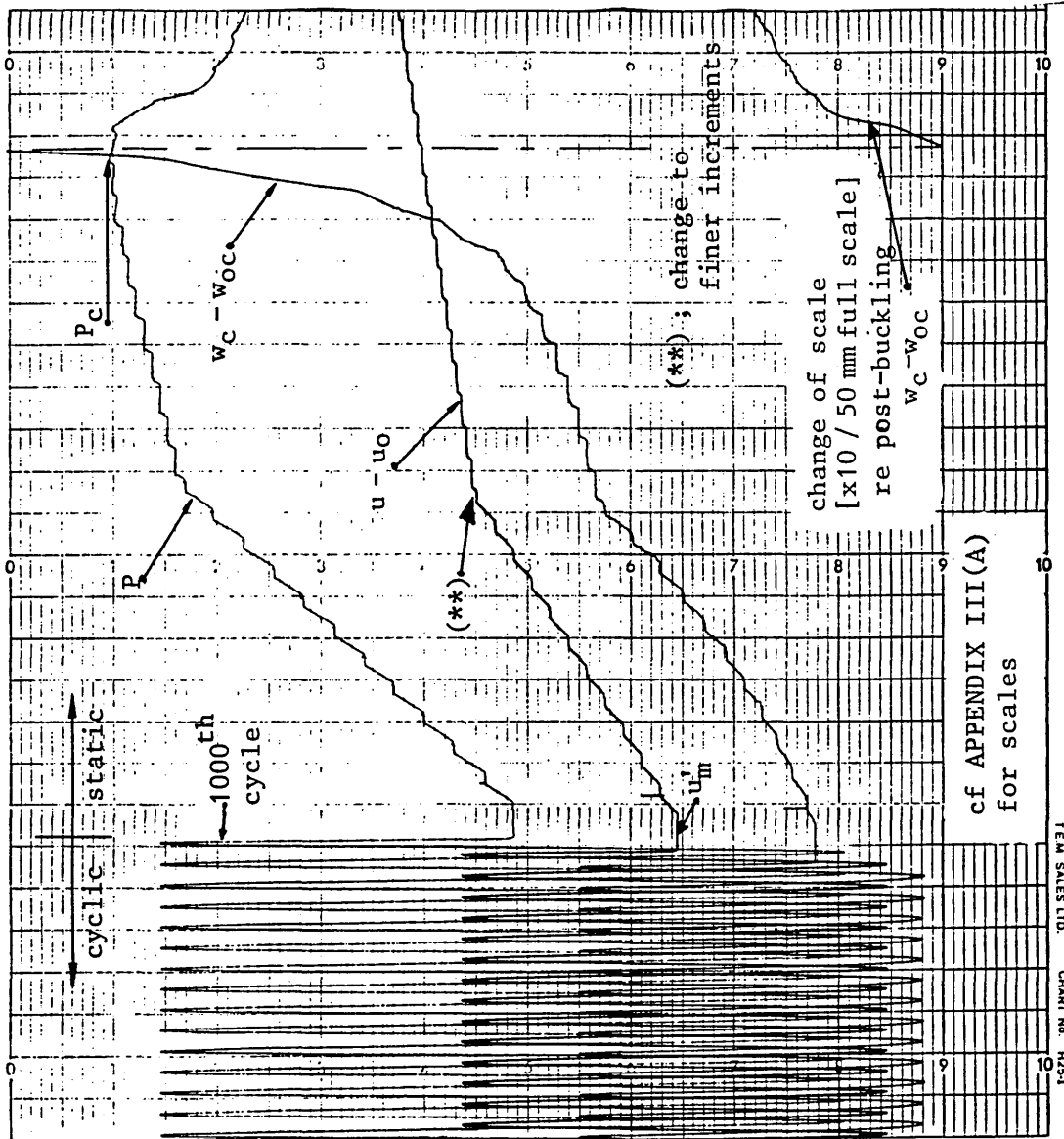
III (A) Static and initial cycles of cyclic phase for Strut Ref. 26C.

III (B) Concluding cycles of cyclic phase and post-cyclic static buckling for Strut Ref. 26C.

APPENDIX III(A)



APPENDIX III (B)



ITEM SALES LTD. CHART NO. H23-1

APPENDIX IV

LIST OF COMPUTER PROGRAMMES

IV (A) RM 380Z Microcomputer Software - BASIC

- (1) Strut test (machine control) drive
- (2) Stub test (machine control) drive
- (3) Initial curvature imperfection drive

IV (B) PDP/1104 Minicomputer Software - BASIC

- (1) Strut test data scanning and acquisition
- (2) Stub test data scanning and acquisition
- (3) Initial curvature imperfection data scanning
and acquisition

IV (C) Experimental Applications; IBM 4341 Mainframe Software
- FORTRAN

- * (1) Strut test — graphical and numerical data
interpretation
- (2) Stub test — graphical and numerical data
interpretation
- (3) Initial curvature test — graphical and numerical
data interpretation

IV (D) Theoretical Applications IBM 4341 Mainframe Software

- FORTRAN

- (1) Formal moment-thrust-curvature contour evaluation
and graphical interpretation
- (2) Formal and curve-fit moment-thrust-curvature contour
graphical interpretation
- (3) Numerical strut modelling solution algorithm
- (4) Pseudo-static enhanced initial imperfection (Δw_{0c})
evaluation
- * (5) Datafile manipulation (pseudo-static path
coordinates)

* Item C(1) accesses D(5) for case study graphical
interpretation.

APPENDIX V

SAMPLE COMPUTER PROGRAMME

Strut test - graphical and numerical data
interpretation programme

FILE: JEANCAL FORTRAN A
DATE: 09JUL1987 AT 13:24:35 HRS

C
C

```
DIMENSION VLVDA(150),TLSA(150),TLVDA(150),RL(150),RRL(150)
DIMENSION LSA1(150),LSA2(150),LSA3(150)
DIMENSION LSA4(150),LSA5(150),IREF(1)
DIMENSION VEC1(100),VEC2(100),VECR(100),ARR(80),ARR2(80)
DIMENSION VEP(120),VEL(120),VELU(120),LODU(120),RLUNP(75)
DIMENSION VEC10(90),VEC20(90),VECRO(90),JUIN(2),JOIN2(2)
DIMENSION VEC3(85),VEC4(85),VECR1(85)
DIMENSION VCP(100),VCPO(80),VCP1(100),YOUT(100),YOUT1(80)
DIMENSION VE(100),VC1(100),VEL1(99),VEP1(99),VEL2(90),VEP2(90)
DIMENSION LOD(80),LOD1(90),LOD2(80),VC2(90),YUT(95),YUT3(80)
DIMENSION VEL3(100),VEP3(100),NPV(50),RRRL(150)
DIMENSION START(2),TO(2)
```

C
C
C

```
DIMENSION PS(500),WCS(500),NS(500),WCSPR(500),WCSPO(500)
DIMENSION PL(500),WCL(500),NLU(500),WCLPR(500),WCLPO(500)
DIMENSION PD(500),WCD(500),ND(500),WCDPR(500),WCDPO(500)
DIMENSION PIN(500),WCI(500),NI(500),WCIPR(500),WCIPO(500)
DIMENSION WAS(3),PAS(3),WAL(3),PAL(3),WAD(3),PAD(3),WAI(3),PAI(3)
DIMENSION PSPR(500),PSPO(500),WS(500),PPS(500)
DIMENSION PLPR(500),PLPO(500),WL(500),PPL(500)
DIMENSION PDPR(500),PDPO(500),WD(500),PPD(500)
DIMENSION PIPR(500),PIPO(500),WI(500),PPI(500),PMX(5)
```

C
C
C
C
C
C
C
C
C
C

"PROGRAMME TO GRAPHICALLY INTERPRET DATA OUTPUT FROM STRUT TESTS"

```
REAL LSA2,LSA3,LSA4,LSA5,MXSTP,MXSTN
REAL MHJM,MHJM1,MGIM,MGIM1,LOD,LOD1,LOD2,LODU
REAL MXST1,MXST2,MXST3,MXST4,LOADMX,JUIN,JOIN2
REAL ICPT,ICPT1,ICP1,INDIA
INTEGER DA,DM,YR,PDT
CALL NULIN(9)
```

```

CALL C1051W
CALL DEVICE(8,0)
CALL DEVPAP(7250.,275.)
C
C
WRITE(6,10)
10 FORMAT(// ' THE FOLLOWING DATA SET WILL HAVE A SYSTEM')
WRITE(6,15)
15 FORMAT(' OF UNITS SET OUT HEREIN')
WRITE(6,20)
20 FORMAT(/ '*****')
WRITE(6,25)
25 FORMAT(// ' MID AXIAL (LONGITUDINAL) STRAIN MEASUREMENTS')
WRITE(6,30)
30 FORMAT(' TO BE IN MICRO=STRAINS (E*10-6)')
WRITE(6,35)
35 FORMAT(//, ' AXIAL LOAD IN KILONEWTONS (KN)')
WRITE(6,40)
40 FORMAT(// ' AXIAL AND LATERAL DISPLACEMENTS IN MILLIMETRES')
WRITE(6,45)
45 FORMAT(// ' TO PROCEED THRU OUTPUT SIMPLY PRESS RETURN KEY!')
C
C INPUT TEST REFERENCE ET. AL.
C
WRITE(6,71)
71 FORMAT(// ' INPUT TEST REFERENCE NUMBER !')
READ(9,*) IR3
WRITE(6,72)
72 FORMAT(/ ' INPUT TEST REFERENCE ALPHABETIC CHARACTER !')
READ(9,77) IREF(1)
77 FORMAT(A3)
C
IREF1=IREF(1)
C
C
C INITIALISE VARIABLES FOR LOOP CALCULATIONS
C
NOT=0
NSAS=10
NPVV=0
LOADMX=0.0
PI=3.141529
C
C CYCLIC TEST - CRIPPLING STATE DISTINCTION ROUTINE
C
WRITE(6,4)
4 FORMAT(/,2X, 'DO YOU REQUIRE A DATA I/P CHECK ? ; 1:-YES , 0:-NO')
READ(9,*) NN
C
C "READ "RAW" DATA TO BE STORED IN ARRAYS"
C
WRITE(6,80)
80 FORMAT(//, ' ARE STRAIN GUAGE RESULTS REQUIRED ? 1 - YES ,0 - NO')
READ(9,55) IEG
55 FORMAT(I1)
87 IF(IEG.EQ.0) GOTO 88

```

```

C
C "STATIC TEST RAW DATA INPUT"
C
  READ(5,*,END=78)I1,I2,I3,IST1
  READ(5,*,END=78)IST2,IST3,IST4,LS,MRA,MXH,MST,MVD
  READ(5,*,END=78)LD1,LD2,LD3,LD4,LOAD
  GOTO 1
C
C "READ CYCLIC TEST RAW DATA"
C
  88  READ(5,*,END=78)I1,I2,I3,LS
      READ(5,*,END=78)MRA,MXH,MST,MVD
      READ(5,*,END=78)LD1,LD2,LD3,LD4,LOAD
C
C
  1  ICHECK=I1+I2+I3+LOAD+MVD+LS
     IF(ICHECK.EQ.0) GOTO 78
     IF(NN.EQ.0) GOTO 991
     WRITE(6,90) LS
  90  FORMAT('/ LS=',I4)
C
C      TRANSFORM INTEGER VARIABLES TO "REAL" VALUES
C
  991 RMST=MST*(-0.001)
      RLOAD=LOAD*(-0.001)
      RMVD=MVD*0.001
      RLD1=LD1*0.001
      RLD2=LD2*0.001
      RLD3=LD3*0.001
      RLD4=LD4*0.001
      RL1=(RLD1-RLD3)/2
      RL2=(RLD4-RLD2)/2
      VEC=SQRT((RL1**2)+(RL2**2))
      VEC=VEC*0.5
C
C      ULTIMATE LOAD SCAN - "PCR"
C
      RLOX=LOADMX-RLOAD
      IF(RLOX)100,110,110
  100  LOADMX=RLOAD
C
C      STORE "REAL" DATA IN ARRAY STORES
C
  110  LSA1(LS+1)=LS
      LSA2(LS+1)=IST1
      LSA3(LS+1)=IST2
      LSA4(LS+1)=IST3
      LSA5(LS+1)=IST4
      TLSA(LS+1)=RMST
      TLVDA(LS+1)=RLOAD
      VLVDA(LS+1)=VEC*2.0
      RL(LS+1)=RL1
      RRL(LS+1)=RL2
      RRR(LS+1)=VEC
      LSCNT=LS+1
      GOTO 87
  78  CONTINUE

```

SUM1=0.
SUM2=0.
SUM3=0.
SUM4=0.
SUM6=0.
SUM7=0.
SUM8=0.
N=0
NC=0
NO=0
LB=0
LB1=0
NA=0
NULT=0

C
C
C
C

FORMATION OF ARRAYS TO PROCESS FAILURE LOCUS
AND SOUTHWELL PLOT(CYCLIC & STATIC TESTS)

WRITE(6,79)
79 FORMAT(/,2X,'DO YOU WISH TO CHOOSE THE UPPER & LOWER LIMITS OF')
WRITE(6,81)
81 FORMAT(/,2X,'THE REGRESSION (STRAIGHT LINE) FIT FOR THE')
WRITE(6,82)
82 FORMAT(/,2X,'SOUTHWELL PLOT ; 1 - YES , 0 - NO! . IF NOT DEFAULT')
WRITE(6,83)
83 FORMAT(/,2X,'VALUES WILL BE SET AT THE CRIPPLING LOAD & 40% OF',
*//,' THE "NOMINAL" EULER LOAD RESPECTIVELY')
READ(9,*) NUTS
IF(NUTS.EQ.1) GOTO 16
SNL=0.4*142.
SNL1=150.
GOTO 17
16 WRITE(6,84)
84 FORMAT(/,2X,'INPUT UPPER & LOWER LIMIT IN TERMS OF LOAD')
READ(9,*) SNL1,SNL
17 CONTINUE
WRITE(6,950)
950 FORMAT(////////,' DO YOU REQUIRE A CHECK ON THE "BREAKDOWN" OF'
*//,' LOAD INCREMENTS USED IN THE SOUTHWELL PLOT ?'
*//,' 1:-YES , 0:-NO')
READ(9,*) SSS

C
C

DO 85 I=1,LSCNT
TLV=TLVDA(I)
IF(TLV) 85,85,59
59 IF(TLV.LT.2.5) GOTO 85
N=N+1
IF(LOADMX~TLV) 65,99,60
99 NULT=15
60 IF(NA.GT.0) GOTO 66
IF(SSS.EQ.0) GOTO 943
WRITE(6,898) TLV,LOADMX
898 FORMAT(/,2X,'STHWELL:LOAD=',2X,1F9.3,'LDMAX=',2X,1F9.3)
943 IF(TLV.GT.SNL) GOTO 130

C
C
C

LOAD , DISPLTS. & SOUTHWELL FACTORS

```

120 NC=NC+1
    VEC10(NC)=RL(I)
    VEC20(NC)=RRL(I)
    VECRO(NC)=RRRL(I)
    VCPO(NC)=(VECR0(NC)/TLV)
    LOD(NC)=TLV
    GOTO 85
C
C     LOAD , DISPLTS. & SOUTHWELL FACTORS
C
130 LB=LB+1
    VEC1(LB)=RL(I)
    VEC2(LB)=RRL(I)
    VECR(LB)=RRRL(I)
    VCP(LB)=(VECR(LB)/TLV)
C
C     LEAST SQUARES REG. : LOOP TO DETERMINE SLOPE (PRE - CYCLIC
C     OR PRE - ULTIMATE LOAD "STATIC")
C
    IF(TLV.GT.SNL1) GOTO 134
    LB1=LB+1
    SUM1=SUM1+(VECR(LB1))
    SUM2=SUM2+(VCP(LB1))
    SUM3=SUM3+(VECR(LB1)*VCP(LB1))
    SUM4=SUM4+(VECR(LB1)**2)
    PUP=TLV
134 LOD1(LB)=TLV
    IF(NULT.EQ.15) NA=1
    GOTO 85
135 CONTINUE
    LSC=(LS)-NCO
C
C     POST CYCLIC SOUTHWELL AND LATERAL DISPLT. VALUES
66 NA=NA+1
    NO=NO+1
    VEC3(NO)=RL(I)
    VEC4(NO)=RRL(I)
    VECR1(NO)=RRRL(I)
    VCP1(NO)=(VECR1(NO)/TLV)
C
C     LEAST SQUARES REG. : LOOP TO DETERMINE SLOPE (POST - CYCLIC)
C
    SUM5=SUM5+(VECR1(NO))
    SUM6=SUM6+(VCP1(NO))
    SUM7=SUM7+(VECR1(NO)*VCP1(NO))
    SUM8=SUM8+(VECR1(NO)**2)
    LOD2(NO)=TLV
    LSCN=LSC-1
85 CONTINUE
65 NNN=1
C
C     SLOPES , INTERCEPTS ET.AL. FROM REGRESSION LOOP
C
156 A=((LB1*(SUM3))-SUM1*SUM2)
    B=((LB1*(SUM4))-((SUM1)**2))
    SLP=A/B
    ICPT=(SUM2/LB1)-SLP*(SUM1/LB1)
    IF(NOT.EQ.0) GOTO 410

```

```

C
C   SLOPES , INTERCEPTS ET.AL. FROM REGRESSION LOOP
C
C= ((NO*(SUM7))- (SUM5*SUM6))
D= ((NO*(SUM8))- ((SUM5)**2))
SLP1=C/D
ICPT1=(SUM6/NO)-SLP1*(SUM5/NO)
C
C   AUTO - SCALING OF VECTOR TRACE (LATERAL MOVEMENT)
C
C
410 IF(NOT.EQ.0) NO=0
    NLN=NC+LB+NO
    NL=NC+LB
    DO 495 I=1,NLN
    IF(I.GT.NC) GOTO 496
    ARR(I)=VEC10(I)
    GOTO 495
496 IF(I.GT.NL.AND.NOT.EQ.1) GOTO 497
    ARR(I)=VEC1(I-NC)
    GOTO 495
497 ARR(I)=VEC3(I-NL)
495 CONTINUE
    RMAX=ARR(1)
    RMIN=ARR(1)
    DO 498 I=2,NLN
    IF(ARR(I).GT.RMAX) RMAX=ARR(I)
    IF(ARR(I).LT.RMIN) RMIN=ARR(I)
498 CONTINUE
    DO 493 I=1,NLN
    IF(I.GT.NC) GOTO 501
    ARR2(I)=VEC20(I)
    GOTO 493
501 IF(I.GT.NL.AND.NOT.EQ.1) GOTO 502
    ARR2(I)=VEC2(I-NC)
    GOTO 493
502 ARR2(I)=VEC4(I-NL)
493 CONTINUE
    RMAX2=ARR2(1)
    RMIN2=ARR2(1)
    DO 504 I=2,NLN
    IF(ARR2(I).GT.RMAX2) RMAX2=ARR2(I)
    IF(ARR2(I).LT.RMIN2) RMIN2=ARR2(I)
504 CONTINUE
C
C   WRITE LATERAL DISPLACEMENTS IN TERMS OF ORTHOGONAL COMPONENTS
C
C
    WRITE(6,491)
491 FORMAT(/,2X,"DO YOU REQUIRE TABULATED OUTPUT OF THE LATERAL")
    WRITE(6,492)
492 FORMAT(2X,"TRANSDUCERS ? - WC ,WC/P ET.AL (1-YES 0-NO)")
    READ(9,*) M1
    IF(M1.EQ.0) GOTO 666
    WRITE(6,490)
490 FORMAT(/" AVERAGED OPPOSING TRANSDUCERS "G & I")
    WRITE(6,510) (ARR(I),I=1,NLN)
    WRITE(6,494)
494 FORMAT(/" AVERAGED OPPOSING TRANSDUCERS "H & J")

```

```

WRITE(6,510) (ARR2(I),I=1,NLN)
WRITE(6,511) RMAX,RMIN,RMAX2,RMIN2
511 FORMAT(// ' G-I"MAX"=',F7.3, ' G-I"MIN"=',F7.3, ' H-J"MAX"=',F7.3,
C ' H-J"MIN"=',F7.3)
525 CONTINUE
C
C WRITE SUB - ULTIMATE LOAD SOUTHWELL VALUES
C
IF(NOT.EQ.0) GOTO 506
WRITE(6,500)
500 FORMAT(// ' VECTOR DISPLT. (PRE-CYCLIC)')
GOTO 523
506 WRITE(6,521)
521 FORMAT(// ' VECTOR DISPLT. (STATIC)')
523 WRITE(6,510) (VECRO(I),I=1,NC)
WRITE(6,510) (VECR(I),I=1,LB)
510 FORMAT(/8F8.3)
IF(NOT.EQ.0) GOTO 526
WRITE(6,520)
520 FORMAT(/// ' VECTOR DISPLT. / LOAD....(PRE-CYCLIC)')
GOTO 889
526 WRITE(6,522)
522 FORMAT(// ' VECTOR DISPLT. / LOAD... (STATIC)')
889 WRITE(6,510) (VCPO(I),I=1,NC)
WRITE(6,510) (VCP(I),I=1,LB)
C
C AUTOMATIC SCALING FOR THE SOUTHWELL PLOTS
C
666 SMAX=VECRO(1)
SMIN=VECRO(1)
SMAX1=VCPO(1)
SMIN1=VCPO(1)
DO 531 I=1,NC
IF(VECRO(I).GT.SMAX) SMAX=VECRO(I)
IF(VECRO(I).LT.SMIN) SMIN=VECRO(I)
IF(VCPO(I).GT.SMAX1) SMAX1=VCPO(I)
IF(VCPO(I).LT.SMIN1) SMIN1=VCPO(I)
531 CONTINUE
TMAX=VECR(1)
TMIN=VECR(1)
TMAX1=VCP(1)
TMIN1=VCP(1)
DO 532 I=1,LB
IF(VECR(I).GT.TMAX) TMAX=VECR(I)
IF(VECR(I).LT.TMIN) TMIN=VECR(I)
IF(VCP(I).GT.TMAX1) TMAX1=VCP(I)
IF(VCP(I).LT.TMIN1) TMIN1=VCP(I)
532 CONTINUE
IF(SMAX.GT.TMAX) SMA=SMAX
IF(SMAX.LT.TMAX) SMA=TMAX
IF(SMIN.GT.TMIN) SMI=TMIN
IF(TMIN.GT.SMIN) SMI=SMIN
IF(SMAX1.GT.TMAX1) SMA1=SMAX1
IF(SMAX1.LT.TMAX1) SMA1=TMAX1
IF(SMIN1.GT.TMIN1) SMI1=TMIN1
IF(TMIN1.GT.SMIN1) SMI1=SMIN1
IF( M1.EQ.0) GOTO 777

```

```

WRITE(6,536) SMA,SMI,SMA1,SMI1
536 FORMAT(/' MAX. DPLT.=',F7.3,2X,'MIN. DPLT.=',F7.3,2X,
C'MAX. DPLT./LD=',F7.3,2X,'MIN. DPLT./LD =',F7.3)
777 IF(NOT.EQ.0) GOTO 580
WRITE(6,540)
540 FORMAT(/' VECTOR DISPLT. (POST - CYCLIC)')
WRITE(6,510) (VECR1(I),I=1,NO)
UMAX=VECR1(1)
UMIN=VECR1(1)
WRITE(6,545)
545 FORMAT(/' VECTOR DISPLT. / LOAD.....(POST - CYCLIC)')
WRITE(6,510) (VCP1(I),I=1,NO)
UMAX1=VCP1(1)
UMIN1=VCP1(1)
DO 575 I=1,NO
IF(VECR1(I).GT.UMAX) UMAX=VECR1(I)
IF(VECR1(I).LT.UMIN) UMIN=VECR1(I)
IF(VCP1(I).GT.UMAX1) UMAX1=VCP1(I)
IF(VCP1(I).LT.UMIN1) UMIN1=VCP1(I)
575 CONTINUE
WRITE(6,576) UMAX,UMIN,UMAX1,UMIN1
576 FORMAT(/' MAX.=',F7.3,2X,'MIN.=',F7.3,2X,'MAX.=',F7.3,2X,
C'MIN.=',F7.3)
C
C AUTOMATIC SCALING OF STRAIN AXIS, AXIAL DISPLACEMENT AXIS ,LOAD AXIS
C AND RESULTANT LATERAL DISPLACEMENT AXIS
C
580 VSTMX=TLISA(LSCNT)+0.5
VLVDAX=1.1*(VLVDA(LSCNT))
MXST1=LSA2(LSCNT)
MXST2=LSA3(LSCNT)
MXST3=LSA4(LSCNT)
MXST4=LSA5(LSCNT)
MXSTN=MXST1
IF(MXST2.LT.MXSTN) MXSTN=MXST2
IF(MXST3.LT.MXSTN) MXSTN=MXST3
IF(MXST4.LT.MXSTN) MXSTN=MXST4
MXSTP=MXST1
IF(MXST2.GT.MXSTP) MXSTP=MXST2
IF(MXST3.GT.MXSTP) MXSTP=MXST3
IF(MXST4.GT.MXSTP) MXSTP=MXST4
MXSTP=MXSTP+100
MXSTN=MXSTN-400
RLOADX=LOADMX*(1.05)
RMSTMX=MSTMX*(1.0)
IF(M1.EQ.0) GOTO 705
C
C WRITE OUT TEST DATA IN FORMAL ENGINEERING UNITS
C
705 IF(NSAS.EQ.0) GOTO 690
WRITE(6,581)
581 FORMAT(2X,'DO YOU REQUIRE TABULATED OUTPUT FROM TEST? 1-YES,0-NO')
WRITE(6,582)
582 FORMAT(/,2X,'INCLUDING LOAD, STRAINS, AXIAL & LATERAL DISPLTS.')
```

READ (9,55) NWOT
IF(NWOT.EQ.0) GOTO 613
WRITE(7,673) IR3,IREF1

```

673 FORMAT(/,10X,' STRUT REFERENCE = ',I2,A4)
```

```

WRITE(6,600)
WRITE(7,600)
600 FORMAT(///, 'LOAD ST.',1X,'STRAIN1',2X,'STRAIN2',2X,
C'STRAIN3',2X,'STRAIN4',2X,'AX.DPLT.',2X,'LOAD',2X,'LAT.DPLT')
WRITE(6,601)
WRITE(7,601)
601 FORMAT('-----')
C-----)
WRITE(6,602)
WRITE(7,602)
602 FORMAT(/)
WRITE(6,610) ((LSA1(I)),(LSA2(I)),(LSA3(I)),(LSA4(I)),(LSA5(I)),
C(TLSA(I)),(TLVDA(I)),(VLVDA(I)),I=1,48)
WRITE(7,610) ((LSA1(I)),(LSA2(I)),(LSA3(I)),(LSA4(I)),(LSA5(I)),
C(TLSA(I)),(TLVDA(I)),(VLVDA(I)),I=1,48)
610 FORMAT(1I4,2X,2F10.0,2F9.0,2X,1F6.3,2X,1F7.3,3X,1F6.3)
IF(N.LT.57) GOTO 613
611 WRITE(6,600)
WRITE(7,600)
WRITE(6,601)
WRITE(7,601)
WRITE(6,602)
WRITE(7,602)
612 WRITE(6,610) ((LSA1(I)),(LSA2(I)),(LSA3(I)),(LSA4(I)),(LSA5(I)),
C(TLSA(I)),(TLVDA(I)),(VLVDA(I)),I=49,96)
WRITE(7,610) ((LSA1(I)),(LSA2(I)),(LSA3(I)),(LSA4(I)),(LSA5(I)),
C(TLSA(I)),(TLVDA(I)),(VLVDA(I)),I=49,96)
WRITE(6,600)
WRITE(7,600)
WRITE(6,601)
WRITE(7,601)
WRITE(6,602)
WRITE(7,602)
WRITE(6,610) ((LSA1(I)),(LSA2(I)),(LSA3(I)),(LSA4(I)),(LSA5(I)),
C(TLSA(I)),(TLVDA(I)),(VLVDA(I)),I=97,N)
WRITE(7,610) ((LSA1(I)),(LSA2(I)),(LSA3(I)),(LSA4(I)),(LSA5(I)),
C(TLSA(I)),(TLVDA(I)),(VLVDA(I)),I=97,N)
613 CONTINUE
690 CONTINUE
C
C PROCESS REG. 'BEST FIT' STRAIGHT LINE THRU STATIC OR PRE & POST
C CYCLIC SOUTHWELL PLOTS
C
DO 300 J=1,LB1
YOUT(J)=(VECR(J)*SLP)+ICPT
300 CONTINUE
C
IF(NOT.EQ.0) GOTO 975
DO 305 K=1,LSC
YOUT1(K)=(VECR1(K)*SLP1)+ICPT1
305 CONTINUE
C
975 CONTINUE
C
C STATIC 'OR' PRE - CYCLIC SOUTHWELL PLOT
C
WRITE(6,301)
301 FORMAT(/,2X,' DO YOU REQUIRE SOUTHWELL PLOT ? : 1:-YES , 0:-NO')

```

```

READ(9,*) NSTH
IF(NSTH.EQ.0) GOTO 309
IF(NSAS.EQ.0) GOTO 39
WRITE(6,310)
310 FORMAT(/,2X,' INPUT STRUT DATA ; E , "EFF. LENGTH" , AV. DIA
C,/, '& AV. WALL THICKNS. (N.B. UNITS IN MM. & KN.)')
READ(9,*) YM,LE, AVDIA,AVWT
INDIA=AVDIA-(2.*AVWT)
SMAR=(PI*((AVDIA**4.)-(INDIA**4.)))/64.
PEU=((PI**2.)*YM*SMAR)/(LE**2.)
IPEU=INT(PE)
39 ASO=ICPT/SLP
SSOP=1./SLP
PLOW=LOD1(1)
IF(SNL1.GE.LOADMX) PUP=LOADMX
CALL WINDOW(2)
CALL SHIFT2(30.,0.)
CALL SCALE2(1.,0.97)
CALL MOVTO2(110.,227.)
CALL LINBY2(149.0,0.0)
CALL CHASWI(0)
CALL CHASWI(1)
CALL SOFCHA
CALL CHASIZ(3.1,3.1)
CALL AXIS2(0.0,SMA,0.0,SMA1)
CALL MOVTO2(8.,125.)
CALL CHASWI(0)
CALL CHASWI(1)
CALL MIXCHA
CALL CHASIZ(3.3,3.2)
CALL CHAHOL(17H(*LMM*U/*LK*UN)*.)
CALL MOVTO2(178.,13.)
CALL CHAHOL(10H(*LMM*U)*.)
CALL CHASWI(0)
CALL CHASWI(1)
CALL CHASIZ(5.5,6.9)
CALL MOVTO2(165.,13.)
CALL CHAHOL(5H*LW*.)
CALL MOVTO2(24.,135.)
CALL CHAHOL(3HP*.)
CALL MOVTO2(15.,137.5)
CALL LINBY2(8.,6.75)
CALL MOVTO2(10.,145.)
CALL CHAHOL(5H*LW*.)
CALL CHASWI(0)
IF(IEG.EQ.1) GOTO 701
CALL CHASWI(0)
CALL CHASWI(1)
CALL CHASIZ(3.5,4.5)
CALL MOVTO2(110.,229.)
CALL CHAHOL(45HSOUTHWELL PLOT : CYCLIC / PRE-ULTIMATE LOAD*.)
GOTO 702
701 CALL MOVTO2(110.,229.)
CALL CHASWI(0)
CALL CHASWI(1)

```

```

CALL CHASIZ(3.5,4.5)
CALL CHAHOL(45HSOUTHWELL PLOT : STATIC / PRE-ULTIMATE LOAD*.)
702 CALL CHASWI(0)
CALL CHASWI(1)
CALL CHASIZ(4.5,4.5)
CALL MOVTO2(14.5,141.5)
CALL CHAHOL(5H*LC*.)
CALL MOVTO2(169.5,9.3)
CALL CHAHOL(5H*LC*.)
CALL CHASWI(0)
CALL CHASWI(1)
CALL CHASIZ(2.65,2.7)
CALL MOVTO2(102.,201.5)
CALL ITALIC(30.0)
CALL CHAHOL(21H:- PRE - REGRESSION*.)
CALL MOVTO2(102.,196.)
CALL CHAHOL(19H          FIT DATA*.)
CALL MOVTO2(102.,185.)
CALL CHAHOL(23H:- LOAD STATES  P*LC*.)
CALL ITALIC(0.0)
CALL HARCHA
CALL MOVTO2(163.5,200.)
CALL CHAHOL(22HP*LE*U"ANALYTICAL" =*.)
CALL MOVTO2(225.2,200.)
CALL CHAHOL(8H*LK*UN*.)
CALL MOVTO2(163.5,190.)
CALL CHAHOL(21HP*LE*U"EMPIRICAL" =*.)
CALL MOVTO2(222.,190.)
CALL CHAHOL(8H*LK*UN*.)
CALL MOVTO2(165.,180.)
CALL CHAHOL(17HAO"EMPIRICAL" =*.)
CALL MOVTO2(222.,180.)
CALL CHAHOL(6H*LMM*.)
CALL ITALIC(0.0)
CALL CHASWI(0)
CALL CHASWI(1)
CALL CHASIZ(3.0,3.25)
CALL SOFCHA
CALL MOVTO2(208.5,200.)
CALL CHAFIX(PEU,5,1)
CALL REFR(IR3,IREF1)
CALL SOFCHA
CALL MOVTO2(142.,185.)
CALL CHAHOL(3H<*.)
CALL MOVTO2(205.5,190.)
CALL CHAFIX(SSOP,5,1)
CALL MOVTO2(205.5,180.)
CALL CHAFIX(AS0,5,2)
CALL CHASWI(0)
CALL CHASWI(1)
CALL MIXCHA
CALL CHASIZ(3.6,3.6)
CALL GRASYM(VECRO,VCPO,NC,1,0)
CALL GRASYM(VECR,VCP,LB,4,0)
CALL GRAPOL(VECR,YOUT,LB1)
CALL CHASWI(0)
CALL CHASWI(1)
CALL CHASIZ(3.4,4.75)
CALL MOVTO2(99.,203.5)

```

```

CALL SYMBOL(1)
CALL MOVTO2(99.,186.5)
CALL SYMBOL(4)
CALL CHASWI(0)
CALL CHASWI(1)
CALL CHASIZ(2.6,2.4)
CALL MIXCHA
CALL MOVTO2(127.,214.)
CALL CHAHOL(50H( LINEAR REGRESSION FIT; P*LU=      K*UN , P*LL=*.)
CALL MOVTO2(200.,214.)
CALL CHAFIX(PUP,5,1)
CALL MOVTO2(236.,214.)
CALL CHAFIX(PLOW,5,1)
CALL MOVTO2(250.,214.)
CALL CHAHOL(10H*IK*UN )*. )
CALL MOVTO2(0.,0.)
CALL SHIFT2(400.,0.)
CALL SCALE2(1.,1.031)

C
C
WRITE(6,306)
306 FORMAT(/,2X,' IS SOUTHWELL PLOT SATISFACTORY ? : 1:-YES , 0:-NO')
READ(9,*) NSAS
IF(NSAS.EQ.0) GOTO 78
309 CONTINUE

C
C
C      CHOOSE LIMITS FOR REGRESSION FIT TO LUNDQUIST PLOT
C
WRITE(6,68)
68 FORMAT(/,2X,' DO YOU REQUIRE LUNDQUIST PLOT? ; 1:-YES , 0:-NO')
READ(9,*) NLUN
IF(NLUN.EQ.0) GOTO 122
WRITE(6,79)
WRITE(6,81)
WRITE(6,86)
86 FORMAT(/,2X,'LUNDQUIST PLOT ; 1 - YES , 0 - NO !. IF NOT DEFAULT')
WRITE(6,83)
READ(9,*) NATS
IF(NATS.EQ.1) GOTO 104
QUST=0.4*142.
QUST1=150.
GOTO 73
104 WRITE(6,84)
READ(9,*) QUST1,QUST
73 CONTINUE

C
C
C      INITIALISE LEAST SQUARES SUMMATION VARIABLES
C
SUM9=0.0
SUM10=0.0
SUM11=0.0
SUM12=0.0
IF(NOT.EQ.0) GOTO 555
SUM13=0.0
SUM14=0.0
SUM15=0.0
SUM16=0.0

```

```

555 CONTINUE
C
C     LOAD & DISPLACEMENTS TO FORM LUNDQUIST PLOT
C
550 FORMAT(/' CENTRAL DISPLACEMENTS (CYCLIC) SUB ULTIMATE LOAD')
551 FORMAT(/' LUNDQUIST LOAD VALUES')
    IF(NOT.EQ.0) GOTO 101
    WRITE(6,550)
    GOTO 103
101 CONTINUE
C     WRITE(6,102)
C 102 FORMAT(/' CENTRAL DISPLACEMENTS (STATIC) SUB ULTIMATE LOAD')
103 NLN1=NLN-1
    DO 119 I=1,NLN
    IF(I.GT.NC) GOTO 109
    VELU(I)=VECRO(I)
    LODU(I)=LOD(I)
    GOTO 119
109 IF(I.GT.NL.AND.NOT.EQ.1) GOTO 114
    VELU(I)=VECR(I-NC)
    LODU(I)=LOD1(I-NC)
    GOTO 119
114 VELU(I)=VECR1(I-NL)
    LODU(I)=LOD2(I-NL)
119 CONTINUE
C     WRITE(6,106) (VELU(I),I=1,NLN)
106 FORMAT(/7F7.3)
    WRITE(6,551)
    WRITE(6,107) (LODU(I),I=1,NLN)
107 FORMAT(/7F8.2)
    WRITE(6,108)
108 FORMAT(/' INPUT "PIVOT" DISPLACEMENT POINT NUMBER')
    READ(9,*) PDT
C
C     AUTO-SCALE & CONSTRUCTION OF LUNDQUIST PLOT
C
    RDL=0.0
    RDL1=0.0
    RLF=0.0
    RLF1=0.0
    NP=0
    DO 162 I=1,NLN
    J=I
    IF(I-PDT) 203,162,201
201 J=I-1
203 VEP(J)=VELU(I)-VELU(PDT)
    VEL(J)=VEP(J)/(LODU(I)-LODU(PDT))
    IF(NOT.EQ.0) GOTO 167
    IF(LODU(J).GE.PV) GOTO 162
167 NP=NP+1
    IF(VEP(NP).GT.RDL) RDL=VEP(NP)
    IF(VEP(NP).LT.RDL1) RDL1=VEP(NP)
    IF(VEL(NP).GT.RLF) RLF=VEL(NP)
    IF(VEL(NP).LT.RLF1) RLF1=VEL(NP)
162 CONTINUE
    RDP=(VEP(NP))
    RDP1=(VEL(NP))
    ROP=VEP(NLN1)
    ROP1=VEL(NLN1)

```

```

GOTO 719
C WRITE(6,116)
C 116 FORMAT(2X, 'DO YOU REQUIRE REDUCED LUNDQUIST DATA ? 1-YES , 0-NO')
C READ(9,55) NOO
C IF(NOO.EQ.0) GOTO 719
C WRITE(6,106) (VEP(J),J=1,NLN1)
C WRITE(6,117) RDL,RDL1
C 117 FORMAT(/ ' LUNDQUIST DISPLTS. , MAX. & MIN =',2X,1F7.4,2X,1F7.4)
C WRITE(6,106) (VEL(J),J=1,NLN1)
C WRITE(6,118) RLF,RLF1
C 118 FORMAT(/ ' LUNDQUIST FACTORS : MAX. & MIN. =',2X,1F7.4,2X,1F7.4)
719 CONTINUE
M=0
IN=0
K=0

```

```

C
C LUNDQUIST CO-ORDINATE BREAKDOWN INTO
C
C
C

```

```

MN=0
M6=0
DO 728 J=1,NLN1
IF (NOT.EQ.0) GOTO 730
IF (LODU(J).EQ.TLVDA(NPVV+1)) MN=10
IF(MN.EQ.10) GOTO 727
730 IF(LODU(J).GT.QUST) GOTO 726
IN=IN+1
VEP1(IN)=VEP(J)
VEL1(IN)=VEL(J)
GOTO 728
726 M=M+1
VEP2(M)=VEP(J)
VEL2(M)=VEL(J)
IF(LODU(J).GT.QUST1) GOTO 3
M6=M6+1
SUM9=SUM9+VEP2(M6)
SUM10=SUM10+VEL2(M6)
SUM11=SUM11+(VEP2(M6)*VEL2(M6))
SUM12=SUM12+(VEP2(M6)**2)
RLUNP(M6)=LODU(J)
3 GOTO 728
727 K=K+1
VEP3(K)=VEP(J)
VEL3(K)=VEL(J)
SUM13=SUM13+VEP3(K)
SUM14=SUM14+VEL3(K)
SUM15=SUM15+(VEP3(K)*VEL3(K))
SUM16=SUM16+(VEP3(K)**2)
728 CONTINUE

```

```

C
C CONSTRUCT LEAST SQUARES REG. FIT
C

```

```

A1=((M6*(SUM11))-(SUM9*SUM10))
B1=((M6*(SUM12))-((SUM9)**2))
SLOP1=A1/B1
ICP1=(SUM10/M6)-SLOP1*(SUM9/M6)
DO 761 I=1,M6

```

```

      YUT(I)=(VEP2(I)*SLOP1)+ICP1
761 CONTINUE
C
C   CONSTRUCT LEAST SQUARES REG. FIT
C
      IF(NOT.EQ.0) GOTO 216
      A3=((K*(SUM15))-(SUM13*SUM14))
      B3=((K*(SUM16))-(SUM13**2))
      SLOP3=A3/B3
      RICP3=(SUM14/K)-SLOP3*(SUM13/K)
      DO 216 I=1,K
      YUT3(I)=(VEP3(I)*SLOP3)+RICP3
216 CONTINUE
      IF(NSTH.EQ.1) GOTO 825
      WRITE(6,310)
      READ(9,*) YM,LE,AVDIA,AVWT
      INDIA=AVDIA-(2.*AVWT)
      SMAR=(PI*((AVDIA**4.)-(INDIA**4.)))/64.
      PEU=((PI**2.)*YM*SMAR)/(LE**2.)
C
C   LUNDQUIST PLOT (STATIC / PRE CYCLIC)
C
825 AO=(ICP1/SLOP1)-VELU(PDT)
      SOP1=(1./SLOP1)+LODU(PDT)
      PIVLD=LODU(PDT)
      PIVDIS=VELU(PDT)
      QQLOW=RLUNP(1)
      QQHI=RLUNP(M6)
      IF(QUST1.GE.LOADMX) QQHI=LOADMX
      IF(AO.LT.0) AO=AO*(-1.)
      CALL SCALE2(1.,0.97)
      CALL SHIFT2(17.,0.)
      CALL CHASWI(0)
      CALL CHASWI(1)
      CALL SOFCHA
      CALL CHASIZ(3.1,3.15)
      CALL AXIS2(RDL1,RDL,RLF1,RLF)
      CALL CHASWI(0)
      CALL CHASWI(1)
      CALL CHASIZ(3.5,3.5)
      CALL MIXCHA
      CALL GRASYM(VEP1,VEL1,IN,1,0)
      CALL GRASYM(VEP2,VEL2,M,4,0)
      CALL CHASWI(0)
      CALL CHASWI(1)
      CALL MIXCHA
      CALL CHASIZ(3.3,3.2)
      CALL MOVTO2(211.,11.)
      CALL CHAHOL(8H*L(MM)*.)
      CALL MOVTO2(3.,116.)
      CALL CHAHOL(17H(*LMM*U/*IK*UN)*.)
      CALL GRAPOL(VEP2,YUT,M6)
      CALL CHASWI(0)
      CALL CHASWI(1)
      CALL MIXCHA
      CALL CHASIZ(4.6,4.6)
      CALL MOVTO2(169.,8.)

```

```

CALL CHAHOL(5H*LC*.)
CALL MOVTO2(191.5,8.)
CALL CHAHOL(5H*LC*.)
CALL CHASWI(0)
CALL CHASWI(1)
CALL MIXCHA
CALL CHASIZ(4.,4.3)
CALL MOVTO2(5.5,147.)
CALL CHAHOL(5H*LC*.)
CALL MOVTO2(21.7,147.)
CALL CHAHOL(5H*LC*.)
CALL CHASWI(0)
CALL HARCHA(1,0)
CALL MOVTO2(127.,178.5)
CALL CHAHOL(5H*LC*.)
CALL MIXCHA
CALL CHASWI(0)
  CALL MOVTO2(110.,229.)
CALL CHASWI(1)
CALL CHASIZ(3.5,4.)
CALL MIXCHA
IF(IEG.EQ.1) GOTO 219
220 CALL CHAHOL(45HLUNDQUIST PLOT : CYCLIC / PRE-ULTIMATE LOAD*.)
  GOTO 221
219 CALL CHAHOL(45HLUNDQUIST PLOT : STATIC / PRE-ULTIMATE LOAD*.)
221 CALL MOVTO2(110.,227.)
  CALL LINBY2(149.,0.)
  CALL CHAESC(1H%)
  CALL CHASWI(0)
  CALL CHASWI(1)
  CALL CHASIZ(5.5,6.7)
  CALL MOVTO2(165.,11.)
  CALL CHAHOL(11H%LW - W *%.)
  CALL CHASWI(0)
  CALL CHASWI(1)
  CALL CHASIZ(4.,5.7)
  CALL MOVTO2(2.,150.)
  CALL CHAHOL(11H%LW - W *%.)
  CALL MOVTO2(2.,134.5)
  CALL CHAHOL(8HP - P*%.)
  CALL MOVTO2(2.,144.)
  CALL LINBY2(20.,0.)
  CALL MOVTO2(90.,205.5)
  CALL CHASWI(0)
  CALL CHASWI(1)
  CALL CHAESC(1H*)
  CALL CHASIZ(3.4,4.9)
  CALL SYMBOL(1)
  CALL MOVTO2(90.,191.)
  CALL SYMBOL(4)
  CALL MOVTO2(95.,203.5)
  CALL ITALIC(30.0)
  CALL CHASWI(0)
  CALL CHASWI(1)
  CALL CHASIZ(2.65,2.7)
  CALL CHAHOL(21H:- PRE - REGRESSION*.)
  CALL MOVTO2(95.,198.)

```

```

CALL CHAHOL(19H          FIT DATA*.)
CALL MOVTO2(90.,190.)
CALL CHAHOL(25H :- LOAD STATES  P*LC*.)
CALL ITALIC(0.)
CALL HARCHA
CALL MOVTO2(163.,200.)
CALL CHAHOL(21HP*LE*U^ANALYTICAL^=*.)
CALL MOVTO2(163.,190.)
CALL CHAHOL(20HP*LE*U^EMPIRICAL^=*.)
CALL MOVTO2(164.,180.)
CALL CHAHOL(16HAO^EMPIRICAL^=*.)
CALL CHASWI(0)
CALL CHASWI(1)
CALL CHASIZ(3.8,4.)
CALL CHAESC(1H%)
CALL MOVTO2(157.,180.)
CALL CHAHOL(3H)%.)
CALL MOVTO2(85.,180.)
CALL CHAHOL(6H(P*=%.)
CALL MOVTO2(123.5,180.)
CALL CHAHOL(10H%LW%U *=%.)
CALL CHASWI(0)
CALL CHASWI(1)
CALL SOFCHA
CALL CHASIZ(3.,3.25)
CALL MOVTO2(137.5,180.)
CALL CHAFIX(PIVDIS,4,2)
CALL MOVTO2(136.,190.)
CALL CHAHOL(3H<%.)
CALL MOVTO2(97.,180.)
CALL CHAFIX(PIVLD,5,1)
CALL MOVTO2(150.5,180.)
CALL HARCHA
CALL CHAHOL(6H%LMM%.)
CALL CHAESC(1H*)
CALL REFR(IR3, IREF1)
CALL CHASWI(0)
CALL CHASWI(1)
CALL SOFCHA
CALL CHASIZ(3.0,3.25)
CALL MOVTO2(205.,200.)
CALL CHAFIX(PEU,5,1)
CALL MOVTO2(203.,190.)
CALL CHAFIX(SOP1,5,1)
CALL MOVTO2(202.,180.)
CALL CHAFIX(A0,5,2)
CALL MIXCHA
CALL MOVTO2(221.5,200.)
CALL CHAHOL(8H*IK *UN*.)
CALL MOVTO2(219.5,190.)
CALL CHAHOL(8H*IK *UN*.)
CALL MOVTO2(218.,180.)
CALL CHAHOL(6H*LMM*.)
CALL MOVTO2(113.,180.)
CALL CHAHOL(10H*IK *UN, *.)
CALL CHASIZ(0.,0.)

```

```

CALL CHASWI(0)
CALL CHASWI(1)
CALL MIXCHA
CALL CHASIZ(2.6,2.4)
CALL MOVTO2(127.,215.)
CALL CHAHOL(50H( LINEAR REGRESSION FIT; P*LU=      K*UN , P*LL=*.))
CALL MOVTO2(200.,215.)
CALL CHAFIX(QQHI,5,1)
CALL MOVTO2(236.,215.)
CALL CHAFIX(QQLow,5,1)
CALL MOVTO2(250.,215.)
CALL CHAHOL(10H*IK*UN )*.))
CALL CHASIZ(0.,0.)
CALL SHIFT2(-17.,0.)
CALL SCALE2(1.,1.031)
CALL CHASWI(0)
CALL MOVTO2(0.,0.)
CALL SHIFT2(400.,0.)

C
C      END OF LUNDQUIST PLOT ! PROCEED OR RE-PLOT?
C
224  WRITE(6,121) -
121  FORMAT(2X,'IS (ARE) LUNQUIST PLOT(S) SATISFACTORY ? :1-YES,0-NO')
      READ(9,*) LUND
      IF(LUND) 309,309,122

C
C      CENTRAL DISPLACEMENT VECTOR TRACE PLOT :
C
122  JUIN(1)=VEC10(NC)
      JUIN(2)=VEC1(1)
      JOIN2(1)=VEC20(NC)
      JOIN2(2)=VEC2(1)
      MP=0
      ZMAX=RL(1)
      ZMIN=RL(1)
      ZMAY=RRL(1)
      ZMINY=RRL(1)
      DO 997 I=2,N
      IF (RL(I).GT.ZMAX) ZMAX=RL(I)
      IF (RL(I).LT.ZMIN) ZMIN=RL(I)
      IF(RRL(I).GT.ZMAY) ZMAY=RRL(I)
      IF(RRL(I).LT.ZMINY) ZMINY=RRL(I)
997  CONTINUE
      WRITE(6,995)
995  FORMAT(/,2X,' DO YOU REQUIRE THE VECTOR TRACES ? 1:-YES , 0:-NO')
      READ(9,*) IVT
      IF(IVT.EQ.0) GOTO 800
      ZER=RRRL(1)
      ZER1=VECRO(1)
      IF(ZER.EQ.ZER1) GOTO 980
      START(1)=RL(1)
      TO(1)=RRL(1)
      START(2)=VEC10(1)
      TO(2)=VEC20(1)
980  CONTINUE
      CALL WINDOW(2)

```

```

IF(MP.EQ.1) GOTO 875
CALL SCALE2(1.0,0.96)
875 CALL AXIPOS(1,40.,140.5,260.,1)
CALL AXIPOS(1,170.,45.,191.,2)
IF (MP.EQ.0) GOTO 981
CALL CHAHAR(0,0)
CALL AXISCA(1,10,ZMAX,ZMIN,1)
CALL AXISCA(1,10,ZMAY,ZMINY,2)
GOTO 982
981 CALL CHAHAR(0,0)
CALL AXISCA(1,10,RMAX,RMIN,1)
CALL AXISCA(1,10,RMAX2,RMIN2,2)
982 CALL AXIDRA(1,1,1)
CALL AXIDRA(-1,-1,2)
CALL CHASWI(0)
IF(MP.EQ.1) GOTO 986
CALL MOVTO2(72.,33.)
CALL CHASWI(0)
CALL CHASWI(1)
CALL SOFCHA
CALL CHASIZ(3.05,3.2)
CALL CHAHOL(44HMID-SPAN LATERAL DISPLACEMENT VECTOR TRACE*.)
CALL CHAHOL(32H (PLAN VIEW) *LRE: *UP < P*LC *.)
CALL MOVTO2(72.,30.5)
CALL LINBY2(200.,0.)
CALL CHASWI(0)
GOTO 989
986 CALL MOVTO2(85.,33.)
CALL CHASWI(0)
CALL CHASWI(1)
CALL SOFCHA
CALL CHASIZ(3.05,3.2)
CALL CHAHOL(44HMID-SPAN LATERAL DISPLACEMENT VECTOR TRACE*.)
CALL CHAHOL(15H (PLAN VIEW) *.)
CALL MOVTO2(85.,30.5)
CALL LINBY2(162.5,0.)
989 CALL CHASWI(0)
CALL CHASWI(1)
CALL REFR2(IR3,IREF1)
CALL HARCHA
CALL CHASIZ(2.9,3.)
CALL MOVTO2(174.,45.)
CALL CHAHOL(11H(J - H)/2*.)
CALL MOVTO2(40.,143.5)
CALL CHAHOL(11H(G - I)/2*.)
CALL MOVTO2(284.,143.5)
CALL CHAHOL(4H(G*.)
CALL MOVTO2(288.,143.5)
CALL CHAHOL(13H ;W*LELD*U)*.)
CALL MOVTO2(172.5,234.)
CALL CHAHOL(6H (J)*.)
CALL MOVTO2(30.,28.)
CALL CHASWI(0)
CALL LINBY2(280.,0.0)
CALL LINBY2(0.0,225.)
CALL LINBY2(-280.,0.0)
CALL LINBY2(0.0,-225.)

```

```

IF(MP.EQ.1) GOTO 987
CALL GRACUR(VEC10,VEC20,NC)
IF(ZER.EQ.ZER1) GOTO 984
CALL GRAPOL(START,TO,2)
984 CALL GRAPOL(JUIN,JOIN2,2)
CALL GRACUR(VEC1,VEC2,LB)
CALL MOVTO2(0.,0.)
IF(NOT.EQ.0) GOTO 985
CALL GRACUR(VEC3,VEC4,NO)
CALL MOVTO2(0.,0.)
985 GOTO 983
987 CALL GRACUR(RL,RRL,LSCNT)
CALL MOVTO2(0.,0.)
983 MP=MP+1
CALL SHIFT2(400.,0.)
CONTINUE
IF(MP.GT.1) GOTO 990
GOTO 980
990 CONTINUE
CALL SCALE2(0.96,1.0)
CALL CHAHAR(0,0)
CALL AXIPOS(0,170.,143.,201.5,1)
CALL AXIPOS(0,170.,143.,201.5,2)
CALL AXISCA(1,10,50.,-50.,1)
CALL AXISCA(1,10,50.,-50.,2)
CALL AXIDRA(2,1,1)
CALL AXIDRA(2,-1,2)
CALL MOVTO2(30.,29.)
CALL LINBY2(280.,0.)
CALL LINBY2(0.,225.)
CALL LINBY2(-280.,0.)
CALL LINBY2(0.,-225.)
CALL GRACUR(RL,RRL,LSCNT)
CALL MOVTO2(51.5,34.2)
CALL CHASWI(0)
CALL CHASWI(1)
CALL SOFCHA
CALL CHASIZ(2.95,3.0)
CALL CHAHOL(44HMID-SPAN LATERAL DISPLACEMENT VECTOR TRACE*.)
CALL CHAHOL(46H PLAN VIEW (A*LXES *US*LCALED *UU*LNIFORMLY)*.)
CALL MOVTO2(51.5,32.)
CALL LINBY2(232.,0.)
CALL CHASWI(0)
CALL CHASWI(1)
CALL MIXCHA
CALL CHASIZ(2.9,2.9)
CALL MOVTO2(282.,142.)
CALL CHAHOL(13H(G ;W*LELD)*.)
CALL MOVTO2(174.,43.)
CALL CHAHOL(5H(H)*.)
CALL MOVTO2(50.,142.)
CALL CHAHOL(5H(I)*.)
CALL MOVTO2(174.,239.)
CALL CHAHOL(5H(J)*.)
CALL REFR2(IR3,IREF1)
CALL CHASWI(0)

```

```

CALL SCALE2(1.04167,1.04167)
CALL MOVTO2(0.,0.)
CALL SHIFT2(400.,0.)
800 CONTINUE
WRITE(6,831)
831 FORMAT(/,2X,' DO YOU REQUIRE "P - U" PLOT ? 1:-YES , 0:-NO')
READ(9,*) IPU
IF(IPU.EQ.0) GOTO 832
CALL SCALE2(1.0,0.96)
CALL SHIFT2(10.,15.)
CALL CHASWI(0)
CALL CHASWI(1)
CALL MIXCHA
CALL CHASIZ(3.4,3.4)
C CALL AXIS(0.0,VSTMX,0.0,RLOADX)
CALL AXIS(0.0,VSTMX,0.0,RLOADX)
CALL CHASWI(0)
CALL CHASWI(1)
CALL MIXCHA
CALL CHASIZ(5.2,5.2)
CALL GRASYM(TLSA,TLVDA,LSCNT,3,0)
CALL CHASWI(0)
CALL CHASWI(1)
CALL MIXCHA
CALL CHASIZ(6.3,7.2)
CALL MOVTO2(165.,9.)
CALL CHAHOL(5H*LU*.)
CALL MOVTO2(21.,135.)
CALL CHAHOL(3HP*.)
CALL CHASWI(0)
CALL CHASWI(1)
CALL MIXCHA
CALL CHASIZ(3.5,4.2)
CALL MOVTO2(135.,228.)
CALL CHAHOL(39HAXIAL LOAD *LVS*U. AXIAL DISPLACEMENT*.)
CALL MOVTO2(135.,225.5)
CALL LINBY2(113.5,0.)
CALL CHASWI(0)
CALL CHASWI(1)
CALL SOFCHA
CALL CHASIZ(2.55,3.2)
CALL MOVTO2(234.,200.)
CALL CHAHOL(11H P*LC*U =*.)
CALL MOVTO2(249.,200.)
CALL CHAFIX(LOADMX,5,1)
CALL MOVTO2(265.,200.)
CALL CHAHOL(8H*IK*UN*.)
CALL CHASWI(0)
CALL GRAPOL(TLSA,TLVDA,LSCNT)
CALL CHASWI(0)
CALL REFR(IR3,IREF1)
CALL CHASWI(0)
CALL CHASWI(1)
CALL CHASIZ(3.5,3.2)
CALL HARCHA
CALL MOVTO2(19.,125.)
CALL CHAHOL(10H(*IK*UN)*.)

```



```

      NSTH=NSTH+1
105 CONTINUE
C
C
C
C
881 NSN=NSLOT2+NSTH
885 IF(NLL.EQ.0) GOTO 886
      NLLOT2=NLLOT/2.
      DO 111 I=1,NLLOT2
        IT=I-1
        WCLPR(I)=WCL(I+IT)
        PLPR(I)=PL(I+IT)
        WCLPO(I)=WCL(2.*I)
        PLPO(I)=PL(2.*I)
111 CONTINUE
C
C
      DO 123 I=1,NLLOT2
        WL(I)=WCLPR(I)
        PPL(I)=PLPR(I)
123 CONTINUE
      NL1=NLLOT2+1
      NLTH=0
      J=-1
      DO 131 I=NL1,NLLOT
        J=J+1
        IF(WCLPO(NLLOT2-J).GT.VLVDAX) GOTO 882
        WL(I)=WCLPO(NLLOT2-J)
        PPL(I)=PLPO(NLLOT2-J)
        NLTH=NLTH+1
131 CONTINUE
C
C
C
C
882 NUN=NLLOT2+NLTH
886 IF(NDD.EQ.0.) GOTO 887
      NDLOT2=NDLOT/2.
      DO 140 I=1,NDLOT2
        IT=I-1
        WCDPR(I)=WCD(I+IT)
        PDPR(I)=PD(I+IT)
        WCDPO(I)=WCD(2.*I)
        PDPO(I)=PD(2.*I)
140 CONTINUE
C
C
      DO 150 I=1,NDLOT2
        WD(I)=WCDPR(I)
        PPD(I)=PDPR(I)
150 CONTINUE
      ND1=NDLOT2+1
      NDIR=0
      J=-1

```

```

DO 160 I=ND1,NDLOT
J=J+1
IF(WCDPO(NDLOT2-J).GT.VLVDAX) GOTO 883
WD(I)=WCDPO(NDLOT2-J)
PPD(I)=PDPO(NDLOT2-J)
NDIR=NDIR+1
160 CONTINUE
C
C
C
C
883 NDN=NDLOT2+NDIR
887 IF(NII.EQ.0) GOTO 191
NILOT2=NILOT/2.
DO 170 I=1,NILOT2
IT=I-1
WCIPR(I)=WCI(I+IT)
PIPR(I)=PIN(I+IT)
WCIPO(I)=WCI(2.*I)
PIPO(I)=PIN(2.*I)
170 CONTINUE
C
C
DO 180 I=1,NILOT2
WI(I)=WCIPR(I)
PPI(I)=PIPR(I)
180 CONTINUE
NI1=NILOT2+1
NINT=0
J=-1
DO 190 I=NI1,NILOT
J=J+1
IF(WCIPO(NILOT2-J).GT.VLVDAX) GOTO 884
WI(I)=WCIPO(NILOT2-J)
PPI(I)=PIPO(NILOT2-J)
NINT=NINT+1
190 CONTINUE
884 NIN=NILOT2+NINT
C
C
191 CONTINUE
C
C
C
C
C
C
DO 195 I=1,NSN
WRITE(6,18) PPS(I),WS(I)
C 195 CONTINUE
C WRITE(6,*) NSN
C
C
C

```

```

        PMX(5)=RLOADX
C
        IF(NSS) 211,211,212
212 PMX(1)=PPS(NSLOT2)
        GOTO 213
211 PMX(1)=0.0
C
C
C
213 IF(NLL) 214,214,215
215 PMX(2)=PPL(NLLOT2)
        GOTO 217
214 PMX(2)=0.0
C
C
C
217 IF(NDD) 218,218,228
228 PMX(3)=PPD(NDLLOT2)
        GOTO 222
218 PMX(3)=0.0
C
C
C
222 IF(NII) 223,223,225
225 PMX(4)=PPI(NILOT2)
        GOTO 226
223 PMX(4)=0.0
C
226 CONTINUE
        PMAX=0.0
        DO 227 I=1,5
        PCH=PMX(I)
        IF(PCH.GT.PMAX) PMAX=PCH
227 CONTINUE
        PMAX=PMAX*1.025
C
908 CONTINUE
C
C
C
C
C
        CALL SCALE2(1.0,0.96)
        CALL CHASWI(0)
        CALL CHASWI(1)
        CALL SOFCHA
        CALL CHASIZ(3.3,3.3)
        IF(NTHWC.EQ.1) PMPM=PMAX
        IF(NTHWC.EQ.0) PMPM=RLOADX
        CALL AXIS(0.0,VLVDAX,0.0,PMPM)
        CALL CHASWI(0)
        CALL CHASWI(1)
        CALL SOFCHA
        CALL CHASIZ(3.3,3.3)
        IF(NTHWC.EQ.1) GOTO 401
        CALL GRASYM(VLVDA,TLVDA,N,4,0)
401 CALL GRAPOL(VLVDA,TLVDA,N,4,0)

```

```

IF(NTHWC.EQ.0) GOTO 302
CALL MOVTO2(72.,100.)
CALL LINBY2(6.,0.)
CALL MOVTO2(80.,100.)
CALL CHAHOL(24H; E*LXPERIMENTAL LOCUS*.)
CALL MOVTO2(145.,100.)
CALL CHAHOL(12H , P*LC*U=*.)
CALL MOVTO2(165.,100.)
CALL CHAFIX(LOADMX,5,1)
CALL MOVTO2(182.,100.)
CALL CHAHOL(8H*LK*UN*.)

```

C
C

```

YDIS=100.0
IF(NSS.EQ.0) GOTO 303
CALL GRACUR(WS,PPS,NSN)
CALL GRASYM(WS,PPS,NSN,7,8)
WS11=WS(1)
PS11=PPS(1)
WAS(1)=0.
WAS(2)=WS11*0.33
WAS(3)=WS11*0.66
PAS(1)=0.
PAS(2)=PS11*0.33
PAS(3)=PS11*0.66
CALL GRAMOV(0.,0.)
CALL GRALIN(WS11,PS11)
CALL GRASYM(WAS,PAS,3,7,0)
YDIS=YDIS-10.
CALL MOVTO2(80.,YDIS)
CALL CHAHOL(33H; S*LOUTHWELL BASED MODEL LOCUS*.)
303 IF(NLL.EQ.0) GOTO 304
CALL GRACUR(WL,PPL,NUN)
CALL GRASYM(WL,PPL,NUN,5,8)
WL11=WL(1)
PL11=PPL(1)
WAL(1)=0.
WAL(2)=WL11*0.33
WAL(3)=WL11*0.66
PAL(1)=0.
PAL(2)=PL11*0.33
PAL(3)=PL11*0.66
CALL GRAMOV(0.,0.)
CALL GRALIN(WL11,PL11)
CALL GRASYM(WAL,PAL,3,5,0)
YDIS=YDIS-10.
CALL MOVTO2(80.,YDIS)
CALL CHAHOL(33H; L*LUNDQUIST BASED MODEL LOCUS*.)
304 IF(NDD.EQ.0) GOTO 311
CALL GRACUR(WD,PPD,NDN)
CALL GRASYM(WD,PPD,NDN,4,8)
WD11=WD(1)
PD11=PPD(1)
WAD(1)=0.
WAD(2)=WD11*0.33
WAD(3)=WD11*0.66
PAD(1)=0.
PAD(2)=PD11*0.33

```

```

PAD(3)=PD11*0.66
CALL GRAMOV(0.,0.)
CALL GRALIN(WD11,PD11)
CALL GRASYM(WAD,PAD,3,4,0)
YDIS=YDIS-10.
CALL MOVTO2(80.,YDIS)
CALL CHAHOL(40H; D*LIRECT "**UW*LOC" BASED MODEL LOCUS*.)
311 IF(NII.EQ.0) GOTO 302
CALL GRACUR(WI,PPI,NIN)
CALL GRASYM(WI,PPI,NIN,1,8)
WI11=WI(1)
PI11=PPI(1)
WAI(1)=0.
WAI(2)=WI11*0.33
WAI(3)=WI11*0.66
PAI(1)=0.
PAI(2)=PI11*0.33
PAI(3)=PI11*0.66
CALL GRAMOV(0.,0.)
CALL GRALIN(WI11,PI11)
CALL GRASYM(WAI,PAI,3,1,0)
YDIS=YDIS-10.
CALL MOVTO2(80.,YDIS)
CALL CHAHOL(42H; I*LNTEGRAL "**UW*LON" BASED MODEL LOCUS*.)
302 CALL MIXCHA
CALL MOVTO2(100.,228.)
CALL CHASWI(0)
CALL CHASWI(1)
CALL CHASIZ(3.5,4.35)
CALL CHAHOL(50HAXIAL LOAD *LVS.*U MID-SPAN RESULTANT LATERAL DI*.)
CALL CHAHOL(12HSPLACEMENT*.)
CALL MOVTO2(100.,226.)
CALL LINBY2(186.,0.)
CALL CHASWI(0)
CALL CHASWI(1)
CALL SOFCHA
CALL CHASIZ(2.55,3.2)
IF(NTHWC.EQ.1) GOTO 404
CALL MOVTO2(235.,200.)
CALL CHAHOL(10HP*LC*U=*.)
CALL MOVTO2(247.,200.)
CALL CHAFIX(LOADMX,5,1)
CALL MOVTO2(264.,200.)
CALL CHAHOL(8H*IK*UN*.)
404 CONTINUE
CALL CHASWI(0)
CALL REFR(IR3,IREF1)
CALL CHASWI(0)
CALL CHASWI(1)
CALL HARCHA
CALL CHASIZ(3.55,3.4)
CALL MOVTO2(197.,13.)
CALL CHAHOL(8H*L(MM)*.)
CALL MOVTO2(20.,125.)
CALL CHAHOL(10H(*IK*UN)*.)
C
IF(NTHWC.EQ.0) GOTO 412

```

```

CALL CHASWI(0)
CALL CHASWI(1)
CALL SOFCHA
CALL CHASIZ(3.5,3.5)
CALL MOVTO2(75.,101.)
IF(NSS.EQ.0) GOTO 406
CALL MOVBY2(0.,-10.)
CALL SYMBOL(7)
406 IF(NLL.EQ.0) GOTO 409
CALL MOVBY2(0.,-10.)
CALL SYMBOL(5)
409 IF(NDD.EQ.0) GOTO 411
CALL MOVBY2(0.,-10.)
CALL SYMBOL(4)
411 IF(NII.EQ.0) GOTO 412
CALL MOVBY2(0.,-10.)
CALL SYMBOL(1)
412 CONTINUE
CALL CHASWI(0)
CALL CHASWI(1)
CALL MIXCHA
CALL CHASIZ(6.3,7.2)
CALL MOVTO2(21.,135.)
CALL CHAHOL(3HP*.)
CALL MOVTO2(163.,13.)
CALL CHAHOL(5H*LW*.)
CALL MOVTO2(180.,13.)
CALL CHAHOL(5H*LW*.)
CALL CHASWI(0)
CALL CHASWI(1)
CALL CHASIZ(4.6,4.6)
CALL MOVTO2(169.,11.5)
CALL CHAHOL(5H*LC*.)
CALL MOVTO2(186.,11.5)
CALL CHAHOL(6H*LOC*.)
CALL MOVTO2(174.5,15.)
CALL LINBY2(3.,0.)
CALL CHASIZ(0.,0.)
CALL CHASWI(0)
CALL MOVTO2(0.,0.)
CALL SHIFT2(400.,0.)
CALL SCALE2(1.0,1.04167)
957 IF(IEG.EQ.0)GOTO 920
WRITE(6,905)
905 FORMAT(/,2X,' DO YOU WANT THE "P - E" GRAPH? , 1-YES 0-NO')
READ(9,*) NSTRM
IF(NSTRM.EQ.0) GOTO 920
CALL SCALE2(1.,0.98)
CALL MOVTO2(169.,11.7)
CALL CHASWI(0)
CALL CHASWI(1)
CALL ITALIC(25.)
CALL SOFCHA
CALL CHAHOL(3H,*.)
CALL ITALIC(0.)
CALL CHASWI(0)
CALL CHASWI(1)
CALL MIXCHA
CALL CHASIZ(3.2,3.3)

```

```

CALL AXIS(MXSTN,MXSTP,0.0,RLOADX)
CALL CHASWI(0)
CALL CHASWI(1)
CALL CHASIZ(6.3,7.6)
CALL MIXCHA
CALL MOVTO2(21.,135.)
CALL CHAHOL(3HP*.)
CALL CHASWI(0)
CALL CHASWI(1)
CALL SOFCHA
CALL CHASIZ(3.,4.75)
CALL MOVTO2(168.6,16.)
CALL ITALIC(32.)
CALL CHAHOL(5H*LC*.)
CALL CHASWI(0)
CALL CHASWI(1)
CALL CHASIZ(6.8,7.6)
CALL ITALIC(0.)
CALL ITALIC(20.)
CALL MOVTO2(165.,11.)
CALL CHAHOL(5H*LC*.)
CALL ITALIC(0.)
CALL CHASWI(0)
CALL CHASWI(1)
CALL MIXCHA
CALL CHASIZ(3.5,3.99)
CALL MOVTO2(115.,229.)
CALL CHAHOL(42HAXIAL LOAD *LV*S*U. MID-SPAN AXIAL STRAIN*.)
CALL MOVTO2(115.,226.5)
CALL LINBY2(125.,0.)
CALL CHASWI(0)
CALL CHASWI(1)
CALL CHASIZ(3.7,3.5)
CALL MOVTO2(171.5,9.6)
CALL CHAHOL(5H*LC*.)
CALL MOVTO2(176.,8.)
CALL HARCHA
CALL CHAHOL(5H*LN*.)
CALL CHASWI(0)
CALL CHASWI(1)
CALL MIXCHA
CALL CHASIZ(3.3,3.3)
CALL MOVTO2(185.,12.)
CALL CHAHOL(19H*L(MICRO-STRAINS)*.)
CALL CHASWI(0)
CALL CHASWI(1)
CALL MIXCHA
CALL CHASIZ(3.45,3.55)
CALL MOVTO2(19.,125.)
CALL CHAHOL(10H(*LK*UN)*.)
CALL CHASWI(0)
CALL CHAHAR(0,0)
CALL REFR(IR3,IREF1)
CALL GRAPOL(LSA2,TLVDA,LSCNT)
YLAB=TLVDA(LSCNT)-3.0
CALL CHAHAR(0,0)
CALL GRAMOV(MXST1,YLAB)
CALL CHAHOL(9H*LN*U=1*.)

```

```

CALL GRAPOL(LSA3,TLVDA,LSCNT)
CALL GRAMOV(MXST2,YLAB)
CALL CHAHOL(9H*LN*U=2*.)
CALL GRAPOL(LSA4,TLVDA,LSCNT)
CALL GRAMOV(MXST3,YLAB)
CALL CHAHOL(9H*LN*U=3*.)
CALL GRAPOL(LSA5,TLVDA,LSCNT)
CALL GRAMOV(MXST4,YLAB)
CALL CHAHOL(9H*LN*U=4*.)
CALL MOVTO2(0.,0.)
CALL SCALE2(1.,1.0204082)
920 CALL DEVEND
STOP
END
SUBROUTINE PAGE
CALL CHAMOD
READ(9,6)
6 FORMAT(A4)
CALL PICCLE
CALL CHAPOS(5.,285.)
RETURN
END
SUBROUTINE AXIS(MINX,MAXX,MINY,MAXY)
CALL AXIPOS(1,45.,30.,273.,1)
CALL AXIPOS(1,45.,30.,180.,2)
CALL AXISCA(1,10,MINX,MAXX,1)
CALL AXISCA(1,10,MINY,MAXY,2)
CALL AXIDRA(1,1,1)
CALL AXIDRA(-1,-1,2)
RETURN
END
SUBROUTINE AXIS2(MINX,MAXX,MINY,MAXY)
CALL AXIPOS(1,45.,30.,256.,1)
CALL AXIPOS(1,45.,30.,180.,2)
CALL AXISCA(1,10,MINX,MAXX,1)
CALL AXISCA(1,10,MINY,MAXY,2)
CALL AXIDRA(1,1,1)
CALL AXIDRA(-1,-1,2)
RETURN
END
SUBROUTINE REFR(IRA,IRA1)
CALL CHASWI(0)
CALL CHASWI(1)
CALL CHAHAR(0,0)
CALL MOVTO2(40.,225.)
CALL CHAHOL(19HS*LTRUT *UR*LEF. *.)
CALL MOVTO2(71.,225.)
CALL CHAINT(IRA,2)
CALL MOVTO2(78.,225.)
CALL CHAARR(IRA1,1,1)
CALL MIXCHA
CALL CHASWI(0)

```

```
RETURN
END
SUBROUTINE REFR2(IRA,IRA1)
CALL CHASWI(0)
CALL CHASWI(1)
CALL CHAHAR(0,0)
CALL MOVT02(38.,245.)
CALL CHAHOL(18HS*LTRUT *UR*LEF.*.)
CALL MOVT02(70.,245.)
CALL CHAINT(IRA,2)
CALL MOVT02(77.,245.)
CALL CHAARR(IRA1,1,1)
CALL MIXCHA
CALL CHASWI(0)
RETURN
END
```

APPENDIX VI

NOMENCLATURE

A	cross-sectional area
A_g	cross-sectional area by geometric measurement
A_m	cross-sectional area by mass measurement
A_{nom}	nominal cross-sectional area
D	outer diameter
D_{av}	average outer diameter
E	direct modulus
E_t	tangent modulus (direct)
E_{tt}	direct modulus determined by tensile testing
I	second moment of area (principal)
L	nominal length
M	bending moment
M_p	fully plastic moment
M_{pn}	reduced plastic moment
M_y	first yield moment
P	axial compression
P_c	buckling load
P_{cs}	equivalent fully static buckling load in cyclic studies
P_e	critical (Euler) load
P_{el}	critical load by Lundquist plot
P_{es}	critical load by Southwell plot
P_m	maximum cyclic load
P_p	Perry (modified/ECCS) load
P_s	squash load

P'	Lundquist pivot state load
P_m'	initial mean cyclic load
Q	conceptual interference force parameter
T_n	transducer measurement at location n
U	strain energy
V	total potential energy
W	external potential work/external (virtual) work
Z	section modulus
a_{01}	Lundquist plot imperfection parameter
a_{0s}	Southwell plot imperfection parameter
a_r	ECCS Robertson factor
c	spring stiffness or sectional constant
e	eccentricity
e_{n1}, e_{n2}	component initial curvatures
f	frequency
k	constitutive function
k_1, k_2	elastic core delineators
n	P/P_s
n_c	cyclic duration/number of cycles
r	minimum radius of gyration
r_s	shape factor
s	standard deviation
t	wall thickness
t_{av}	average wall thickness
t'	time
u	global end-shortening
u_a	axial end-shortening

u_{am}	half amplitude
u_f	flexural end-shortening
u_m	peak cyclic amplitude
u_0	initial end-shortening
u'_m	mean cyclic stroke or displacement
w_c	central transverse displacement with respect to the effective length
w_{cL}	central transverse displacement with respect to the nominal length
w_{oc}	initial central transverse displacement with respect to the effective length
w_{ocE}	initial central transverse displacement with respect to the nominal length under encastré end conditions
w_{on}	n^{th} initial central transverse displacement with respect to the nominal length under pinned end conditions
w_{om}	maximum value of w_{on}
w_{ocL}	central value of w_{on}
w'	Lundquist pivot state displacement
w'_c	cyclic step with respect to the effective length
w'_{cL}	cyclic step with respect to the nominal length
x, y	Cartesian coordinates
\bar{x}	mean
α_i	i^{th} angular displacement with respect to adjacent model links
α_{oi}	initial/unloaded value of α_i
β_{on}	n^{th} angular orientation of w_{on} with respect to the

	weld location
ΔP	load shedding at P_m'
ΔP_c	theoretically based load loss at buckling due to cyclic action
δU	internal virtual work
δW	external virtual work
ϵ	strain
ϵ_m	maximum strain
ϵ_n	n^{th} strain gauge value
ϵ_y	yield strain
ϵ_1	maximum compressive strain
ϵ_2	maximum tensile direct strain
η	Perry factor/ECCS imperfection parameter
θ_i	model link rotation
θ_{oi}	initial/unloaded value of θ_i
λ	slenderness ratio
$\lambda_m = \lambda / \lambda_1$	modified slenderness ratio
λ_0	ECCS limiting slenderness ratio
l	effective length
l_i	model link length
l_1	Lundquist plot based effective length
l_s	Southwell plot based effective length
v	curvature
v_i	i^{th} model-spring curvature
v_y	yield curvature
σ	stress
σ_a	applied stress
σ_m	maximum stress

$\sigma_y/\sigma_{0.2}$ yield/proof stress
 σ_{ytt} yield/proof stress evaluated from tensile testing
 σ_1 maximum compressive stress
 σ_2 maximum tensile stress

APPENDIX VII

BIBLIOGRAPHY

- (1) Trahair, N.S. The Behaviour and Design of Steel Structures, Chapman and Hall, 1977.
- (2) Supple, W.J. Structural Instability - fundamentals of post-buckling behaviour of structures. IPC Science and Technology Press Ltd, 1973.
- (3) Croll, J.G.A. and Walker, A.C. Elements of Structural Stability. Macmillan Press, 1972.
- (4) Gould, P.L. and Abu-Sitta. Dynamic Response of Structures to Wind and Earthquake Loading. Pentech Press, 1980.
- (5) Hudson, D.E. Resonance Testing of Full-Scale Structures. Journal of the Engineering Mechanics Division, ASCE, 90, EM3, 1964, Jun.
- (6) Timoshenko, S.P. and Young, D.H. Theory of Structures, McGraw-Hill, 1966.
- (7) Hurty, W.C. and Rubinstein, M.F. Dynamics of Structures. Prentice-Hall, 1964.

- (8) Lawrence, H.N.L. Dynamic Buckling of an Inelastic Column. International Journal of Solids and Structures, 17, Pergamon Press, 1981.
- (9) Horne, M.R. Plastic Theory of Structures. 2nd Edition, Pergamon Press, 1979.
- (10) Neal, B.G. The Plastic Methods of Structural Analysis. 3rd Edition, Chapman and Hall, 1977.
- (11) CIRIA Report SP18. Long Term Research and Development Requirements in Civil Engineering. CIRIA/Institution of Civil Engineers, 1981.
- (12) Bjorhovde, R. Research Needs in Stability of Metal Structures. Journal of the Structural Division, ASCE, 106, ST12, 1980, Dec.
- (13) Ikeda, K. and Mahin, S.A. Cyclic Response of Steel Braces. Journal of Structural Engineering, 112, 2, 1986, Feb.
- (14) Popov, E.P. and Black, R.G. Steel Struts under Severe Cyclic Loadings. Journal of the Structural Engineering Division, 107, ST9, 1981, Sep.
- (15) Toma, S. and Chen, W.F. Inelastic Cyclic Analysis of Pin-Ended Tubes. Journal of the Structural Division, 108, ST10, 1982, Oct.

- (16) Jain, A.K., Subhash, C.G. and Hanson, R.D. Hysteretic Cycles of Axially Loaded Steel Members. Journal of the Structural Division, ASCE, 106, ST8, 1980, Aug.
- (17) Higginbottom, A.B. and Hanson, R.D. Axial Hysteretic Behaviour of Steel Members. Journal of the Structural Division, ASCE, 102, ST7, 1976, Jul.
- (18) Prathuangsit D., Subhash, C.G. and Hanson, R.D. Axial Hysteresis Behaviour with End Restraints. Journal of the Structural Division, ASCE, 104, ST6, 1978, Jun.
- (19) Nonaka, T. An Elastic-Plastic Analysis of a Bar under Repeated Axial Loading. International Journal of Solids and Structures, 9, 1973.
- (20) Shibata, M. Analysis of Elastic-Plastic Behaviour of a Steel Brace Subjected to Repeated Axial Force. International Journal of Solids and Structures, 18, 3, 1982.
- (21) Jain, A.K., Subhash, C.G. and Hanson, R.D. Inelastic Response of Restrained Steel Tubes. Journal of the Structural Division, ASCE, 104, ST6, 1978.
- (22) Mulcahy, T.M. and Shoemaker, E.M. Column Instabilities caused by Cyclic Loading. International Journal of Solids and Structures, 6, 1970.

- (23) Todd, J.D. Structural Theory and Analysis. Macmillan, 1974.
- (24) Taylor, N. and Hirst, P. Regarding Flexural Curvature. Proceedings of the Institution of Civil Engineers, 2, 77, 1984.
- (25) British Standards Institution. Methods for Tensile Testing of Metals, Part 4: Steel Tubes, BSI, London, BS18, Part 4.
- (26) Tall, L. Stub Column Test Procedure, Document X-282-61, Laboratory Report No 220A, Lehigh University, Bethlehem Pa, 1961.
- (27) Coates, R.C., Coutie, M.G. and Kong, F.K. Structural Analysis. Nelson, 1975.
- (28) Thompson, J.M.T. and Hunt, G.W. A General Theory of Elastic Stability. Wiley, 1973.
- (29) Thompson, J.M.T. Instabilities and Catastrophes in Science and Engineering. Wiley, 1982.
- (30) Benham, P.P. and Warnock, F.V. Mechanics of Solids and Structures. Pitman, 1973.
- (31) Timoshenko, S.P. and Gere, J.M. Theory of Elastic Stability. 2nd Edition, McGraw-Hill, 1961.

- (32) Stamenkovic, A. and Gardner, M.J. Effect of Residual Stresses on Column Behaviour of Hot Finished Steel Structural Sections. Proceedings of the Institution of Civil Engineers, Part 2, 75, 1983.
- (33) Chen, W.F. and Ross, D.A. Tests of Fabricated Tubular Columns. Journal of the Structural Division, ASCE, 103, ST3, 1977, Mar.
- (34) Narayanan, R. Axially Compressed Structures - Stability and Strength. Applied Science Publishers, 1982.
- (35) Allen, H.G. and Bulson, P.S. Background to Buckling. McGraw-Hill, 1980.
- (36) British Standards Institution: Structural use of steelwork in building, Part 1: Code of practice for design in simple and continuous construction; hot rolled sections, BSI, London, BS 5950, Part 1, 1985.
- (37) CONSTRADO/Instn. of Struct. Engrs. Structural Use of Steelwork in Building: Introduction to BS 5950, Part 1, CONSTRADO/Instn. of Struct. Engrs., 1986, Feb.
- (38) Bell, B. Presidential Address. Journal of the Society of Engineers, Proceedings Paper, 62, 1971.

- (39) Lord Baker of Windrush. Early Steelwork Research. Journal of Constructional Steel Research, 1, 1980, Sept.
- (40) Johnston, B.G. Column Buckling Theory: Historical Highlights. Journal of Structural Engineering, ASCE, 109, 9, 1983, Sept.
- (41) Shanley, F.R. Inelastic Column Theory. Journal of the Aeronautical Sciences, 14, 5, 1947, May.
- (42) Johnston, B.G. Third SSRC Guide with Column Design Applications. Journal of the Structural Division, ASCE, 103, ST7, 1977, Jul.
- (43) Ellinas, C.P. et al. Buckling of Offshore Structures. Granada, 1984.
- (44) Hall, D.H. Proposed Steel Column Strength Criteria. Journal of the Structural Division, ASCE, 107, ST4, 1981, Apr.
- (45) British Standards Institution. Materials Testing Machines and Force Verification Equipment, Parts 1 and 2, BSI, London, BS 1610, 1985.
- (46) Smith, G.N. Elements of Soil Mechanics. Crosby Lockwood, 1968.

- (47) British Standards Institution. Hot-Rolled Structural Steel Sections, Part 2: Hollow Sections, BSI, London, BS 4848, Part 2, 1975.
- (48) British Standards Institution. Method for Determination of K-Values of a Tensile Testing System, BSI, London, BS 4759, 1971.
- (49) British Standards Institution. Specification for Weldable Structural Steels, BSI, London, BS 4360, 1979.
- (50) British Standards Institution. Specification for Structural Steel Sections: Part 2, Hot-Rolled Hollow Sections, BSI, London, BS 4, Part 2, 1969.
- (51) Wood, W.A. The Study of Metal Structures and their Mechanical Properties. Pergamon Press, 1979.
- (52) Gaylord, E.H. and Gaylord, C.N. Structural Engineering Handbook. McGraw-Hill, 1968.
- (53) CIRIA Report 63. Rationalisation of Safety and Serviceability Factors in Structural Codes, CIRIA, London, 1977.
- (54) TRRL Supplementary Report 254. Recommended Standard Practices for Structural Testing of Steel Models. TRRL, Crowthorne, 1977.

- (55) Smith, C.S., Kirkwood, W. and Swan, J.W. Buckling Strength and Post-Collapse Behaviour of Tubular Bracing Members Including Damage Effects. Dept. of Energy Report No. OT-R7837, 1979, Jul.
- (56) Spencer, H.H. and Walker, A.C. Critique of Southwell Plots with proposals for alternative methods. Journal of Experimental Mechanics, 15, 8, 1975.
- (57) Southwell, R.V. On the Analysis of Experimental Observations in the Problems of Elastic Stability. Proceedings of the Royal Society, London, Series A, 135, 1932.
- (58) Leicester, R.H. Southwell Plot for Beam Columns. Journal of the Engineering Mechanics Division, ASCE, 96, EM6, 1970.
- (59) Taylor, N. and Hirst, P. Computerised Large Scale Strut Testing - Interaction Between Experimental and Numerical Models. Proc of the Third Int. Conf. on Comp. Meths. and Exptl. Meas., 1, Porto Carras, 1986, Sept.
- (60) British Standards Institution. Specification for the Use of Structural Steel in Building: Part 2, BSI, London, BS 449, Part 2, 1969.

- (61) Wood, W.A. Technical Elasticity and Elastic Fatigue. Journal of Engineering Fracture Mechanics, 8, Pergamon Press, 1976.
- (62) Snijder, H.H. and Bijlaard, F.S.K. The Influence of End Restraints on the Maximum Strength of Centrally Loaded Steel Columns in Braced Frames. Journal of Constructional Steel Research, 5, 1985.
- (63) Stubbins, J.F. and Alexander, W.R. Effects of Fatigue in the Elastic Régime on the Mechanical Properties of Nuclear Pressure Vessel Steels. Conf. Proc. on Ferrific Alloys for Use in Nuclear Energy Technologies, Snowbird, Utah, USA, 1983, Jun.
- (64) Sandor, I.S. Fundamentals of Cyclic Stress and Strain. University of Winsconsin Press, 1972.
- (65) Dolan, T.J. Non-Linear Response Under Cyclic Loading Conditions. Proc. of the 9th Midwestern Mechanics Conference, Madison, Wisconsin, USA, 1965, Aug.
- (66) Shen, Z.Y. and Lu, L.W. Analysis of Initially Crooked, End Restrained Steel Columns. Journal of Constructional Steel Research, 3, 1, 1983.

- (67) Ross, D.A., Chen, W.F. and Tall, L. Fabricated Tubular Steel Columns. Journal of the Structural Division, ASCE, 106, ST1, 1980, Jan.
- (68) Ballio, G. and Perotti, F. Cyclic Behaviour of Axially Loaded Members: Numerical Simulation and Experimental Verification. Journal of Constructional Steel Research, 7,1, 1987.
- (69) Sherman, D.R. Ultimate Capacity of Tubular Members. Shell Oil Company. Report CE-15, Houston, Texas, 1975, Aug.
- (70) Chen, W.F. and Atsuta, T. Inelastic Response of Column Segments under Biaxial Loads. Journal of the Engineering Mechanics Division, ASCE, 99, EM4, 1973, Aug.
- (71) Santathadaporn, S. and Chen, W.F. Tangent Stiffness Method for Biaxial Bending. Journal of the Structural Division, ASCE, 98, ST1, 1972, Jan.
- (72) Snyder, J.S. and Lip-Seng, L. Buckling of Elastic-Plastic Tubular Columns. Journal of the Structural Division, ASCE, 94, ST1, 1968, Jan.
- (73) Tauchert, R.T. Energy Principles in Structural Mechanics. McGraw-Hill, 1974.

- (74) Wang, R.L. Elasto-Plastic Deflection of Tubular Beams. Journal of the Structural Division, ASCE, 95, ST2, 1969, Feb.
- (75) Wagner, A.L., Wendelin, H.M. and Erzurumlu, H. Ultimate Strength of Tubular Beam-Columns. Journal of the Structural Division, ASCE, 103, ST1, 1977, Jan.
- (76) Saleeb, A.F. and Chen, W.F. Elastic-Plastic Large Displacement Analysis of Pipes. Journal of the Structural Division, ASCE, 107, ST4, 1981, Apr.
- (77) Moy, F.C.S Method of Analysis of Laterally Loaded Columns. Journal of the Structural Division, ASCE, 100, ST5, 1974, May.
- (78) Gan, A.B. The Effect of Frictional and Thermal Forces upon Sea Bed Pipeline Buckling Behaviour. PhD Thesis, Sheffield City Polytechnic, 1985.
- (79) Sidney, A.G., Erber, T., Stefanis, J. and Soudan, O. Plastic Collapse, Shakedown, and Hysteresis of Multistorey Steel Structures. Journal of Structural Engineering, ASCE, 112, 12, 1986, Dec.
- (80) Frederick, C.O. Shakedown of a Rectangular Beam under Combined Loading. CEGB, RD/B/N663, Berkeley Nuclear Laboratories, 1966.

- (81) Esin, A. Prediction of the Cyclic Hardening Stress-Strain Curve. Journal of Strain Analysis, 4, 15, 1980.
- (82) Hirst, P. and Taylor, N. Strut Behaviour Subject to Pre-Buckling Cyclic Loading. Applied Solid Mechanics - 2, Strathclyde University, 1987, Apr.